University *of*
Leicester

BROWN DWARFS IN OPEN CLUSTERS

A thesis submitted for the degree of
Doctor of Philosophy
at the University of Leicester.

by
Samantha Louise Osborne

X-ray and Observational Astronomy Group
Department of Physics and Astronomy
University of Leicester

September 2005

ProQuest LLC
789 East Eisenhower Parkway
P.O. Box 1346
Ann Arbor, MI 48106-1346

Abstract

Brown Dwarfs in Open Clusters

Samantha Louise Osborne

This thesis presents the results of the work undertaken during the course of this PhD.

Firstly, the results of a large, deep survey of 5.65 sqaure degrees of the Taurus Dark Clouds are presented. Using a combination of three colour-magnitude diagrams, 165 brown dwarf candidates are identified from RIZ photometry. The presence of deep TiO absorption bands and weak Hα emission in follow-up far-optical spectra revealed 3 borderline brown dwarfs, and the presence of gravity sensitive H_2O absorption features and weak NaI lines in follow-up infrared spectra confirmed 3 more brown dwarfs.

Secondly, the results of a detailed study of brown dwarfs in the Pleiades are presented. The proper motion for 48 brown dwarf candidates is calculated to determine their membership status, with 37 being confirmed as genuine members. Theoretical models indicate that these objects have masses in the range 0.087 - 0.031 $M_\odot$ ($\pm$0.015 $M_\odot$). The effects on the IMF of the cluster are then described. In addition, infrared spectra for 12 of the candidates are presented, with all but 1 of these showing the broad H_2O absorption features typical of brown dwarfs.

Finally, the results of an extremely large scale survey of the Hyades are presented. Data from the USNO and 2MASS catalogues are analysed in terms of proper motion and photometry in order to compile a complete list of the very low mass and brown dwarf cluster members. Unfortunately, no brown dwarfs are found. The core radius of the cluster is calculated for objects of typical brown dwarf mass, and their escape velocity is found to be greater than that of the cluster. Therefore any substellar objects originally formed within the Hyades would have since been ejected.

Declaration

I hearby declare that no part of this thesis has been previously submitted to this or any other University as part of the requirement for a higher degree. The work described herein was conducted by the under signed except for contributions from colleagues as acknowledged in the text.

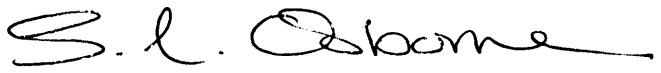

Samantha Louise Osborne
21/09/05

Acknowledgements

I would like to pass on my sincerest thanks to all of the following people, as without their help and support the completion of this thesis would not have been possible.

Firstly to my supervisor, Richard Jameson, for excellent guidance and advice during the course of my PhD.

Secondly to Paul Dobbie for showing me how to use a professional telescope and how to analyse data, and for always having the patience to help with my (frequent!) computing problems.

Thirdly to Simon Hodgkin for being a great companion in Hawaii.

Then to my office-mates: Owen, Dave, Tim, Rosie, Louise, Jon, Yohann, Paul and Mike; for providing good friendship over the last few years.

And next to my parents for their continual support during the entire course of my education, and to my mother in particular for accompanying me on my first trip to the local observatory. That was when I looked through a telescope and saw Saturn's rings, and was the point at which my astronomical journey began.

And lastly, but most importantly, to my husband, Steven, for his constant and unwavering love and support, without which I never would have got this far.

Publications

1. A Large, Deep Survey of the Taurus Dark Clouds
   S. L. Osborne, R. F. Jameson, P. D. Dobbie, E. L. Martín
   2003, *IAU Symposium 211 - Brown Dwarfs*, Edited by E. L. Martín , 79

2. The Substellar Members of the Pleiades
   P. D. Dobbie, R. F. Jameson, S. L. Osborne, S. T. Hodgkin, D. J. Pinfield
   2003, *IAU Symposium 211 - Brown Dwarfs*, Edited by E. L. Martín, 181

3. A Deep IZ Survey of 1.1 deg^2 of the Pleiades Cluster: Three Candidate Members with $M \leq 0.04\ M_{\odot}$
   P. D. Dobbie, F. Kenyon, R. F. Jameson, S. T. Hodgkin, D. J. Pinfield, S. L. Osborne
   2002, *MNRAS*, **335**, 687

In preparation

1. Proper Motions in the Pleiades
   S. L. Osborne, P. D. Dobbie, R. F. Jameson
2. A Survey of the Entire Hyades for Low Mass Members
   S. L. Osborne, S. L. Casewell, R. F. Jameson

Contents

Chapter 1

Introduction

This chapter acts as an introduction to this thesis. Firstly, a brief descrption of what brown dwarfs actually are is given. This is followed by an explanation of why the study of brown dwarfs is important, with particular emphasis on the aims of the work carried out during the course of this PhD. Finally, an outline of the structure of this thesis is provided.

1.1 What are Brown Dwarfs?

Brown dwarfs are best decribed as failed stars. They form from the collapse of interstellar clouds in the same manner as main-sequence stars, but because of their low mass they are unable to reach a core temperature high enough to initiate the fusion of hydrogen into helium. As there is no energy released from nuclear fusion, brown dwarfs 'shine' via the energy released through gravitational contraction and the cooling of their interiors, which means that they are intrinsically both very cool and very faint.

Brown dwarfs are thought to fill the gap in mass between very low mass (VLM) stars and planets, that is to say the mass range between $0.08\,M_{\odot}$ and $0.01\,M_{\odot}$, or 80 and 10 Jupiter masses (M_J). Brown dwarfs and planets are classed as different types of object because they form via two distinct formation mechanisms. Brown dwarfs form as outlined above, whereas planets form via a number of different processes, such as protostellar disk instabilities, the accretion of stellar debris onto a rocky or icy core, the collision of several planetessimals, or through interactions with, or capture by, other more massive objects.

The idea that there could be astronomical objects lying below the hydrogen burning

mass limit was proposed independently in two papers published in 1963, Kumar (1963) and Hayashi & Nakano (1963), although at this stage they were named 'black dwarfs'. The term 'brown dwarfs' was introduced in 1975 by J. C. Tarter (Tarter 1975), but the first bone-fide brown dwarfs were not identified until 20 years later, with the discovery of GL 229B (Nakajima et al. 1995) and Teide 1 (Rebolo, Zapatero-Osorio & Martín 1995). However, it should be noted that several potential brown dwarfs were identified in surveys carried out prior to 1995, but did not have their status confirmed until later, such as GD 165b (Becklin & Zuckerman 1988) and HD 114762 (Latham et al. 1989).

1.2 Why Study Brown Dwarfs?

Originally, the study of brown dwarfs was important because it was thought that they could have been the answer to the problem of the 'missing mass' of the Galaxy (Napier & Guthrie 1975). However, as a result of studies of clusters such as the Pleiades, where it has been shown that brown dwarfs contribute only a few percent towards the total mass of the cluster (Hambly et al. (1998), Hodgkin & Jameson (2000)), brown dwarfs are no longer believed to be the solution. However, this is not definitive since the Pleiades could have lost some brown dwarf members, via interactions with other objects whilst orbiting the Galaxy or during its evolution (Kroupa, Aarseth & Hurley 2001).

Today, the observational study of brown dwarfs remains important for several reasons:

- placing constraints on star formation theories, especially towards the lower end of the mass spectrum.
- providing observational tests for current evolutionary and atmospheric models.
- helping towards the discovery of more extra-solar planets, and ultimately furthering the understanding of extra-solar planet theory, as the two fields are closely related.
- developing a deeper understanding of degenerate physics.
- providing the motivation to develop new and improved technologies, since brown dwarfs push to the limit current observational instruments and techniques.

The aim of this thesis is to study the observational properties of brown dwarfs, and investigate the lower end of the Inital Mass Function (IMF). This will be achieved by continuing the search for brown dwarfs in the Pleiades, Hyades and Taurus clusters, by using both colour-magnitude diagrams and proper motion surveys. Follow-up spectroscopy and infrared photometry will then be used to confirm the membership of the brown dwarf candidates identified. Further studies on the properties of brown dwarfs

will help to improve the accuracy of current evolutionary theories and atmospheric models. After cluster membership has been established, the results will be used to try and determine the substellar mass function. Investigating the Mass Functions (MF) of stellar clusters is also important, since the MF of a group of young stars can be assumed to be a close approximation of their IMF. The lower end of the IMF is of interest because exactly how very low mass objects are formed within a group of higher mass stars and what the minimum mass of an object formed in isolation can be is still unknown. Therefore, observations of young brown dwarfs will help in developing a deeper understanding of star formation processes.

1.3 Structure of Thesis

This thesis is split into two main parts, with the first part covering all of the relevant background information (Chapters 1 to 4) and the second part covering all of the science work undertaken during the course of this PhD (Chapters 5 to 7).

The following two chapters of this thesis provide a review of the observational and theoretical work currently being carried out in the field of brown dwarfs. Chapter 2 provides a summary of the main results obtained from the various surveys aimed at detecting brown dwarfs, both in the field and in open clusters, whilst on the theoretical side, the formation, evolution and atmospheres of brown dwarfs are detailed in Chapter 3. Chapter 4 gives an overview of the technical side of modern observational astronomy, and discusses the telescopes, detectors and data analysis techniques utilised during the course of this PhD.

Chapter 5 presents the results of the first project undertaken during this PhD; a large, deep survey of the Taurus Dark Clouds in the far optical R, I and Z filters. Also included in this chapter are the results of follow-up spectroscopy and infra-red J, H and K photometry. The results of a detailed study of candidate brown dwarfs in the Pleiades cluster are presented in Chapter 6. The membership status of 48 potential brown dwarfs is assessed by calculating their proper motion. The resulting list of definite Pleiades members is then used to determine the form of the mass function for the cluster. In addition, the infrared spectra of 12 of these possible Pleiades brown dwarfs are presented. Chapter 7 presents the results of an extremely large survey of the Hyades, carried out using archive catalogue data from both the Palomar Sky Surveys and 2MASS . The results of the survey are then used to determine the kinematic properties of the Hyades. The thesis is concluded in Chapter 8 with a summary of the findings from the three main

science chapters (5,6 and 7), along with suggestions for further work. Finally, lists of the brown dwarf candidates found in Taurus and the Hyades are included in Appendices A and B respectively.

Chapter 2

Review of Observational Brown Dwarf Work

This chapter summarises the current state of the observational side of brown dwarf research. The first two sections describe the photometric and spectroscopic properties of brown dwarfs. This is followed by a summary of how brown dwarfs can be found, either in the field, in binaries or in clusters. The most recent observational work carried out in a variety of different surveys and clusters is then reviewed.

2.1 The Photometric Properties of Brown Dwarfs

Photometry is the science of the measurment of light. The amount of light emitted from a star is obviously one of the most important characteristics available to an astronomer as this measurement allows other valuable information about the star to be derived, such as luminosity, distance and temperature.

2.1.1 The Stellar Magnitude Scale

The first known magnitude scale was devised by the Greek astronomer Hipparchus around 2000 years ago. He compiled a list of positions of some 850 stars, and assigned to each of these an apparent brightness on a scale of 1 to 6, with 1 being the brigthest and 6 being the faintest, as visible with the naked eye. This system remained relatively unchanged until 1856, when British astronomer N. R. Pogson quantified the scale by proposing that a first magnitude star is 100 times brighter than a sixth magnitude star. As

a result of this, a difference of one magnitude is equivalent to a factor of 2.512 difference in brightness, which reflects the logarithmic nature of the detection of light by the human eye. The difference in *apparent magnitude* between two stars, a and b, corresponds to the ratio of their flux:

$$m_a - m_b = 2.5 \log_{10} \left(\frac{F_b}{F_a} \right). \tag{2.1}$$

The scale has since been extended to include much fainter stars, down to $\sim$ 25th magnitude, and very bright objects, which have negative magnitudes. Specific standard stars, such as Vega (α Lyrae), are used to define zero magnitude.

The flux received on Earth from an astronomical object depends on both its intrinsic luminosity and its distance. These considerations lead to the idea of *absolute magnitude*, which is defined as the apparent magnitude a star would have if it were at a distance of 10 parsces from the Earth. As the flux of a star is related to its distance by an inverse square law, the *distance modulus* is defined by:

$$m - M = 5 \log_{10} d - 5. \tag{2.2}$$

Information collected from Carroll & Ostlie (1996) and Zeilik et al. (1992).

2.1.2 Photometric Wavebands

The measured magnitude of a star depends upon the wavelength at which it has been observed, because the emitted flux varies with wavelength. In addition to this, the light is further affected by absorption in the interstellar medium and/or the atmosphere of Earth.

At optical wavelengths, the atmosphere of the Earth is effectively transparent and is split into several wavebands. The most common wide band system in use in astronomy today is the *UBV* system developed by H. L. Johnson in the 1950's, which covers the ultraviolet, blue and visible wavebands. The longer wavelength *R* and *I* bands were added later. At infrared wavelengths, the atmosphere of the Earth is mostly opaque due to absorption by water vapour and carbon dioxide, with only a few transparent 'windows'. These windows correspond to the *JHKLMN* system. Information collected from Zeilik et al. (1992).

2.1.3 Colour Index

The *colour index* of a star is defined as the difference between magnitudes at two different wavelengths:

$$CI = m(\lambda_1) - m(\lambda_2). \tag{2.3}$$

In this equation, $m(\lambda_1)$ is the short-wavelength magnitude and $m(\lambda_2)$ is the long-wavelength magnitude. As the colour index depends only on the difference between magnitudes, it is equivalent to a flux ratio, which in turn is equivalent to the ratio of the Planck function at two different wavelengths, if the star behaves like a black body. Therefore, the colour index is indicitive of the temperature of the star.

Since stars have different temperatures, their Planck curves will peak at different wavelengths, making hot stars bluish and cooler stars reddish. A comparison of colour indices, for example between $B - V$ and $R - I$, allows astronomers to differentiate between blue stars and red stars.

Colour indices are also affected by *interstellar reddening* because the light emitted by a star is absorbed and scattered by dust grains in the interstellar medium. The difference between the observed and intrinsic colour indices is known as the *colour excess*. Therefore, photometry in at least three different wavebands is required to separate out the effects of interstellar reddening and determine the temperature of a star. Information collected from Carroll & Ostlie (1996) and Zeilik et al. (1992).

2.1.4 H-R Diagrams

The first H-R diagrams were plotted by E. Hertzsprung and H. N. Russell in 1911 and 1913 respectively. The diagrams showed the relationship between absolute visual magnitude versus spectral type for nearby stars. However, since spectral types are more difficult to determine than magnitudes for large numbers of stars it is often easier to plot absolute magnitude versus colour in a colour-magniude diagram (CMD). This still results in an H-R diagram for stars in a cluster since stellar colours and spectral types are closely related and the distance to each member is about the same. In particular, stars belonging to a stellar cluster form a distinctive sequence in a CMD which can often be easily identified from other stars, thus making it possible to determine which of the observed stars are actually members of the cluster being studied. Information collected from Carroll & Ostlie (1996) and Zeilik et al. (1992).

2.1.5 Photometric Properties of Brown Dwarfs

Due to their coolness the spectral energy distribution of a brown dwarf peaks in the infrared, and, therfore, when searching for brown dwarfs it is best to use a far-red or infrared filter. A CMD plot will then usually reveal a cluster of objects located towards the left hand side of the diagram, which gradually decreases redward, followed by the thin but distinctive sequence of cluster stars (see Figure 2.1). Therefore when searching for brown dwarfs in stellar clusters, potential members can be identified from the CMD by extrapolating the main sequence distribution down into the brown dwarf regime. Unfortunately, this sequence becomes somewhat less distinctive at fainter magnitudes and redder colours (the domain of brown dwarfs), so a simple single selection procedure is likely to be highly contaminated with backgroud objects. To overcome this problem, it is usually best to combine selections from two or three CMDs in order to reduce the number of contaminating objects.

When compared to their warmer L dwarf (Kirkpatrick et al. (1999); Martín et al. (1999*a*)) cousins, the identification of the coolest T dwarfs (Kirkpatrick et al. 1999) from infrared surveys is complicated by the fact their infrared colours begin to turn blueward due to CH_4 absorption in the H and K bands. Thus, the identification of T dwarfs requires much wider selection criteria, and hence more field star contaminants to sift through.

The identification of brown dwarfs from CMDs can be further complicated by interstellar reddening. However, for most nearby clusters the reddening is the same across the whole cluster and is usually quite low, making it fairly straightforward to take the effects into account. Unfortunately, the same does not apply for star forming regions, where the levels of reddening can be both high and variable. A reddened object may be dereddened by comparing the observed colour index and the intrinsic colour index as determined from the objects' spectrum, or by comparing two colour indices, such as $J - H$ and $H - K$.

2.2 The Spectroscopic Properties of Brown Dwarfs

The spectrum of a star is the distribution of its emitted radiation, and it can provide an astronomer with a great deal of information. A spectrum is created when light is passed through a prism or grating because different wavelengths have different degrees of refraction. The exact distribution of energy is determined in the star's atmosphere,

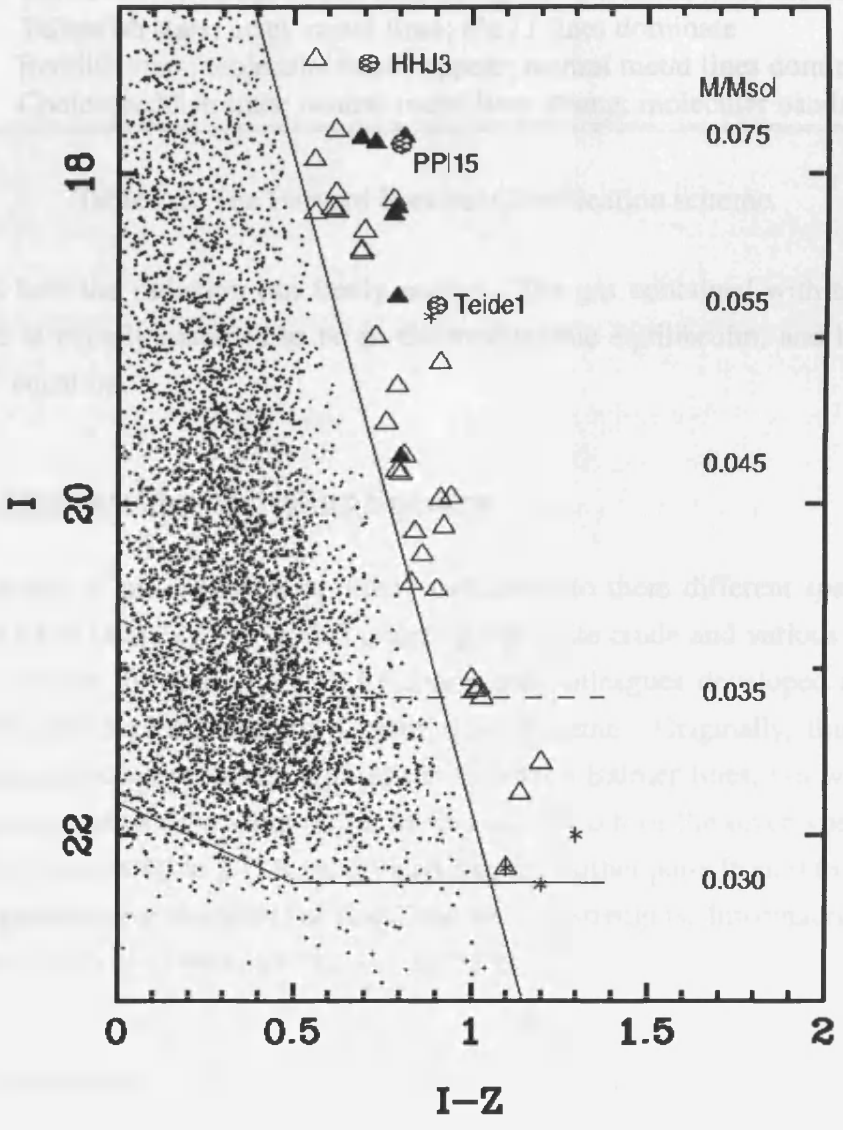

FIGURE 2.1. An example CMD for the Pleiades cluster from Zapatero-Osorio et al. 1999.

Spectral Type	Principle Characteristics
O	Hottest bluish-white stars; relatively few lines; $He\,II$ dominates
B	Hot bluish-white stars; more lines; $He\,I$ dominates
A	White stars; ionized metal lines; hydrogen Balmer lines dominate
F	White stars; hydrogen lines decreasing; neutral metal lines increasing
G	Yellowish stars; many metal lines; $Ca\,II$ lines dominate
K	Reddish stars; molecular bands appear; neutral metal lines dominate
M	Coolest reddish stars; neutral metal lines strong; molecular bands dominate

Table 2.1. The Harvard Spectral Classification scheme.

since from here the radiation can freely escape. The gas contained within the stellar atmosphere is usually assumed to be in thermodynamic equilibruim, and to obey the perfect gas equation.

2.2.1 Classification of Stellar Spectra

The first person to place spectra in order, and assign to them different *spectral types* was A. Secchi in 1863. However, this ordering was quite crude and various other classification schemes followed, until A. J. Cannon and colleagues developed a new system in 1910, the Harvard Spectral Classification scheme. Originally, this sequence was ordered according to the strength of the hydrogen Balmer lines, but was later altered to correspond to decreasing stellar temperature. Each of the seven spectral types (*O,B,A,F,G,K,M*; see Table 2.1) is subdivided into ten further parts from 0 to 9, depending on the presence (or abscence) of lines, and the line strengths. Information collected from Carroll & Ostlie (1996) and Zeilik et al. (1992).

2.2.2 Spectroscopic Properties of Brown Dwarfs

Since the discovery of the first brown dwarfs in the mid-1990's, and the numerous other discoveries since, the study of cool atmospheres has become a popular topic. As a result of the follow-up spectroscopic work carried out on brown dwarfs it has been necessary to introduce two new spectral classes to the Harvard scheme to account for the different features observed in the atmospheres of cool, substellar objects. The exact definitions of these two new classes are given in the review by Reid (1999*b*), and the key spectral features are outlined in Table 2.2.

Spectral Type	Principle Characteristics
L	Coolest very low mass stars and brown dwarfs; TiO and VO weaken; prominent molecular bands from metal hydrides; atomic lines increasing
T	Cool brown dwarfs; H_2O increases, CH_4 present

Table 2.2. The key features of the L and T spectral classes.

The first new spectral class introduced was L (Kirkpatrick et al. (1999); Martín et al. (1999*a*)), which describes objects that are just cooler than standard M class objects. L dwarfs can be either very low mass stars or warm, massive brown dwarfs, and range in temperature from around 2500 K (L0) to 1200 K (L9). The spectra show increasing water absorption bands, along with strong Na, Rb and Cs resonance lines. After this lie the T dwarfs (Kirkpatrick et al. 1999), which at temperatures below about 1200 K are characterised by the presence of methane in their atmospheres. In addition, a further spectral class, Y (Kirkpatrick et al. (1999); Burgasser et al. (2005) and references therein), has also been proposed, although no definite candidates have yet been observed.

2.3 Finding Brown Dwarfs

In order to find brown dwarfs there are three key locations that can be searched: in the field, in binary sytems, or in open clusters. Brown dwarfs can also be found indirectly by looking for the slight increase in intensity of a star which occurs when a brown dwarf acts as a gravitional microlens, see for example Smith, Mao & Woźniak (2003).

2.3.1 In the Field

Since there are thought to be many brown dwarfs in the Milky Way, it is likely that a large number could be found by surveying very large areas of sky for very cool, faint objects. Unfortunately, when using this method there is no way of knowing the age of any object detected, and hence no way of determining whether it is a definite brown dwarf without further observations. However, if the object has an effective temperature consistent with a mid-L spectral type ($T_{eff} \sim 1800$) then it must be a brown dwarf since a star with $M \geq 0.075\,M_{\odot}$ (Baraffe et al. 2002*b*) can never reach this temperature.

2.3.2 In Binaries

Stars which are near to Earth (say within 10 pc) are observed to have a 'proper motion' due to the velocity component of the star relative to the Sun which is perpendicular to the line of sight. If the star is an astrometric binary, and has a brown dwarf companion, it will rotate around the centre of mass of the system and hence display a sinusoidal proper motion. Brown dwarf binaries can also be detected by using the Doppler shift of the star to measure the component of velocity along the line of sight. This method is particularly useful if the binary period is short or if the primary star is bright. If the binary separation is wide enough, the brown dwarf may be visible directly. One advantage of searching for brown dwarfs in binary systems is that the dynamical mass of the system may be able to be determined, meaning that the brown dwarf mass can be found independently, without the need for evolutionary models (Zapatero-Osorio et al. 2004).

2.3.3 In Clusters

For a given cluster of stars, the distance, age, metallicity and extinction can be determined, thus making them an ideal place in which to search for brown dwarfs. Also, if the cluster is young, the brown dwarfs will be brighter and so easier to find. The same reasoning also applies to star formation regions (SFRs), although these areas often have high, and sometimes variable, levels of reddening due to dust which can make calculating accurate photometric magnitudes problematic.

2.4 Observational Review

There is currently much activity in the observational study of brown dwarfs, with many different groups from around the world focusing on a variety of observational investigations. What follows is a brief review of brown dwarf observations up to the current time, highlighting the key areas of research and summarising the most important findings.

2.4.1 Brown Dwarf Surveys

Despite the dificulties associated with finding field brown dwarfs, many brown dwarfs have been identified from data collected from large scale all-sky surveys such as the Two Micron All Sky Survey (2MASS; Skrutskie et al. (1997)), the Deep Near-infrared

Survey (DENIS; Epchtein (1997)) and the Sloan Digital Sky Survey (SDSS; York (2000)). Other large scale surveys undertaken with the sole purpose of finding brown dwarfs and planetary mass objects, include the ELODIE (Naef et al. (2004)) and CORALIE (Pepe et al. 2002) surveys.

Despite not having their status recognised at the time, GD 165b (Becklin & Zuckerman 1988) and HD 114762 (Latham et al. 1989) were the first field brown dwarf candidates to be identified. Other early discoveries of field brown dwarfs were made by Jones, Miller & Glazebrook (1994), Ruiz, Leggett & Allard (1997) and Tinney (1998), however, 2MASS has by far been the most successful survey in finding field brown dwarfs. To date, over 170 L and T dwarfs have been discovered by using 2MASS data (Kirkpatrick 2003), more than twice as many as any other survey. Many of the initial brown dwarf discoveries made by 2MASS had spectral types later than M9.5, which led to the definition of the new 'L' spectral type and the proposal of the 'T', or methane, dwarf status for Gl 229B (Kirkpatrick et al. 1999). As the survey neared completion, many more L dwarfs were discovered (Cruz et al. 2003), along with numerous T dwarfs (Burgasser et al. (2002*e*), Burgasser et al. (2004)), including one T dwarf which is very close (< 10 pc) to the Sun (Burgasser et al. 2003). Thus the T spectral class was able to be fully characterised (Burgasser et al. (2002*e*), Geballe et al. (2002)). 2MASS data have also been responsible for the discovery of the rare phenomenon of strong $H\alpha$ emission in L and T dwarfs (Hall (2001), Burgasser et al. (2002*a*)), which is possibly a result of the brown dwarf having an accretion hot spot (Burgasser et al. 2002*c*). Also, since the completion of the entire survey, and the subsequent easy online accessibilty of 2MASS data, such data have been used to supplement many other brown dwarf investigations.

The first brown dwarf candidates found from DENIS were identified by Delfosse et al. (1997), with three objects showing properties indicitive of a substellar nature. Further very low mass and brown dwarf candidates have since been discovered, including several L-type objects (Delfosse et al. (1999), Martín et al. (1999*b*) and Kendall et al. (2004)), resulting in an L dwarf classification scheme (Martín et al. 1999*a*). DENIS data has also been used to help complete the census of very low mass stars within the solar neighbourhood by identifying 62 nearby (< 30 pc) late M dwarfs (Phan-Boa et al. (2001), Phan-Boa et al. (2003)).

Data obtained from the SDSS has also played a significant role in the identification, classification and characterisation of L and T dwarfs, since the survey includes spectroscopic data in addition to photometric data. Just under a third of all the known L and T dwarfs have been discovered by the survey (Kirkpatrick 2003). SDSS photometry resulted in 20 L dwarfs being uncovered by Fan et al. (2000) and Schneider et al. (2002),

and 2 T dwarfs being found by Strauss et al. (1999) and Tsvetanov et al. (2000). More significantly, Hawley et al. (2002) identified 629 new M dwarfs and 48 new L dwarfs, each with spectral data, which when combined with 41 previously known objects allowed for the complete characterization of the M, L, T, spectral sequence.

These three large-scale surveys have been responsible for almost all of the L and T dwarf discoveries made to date (over 400 L dwarfs, and around 70 T dwarfs), but since the data collected were analysed by different groups of researchers this led to several classification schemes being proposed (Kirkpatrick et al. (1999); Martín et al. (1999*a*); Geballe et al. (2002); Burgasser et al. (2002*b*)). Despite basing the classification on different features within the L dwarf spectrum, the L subclasses from the different schemes are in fairly good agreement with each other. The L dwarf spectral sequence, in the far optical waveband, is shown in Figure 2.2.

In contrast, agreement upon the classification of the T dwarfs has been somewhat more difficult, perhaps due to the fact that when compared to the L dwarfs, there are significantly fewer example T dwarf spectra to work with. However, with the growing number of T dwarf discoveries this situation has improved, and a unified T dwarf classification scheme has recently been proposed (Burgasser et al. 2005). The T dwarf spectral sequence, in the infrared, is shown in Figure 2.3, whilst the transition region between L and T, showing the onset of methane absorption, is illustrated in detail in Figure 2.4.

2.4.2 Brown Dwarfs in Binary Systems

Searches for brown dwarfs in binary systems fall into two main catagories: searches for brown dwarfs as companions to stars and searches for brown dwarf/brown dwarf binaries; although more recently some emphasis has been placed on the search for planets around brown dwarfs (Guenther & Wuchterl 2003). Most searches for brown dwarfs in binary systems rely either upon precise radial velocity measurements or extremely high resolution adaptive optics imaging, with the Hokupa'a curvarture wave-front sensor allowing the Gemini telescope to guide even on faint, low mass stars and brown dwarfs (Close et al. (2002*a*), Close et al. (2002*b*)).

Regarding the search for brown dwarfs as companions to stars, there are too many published papers on too many individual systems to be reviewed here in a succinct manner, so only the key points and most recent highlights will be outlined here. Perhaps the most prominent feature of brown dwarfs in binaries is the rarity of systems which have a solar-type primary and a brown dwarf secondary (Endl et al. 2004). This sudden drop in the mass function is known as the 'Brown Dwarf Desert' (Halbwachs et al. 2000). From

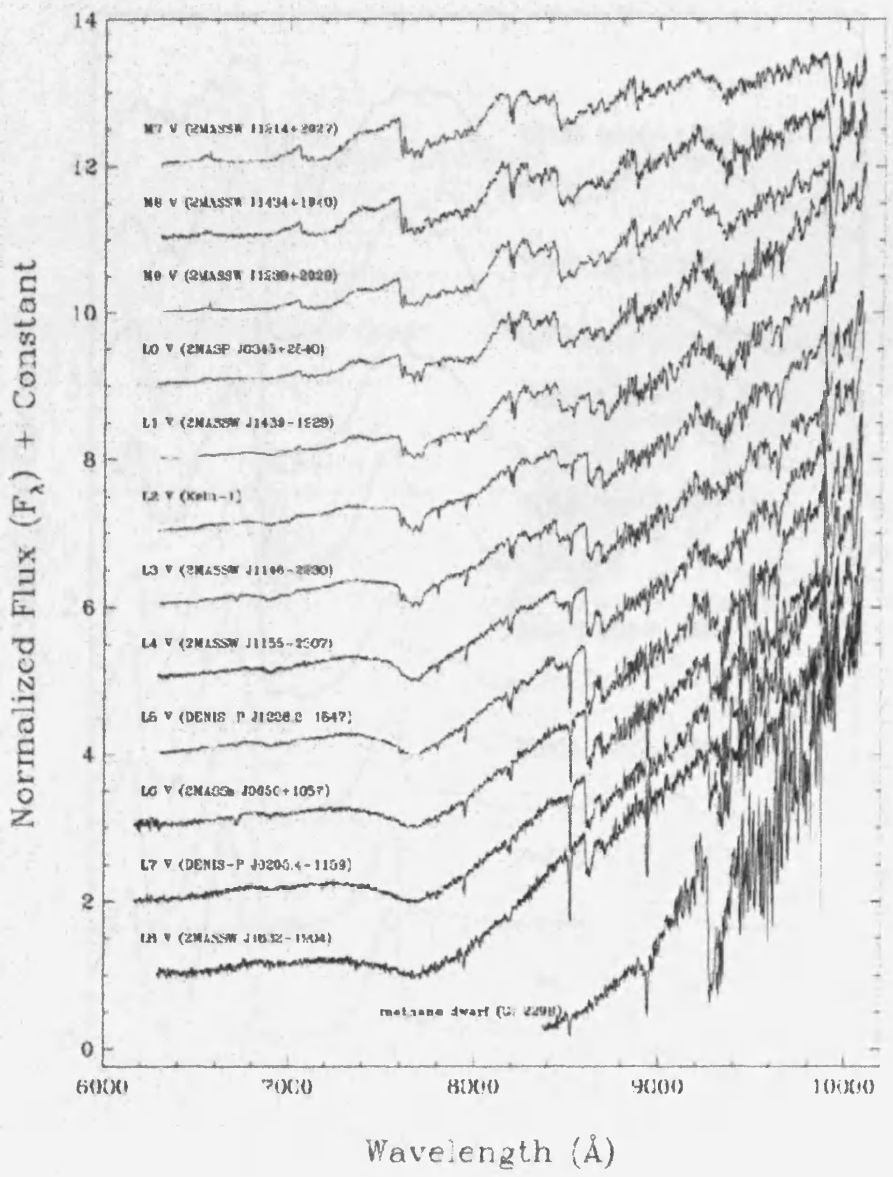

FIGURE 2.2. The L dwarf spectral sequence as defined by Kirkpatrick et al. 1999.

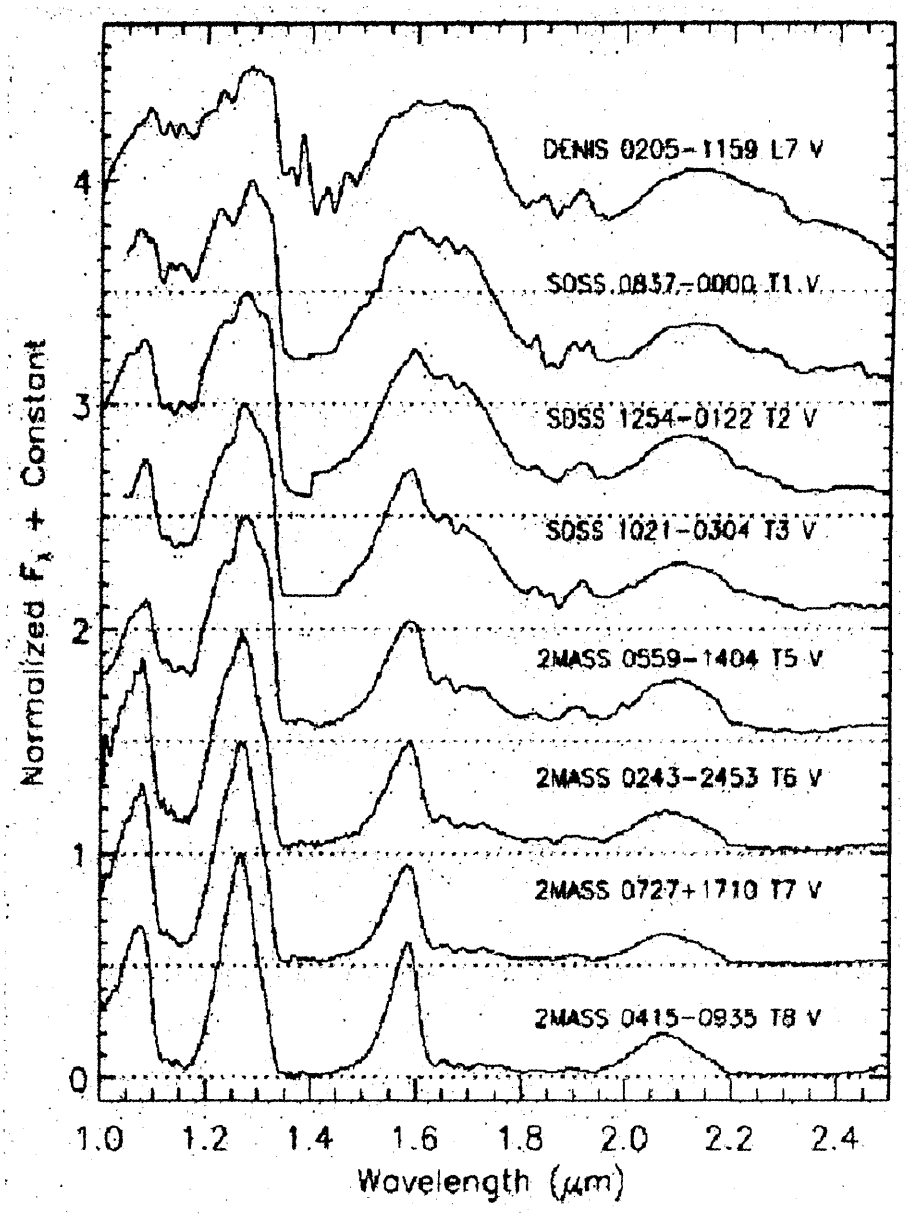

FIGURE 2.3. The T dwarf sequence as defined by Burgasser et al. 2002.

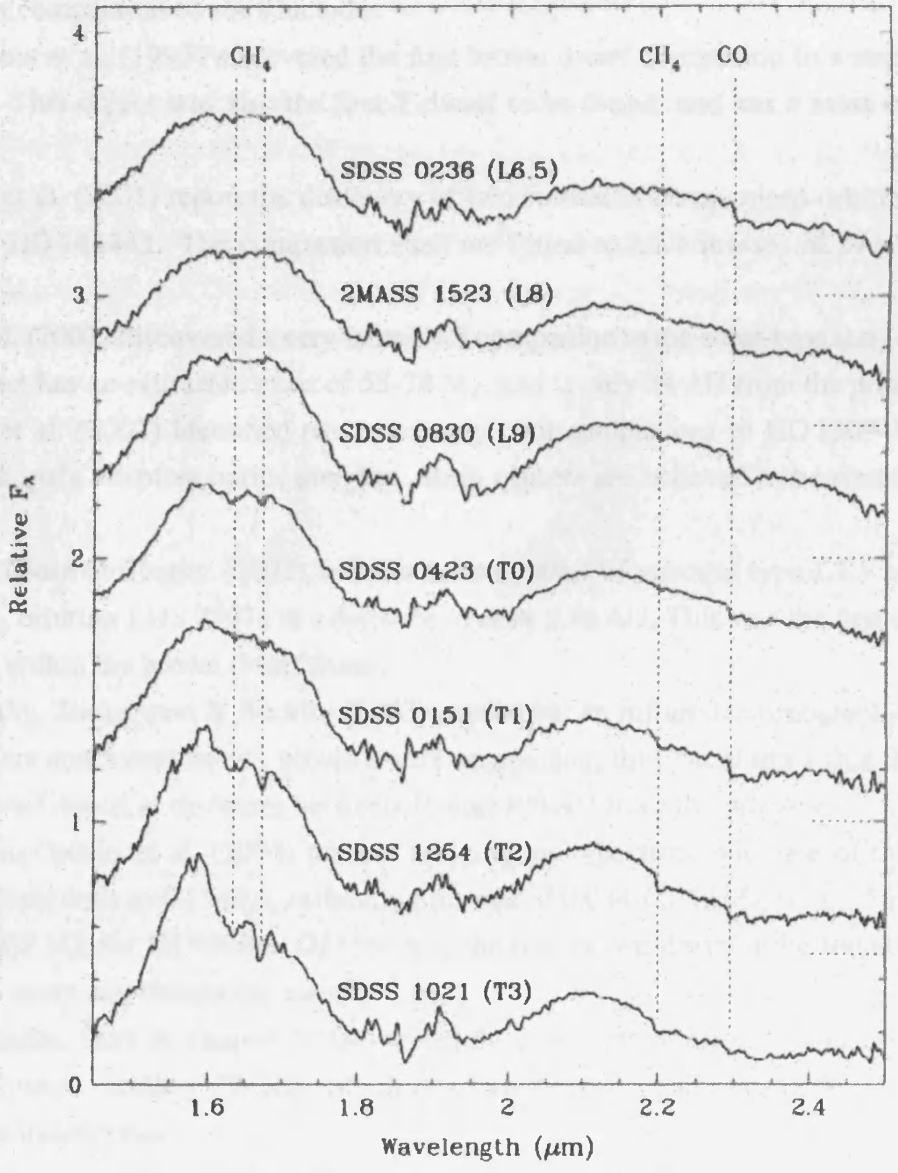

FIGURE 2.4. The L/T dwarf boundary, showing the onset of methane absorption, from Geballe et al. 2002.

the surveys carried out to date, it seems that this desert is only apparent for close binaries, and does not exist for binaries with wider separations (Gizis et al. (2001), Neuhäuser & Guenther (2004)). However, it should be noted that there are a few exceptional systems that lie within the brown dwarf desert such as HD 114762, which has a semi-major axis of only 0.3 AU (Latham et al. 1988). Some highlights during the last few years on brown dwarfs as companions to stars include:

• Nakajima et al. (1995) discovered the first brown dwarf companion to a star, namely Gl 229B. This object was also the first T dwarf to be found, and has a mass of around 43 M_J.

• Marcy et al. (2001) report the discovery of two substellar companions orbiting the G-type star HD 168443. The companion stars are found to have masses of $M \sin i = 7.7$ and 17.2 M_J.

• Lui et al. (2002) discovered a very faint L4.5 companion to the solar-type star HR 7672. This object has an estimated mass of 55-78 M_J, and is only 14 AU from the primary.

• Potter et al. (2002) identified two extremely cool companions to HD 130948 (G2V) from Hokupa'a adaptive optics imaging. Both objects are believed to be contracting L dwarfs.

• Freed, Close & Siegler (2002) found a brown dwarf of spectral type L7.5 and mass 0.068 $M_\odot$ orbiting LHS 2397a at a distance of only 2.96 AU. This was the first object to be found within the brown dwarf desert.

• McCarthy, Zuckerman & Becklin (2003) carried out an infrared coronographic survey of 280 stars and found only 1 brown dwarf companion, thus concluding that there is a brown dwarf desert at distances between 75 and 300 AU from the primary.

• Zapatero-Osorio et al. (2004) present imaging and spectroscopic data of the brown dwarf companions to GJ 569A, estimating masses of 0.034-0.070 $M_\odot$ for GJ 569Bb and 0.055-0.087 $M_\odot$ for GJ 569Ba. GJ 569Bb is the first brown dwarf to be found without having to make any theoretical assumptions.

• Mennickent, Diaz & Tappert (2004) report the discovery of an L0 secondary around the cataclysmic variable VW Hyi, which is unusual because the system has a relatively high mass transfer rate.

• Farihi & Christopher (2004) identified an unresolved, possible L dwarf companion to the white dwarf GD1400, and which is only the second white dwarf/brown dwarf binary known.

• Dobbie et al. (2005) report on an unsuccessful search for low mass stars around DA white dwarfs, however there is some evidence that these white dwarfs may have as yet unresolved substellar companions.

As a result of improved observational instruments, detectors and techniques, it is now possible to directly detect faint, multiple brown dwarf systems, and resolve them in order to determine the properties of the individual members. Some examples of work carried out on substellar binary systems includes:

• Gizis et al. (2003) analysed 82 nearby M and L dwarfs and found that 13 were double M/L dwarf binaries. This sample includes one system with an early T dwarf secondary.

• McCaughrean et al. (2004) re-examined ϵIndiB (Scholz et al. 2003), the closest known brown dwarf, and determined that it is actually a T dwarf binary, with ϵIndiBa having a spectral type T1 and ϵIndiBb having a spectral type T6. The masses are estimated at 44 and 28 M_J respectively.

• Cruz et al. (2004) present the spectrum of an unresolved L/T binary system, and discuss the importance of this system in understanding the L/T dwarf transition.

• Bouy et al. (2004*a*) report the possible discovery of the first accreting substellar multiple system from imaging and spectroscopic observations of the ultra-cool dwarf DENIS-P J185950.9-370632.

• Bouy et al. (2004*b*) determine the orbit and dynamical mass of 2MASSW J0746425 +2000321, a binary L dwarf. The orbital period is found to be 3850.9 days, and the primary and secondary masses are estimated at 0.085 and 0.066 $M_\odot$ respectively.

From this long, but far from complete, summary of the current status of research on brown dwarf binaries, it can be seen that much progress has been made not only with brown dwarf binaries, but also with extra-solar planets (over 180 systems have now been identified). These studies are helping to constrain star formation theories through the determination of the binary/multiple system fractions, and are also helping to improve theoretical models since the mass of a brown dwarf in a binary system can be determined without the use of such models, and therefore can provide an independent test of their accuracy.

2.4.3 The Pleiades

As stated above, stellar clusters provide an ideal hunting ground for brown dwarfs, with the Pleiades cluster (also known as M45), located in the constellation of Taurus (RA = $03^h\ 40^m$, DEC = +24°), being no exception. The low mass and substellar population of the Pleiades is perhaps one of the most well studied and well understood of all open clusters, since its young age and relatively close proximity mean that potential cluster brown dwarfs are easy to find, and are still fairly bright.

Stauffer, Schultz & Kirkpatrick (1998) estimate that the cluster lies at a distance of around 130 pc, which disagrees slightly with the distance of 118 pc determined by Hipparcos. However, the Hipparcos distance has been shown to be somewhat inaccurate due to the systematic errors associated with the measurement of parallaxes on small angular scales (Pinsonneault et al. 1998). Stauffer et al. (1998) also estimate that the cluster has an age of 125 $\pm$ 8 Myrs, which they determined from the lithium abundance in a sample of low mass Pleiades members and the theoretical models of Baraffe et al. (1998). The same age was found when the analysis was recalculated using the Burrows et al. (1997) models, whereas an age of 130 Myrs was found when using the models of D'Antona & Mazzitelli (1997). Other calculations of the age of the cluster determined from theoretical stellar evolution models give a range of ages about this value, depending upon how convective core overshoot has been treated within the model (Stothers & Chin 1992).

The first genuine brown dwarf discovered in the Pleiades was Teide 1 (Rebolo et al. 1995), originally identified from a photometric survey of the cluster in the R and I wavebands. The spectrum of Teide 1 showed no evidence of lithium depletion and was dominated by TiO and VO molecular bands, which theory suggested were the typical properties of brown dwarfs. It also had a proper motion and radial velocity consistent with that of the Pleiades, which confirmed it as a definite member of the cluster. The mass of Teide 1 has been estimated at 55 ± 15 M_J (Rebolo et al. 1996).

However, for several years before the discovery of Teide 1 the cluster had been the focus of a variety of survey work by many different groups. The first CCD survey of the Pleiades was carried out by Jameson & Skillen (1989), and although the survey identified numerous candidates from R and I photometry, none turned out to be brown dwarfs. Other early work in the Pleiades includes:

- Hambly, Hawkins & Jameson (1991) carried out a deep proper motion survey of the Pleiades using COSMOS measurements of the red POSS and UKSTU Schmidt plates. This survey unearthed 441 low mass stars and a few brown dwarf candidates (assuming the age of the cluster to be 70 Myrs, as was believed at the time).
- Simons & Becklin (1992) conducted a 200 arcmin^2 survey in the I and K wavebands, identifying 22 potential low mass candidates located near the main-sequence/brown dwarf boundary.
- Steele et al. (1995) present low-resolution infrared spectra for a number of low-mass stars and brown dwarf candidates identified by Hambly et al. (1991).

After the discovery of Teide 1 in 1995, the search for brown dwarfs in the Pleiades in-

tensified, although as a result of previous work and several theoretical developments, the surveys carried out now moved away from the far optical wavebands and instead focused further into the infrared. The first I, Z survey was carried out by Cossburn et al. (1997), resulting in the discovery of the brown dwarf PIZ 1. This object was found to have an effective temperature of around 2800 K, and a mass of around 0.048 $M_{\odot}$. Since 1995, many more substellar candidates have been unearthed in the Pleiades by the numerous multi-waveband surveys carried out, and much more work has been done in order to understand the substellar population of the cluster, including:

- Zapatero-Osorio et al. (1999*b*) conducted an IZ survey of $\sim 1\,\mathrm{deg}^2$ of the Pleiades, finding 47 potential candidates.
- Bouvier et al. (1998) carried out an R and I band survey which identified 26 very low mass (VLM) and brown dwarf candidates.
- Pinfield et al. (2000) completed a large $\sim 6.25\,\mathrm{deg}^2$ IZ survey of the cluster, from which 169 new very low mass and substellar members were found.
- Dobbie et al. (2002*b*) carried out a $1.1\,\mathrm{deg}^2$ survey in the I and Z wavebands, and identified 23 potential low mass cluster members, of which 15 were new.
- Moraux, Bouvier & Stauffer (2001) present the results of a proper motion analysis of 25 VLM candidates, confirming 18 as likely cluster members and estimating the IMF of the Pleiades to have $\alpha \sim 0.51 \pm 0.15$ for $0.3\,M_{\odot} > M > 0.04\,M_{\odot}$.
- Martín et al. (2000) assess the membership status of 45 VLM and brown dwarf candidates from near-infrared photometry and optical spectroscopy, finding only 8 apparent non-members and a slope of $\alpha = 0.53$ for the cluster IMF.
- Pinfield et al. (2003) identify non-members from the BPL list of VLM and brown dwarf candidates (Pinfield et al. 2000) using JHK photometry and optical spectroscopy, and estimate a brown dwarf binary fraction of 50% for the cluster.
- Moraux et al. (2003*b*) present the results of a $6.4\,\mathrm{deg}^2$ IZ survey of the Pleiades in which 29 new brown dwarf candidates are identified.
- Briggs & Pye (2001) have carried out X-ray observations of the Pleiades, and have detected X-ray emission in several very low mass members and brown dwarf candidates, including Roque9 and Roque14 (Briggs & Pye 2004).

Despite this vast amount of work, there is still much to be learned about the substellar population of the Pleiades. In particular, the most recent studies have focused upon trying to determine the form of the Pleiades IMF (see for example Bouvier et al. (1998), Martín et al. (2000), Jameson et al. (2002)) in order to accurately describe the brown dwarf population and provide information on the formation of open stellar clusters. However, to date, there has been no complete survey of the entire cluster, and so the exact number

of brown dwarfs within the Pleaides is undetermined. In addition, many of the brown dwarf candidates identified so far have been found on the basis of photometry alone, which is insufficient because not all of the contaminating field stars can be identified from the photometry.

2.4.4 The Hyades

The Hyades (RA = $04^h\ 27^m$, DEC = +15° 52′) is the closest open cluster to the Sun, lying at a distance of only 46.3 pc (Perryman et al. 1998). This results in a significantly large cluster depth to distance ratio, and a large cluster motion. Estimates of the age of the cluster range from 500 Myrs to 900 Myrs, making it significantly older than other clusters which have been studied in relation to finding brown dwarfs, such as the Pleiades. The best current estimate for the age of the Hyades is 625 Myrs, which is based on the best theoretical isochrone fit to the cluster Hertzsprung-Russell diagram, as measured by Hipparcos (Perryman et al. 1998). The combination of these two factors make it quite difficult to search for low mass and substellar objects in the Hyades, due to the large area of sky covered by the cluster, and the fact that any brown dwarfs in the cluster have had a long period of time to cool and fade.

Over the years, many studies of the higher mass members of the Hyades cluster have been carried out, but it was not until the work of Leggett & Hawkins (1988) and Leggett & Hawkins (1989) that the fainter members of the cluster also began to be detectable by astronomers. This work led to the calculation of the IMF for very low mass stars in the cluster (Hubbard, Burrows & Lunine 1990), and it was concluded that the IMF of the Hyades did not increase with decreasing mass. Other early work carried out on the low mass population of the Hyades includes:

- Bryja et al. (1992) identified 12 brown dwarf candidates from a proper motion survey, although these candidates were later shown to be very low mass M dwarfs rather than brown dwarfs (Bryja, Humphreys & Jones 1994).
- Macintosh et al. (1992) conducted an infrared survey of 49 90″ × 90″ fields, finding only three potential VLM objects.

Upon completion of the POSS II survey in the Hyades region the first comprehensive list of all Hyades members, including the very low mass members, was compiled by Reid (1993). Bryja (1993) also used POSS II data to complete a proper motion survey of the central region of the Hyades. Since then there have been several more detailed studies of the cluster, including:

- Leggett, Harris & Dahn (1994) used VI photometry, colour-magnitude diagrams and

proper motion data to identify 49 potential very low mass stars and 13 potential brown dwarfs, and thus estimated that at very low masses the mass function is flat.
• Gizis, Reid & Monet (1999) obtained 2MASS and POSS II photometry in order to search for potential very low mass and brown dwarf candidates, although follow-up spectroscopic work revealed that none of the candidates found were genuine cluster members.
• Ali et al. (2000) carried out a mid-infrared survey of the Hyades using ISOCAM, finding four potential very low mass companions. These objects were then followed-up using near-infrared photometry.
• Dobbie et al. (2002*a*) surveyed 10.5 square degrees of the Hyades cluster in the I and Z wavebands, and identified 20 low mass and substellar candidates. Follow-up observations have shown that only one of these candidates is a genuine low mass stellar member.
• Siegler et al. (2003) conducted a binary survey of 30 nearby dwarf stars and discovered three new binary systems. Of these, two of the companions are probable very low mass Hyades members.

Despite this intensive study no confirmed brown dwarf members have been discovered in the Hyades to date. The exact reasons for this are still uncertain, although the most popular theory is that during its lifetime the cluster has undergone several gravitational interactions with other bodies in the Galaxy, resulting in the ejection of many of the lowest mass members. However, since there has yet been no complete analysis of the entire cluster in order to accurately determine its low mass and brown dwarf population, then this hypothesis remains untested.

2.4.5 Taurus

As was described in Section 3.1, studying the IMF of a cluster can significantly improve our understanding of star formation processes. However, in order to determine an accurate value for the form of the IMF, brown dwarfs of very low mass need to be observed. Unfortunately, this is difficult to do in typical open clusters of medium age since objects of sufficiently low mass are too faint to detect. In order to overcome this problem it is useful to search for extremely low mass substellar objects in a young population of stars, such as in a star forming region (SFR) or within a molecular cloud, where such objects are still relatively bright.

In the last few years, a number of surveys of the Taurus Dark Clouds (TDC), or the Taurus star forming regions (located around RA = $4^h\,30^m$, DEC = 24°) have been carried out. This region lies in the Taurus-Auriga molecular cloud complex at a distance of about 140 pc (Martín et al. 2001*b*), and has an estimated age of only 4 Myrs (Palla &

Stahler 2000). These factors combine to make this an ideal area in which to search for very young low mass brown dwarfs. However, the search for brown dwarfs in the Taurus Dark Clouds is complicated by the variable levels of reddening.

The first low mass candidates identified in the Taurus Dark Clouds were found by Strom & Strom (1994), who conducted a deep X-ray survey of the L1495E cloud, covering an area of 50′ in diameter. In this work 8 VLM candidates were found, most with spectral types later than M3, representing a previously unknown fraction of the cloud's population. Other early surveys of the region include:

- Itoh, Tamura & Gatley (1996) carried out a JHK survey of 1 square degree of the Heiles cloud 2 in the Taurus star forming region, identifying 50 young stellar object candidates. Itoh, Tamura & Nakajima (1999) then obtained high resolution images for 23 of these objects, identifying 5 potential brown dwarf companions.
- Briceño et al. (1998) surveyed just over half a square degree of the Taurus Dark Clouds in the VRI wavebands, finding 9 very low mass pre-main-sequence objects, of which 5 were believed to be probable substellar members.
- Luhman & Rieke (1998) followed-up the work of Strom & Strom (1994), using infrared spectra and photometry to identify 17 new VLM candidates in the L1495E region.
- Luhman (2000) conducted an IZ survey of 0.7 square degrees of the Taurus Dark Clouds (the same fields as surveyed by Briceño et al. (1998)) and used infrared spectroscopy to analyse the 53 previously identified members of the region.

Although numerous VLM candidates were found from these searches, unfortunately none were successful in identifying any substellar members, given that the hydrogen mass burning limit has been estimated to fall at a spectral type of M6.5 (Martín, Basri & Zapatero-Osorio 1999). However, more recently there has been much new work undertaken in order to find brown dwarfs in Taurus, including:

- Martín et al. (2001*b*) carried out a 2.29 square degree survey of the star forming region in the R, I and Z wavebands, and used 2MASS data and optical spectroscopy to identify 4 brown dwarfs.
- Briceño et al. (2002) conducted a large survey of 8 square degrees of the Taurus Dark Clouds at I and Z, finding numerous VLM candidates, of which 9 were confirmed as new substellar members from 2MASS data and follow-up spectroscopy.
- White & Basri (2003) present the optical spectra of 10 potential low mass/substellar members of the Taurus Dark Clouds, confirming 5 as brown dwarfs.
- Luhman et al. (2003) continued the work of Briceño et al. (2002), using optical imaging, 2MASS data and spectroscopy to identify 5 new VLM members and 1 brown dwarf.

Although significant progress has been made in recent years, the discovery and anal-

ysis of brown dwarfs in the Taurus star forming region is still relatively new when compared to other clusters such as the Pleiades, and as such there still remains a lot of uncharted territory. Therefore any new brown dwarf discoveries in the region would have a lot of impact in the effort to determine the IMF of Taurus, which is an important quantitiy to determine so that it can be seen whether or not there is any difference between it and the IMFs of other star formation regions and young clusters.

2.4.6 Other Clusters

As well as the work that has been carried out in the Pleiades, Hyades and Taurus Dark Clouds, as outlined above, there have also been a large number of surveys carried out in other clusters, such as σ Orionis, Praesepe, Trapezium, Chamaeleon I and IC 2391.

σ Orionis

The σ Orionis star cluster is located within the Orion 1b association in the Orion complex. The cluster has an age of between 1 and 7 Myrs (Zapatero-Osorio et al. (2002*b*) and references therein), and a distance of around 350 pc (Bejar, Martín & Zapatero-Osorio 2001). Due to the young age of the cluster any brown dwarfs will be intrinsically brighter and therefore easier to detect.

Early studies of the cluster by ROSAT (Walter et al. (1994), Wolk (1996)) uncovered a significant low mass stellar population, which in turn indicated that there could also be a fairly large population of substellar members. Béjar, Zapatero-Osorio & Rebolo (1999) conducted a near-infrared R, I and Z survey of 870 square arcminutes, identifying 49 very low mass and brown dwarf candidates. Follow up optical spectroscopy for several of these candidates revealed objects with spectral types between M6 and L1.5 (Zapatero-Osorio et al. 1999*a*). Further work, probing with greater sensitivity in the same region resulted in the discovery of yet more substellar objects, with spectral types down to L5 (Zapatero-Osorio et al. 2000).

Since then the cluster has been the focus of many more observations. Numerous large scale surveys have been conducted, including: an analysis of 2MASS data to investigate disk dissipation in low mass and substellar objects (Oliveira et al. 2001); K and L band imaging of a sample of cluster members in order to search for circumstellar disks (Oliveira, Jeffries & van Loon 2003); spectroscopy and 2MASS photometry in order to determine the key properties of a selection of very low mass cluster members (Barrados

y Navascués et al. 2003); a ROSAT search for X-ray emission from brown dwarf candidates (Mokler & Stelzer 2002); J and K band spectra of ~ 100 candidate substellar members (Slesnick, Hillenbrand & Carpenter 2004). In addition, the properties of several individual cluster members have been studied, including: the variable $H\alpha$ emission of S Ori 55 (Zapatero-Osorio et al. 2002*a*); the strong $H\alpha$ emission from S Ori 71 (Barrados y Navascués et al. 2002); the photometric variability of S Ori 45 (Zapatero-Osorio et al. 2003).

Praesepe

Praesepe is a relatively old and distant open cluster. It has an age of ~ 700 Myrs and lies at a distance of ~ 175 pc from Earth (Hauck 1981). Due to its age, any brown dwarfs in Praesepe will have had a lot of time during which to cool and fade, and thus their detection will be more difficult.

Identification and measurement of the brighter members of Praesepe began in the late 1920's (Klein-Wassnik 1927), but the accurate measurement of the fainter members didn't begin until almost 60 years later (Jones & Cudworth 1983). The proper motions determined by Jones & Stauffer (1991) extended the list of known members further still, however, the first brown dwarf wasn't discovered until 1998, when Magazzù et al. (1998) identified the spectrum of a very late type object, designated RPr 1, and estimated a mass of between 0.063 and 0.084 $M_{\odot}$.

A large scale, deep proper motion and photometric survey carried out by Hambly et al. (1995) identified over 500 objects with properties consistent with the cluster. 90 of these objects were followed up using infrared photometry, and 81 were found to be likely cluster members (Hodgkin & Jameson 2000). Pinfield et al. (1997) conducted a 1 square degree R, I and Z survey of the central region of Praesepe, and identified 19 potential brown dwarfs . Follow up infrared photometry was obtained for 17 of these objects, with 9 found to be probable cluster members (Hodgkin & Jameson 2000).

Trapezium

The Trapezium cluster forms a part of the rich Orion Nebula cluster, lying within 5 arcmin^2 of the centre. It is an active star forming region, and has an estimated average age of ~ 6 Myrs (Luhman et al. 2000). One of the unique features of this cluster is the fact that it lies on the edge of the molecular cloud, and therefore the vast majority of contaminating background stars are obscured. This, combined with the proximity of the

cluster (distance ~ 450 pc), makes it an ideal location in which to search for young brown dwarfs.

Previous surveys of the Trapezium have been carried out by McCaughrean & Stauffer (1994) and Hillenbrand (1997), resulting in the identification of numerous potential very low mass objects. In Luhman et al. (2000) all these objects were re-observed using the HST, and many new potential stellar and substellar members were found. From this data ~ 50 likely brown dwarfs were identified, and the IMF was shown to have a form similar to that of other young clusters. After completing a new multi-epoch and multi-wavelength near-infrared study of the cluster, Muench et al. (2002) reach a similar conclusion on the form of the IMF, with the IMF having a Salpeter-like slope down to about $0.6\,M_{\odot}$, where it then flattens out and remains flat into the substellar regime. In addition, Lucas & Roach (2000) carried out a JHK photometric survey of the cluster, finding 165 brown dwarf candidates. This was followed up by obtaining broad-band H and K spectra for 21 objects, resulting in the identification of 20 substellar members, of which 15 are planetary mass candidates (Lucas et al. 2001).

Chamaeleon I

Chamaeleon I is one of the three dark clouds located in the nearby, 160 pc (Wichmann et al. 1998), Chamaeleon complex, as identified by Gregorio-Hetem, Sanzovo & Lepine (1989). It is the largest of the three clouds, and also the oldest, with an estimated age of about 3 Myrs (López Martí et al. 2004).

The first brown dwarf in this cluster was found by Neuhäuser & Comerón (1998) via the detection of X-ray emission. Further work in the region increased the number of known very low mass and brown dwarf members to 18 (Comerón, Rieke & Neuhäuser 1999), and seven more objects with spectral types up to M8 were found by Comerón, Neuhäuser & Kaas (2000). The results of a R, I and $H\alpha$ survey carried out by López Martí et al. (2004) indicates a large population of brown dwarfs in the Chamaeleon I cloud, and suggests that there may be as many brown dwarfs as low mass stars. Joergens et al. (2003) measured the photometric variability of a sample of young very low mass stars and brown dwarfs in the cluster. They suggest that this variability is due to the rotation period of magnetically driven surface features, and thus that the accretion disk of a brown dwarf dissipates between a few Myrs and 36 Myrs. In addition, one of the first widely separated brown dwarf/brown dwarf binaries was discovered in this region (Luhman 2004).

IC 2391

IC 2391 is a young open cluster which has only fairly recently become popular as a region in which to search for brown dwarfs. It has an estimated age of 35 Myrs (Mermilliod 1981), and a distance modulus of (m - M) = 5.82 (Robichon et al. 1999).

The first work carried out in this region regarding brown dwarfs was the analysis of spectra of a number of very low mass cluster members (Barrados y Navascués, Stauffer & Patten 1999). This work was followed by a large optical survey which identified numerous potential low mass and brown dwarf cluster members (Barrados y Navascués et al. 2001). Follow up optical spectroscopy was obtained for 44 candidate very low mass members of the cluster (Barrados y Navascués, Stauffer & Jayawardhana 2004), of which 33 appear to be likely cluster members, including the first brown dwarf member of IC 2391 (namely CTIO-160).

Chapter 3

Theory of Brown Dwarfs

This chapter outlines the theoretical considerations relating to brown dwarf formation and evolution. Firstly, basic star formation processes are explained, and current theories on brown dwarf formation mechanisms are discussed. This is followed by a description of the life cycle of a brown dwarf, from initial collapse, through deuterium burning and gravitational contraction, to the final stages of degeneracy. The main spectral properties of brown dwarf atmospheres are described in the third section of this chapter, along with the importance of the lithium test. Finally, the basic theory behind brown dwarf models is outlined, including the equations of stellar structure and the equation of state, and the key features of current evolutionary and atmospheric models are summarised.

3.1 The Formation of Brown Dwarfs

All stars begin their lives in dense interstellar clouds of gas and dust, either in giant molecular clouds (GMCs) or Bok globules. Star formation is indicated in GMCs because of their physical association with very young O and B main-sequence stars, whilst infrared surveys show that most Bok globules have young stars in their centres. Although the formation of stellar mass objects is well understood, and can be simulated fairly accurately, the exact processes involved in the formation of lower mass substellar objects are not yet fully understood.

3.1.1 The Jeans Mass

The conditions required to initiate star formation were first studied by J. Jeans in 1902 (Jeans 1902). If a gas cloud is assumed to obey the perfect gas law, and rotation and

magnetic fields are neglected, then gravity will overcome the gas forces trying to expand the cloud if the cloud has a mass greater than the Jeans mass, defined by:

$$M_{Jeans} = \left(\frac{5kT}{G\mu m_H}\right)^{3/2} \left(\frac{3}{4\pi\rho}\right)^{1/2}, \tag{3.1}$$

where T is the temperature of the cloud, ρ is the density of the cloud, k is Boltzmann's constant, G is the gravitational constant, m_H is the mass of hydrogen and μ is the mean atomic weight of the material in the cloud relative to hydrogen.

If the cloud remains optically thin, and it is able to radiate away some of its gravitational potential energy during the collapse, then the cloud may fragment. The fragments produced will have a higher density than the original cloud and may exceed a smaller Jeans mass, resulting in collapse. Further fragmentation may occur, and so from a single cloud a cluster containing stars of a variety of different masses will be produced.

However, the process of fragmentation and collapse cannot continue indefinitely, and there are several processes that have been ignored in the simplistic model outlined above which can affect the value of the Jeans mass, such as:

- the point at which the collapse becomes adiabatic, and radiation ceases to escape from the cloud.
- whether or not the original cloud has any large scale turbulence.
- the conservation of angular momentum, which means that the angular velocity must increase with decreasing radius, and, therefore, that the centrifugal forces must also increase.
- whether or not a massive star forms first in the cloud centre, evolves and becomes a supernova and blows the cloud apart.
- the cooling rates of dust and molecules, and thus the abundances of heavy elements.
- the onset of degeneracy.
- the presence of magnetic fields, and the effects of ionization and magnetic flux freezing.

Information collected from Prialnik (2000) and Carroll & Ostlie (1996).

It has been calculated that the minmum Jeans mass is about $0.007\,M_\odot$ (Low & Lynden-Bell (1976), Rees (1976)), which indirectly predicts the existence of brown dwarfs since the limiting main-sequence mass below which hydrogen burning cannot take place is $0.07\,M_\odot$ for population I stars and $0.09\,M_\odot$ for population II stars (Kumar 1963). As a result of improved theoretical models and more advanced computer simulations, the minimum hydrogen burning mass is now in the estimated to be around

0.075 $M_{\odot}$(Baraffe et al. 2002*b*), with the exact value depending upon metallicity and the way in which atmospheric dust is treated in the model (Chabrier et al. 2000). Burrows et al. (1997) define the mass used to distinguish between a brown dwarf and a planet to be 0.013 $M_{\odot}$, the point below which deuterium burning cannot take place. However, it should be noted that both the formation method and the interior structure also need to be taken into account when classifying planetary mass objects.

3.1.2 Formation Mechanisms

Although the general formation scenario of brown dwarfs, as outlined above, is fairly well understood, the exact details are still unclear. For many years it was beleived that brown dwarfs formed directly from the collapse of small, low-mass fragments in the nascent gas cloud, though such regions have not yet been observed. The formation mechanism currently favoured is that the brown dwarf embryos are ejected from the gas cloud before they can accrete enough matter to become stellar objects. It is believed that this ejection is due to the interaction of the brown dwarf embryo with other more massive stellar embryos that are forming together in a small unstable multiple star system. This idea was first proposed by Reipurth & Clarke (2001), who suggest that embryos in a small multiple system compete with their siblings to accrete infalling matter, and that the one which grows the slowest is the one most likely to be ejected.

Bate, Bonnell & Bromm (2002) present a hydrodynamical simulation of the collapse and fragmentation of a turbulent molecular cloud, and show that brown dwarfs form in localised regions of dense gas where the Jeans mass is lower than average. In the simulation, around three-quarters of the brown dwarfs fragment from gravitationally-unstable circumstellar disks, with the remainder formed in collapsing filaments of molecular gas. In both cases the brown dwarfs form in unstable mulitple systems, from which they are quickly ejected, thus supporting the formation mechanism proposed by Reipurth & Clarke (2001).

3.1.3 The Initial Mass Function

The exact formation mechanisms of brown dwarfs depends strongly upon any assumptions made about the distribution of mass during the formation period. In general, when an interstellar cloud fragments, the probability of the formation of massive stars is much smaller than that of low mass stars, which in turn implies that the number of stars that

form per mass interval per unit volume is highly mass dependent. The mathematical representation of this dependence is known as the initial mass function (IMF).

The number of stars, N, formed in a given time within a given volume, with masses between M and $M + dM$, is only dependent on M:

$$dN = \Phi(M)dM. \tag{3.2}$$

Salpeter (1955) found that for main-sequence stars in the mass range $0.4\,M_\odot < M < 10\,M_\odot$, the number of stars per unit logarithmic mass interval was described by an inverse power law:

$$\frac{dN}{d\log_{10}(M)} = 0.03M^{-1.35} \tag{3.3}$$

or

$$\Phi(M) = 0.013M^{-2.35}. \tag{3.4}$$

Therefore, the number of low mass stars in the population is greater than the number of high mass stars. Information collected from Carroll & Ostlie (1996).

The form of the IMF is different both for very high mass stars and for low mass and substellar objects, deviating considerably from the inverse power law which describes the function for main-sequence stars. It is thought that the function again changes significantly at the brown dwarf/planet transition. Unfortunately, deriving an accurate form for the IMF in these mass regimes is problematic due to the difficulties involved in observing faint, low mass objects.

In addition to the variations with mass, the IMF also changes slightly within different environments. For example, recent estimates of the low mass and substellar IMF in the Pleiades open star cluster have revealed a slowly rising mass function, with a power law index of between 0.4 and 0.8 (Bouvier et al. (1998), Martín et al. (2000), Jameson et al. (2002)). In star forming regions, such as Taurus, Trapezuim and ρ Ophuichi, the shape of the IMF is similar to that of the Pleiades, with $\alpha \sim 0.3$ (Luhman et al. 2000), although the peak in the mass function tends to be sharper and more pronounced (Briceño et al. 2002)). Finally, Reid (1999*a*) constrained the slope of the field substellar IMF to lie between 0 and 1. Therefore whilst these IMFs do differ slightly, they are all consistent with an IMF in the substellar regime which is flat or slowly rising.

3.2 The Evolution of Brown Dwarfs

Throughout their lifetime, brown dwarfs grow fainter and cooler. During their evolution both nuclear and degenerate physics are important, with each defining a different stage in the brown dwarf life cycle.

3.2.1 The Deuterium Burning Phase

After the preliminary formation phase the brown dwarf evolves with a constant effective temperature, whilst its radius, and hence its luminosity, decreases under the influence of gravity. This first stage of evolution typically lasts around one million years, until the brown dwarf reaches the point where it has contracted enough so that its interior temperature is hot enough to burn deuterium:

$$^2H + {}^1H = {}^3He. \tag{3.5}$$

The energy released in this process balances the inward attraction of gravity and so the brown dwarf is temporarily stable. However, since the relative abundance of deuterium is low this phase lasts only for a relatively short period of time, typically up to 10^7 years. In the most massive brown dwarfs the temperature may get hot enough to burn hydrogen, but this is both rare and short-lived. Due to the fact that the phases of nuclear burning do not last for long, brown dwarfs are never able to reach a stable temperature and luminosity, and this is one of the most significant properties that distinguishes brown dwarfs from main-sequence stars. However, it can be difficult to identify a very low mass star from a brown dwarf because very low mass stars cool very much like brown dwarfs during the 10^9 years it may take them to reach the main-sequence.

3.2.2 The Degenerate Phase

When the source of deuterium fuel has been exhausted the temporary state of hydrostatic equilibrium breaks down, and gravity dominates once again. This second phase of contraction continues until the onset of electron degeneracy, which limits the radius of the brown dwarf. At this point the Fermi energy of the electrons is greater than their thermal energy, and the electron degeneracy pressure balances gravity, therefore the object becomes stable in radius once more. The brown dwarf will then slowly cool and fade with time, until the Universe reaches the final stages of its evolution. Adams & Laughlin

(1997) suggest that brown dwarfs have a significant role to play in the dying Universe, by continuing the process of star formation through brown dwarf/brown dwarf collisions after the supply of interstellar gas and dust has been depleted. Eventually though, even this will cease as the brown dwarfs are lost due to ejection and accretion onto black holes.

3.3 Brown Dwarf Atmospheres

Having a clear understanding of brown dwarf atmospheres is important for several reasons. Firstly, we need to know what they look like so that we can adopt the most appropriate observing techniques, and so that we are able to recognise them when we find them. Secondly, we want to be able to relate what we observe to the actual physical properties of brown dwarfs. Finally, we need accurate atmospheric information in order to provide the evolutionary models with realistic boundary conditions.

3.3.1 Spectral Features

Brown dwarf atmospheres are almost perfect gases, but their very cool temperatures mean that the chemistry describing them is extremely complex. In an atmosphere around 3000 K the majority of atoms are locked up in molecules: H in H_2, C in CO and O in H_2O, TiO, VO, etc. The spectrum of such a star is dominated by absorption due to TiO and VO in the optical and H_2O in the infrared. In cooler atmospheres the strength of the water vapour absorption bands increases.

When the temperature falls below about 2500 K the molecules condense into grains, particularly corundum (Al_2O_3), enstatite ($MgSiO_3$), vanadium oxide (VO) and iron, and the strength of the TiO and VO absorption bands decreases. These are replaced by the molecular bands of the metal hydrides, with the most prominent being CaH, FeH and CrH, and strong atomic lines due to Cs, Rb, Na and K. The point at which this condensation process begins also signifies the transition of spectral type from M to L (see Section 2.2).

In the coolest atmospheres, below about 1200 K, there are strong methane absorption bands. It is believed that eventually all brown dwarfs cool to this level. Brown dwarfs with methane present in their atmosphere fall into a later spectral class (see Section 2.2), and are known as T dwarfs.

3.3.2 The Lithium Test

The description given above of a brown dwarf atmosphere indicates that a young brown dwarf looks very similar to an older field M dwarf, and therefore a method of distinguishing between the two is required. Unfortunately, neither the luminosity or the temperature of the object is a definitive indicator, since the properties of a young, massive brown dwarf overlap those of an M dwarf. In order to overcome this ambiguity, the *lithium test* was proposed (Pozio (1991), Rebolo, Martín & Magazzù (1992)), which is a spectroscopic test using the resonance line of lithium at 6707 Å.

In contrast to an older field M dwarf, a brown dwarf with a mass less than roughly $60\,M_J$ will never have a core temperature high enough to allow it to burn lithium (the fusion of lithium requires a core temperature of at least 2.5×10^6 K):

$$^6Li + {}^1H = {}^3He + {}^4He, \tag{3.6}$$

$$^7Li + {}^1H = 2(^4He). \tag{3.7}$$

Therefore the presence of the lithium absorption line indicates an undepleted supply of lithium, and hence a brown dwarf. However, it should be noted that the application of this test does require knowledge of the age of the object. This is because lithium is mixed and destroyed on a time-scale of less than 10^8 years in the fully convective interiors of very low mass main sequence stars, and so a star younger than this could still have some lithium present in its atmosphere.

3.4 Theoretical Models

In order to generate a theoretical model of brown dwarf evolution, it is necessary to consider all of the following:

- the standard equations of stellar structure, including hydrostatic and thermal equilibrium, mass continuity and radiative and convective energy transport mechanisms.
- the equation of state, describing the relationship between pressure and density.
- the surface boundary conditions, governed by the atmospheric propeties of the brown dwarf, including the molecular species present, the surface opacities and dust (see Section 3.3).
- the initial conditions during formation, such as the nature of the gravitational collapse

and the role of rotation and magnetic fields. In practice, theoretical models are usually either solely of the formation processes (see Section 3.1) or solely of the evolutionary processes, starting at around one million years after the intial formation.

3.4.1 The Equations of Stellar Structure

The strucure of a star, whether stellar or substellar, is governed by the solutions to the set of differential equations known as the equations of stellar structure (Equations 3.8 to 3.12). These equations consider the main forces at work in the interior of the star, and determine its physical properties.

Hydrostatic Equilibrium

Stars can be described as self-gravitating balls of gas, and as such, their structure and evolution are governed by the opposition of gravity and internal pressure. For non-degenerate matter the pressure results from a combination of gas and radiation pressure, although for low mass stars the contribution from radiation pressure is usually negligable when compared to the contribution from gas pressure. For degenerate matter, the polytropic pressure-density relationship depends upon whether the situation is relativistic or not. When pressure and gravity are in balance, a star is said to be in hydrostatic equilibrium, which is the case for main-sequence stars.

$$\frac{dP}{dr} = -\frac{Gm(r)\rho}{r^2} \tag{3.8}$$

where P is the pressure, r is the radius of the star, $m(r)$ is the mass of the star within a given radius, ρ is the density and G is the gravitational constant.

Mass Conservation

Since a star is a physical system, it is subject to the basic conservation laws that apply to all physical systems, and thus mass must be conserved at all times.

$$\frac{dm}{dr} = 4\pi r^2 \rho \tag{3.9}$$

where m, r and ρ are the mass, radius and density of the star respectively, and π has its usual value.

Energy Generation

Stars lose energy via radiation, but in order to be in thermal equilibrium, there must be some form of energy generation to balance these losses and to keep the luminosity

and effective temperature constant. Thus for a region where energy is being generated per unit mass at a rate ϵ, then $dL = \epsilon dm$. The rate of energy generation will depend on the internal properties of the star, including the density, temperature and chemical composition.

$$\frac{dL}{dr} = 4\pi r^2 \rho \epsilon \tag{3.10}$$

where L, r and ρ are the luminosity, radius and density of the star respectively, ϵ is the rate of energy generation and π has its usual value.

Energy Transport

Energy can be transported through a star by radiation or convection (energy transfer via conduction can be ignored in the majority of stellar systems), and like mass, energy must also be conserved at all times.

• Radiative Temperature Gradient

Since a photon carries momentum of $p = h\nu/c$, the radiation field in a star also carries momentum. By considering the intensity of this radiation, and the balance between emission and absorption, the radiative transfer equation can be solved in order to determine the temperature stratification required for radiative energy transport.

$$\frac{dT}{dr} = -\frac{3}{4ac}\frac{\kappa\rho}{T^3}\frac{F}{4\pi r^2} \tag{3.11}$$

where dT/dr is the temperature gradient, κ is the Rosseland mean opacity, ρ is the density, F is the flux, a is the radiation constant ($= 4\sigma/c$; σ is the Stefan-Boltzmann constant), c is the speed of light, T is the temperature of the star, r is the radius of the star and π has its usual value.

• Adiabatic Temperature Gradient

By considering the conditions required for a bubble of gas to rise and expand adiabatically in the stellar interior, it can be deduced that a convective instability will set in if the adiabatic temperature gradient becomes small or the radiative temperature gradient becomes large.

$$\frac{dT}{dr} = -\frac{\mu m_H}{k}\frac{Gm(r)}{r^2}\frac{\gamma - 1}{\gamma} \tag{3.12}$$

where μ is the mean atomic weight relative to hydrogen, m_H is the mass of the hydrogen atom, G is the gravitational constant, $m(r)$ is the mass of the star within a given radius,

γ is the ratio of specific heats, k is the Boltzmann constant and r is the radius of the star. Information collected from Prialnik (2000) and Carroll & Ostlie (1996).

3.4.2 The Equation of State

There can be some difficulty in deciding which equation of state to use when modelling brown dwarfs since there are a number of different physical processes at work at different times and places within the brown dwarf interior. For example, in the early evolutionary stages during deuterium burning the interior has radiative properties, whilst later the core becomes almost, but not totally, degenerate. In addition, the outer layers of the brown dwarf atmosphere can be descibed by the perfect gas law.

However, if the brown dwarf is considered to be a fully convective object (since a star loses its radiative core if it has a mass is less than about $0.3\,M_{\odot}$) the problems surrounding the equation of state can be simplified. In this case, the interior physics are governed by an $n = 3/2$ polytrope, with the polytropic index, n, defined by:

$$1 + \frac{1}{n} = \gamma = \frac{C_p}{C_v}. \tag{3.13}$$

Therefore the polytropic equation of state is of the form:

$$P \propto \rho^{1+\frac{1}{n}} \propto \rho^{5/3}. \tag{3.14}$$

3.4.3 Current Models

The biggest problem in calculating accurate theoretical brown dwarf models comes from the presence of the cool atmosphere, with its complex molecules and grains (see Section 3.3). In addition, black-body models may not be used as brown dwarfs show no evidence of having a true continuum, and grey atmospheric models are of little use since the molecular absorption coefficients are highly wavelength dependent. The first evolutionary models of brown dwarfs were presented by Nelson, Rappaport & Joss (1986), who describe how the luminosity, radius, core temperature and effective temperature change with time for brown dwarfs with masses between 0.01 and $0.1\,M_{\odot}$. Since then, several different models have been developed by a number of theoretical astrophysics groups. The most recent calculations include detailed atmospheric boundary conditions, the presence of dust and fewer uncertainties in the treatment of surface opacity.

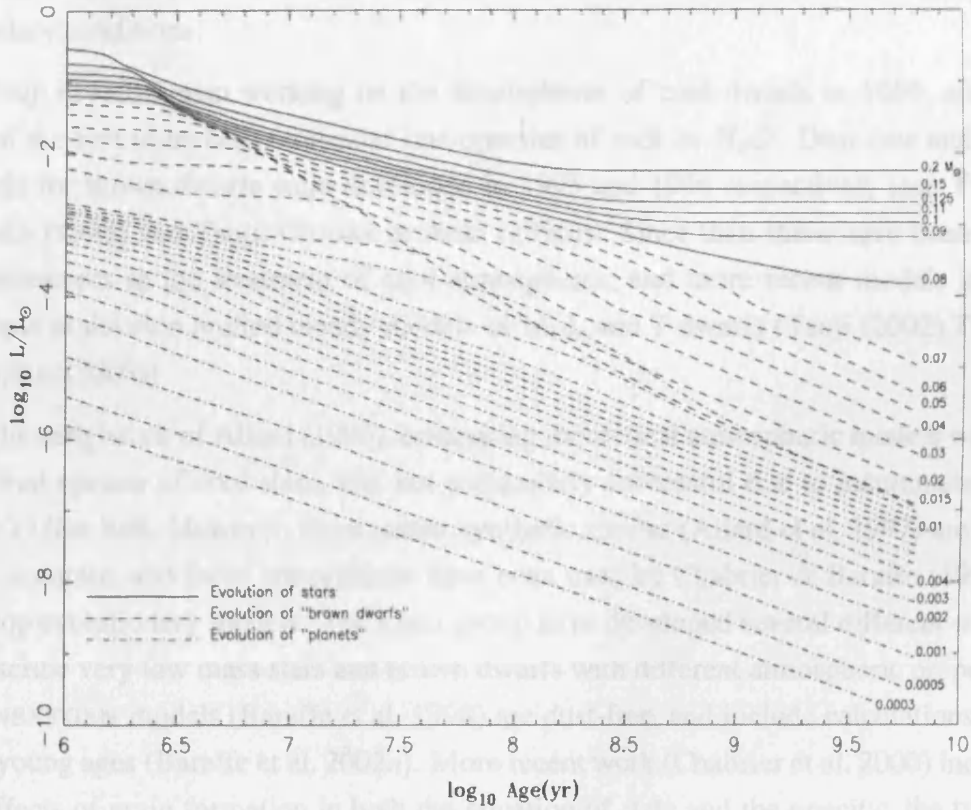

FIGURE 3.1. The evolution of luminosity with time according to the models of Burrows et al. 1997.

Burrows et al. (1993) presented their first evolutionary models in 1993, and showed that it is the surface boundary condition that governs the evolution of a brown dwarf. These models were later reworked and improved to include calculations of the atmospheres, spectra, colours and evolution of brown dwarfs and planetary mass objects with tempertures less than 1300 K (Burrows et al. 1997). Key findings from this work include: the domination of the spectrum by H_2O, H_2 and CH_4 for $T_{eff} \leq 1200$ K; the fact the some infrared colours get bluer with age; the existence of a radiative zone in objects with effective temperatures between 200 and 1000 K; and the formation of H_2O clouds at $T_{eff} < 400$ K and NH_3 clouds at $T_{eff} < 200$ K. The evolution of luminosity with time is illustrated in Figure 3.1, which clearly shows how objects of typical brown dwarf mass, or lower, gradually grow fainter.

Electronic versions of these models can now be found on the world wide web, including an automatic calculator which returns the effective temperature of a brown dwarf given its age and estimated mass. More recently, this group have been working on modelling the line profiles of neutral alkali metals (Burrows & Volobuyev 2003) and metal-

bearing condensate clouds (Burgasser et al. 2002*d*) to further improve the atmospheric boundary conditions.

Tsuji (1969) began working on the atmospheres of cool dwarfs in 1969, and was one of the first to include molecular line opacties of such as H_2O. Dust-free and dusty models for brown dwarfs were developed in 1995 and 1996 respectively (see Tsuji & Ohnaka (1995) and Tsuji, Ohnaka & Aoki (1996)). Since then there have been many improvements in the treatment of cool atmospheres, and more recent models include attempts to develop unified cloudy models of M, L and T dwarfs (Tsuji (2002),Tsuji & Nakajima (2003)).

The early work of Allard (1990), comparing theoretical atmospheric models with the observed spectra of cool stars, was not particularly successful due to incomplete H_2O and VO line lists. However, more recent synthetic spectra (Allard et al. 1997) are much more accurate, and these atmospheres have been used by Chabrier & Baraffe (1997) to develop evolutionary models. The Lyon group have developed several different models to describe very low mass stars and brown dwarfs with different atmospheric properties. The NEXTGEN models (Baraffe et al. 1998) are dust-free, and include calculations from very young ages (Baraffe et al. 2002*a*). More recent work (Chabrier et al. 2000) includes the effects of grain formation in both the equation of state and the opacity: the DUSTY models account for the formation of dust, and the resulting atmospheric absorption and scattering, whilst the COND models account for the formation of grains, their subsequent sinking beneath the photosphere, and thus the removal of heavy elements from the atmosphere above the photosphere. These two models correspond approximately to the L and T dwarfs respectively. Figure 3.2 (Chabrier et al. 2000) shows the evolution of luminosity and effective temperature with time for very low mass stars and brown dwarfs, for both the NEXTGEN (solid lines) and DUSTY (dotted lines) models. From this diagram it can be seen that in the brown dwarf mass regime the inclusion of dust within the theoretical models has the effect of slightly lowering the expected effective temperature. Perhaps the most useful feature of these models is that they predict the absolute magnitudes of the objects in the wavebands used by observers. This makes the comparison between theory and observation much more simple, providing that the age and distance of the object is known.

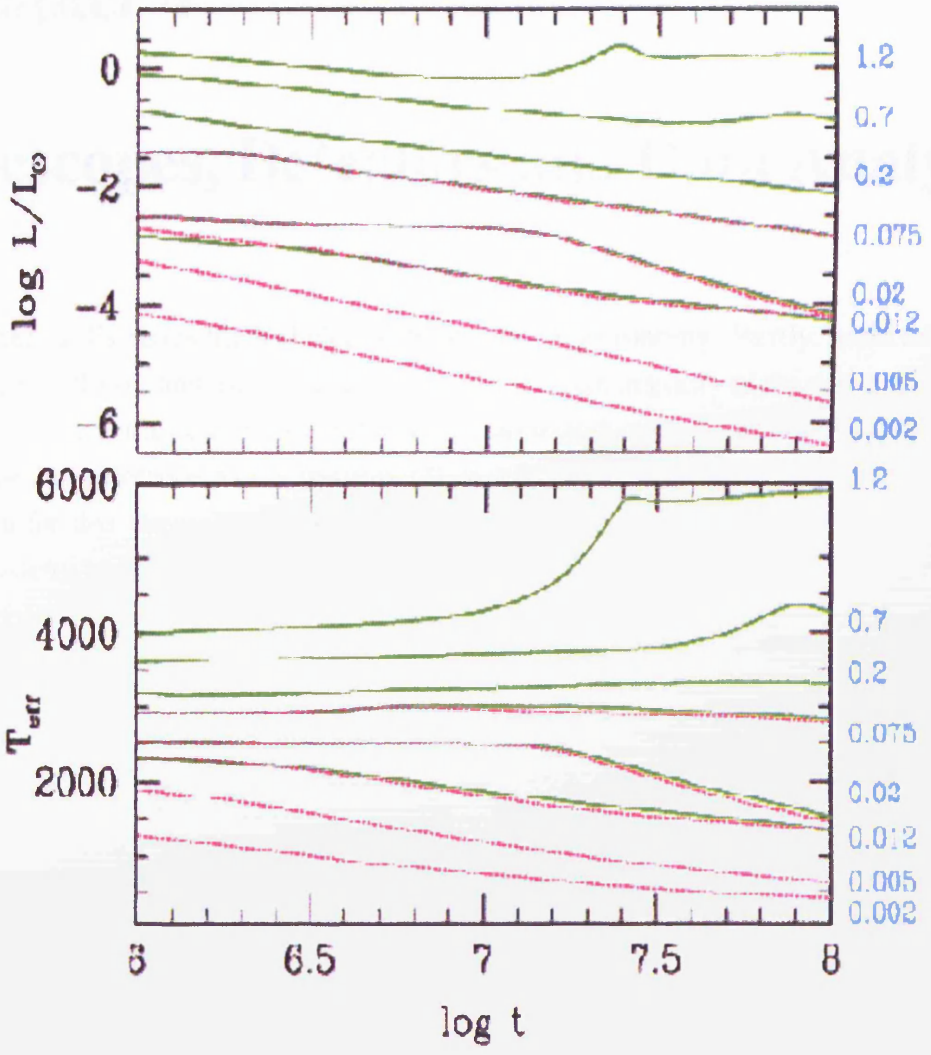

FIGURE 3.2. The evolution of luminosity and effective temperature with time for various masses according to the models of Baraffe et al. 2002. The NEXTGEN models (Baraffe et al. 1998) are shown as solid lines and the DUSTY models (Chabrier et al. 2000) are shown as dashed lines.

Chapter 4

Telescopes, Detectors and Data Analysis

This chapter discusses the technical side of modern astronomy. Firstly, basic telescope optics are outlined, and the telescopes used to obtain the majority of the data presented in this thesis are described. This is followed by an introduction to astronomical detectors, with specific reference to the instruments and detectors used in the process of gathering data for this thesis. The third section moves on to discuss filters, and the different filter systems available in both the far optical and infrared wavebands. Finally, the methods and procedures used to reduce and analyse both imaging and spectroscopic data are explained.

4.1 Telescopes

Telescopes were invented during the early 17th Century, firstly utilising the refraction of light, and then about 10 years later taking advantage of the reflection of light. A refracting telescope collects light through an 'objective' lens, which brings the light into focus and creates an image. This image is usually magnified by an eyepiece and, unless an extra lens system is used, is also inverted. A reflecting telescope collects light via a concave primary mirror, which produces an image between it and the object in view. This image is then reflected by a second mirror to the eyepiece.

In reflecting telescopes, the location of the secondary mirror depends upon the type of optical system being used. In a Newtonian system the secondary mirror is flat, and lies at a 45° angle to the telescope axis, reflecting the image to an eyepiece at the side of the telescope. In a Cassegrian system the secondary mirror is convex, which reflects the image back to the eyepiece through a hole in the primary. A Coudé system has a convex

secondary mirror, like the Cassegrian, and an extra rotatable mirror set at 45° to the polar axis of the telescope.

In order to obtain sharp images from observations, the telescope needs to be mounted on a rigid structure which will allow smooth, regular movement in all directions. The simplest form of mount is an altazimuth system, which allows the telescope to be moved freely in both the vertical and horizontal directions. On an equatorial mount, the telescope is set on an axis parallel to the axis of the Earth. In this set-up, as the telescope is moved from east to west, the correct movement in altitude is naturally accounted for. If a computerised clock drive is fitted, the telescope is able to track a given object for long periods of time. Information collected from Moore (1992).

A large proportion of the data presented in Chapters 5 and 6 of this thesis was obtained using the Isaac Newton Telescope and the United Kingdom Infra-Red Telescope. A small amount of data was obtained with the Keck II telescope. Brief descriptions of these telescopes are given below. Data has also been obtained from several other sources, but these will be described elsewhere when appropriate.

4.1.1 Isaac Newton Telescope

The Isaac Newton Telescope (INT) is a part of the Isaac Newton Group of Telescopes, and is located at the Roque de Los Muchachos Observatory (ORM) on the island of La Palma, in the Canaries (www.ing.iac.es/PR/int_info). It stands at an altitude of 2350 m. The telescope is equatorially mounted, and has a 2.54 m paraboloidal primary mirror, with a corrected focal ratio of $f/3.29$. There is also an $f/15$ cassegrian focus. The telescope is used mostly for wide-field imaging and intermediate to low dispersion spectroscopy.

4.1.2 United Kingdom Infrared Telescope

The United Kingdom Infrared Telescope (UKIRT; www.jach.hawaii.edu/UKIRT) is located close to the summit of Mauna Kea, on the island of Hawaii, at an altitude of 4194 m. It has a 3.80 m primary mirror, with a focal ratio of $f/36.4$. Unusally, UKIRT has a mount of English yoke design, which basically means that the telescope is placed between two separate fork mounts. A secondary mirror is used to form a tip-tilt system, with the principal function of correcting image movements, whilst a tertiary mirror has an infrared reflecting dichroic coating. UKIRT is the largest telescope in the world devoted to infra-red astronomy.

4.1.3 Keck II

The Keck II Telescope is one of the twin Keck telescopes, located on Mauna Kea, Hawaii (www.keckobservatory.org/geninfo/about). Each of the telescopes has a 10 m primary mirror composed of 36 hexagonal segments which work together to form a single piece of glass. The complete mirror is hyperbolic in shape, with a focal ratio of $f/1.75$, and is mounted on an altitude-azimuth system. Both telescopes have an adaptive optics system which uses a small, deformable mirror that changes its shape 670 times per second to cancel out atmospheric distortion.

4.2 Detectors

Historically, the first astronomical measurements were made visually using the human eye as a detector, firstly without, and then with the aid of a telescope. Unfortunately, the human eye is not a very useful tool for astronomical detection as it is unable either to store or to quantify the input it receives. With the invention of photographic plates and emulsions in the early- to mid-1800's, the eye was surpassed as an astronomical detector, and the first quantitive measurements were made. The photographic plate remained the key astronomical detection method for about a century, until it began to be superseded by modern electronic devices in the early 1970's. Firstly, intensifier tubes exploited the photoemissive properties of electromagnetic radiation, then charged coupled devices (CCDs) exploited the photoconductive processes. During the 1980's, CCDs grew rapidly in popularity as astronomical detectors, and are today seen as standard equipment on almost all professional telescopes. When observing in the infrared regime, originally most cameras used a single element detector, which built up an image by scanning the telescope across the sky. However, in 1984 infrared arrays were introduced, and although small to begin with, recent technological developments have seen them increase significantly in size. Information collected from Eccles (1983).

4.2.1 Charged Coupled Devices

A charged coupled device (CCD) is a solid state imaging detector, made from a silicon wafer which has a silicon dioxide (SiO_2) insulating layer grown onto a p-type semiconductor substrate. A large number of 'gates' are then inserted into the insulating layer in an array strucure to a depth of around 0.1 μm. The gates act as electrodes, and are often made from polysilicon, a form of silicon which has metallic properties. When a positive

voltage is passed through the gate, the holes are repelled from the $Si - SiO_2$ junction and a depletion layer forms. As the voltage is increased the depletion layer moves further into the semiconductor substrate. Once the junction has a sufficiently positive charge any free electrons are attracted to it, and an inversion layer is formed. In an uncooled device thermal electrons will quickly flow into the junction, but if the device is cooled (typically with liquid nitrogen to a temperature around 150 K) these electrons are suppressed, and an inversion layer will not form unless free electrons are generated by photon bombardment. In this case, the magnitude of the electron charge formed is proportional to the intensity of the illuminating radiation. Three gates are used for each imaging element, or *pixel*, hence creating a spatially digitised electric analogue of the original optical image. The charge is then transferred from one pixel to the other and finally to an output amplifier. Information collected from Eccles (1983).

CCD detectors are currently so popular because they exhibit many of the features that would be desirable in an ideal device:

- they have the obvious practical benefits of being small in size, light in weight and economic on power consumption.
- they have a high level of quantum efficiency (QE), with between 60% and 90% of incident photons being able to excite free electrons in the semiconductor.
- they have a very low readout noise when cooled, typically less than 10 electrons per pixel.
- they are highly linear detectors, and have a large dynamic range (usually larger than 1000 to 1), making the accurate photometric measurement of stars that differ in brightness readily achievable.
- typical CCD array sizes (2000 by 4000 pixels) give a relatively large field of view, and modern arrays using multiple CCD chips allow large scale surveys to be carried out with ease.
- when coupled with the optical capabilities of modern telesopes, the typical pixel size (approximately 15 μm) of a CCD results in a high spatial resolution, usually better than 0.5″ per pixel.
- the nature of the CCD allows for long integration times to obtain deep images.
- the final output images are digitized, which makes them suitable for processing on computers.

The main disadvantage of the CCD is the relatively large number of flaws present in the image, caused by cosmic rays, hot spots, dead pixels and inefficiencies in the pixel transfer process. However, many of these flaws can be eliminated during the data reduction stages (see Section 4.4).

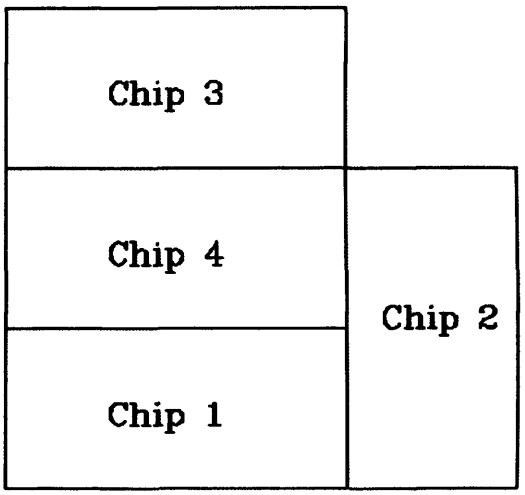

FIGURE 4.1. The spatial layout of the four EEV chips of the WFC.

The Wide Field Camera

In the work carried out in Chapters 5 and 6, the optical CCD used was the Wide Field Camera (WFC; www.ing.iac.es/Astronomy/instruments/wfc) (Ives, Tulloch & Churchill 1996) on the INT. This instrument consists of four thinned EEV 2k × 4k CCDs, arranged as shown in Figure 4.1. Each pixel measures 13.5 μm, which results in a 0.33″ per pixel resolution and a sky coverage of 22.8′ × 11.4′. The total field of view for the four CCDs is 0.29 square degrees.

The quantum efficiency curve of the detector is shown in Figure 4.2. It can be seen that the efficiency of the detector peaks between 4000 and 8000 Å, and therefore that the detector is most sensitive to optical and far optical wavelengths.

4.2.2 Infrared Arrays

An infrared array operates in a similar manner to an optical CCD, however, in order to be sensitive to infrared wavelengths, the detector must be made from a different semiconducting material. Unfortunately there is no infrared counterpart to silicon, which has all of the necessary properties for making an efficient optical detector. Therefore hybrid arrays are used, whereby an infrared sensitive semiconductor (for detecting the arriving photons), such as indium antimonide ($InSb$) or mercury cadmium telluride ($HgCdTe$),

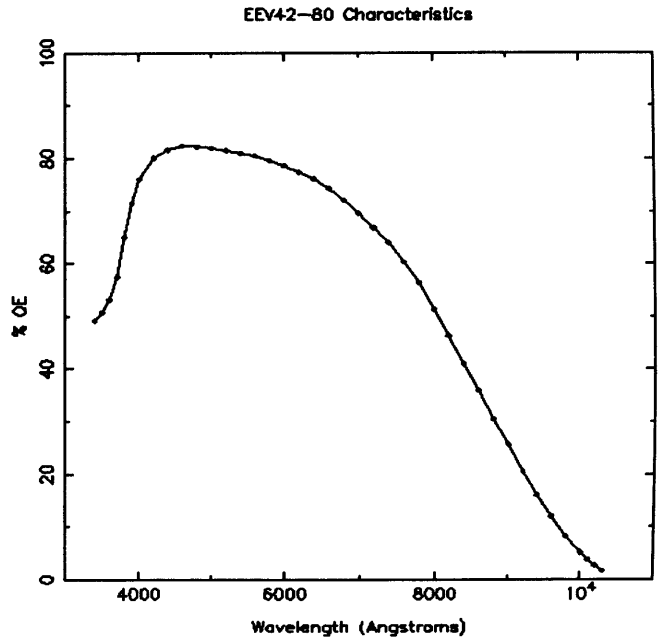

FIGURE 4.2. The quantum efficiency (QE) curve for the WFC. Image from www.ast.cam.ac.uk/~wfcsur/technical/ccd/qe.gif.

is bonded to a silicon based device which is used for the readout. When a photon is incident on the detector material, it is absorbed and an electron is produced; however, for it to be detected it must be produced near to the connection to the readout circuit. This means that the detector layer must be thin, which can be achieved either by growing the detector layer on an inert substrate, or by etching and polishing the material in its bulk form. The local electric field is produced by diodes implanted into the semiconductor, which are insulted from each other to form the pixels, and the electron produced in the detector layer is then passed to the readout circuit through a column of metallic indium. In such an array, each pixel has its own individual storage site and amplifier, with a device known as a multiplexor providing a path between the pixels and the output amplifier, although only one pixel is connected to the output at any time. Information collected from Eccles (1983).

Although infrared arrays can be thought of as analagous to CCDs, there are several important differences:

• an infrared array uses a non-destructive readout mode, in which only the difference in charge between the beginning and end of the exposure is measured for each pixel.

• each pixel in an infrared array is entirely separate from the others, and so it is not possible to combine the charge from adjacent pixels before readout.
• the readout noise of an infrared array is greater than that of a CCD due to the more complicated circuitry and the extra amplifier for each pixel.
• infrared arrays need to be cooled to much lower temperatures (typically around 35 K) in order to operate efficiently and minimise thermal excitation of electrons.
• infrared arrays are not linear detectors, although the relationship between input and output is monotonic and can be calibrated.
• the size of the array is limited by the thermal properties of the two hybrid materials, since a difference in expansion between the two layers could cause the device to split apart.
• infrared arrays have much smaller fields of view.

The main disadvantages of infrared arrays are that the insulating regions between the pixels produce dead space in which incident photons are lost; the dark current is harder to define, since additional electrons can be produced not only by thermal excitation in the semiconductor, but also by warm components in the detector field of view, out-of-band filter leakage and luminescence from circuitry on the detector chip; due to the high level of sky background, especially at far infrared wavelengths, it can be difficult to read out the array fast enough to prevent saturation of the pixels (Beckett 1995).

The UKIRT Fast Track Imager

The infrared image data obtained in Chapter 5 was obtained with the UKIRT Fast Track Imager (UFTI; www.jach.hawaii.edu/UKIRT/instruments/ufti). UFTI is a 1024×1024 HgCdTe Rockwell array, sensitive to infrared radiation over a wavelength range of 1.0 to 2.5 μm. The pixels measure 18.5 μm and the plate scale is 0.091″ per pixel, giving a field of view of 92.9″ with a full array readout.

4.2.3 Spectrographs

As explained in Section 2.2, a star's spectrum is the wavelength distribution of the intensity of the radiation. This dispersion of light can be achieved by passing the light through either a prism, grating or grism.

Prism spectroscopy is governed by Snell's law. The incident light is split because the refractive index of glass is dependent upon wavelength, and therefore the refracted angle out of the prism is also dependent upon the wavelength. This type of spectroscopy is not

often used in astronomy since the finish of the prism surface must be almost perfect, and the relationship between the refractive index of glass and wavelength is complex, making the resultant spectrum highly non-linear and difficult to calibrate. However, prisms are sometimes used in infrared spectroscopy, for example SpeX on the Infrared Telescope Facility (IRTF; http://irtfweb.ifa.hawaii.edu/ spex) is a prism spectrograph covering a wavelength range of 0.8 - 5.4 μmwith a resolution of R $\sim$ 1000 - 2000.

Grating spectroscopy works because of the constructive interference of light. After passing through a narrow slit and a collimator, the light is directed onto a diffraction grating, which will either transmit the light or reflect it. The grating acts like a large number of double slits, causing different wavelengths to have maxima at different angles:

$$d \sin \theta = n\lambda \tag{4.1}$$

where d is the spacing of the lines on the grating, θ is the diffraction angle, n is the order of the spectrum and λ is the wavelength. A spectrum is produced when $n \geq 1$, with higher levels of dispersion at larger values of n. The dispersion is approximately linear with wavelength since $\sin \theta \simeq \theta$ for small angles. However, at high orders the maxima overlap and are no longer useful, and so an echelle grating is used instead. This type of grating is illuminated at a very oblique angle, and when combined with a low dispersion grating perpendicular to the echelle's axis of dispersion, the overlapping orders are moved adjacent to each other.

Spectroscopy using a grism combines the effects of both prisms and gratings. A grism is made by ruling a grating onto one face of a prism, with the net effect being that the dispersions add whilst the deflections cancel so that the central wavelength is undeflected.

The ability of a spectrograph to distinguish two closely spaced wavelengths separated by an amount $\delta\lambda$ is known as the *resolving power*, and is given by the ratio $\lambda/\delta\lambda$. This quantity depends on many factors, including the order of the spectrum, the number of lines on the grating and the slit width. Information collected from Carroll & Ostlie (1996) and Zeilik et al. (1992).

The UKIRT Imaging Spectrometer

The spectra obtained in Chapters 5 and 6 were obtained using the UKIRT Imaging Spectrometer (UIST; www.jach.hawaii.edu/UKIRT/instruments/uist). UIST consists of a 1024 $\times$ 1024 InSb array, which can be used either for imaging or spectroscopy. In

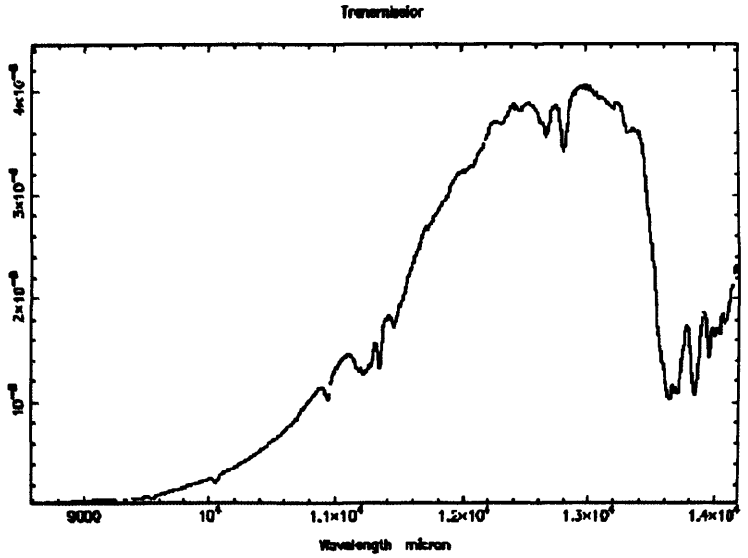

FIGURE 4.3. The relative transmission across the passband of the IJ grism on UIST. The spectrum is of a bright standard star which has been normalised by the division of an appropriate blackbody function. The absolute scale on the y-axis is arbitrary. Image from www.jach.hawaii.edu/UKIRT/instruments/uist/spectroscopy/spectra.

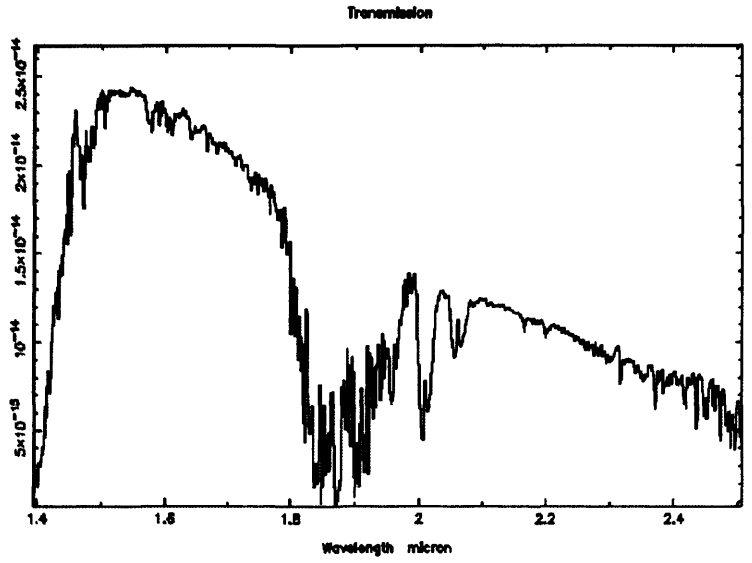

FIGURE 4.4. The relative transmission across the passband of the HK grism on UIST. The spectrum is of a bright standard star which has been normalised by the division of an appropriate blackbody function. The absolute scale on the y-axis is arbitrary. Image from www.jach.hawaii.edu/UKIRT/instruments/uist/spectroscopy/spectra.

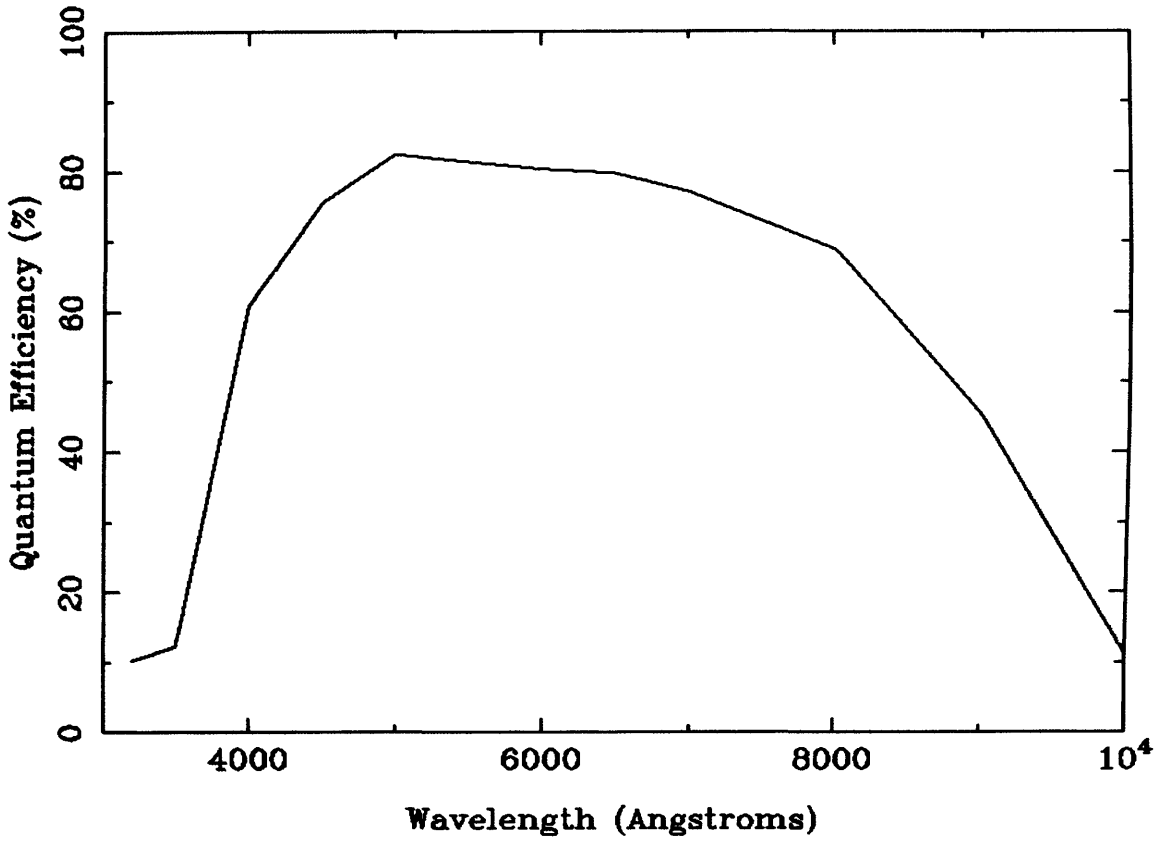

FIGURE 4.5. The quantum efficiency (QE) curve for the ESI. Image created using data from www2.keck.hawaii.edu/inst/esi/ccd.html.

spectroscopic mode the CCD has a 0.12″ plate scale, and is sensitive to wavlengths between 1.05 and 3.84 μm. The detector is equipped with five different spectroscopy slits, offering widths of 1, 2, 4, 5, and 7 pixels. The spectra obtained with UIST which are presented in this thesis used only the IJ or HK grism, and the relative transmission of the grisms are shown in Figure 4.3 and Figure 4.4 respectively.

The Echellette Spectrograph and Imager

In addition to the spectra obtained with UIST in Chapter 5, several more spectra were obtained using the Echellette Spectrograph and Imager (ESI) on the Keck II telescope (www2.keck.hawaii.edu/inst/esi). This detector consists of a 2k×4k MIT-LL CCD with 15 μm pixels and a pixel scale of 0.15″ per pixel. The total wavelength coverage is 0.39 to 1.10 microns, and the corresponding spectral resolution ranges from R=6000 to R=1000. The CCD has a high level of quantum efficiency between $\sim$3900 Å and $\sim$ 8000 Å, although this starts to drop significantly by 9000 Å, as shown in Figure 4.5.

Band	Effective Wavelength	Bandwidth
U	350 nm	100 nm
B	430 nm	100 nm
V	550 nm	100 nm
R	640 nm	150 nm
I	790 nm	150 nm
J	1.25 μm	0.12 μm
H	1.66 μm	0.16 μm
K	2.22 μm	0.22 μm
L	3.45 μm	0.35 μm
M	4.65 μm	0.46 μm
N	10.3 μm	1.00 μm

Table 4.1. Key properties of the Johnson photometric waveband system.

4.3 Filters

As explained in Section 2.1, the incoming radiation from an object can be split into different wavebands in both the optical and infrared regimes. At the telescope, these wavebands are created by using filters which only transmit incident radiation in the desired wavelength range. Modern photometric filter systems are designed to work with CCD detectors and may be catagorised in terms of bandwidth:

- *wide band* systems have bandwidths of at least 300 Å wide.
- *intermediate band* systems have bandwidths between 100 Å and 300 Å.
- *narrow band* systems have bandwidths of no more than a few tens of Å wide.

The key properties of the Johnson system are outlined in Table 4.1 (information collected from Zeilik et al. (1992)). There are also several other filter systems in use, including Kron-Cousins, Sloan and 2MASS . However, because the many detectors used have different properties, and in particular different levels of quantum efficiencies, the effective pass band of a filter varies between detectors. These variations in transmission mean that care should be taken when comparing results with other observations or theory.

4.3.1 Far Optical Filters

Although the key properties of the Johnson photometeric system were outlined above, in actual fact there is no standard set of filters for far optical wavelengths because of the large number of filter combinations available at different telescopes. Usually the Kron-

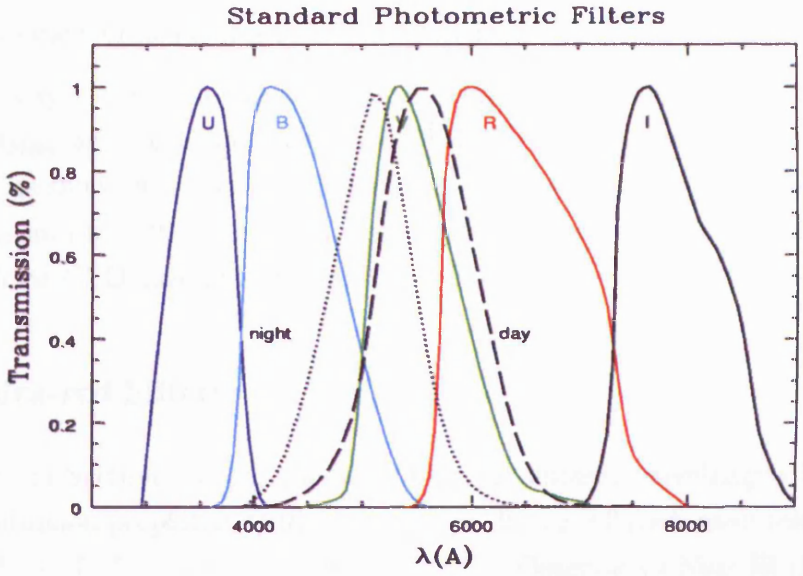

FIGURE 4.6. The standard Kron-Cousins RIZ filter transmission profiles. Image from www.physics.hmc.edu/faculty/esin/a101/lectures.html.

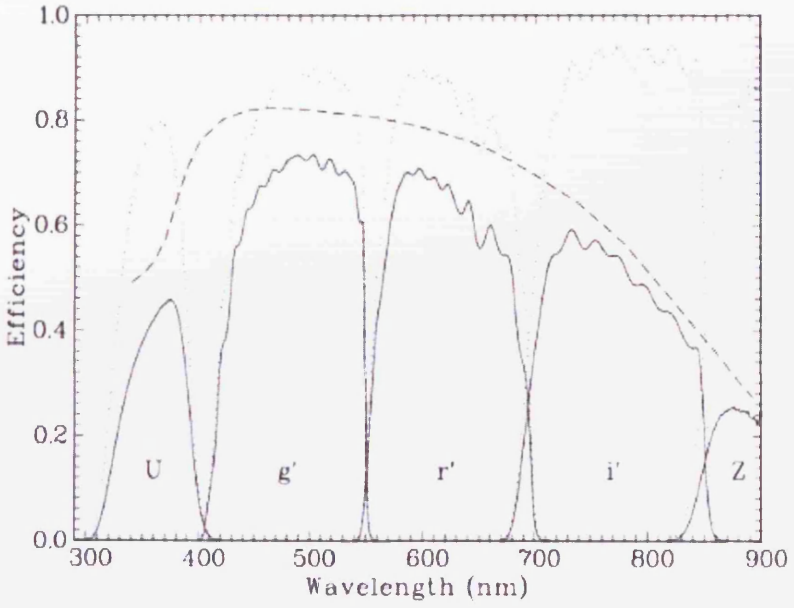

FIGURE 4.7. The RIZ filter transmission profiles for the WFC. The dotted lines are the filter transmission profiles, whilst the solid lines are the overall filter responses. The QE of the CCD is shown as a dashed line. Image from www.ast.cam.ac.uk/∼wfcsur/technical/filters.

Cousins system is adopted as the standard at R and I (see Figure 4.6), with data from other systems transformed to this by using polynomial conversion equations.

The majority of the data obtained throughout the course of this PhD, was taken using the R_{Sloan}, I_{Sloan} and Z_{RGO} filters on the WFC at the INT. The transmission profiles of these filters are shown in Figure 4.7 (dotted lines). Also shown in this plot are the overall transmission profiles of the filters (solid lines), resulting from the convolution of the filter profiles with the CCD quantum efficiency (dashed line).

4.3.2 Infra-red Filters

As explained in Section 2.1, the choice of filters at infrared wavelengths is governed by the transmission properties of the atmosphere. In the infrared, most telescopes use the standard set of *JHK* filters from the Mauna Kea Observatory Near-IR (MKO-NIR) photometric system.

All of the infrared data presented in this thesis was taken using the MKO-NIR *JHK* filters on UFTI at UKIRT. Additional infrared data was obtained in Chapter 7 using the infrared filters of 2MASS (see Section 7.2 for more details). The transmission profiles of the MKO-NIR JHK filters are illustrated in Figures 4.8, 4.9 and 4.10 respectively.

4.4 Data Reduction Procedures

The raw images obtained at the telescope are not suitable for immediate use due to the 'additive' effects of the detector. The images therfore need to be calibrated in order to remove the signature of the detector before they can be analysed. On the other hand, infrared images are dominated by the high level of the sky background. The array is therefore read out frequently to avoid saturation, which produces a stack of images which are subsequently added together, usually by a process internal to the instrument. The co-added infrared image can then be reduced in a manner similar to that used for an optical CCD image, as outlined below.

4.4.1 Bias Level Removal

Bias frames are zero time exposures which provide an estimate of the pedestal or 'bias' level introduced to the output to avoid detecting negative signals from background noise, and an estimate of the second order pattern introduced by the electronics. The bias

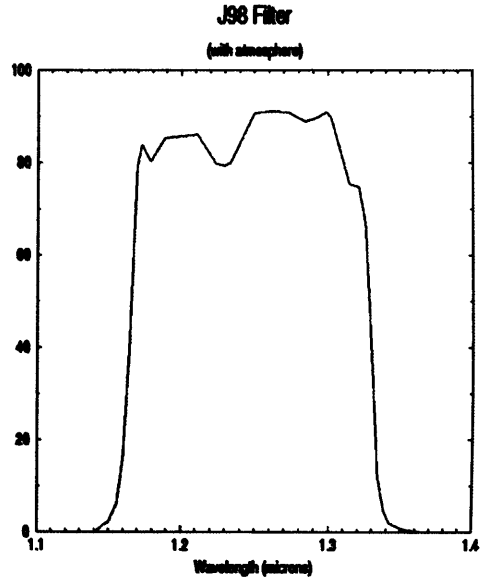

FIGURE 4.8. The MKO J filter transmission profile for UFTI. Image from www.jach.hawaii.edu/UKIRT/instruments/ufti/PARAMETERS.

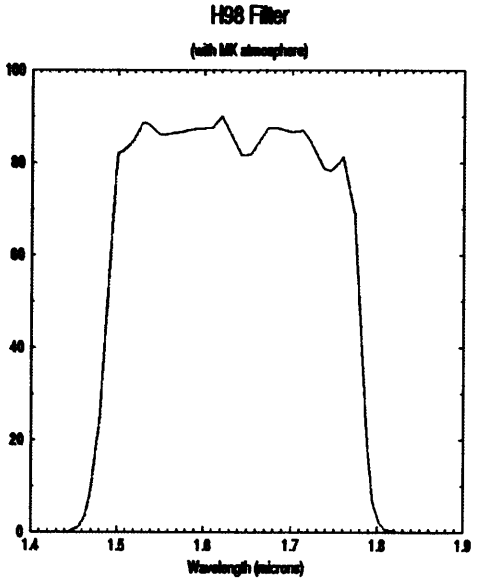

FIGURE 4.9. The MKO H filter transmission profile for UFTI. Image from www.jach.hawaii.edu/UKIRT/instruments/ufti/PARAMETERS.

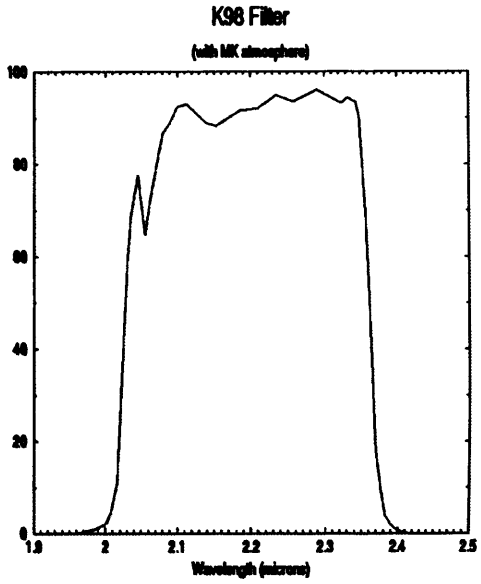

FIGURE 4.10. The MKO K filter transmission profile for UFTI. Image from www.jach.hawaii.edu/UKIRT/instruments/ufti/PARAMETERS.

level is monitored in an area of the image known as the overscan region, and is ususally constant. This level needs to be subtracted from all images, and can be done relatively easily using a routine such as CCDPROC in IRAF. IRAF (Image Reduction and Analysis Facility), is a software system designed for the reduction and analysis of astronomical data (iraf.noao.edu; star-www.rl.ac.uk/iraf/web/iraf-homepage). If good quality science images are required in order to determine accurate photometry measurements, then the second order bias pattern can also be removed by subtracting from each image a master bias frame. This frame is made by combining the overscan corrected bias frames, which consist only of this pattern. Once all the images have had the bias level removed, the overscan region and any other unwanted strips of the image are trimmed off.

4.4.2 Dark Current Correction

Dark current is the intrinsic level of the detector, due to the presence of thermal electrons. In modern CCDs, the level is usually low enough (typically one electron per hour) to be ignored. However, the dark current becomes important when using infrared arrays, as these detectors are sensitive to electrons with a much lower energy and are therefore more likely to detect the thermal background, particularly during long integrations. Indeed, for

most infrared observations, the dark current dominates, meaning bias level corrections need not be applied. Dark frame exposure times are usually matched to the science frame exposure times, and are taken with the shutter closed. They are then stacked together and subtracted from the observed images using an image manipulation routine, such as IMARITH in IRAF.

4.4.3 Flat Fielding

The purpose of flat fielding is to remove pixel-to-pixel variations and large scale spatial variations. These variations in sensitivity are multiplicative, and so the science images need to be divided by the flat field images to remove the effects. Again, a routine such as IMARITH can be used to perform the division. The variations are also wavelength dependent, and therefore flat fields need to be obtained for each different filter used. Flat fields are created by observing a uniformly bright source such as the interior of the telescope dome, a projector screen illuminated by a tungsten light source, or the twilight sky, which is the best method. Alternatively, using a dither pattern in the observation of the science object, and then median adding the frames will also create an effective flat field. This is the most common method used in the infrared.

4.4.4 Other Effects

Fringing

Fringing is an optical effect caused by the interference of narrow night sky emission lines with thinned CCDs at the red end of the spectrum (R, I and Z). Fringing patterns have both spatial and wavelength dependence, and also vary with atmospheric conditions. The complete removal of all fringing effects is difficult, but the majority can be subtracted out by creating a master fringe from a stack of offset target exposures taken under similar atmospheric conditions. For the majority of the images analysed in this work, fringing effects were not a problem. The only data in which they were visible were the second epoch Pleiades images obtained with the WFC (see Chapter 6), however, since these images were only used for astrometric measurements and not photometry then the fringing was not an issue.

Cosmic Rays

A cosmic ray is a random radiation event incident upon the detector, and is typically only contained in a single, isolated pixel. Cosmic rays can be removed in three ways: by modifying analysis programs to ignore them; by using a 'cosmic ray remover', which searches for individiual pixels with unusally high counts; or by using multiple frames to perfom a pixel-by-pixel comparison, along with some sort of rejection algorithm. A large number of cosmic rays can also be easily removed if a dither pattern is used to create a flat field, which was the method used for all of the infrared data obtained.

Bad Pixels

The majority of CCDs have some pixels and/or partial rows or columns whose response is not linear. In direct imaging, these are not usually a problem, as they are clearly apparent in the final reduced image. However, for spectroscopic reductions it is necessary to interpolate over these bad pixels using a 'bad pixel mask'. This step was carried out by using the predetermined masks available within the standard ORAC_DR recipes.

4.4.5 Spectral Extraction

Since the spectrum of an object will be detected on a CCD in the same way as an image would be, the first step in the reduction procedure is to subtract the bias level and flat field the data. If there are several subsets of data, as is usually the case, these need to be combined to produce a single integrated image with a higher signal-to-noise ratio. This image will generally consist of a pair of spectra, one positive and one negative, due to the nodding of the slit at the telescope and the subsequent sky subtraction. Suitable routines for all of the stages of spectral reduction can be found in IRAF and the STARLINK package FIGARO.

Once the integrated image has been formed the spectrum needs to be located, and then extracted. This is done by defining a window around the peak of the spectrum, and forming a profile which is then used to optimally extract the spectrum. The positive and negative images will each have a different profile, and so this step needs to be carried out on both spectra. The spectra are then co-added, and if necessary de-rippled, to form the final positive optimally extracted spectrum.

When spectra are obtained from ground based telescopes, the data will include emission lines and continuum due to the night sky, which need to be removed. This can be

done by using a backgound window to define the areas that are to be considered as sky, and subtracting the result from the object spectrum.

In order to calibrate the spectrum in terms of wavelength, a comparison arc spectrum is used to create a dispersion curve, which relates the pixel position to the known arc emission lines. The dispersion relation can then be applied to the object spectrum.

The spectrum also needs to be calibrated in terms of flux, which can be achieved by dividing the object spectrum by the spectrum of a standard star with a known temperature, and then multiplying the result by a blackbody of the same temperature. Finally, the spectrum is smoothed and plotted.

Chapter 5

Brown Dwarfs in the Taurus Dark Clouds

This chapter presents the results of the first major project undertaken during the course of this PhD; a large scale survey of the Taurus Dark Clouds. The first section discusses the main properties of the Taurus Dark Clouds, and this is followed by a description of the data aquisition and reduction. The data is analysed using colour-magnitude diagrams, and the results of follow-up spectroscopy and infrared photometry are presented and discussed.

5.1 The Taurus Dark Clouds

Star formation regions (SFRs) are ideal sites in which to search for brown dwarf members because their young age means that these are relatively bright. Hence very low mass objects ($M \leq 10\,M_J$) can be observed with only 2 m class telescopes. Furthermore, the members of an SFR have a common distance and metallicity, and are approximately of the same age, making the transition between theory and observation relatively straightforward. The Taurus Dark Clouds (TDC), which lie at a distance of 140 pc (Martín et al. 2001*b*) and have an estimated age of 4 Myrs (Palla & Stahler 2000), are potentially a very interesting region to study.

5.2 Observational Data and Analysis

The identification of potential brown dwarfs in an area usually begins with a survey of the area in at least two different wavebands. This allows the objects found to be plotted on colour-magnitude diagrams, from which the brown dwarf candidtaes can be identified.

5.2.1 RIZ Observations in Taurus

Far optical R, I and Z band data were obtained in December 2000 with the WFC on the INT. The survey covered an area of 5.65 square degrees, with the majority of the fields concentrated around the TA I, TA II, TA IV and TA VI groups of pre-main-sequence stars idenified by Gómez et al. (1993) (see Figure 5.1). Unfortunately the weather was variable during the observing run, and the conditions were not photometric. Therefore during one period of photometric conditions a series of short calibration fields were observed. Approximately 40% of the data obtained was analysed by Kenyon (2001), who determined that the survey was 90% complete to R = 23.8, I = 22.4 and Z = 21.3, with limiting magnitudes of ~25, ~23 and ~22 at R, I and Z respectively. However, for consistency, these data have been re-analysed in terms of determining the magnitudes for inclusion in this thesis, along with the first analysis of the remaining 60% of the data.

5.2.2 Data Analysis

The observational data were intially reduced in Cambridge using the WFC pipeline processes (www.ast.cam.ac.uk/ wfcsur/technical/pipeline), which applies the standard reduction steps to the CCD images (de-biasing, bad pixel removal, non-liearity correction, flat-fielding and astrometric calibration). The pipeline is fairly robust, although the non-linearity characteristics do change with time, and both I and Z band images suffer from significant sky fringing. However, for the data analysed here non-linearity was not a problem, and the fringing effects were removed during the pipeline process using a master fringe frame. The short calibration fields were then calibrated in terms of magnitude by constructing airmass curves using stars from the Landolt catalogues (Landolt 1992), after the standard star magnitudes had been converted to the WFC photometric system. The offsets in magnitude between the short calibration fields and the deep science fields were then calculated. Finally, the deep science fields were calibrated using the short calibration fields and the calculated offsets.

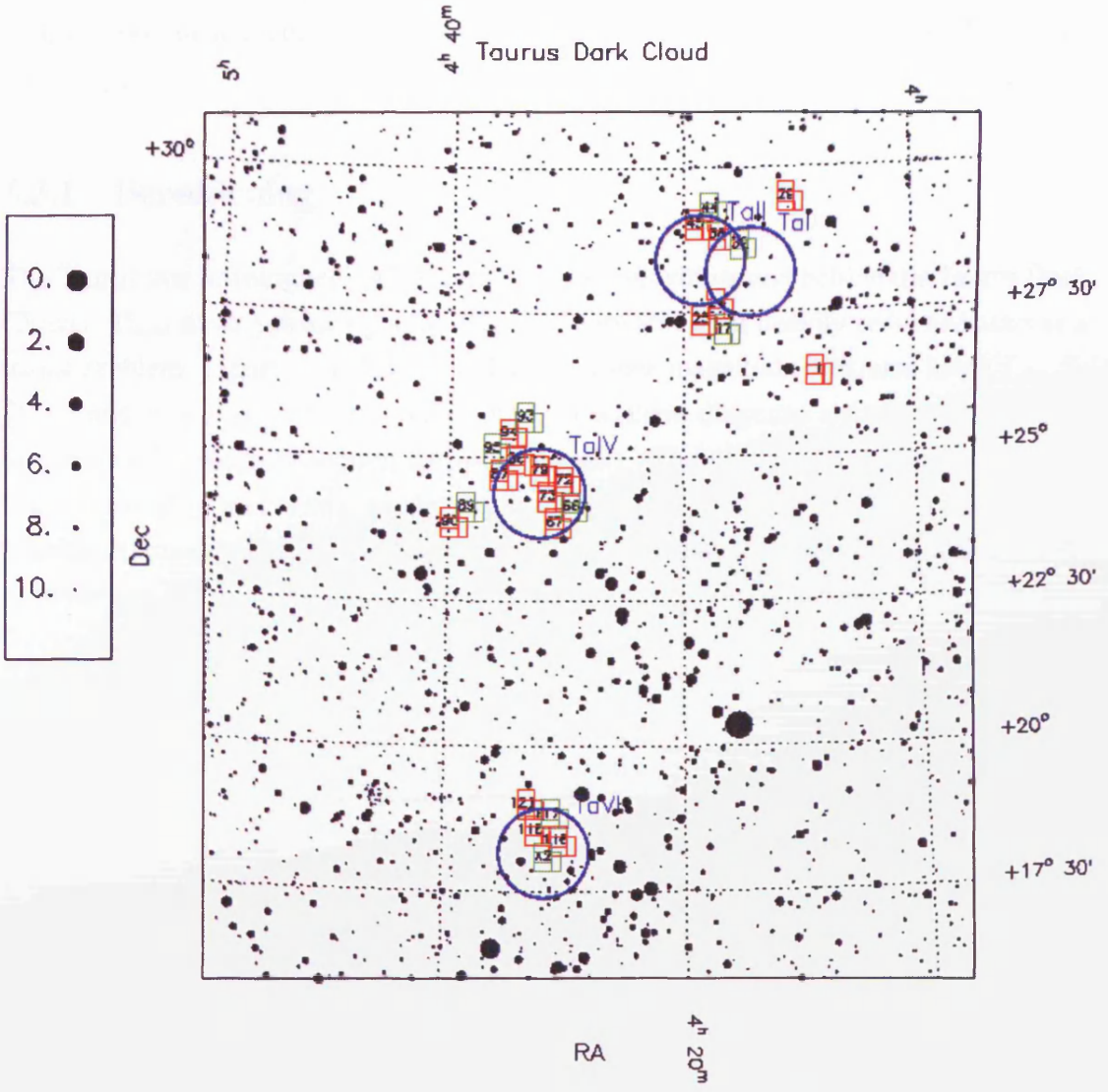

FIGURE 5.1. The fields observed in the Taurus Dark Clouds region with the WFC. Deep science fields are shown in red and short calibration fields are shown in green. The groups of pre-main-sequence stars identified by Gomez et al. (1993) are identified as blue circles.

5.3 Candidate Brown Dwarf Selection

Potential brown dwarf candidates in the Taurus Dark Clouds were identified from three colour-magnitude diagrams. The decision to use three diagrams instead of two was made because it was thought that this third selection step would increase the accuracy of the identification of potential brown dwarfs, given that the reddening levels in Taurus are quite high.

5.3.1 Dereddening

The Taurus star forming region is located in front of, within, and behind the Taurus Dark Clouds. Thus distinguishing young, red brown dwarfs from heavily reddened stars is a major problem. Figures 5.2, 5.3 and 5.4 show colour-magnitude diagrams using $I - Z$, $R - I$ and $R - Z$ respectively. Superimposed on these diagrams are models for young brown dwarfs (see next section for more details). The problem is that the reddening vectors are steep and nearly parallel to the isochrones, so disentangling brown dwarfs is difficult from such diagrams. However, these diagrams can be used to select possible candidates.

5.3.2 Far Optical Colour-Magnitude Diagrams

Potential brown dwarf candidates were initially identified using two colour-magnitude diagrams (CMDs): I vs $I - Z$ and R vs $R - I$ (see Figures 5.2 and 5.3 respectively). In these diagrams the dark mass of points on the left of the figure represents the large number of predominantly background stars. The selection criterion used was to class any objects that were positioned redward of the solid diagonal blue line in both CMDs as candidates, and these are shown as filled blue stars. The 1, 5 and 10 Myr NEXTGEN models of Baraffe et al. (1998) are shown in blue, pink and red respectively, and the 1, 5 and 10 Myr DUSTY models of Chabrier et al. (2000) are shown in turquoise, yellow and green respectively. The previously identified candidates of Luhman (2000) are shown as open pink circles, and candidates identified in σ Orionis by Béjar et al. (1999), transformed to the appropriate distance modulus, are shown as open red squares. The use of two CMDs, rather than just one CMD, to select potential brown dwarfs has been shown to be an effective method of identification (Zapatero-Osorio et al. 1999*b*). Using this method 186 brown dwarf candidates were found, but of course this number also includes a large number of contaminating stars.

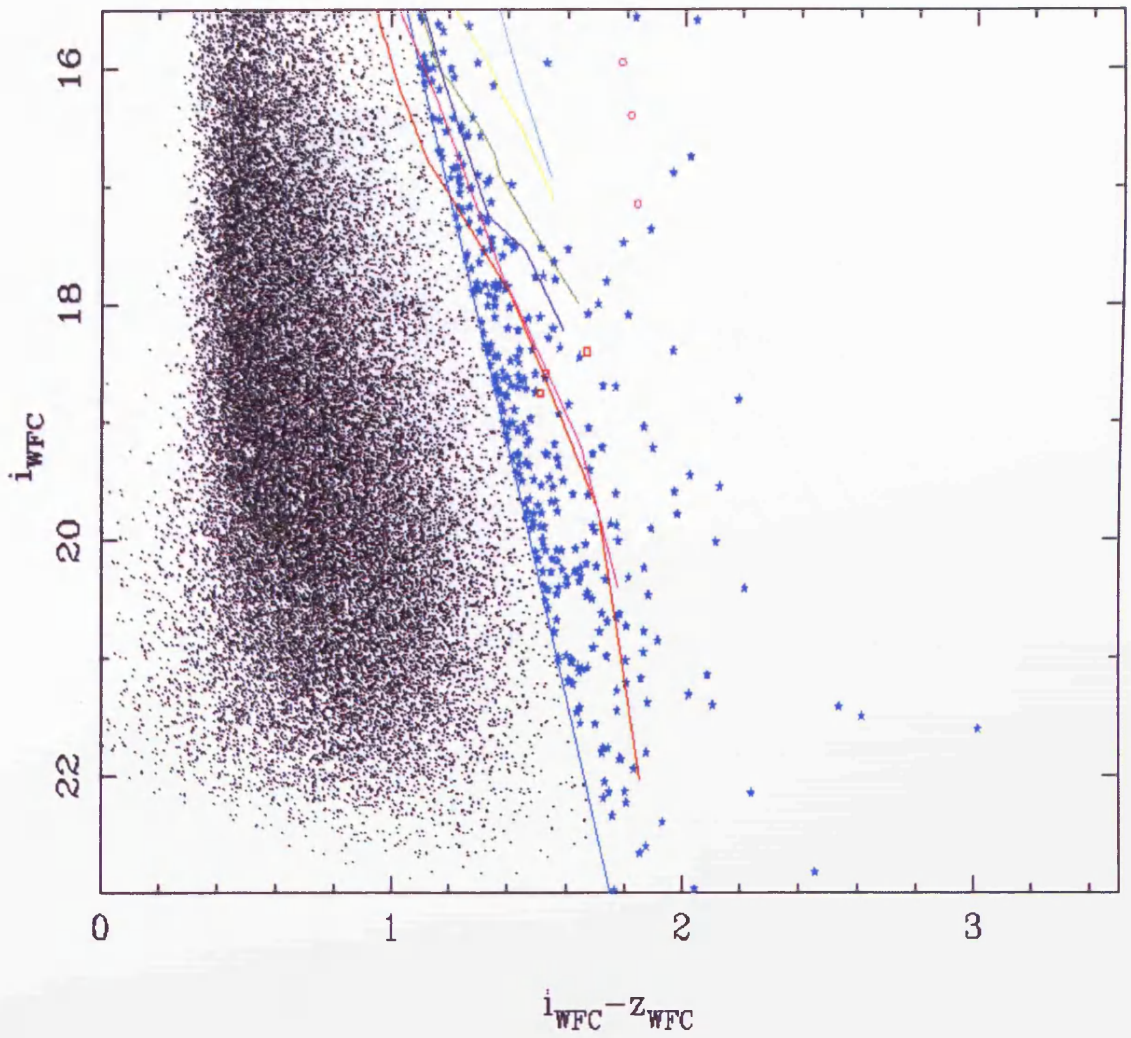

FIGURE 5.2. The I vs $I - Z$ CMD for the 5.65 square degree region of the Taurus Dark Clouds surveyed with the INT. The criterion for selecting candidate substellar members is shown as a solid diagonal blue line, with objects to the right of this line being considered as potential brown dwarfs (shown as blue stars). The 1, 5 and 10 Myr NEXTGEN models of Baraffe et al. (1998) are shown in blue, pink and red respectively, and the 1, 5 and 10 Myr DUSTY models of Chabrier et al. (2000) are shown in turquoise, yellow and green respectively. Previously identified candidates of Luhman 2000 are shown as open pink circles, and candidates identified in σ Orionis by Bejar et al. (1999), transformed to the appropriate distance modulus, are shown as open red squares.

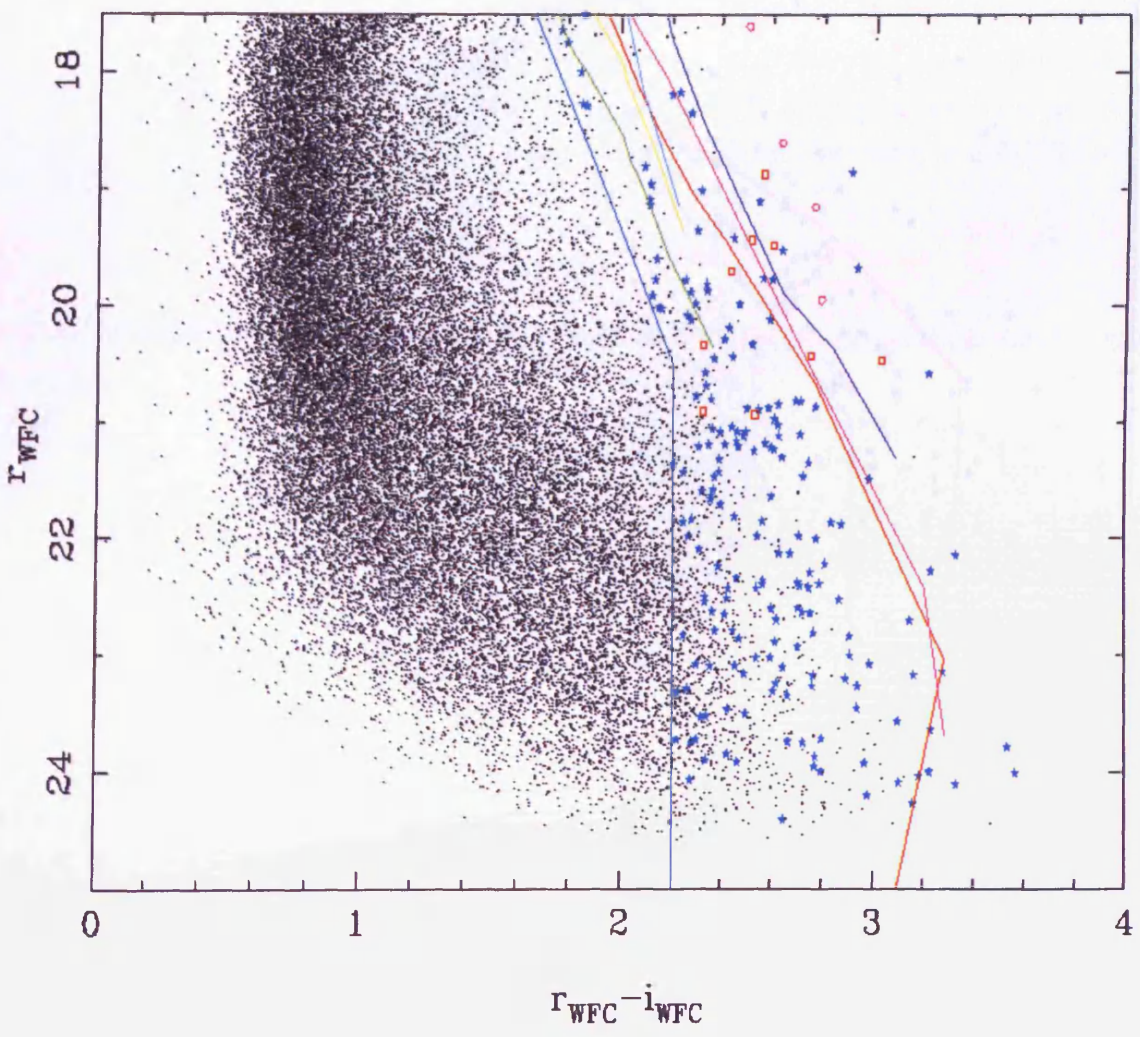

FIGURE 5.3. The R vs $R - I$ CMD for the 5.65 square degree region of the Taurus Dark Clouds surveyed with the INT. The criterion for selecting candidate substellar members is shown as a solid blue line. Objects which satisfy both this and the I vs $I - Z$ criterion are shown as blue stars. The theoretical isochrones and previously identified objects have the same colours and symbols as in Figure 5.2.

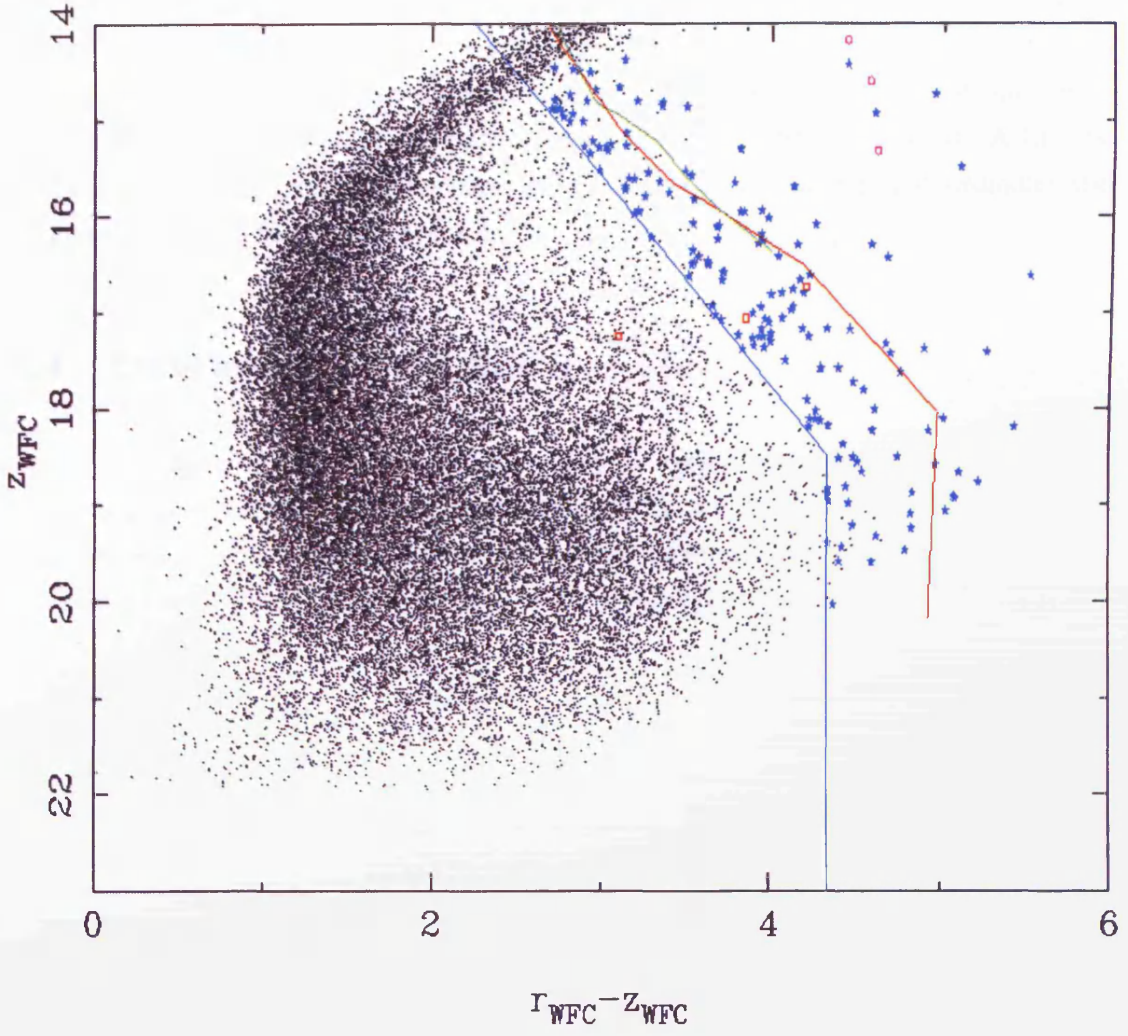

FIGURE 5.4. The Z vs $R - Z$ CMD for the 5.65 square degree region of the Taurus Dark Clouds surveyed with the INT. The 10 Myr NEXTGEN model (Barrafe et al. 1998) is shown in green, and the 10 Myr DUSTY models Chabrier et al. 2000 is shown in red. The criterion for selecting candidate substellar members is shown as a solid blue line. Objects which satisfy all three selection criteria are shown as blue stars. The previously identified objects have the same colours and symbols as in Figure 5.2.

In order to assess the effect of colour on the selection of brown dwarf candidates an R vs $R - Z$ CMD was also plotted (see Figure 5.4). This allowed the colour to be maximised, and therefore stretched the cluster sequence on the plot. It can be seen from Figure 5.4 that the reddest objects are pushed further to the right of the background stars, thus making them more readily identifiable. The 10 Myr NEXTGEN model (Baraffe et al. 1998) is shown in green, and the 10 Myr DUSTY models (Chabrier et al. 2000) is shown in red. A further selection was then performed (shown as a solid blue line), reducing the number of potential Taurus brown dwarfs to 165 (blue stars). A full list of these candidates, in order of decreasing $R - Z$ colour and including coordinates and magnitudes, can be found in Table A.1.

5.4 Follow-up Observations

In order to follow-up the work carried out on the R, I and Z waveband data, both infrared photometry and spectroscopic data was acquired for a selected number of candidates. This follow-up work enabled more data and information to be gathered for the most promising brown dwarf candidates in order to unambiguously determine their status.

5.4.1 ESI Spectra

From the list of brown dwarf candidates drawn up by Kenyon (2001), seven objects at around I = 18-19 were selected by the author for follow-up spectroscopy. These observations were made in November 2001 by E. L. Martín with the ESI on the Keck II telescope, and have been reduced and analysed as part of this work.

The ESI spectra were reduced using the packages available in IRAF, following the usual standard procedures: CCD reduction (*ccdproc*), sky subtraction (*imarith*), optimal extraction (*apall*) and calibration (*identify*, *dispcor*, *standard*). There were some difficulties encountered in the reduction stages when trying to get an accurate sky subtraction due to the curvature of the raw spectral image, but this was overcome by using a relatively small window, located right next to the end of the object spectrum, in order to define the background region.

Of the seven spectra obtained with the ESI, only three show properties consistent with late-type dwarf stars: dtau17, dtau31 and dtau33 (see Figure 5.5). The remaining four spectra indicate that these objects are reddened background stars of earlier spectral type. For reference purposes, the objects denoted as dtau17, dtau31 and dtau33 (identified

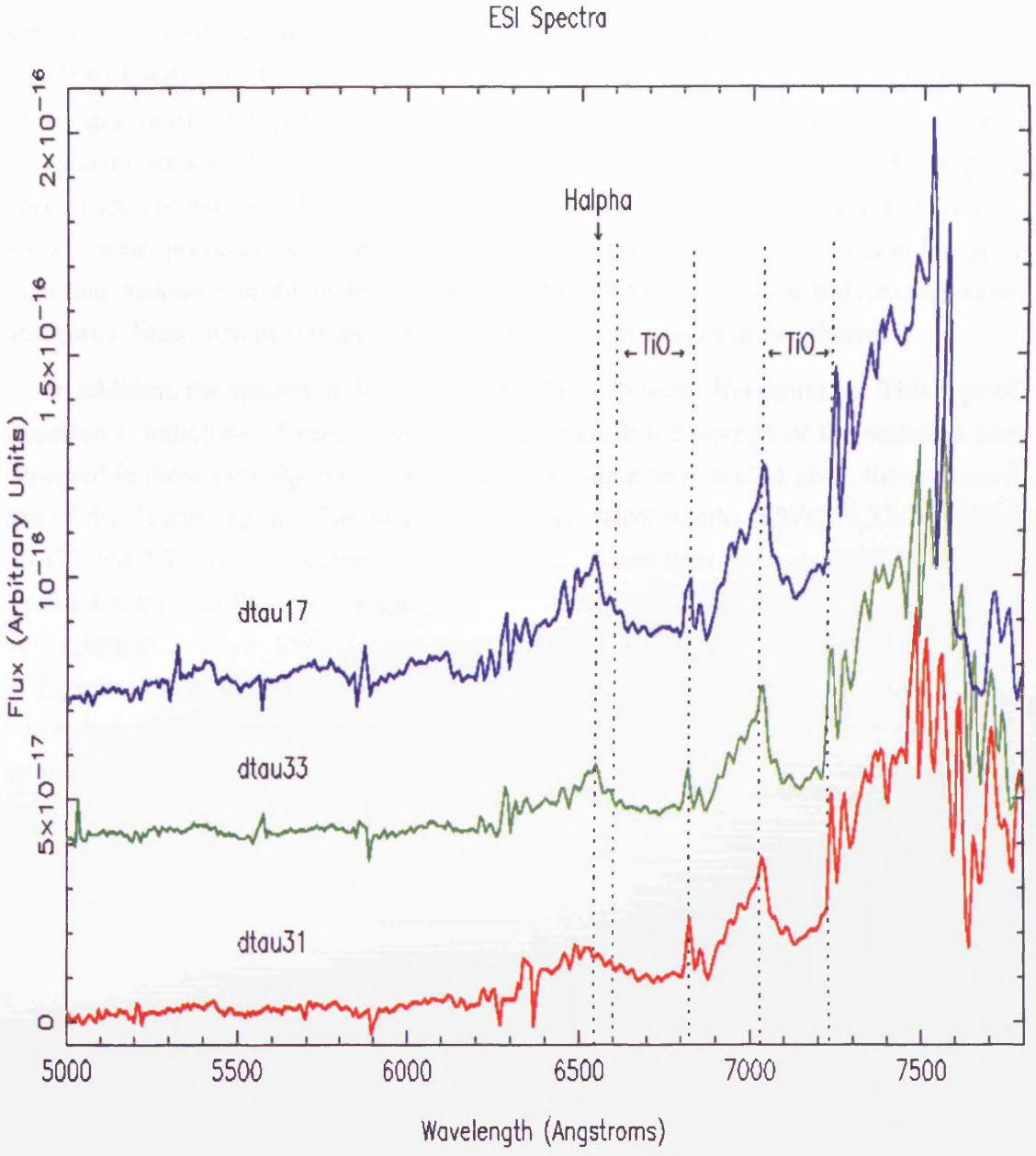

FIGURE 5.5. The ESI spectra of the three late-type M dwarfs discovered in the Taurus Dark Clouds region.

originally by Kenyon (2001)), were duplicated in the CMD analysis presented in this work, and correspond to the objects denoted as tau154, tau243 and tau129 respectively. The details for tau154 and tau129 can be found in Appendix A.1, but tau243 is not listed here since its $R - Z$ colour is less than 4 and therefore it was rejected during the Z vs $R - Z$ selection procedure.

The photometry of the three dwarf objects suggest that they are all of spectral type M6 or M7, whilst the presence of deep TiO absorption bands centered around 6700 Å and 7150 Å indicates that these objects are very cool. These features have been identified in the spectra of other potential Taurus brown dwarfs (Martín et al. 2001*a*), and when compared over a wavelength range of 6500-8000 Å, the similarities in the shape of the spectra are obvious (see Figure 5.6 for comparison). The KI lines near 7700 Å may show a weak presence in all three objects, but the noise levels in this region are quite high thus making it problematic to make a definite detection. This is unfortunate, since absorption lines such as this are good indicators of low gravity atmospheres.

In addition, the spectra of dtau17 and dtau33 show weak $H\alpha$ emission. This type of emission is indicitive of very young objects, although the strengh of the emission line observed in these two objects is not as strong as might be expected given the estimated age of the Taurus region. The measured Hα equivalent widths (EWs), 5.3 ± 0.1 Å for dtau17 and 2.7 ± 0.1 Å for dtau33, are somewhat lower than those measured for other Taurus brown dwarfs (EWs ranging from 13 Å to 340 Å; Martín et al. (2001*a*)), but are comparable to the EWs derived for some Pleiades brown dwarfs (Martín, Rebolo & Zapatero-Osorio 1996). When compared with the field, most M dwarfs show Hα in absorption, although for spectral types later than M3 many show Hα in emission (EWs up to 10 Å), which is thought to be related to the point at which M dwarfs become fully convective (Gizis, Reid & Hawley 2002). For the latest M dwarfs and L dwarfs, Hα emission is also typically between 0 and 10 Å, although the emission level seems to decrease in the L dwarf regime (Martín et al. 1999*a*).

5.4.2 Infrared Data

A useful approach to follow-up observations is to get additional JHK data, which allows for further photometric analysis and makes it possible to de-redden the data. Although much of this can now be obtained from 2MASS, some UKIRT data was obtained for the faintest Taurus candidates. Infrared JHK photometry for 21 of the reddest candidates identified from the analysis of the RIZ data was obtained using UFTI in November 2002.

The photometric data was reduced automatically using the ORAC_DR scripts available on STARLINK. Initially, the *array_tests* and *reduce_dark* recipes were used to calculate the readout and dark current. The *jitter_self_flat* recipe was then used to carry out all of the bias removal, bad-pixel masking, dark subtraction and flat fielding (from a 5 point

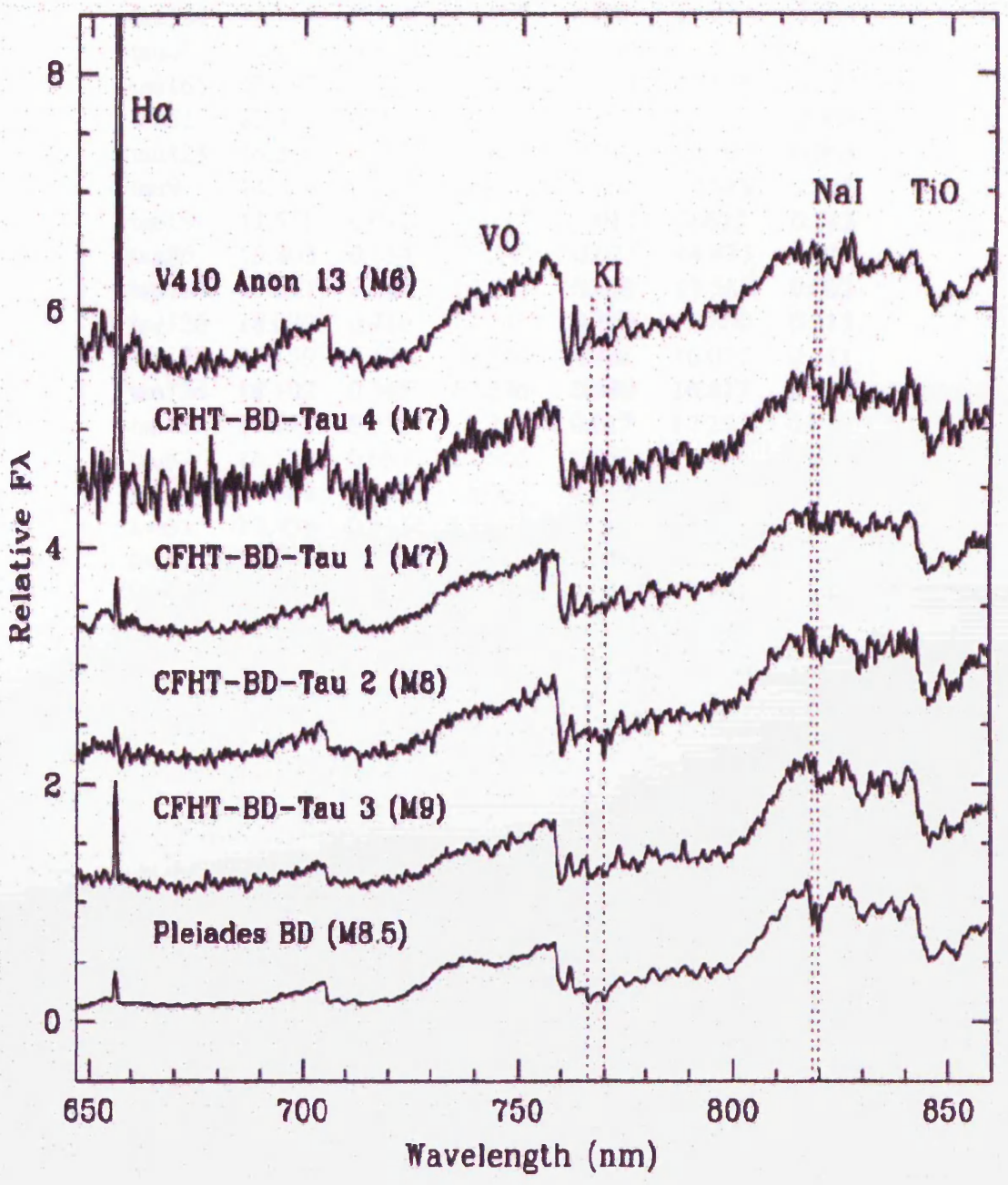

FIGURE 5.6. The spectra of four potential brown dwarfs in Taurus. Also shown for comparison are spectra for the known Taurus member V410 Anon 13, and a Pleiades brown dwarf. Diagram from Martín et al. (2001).

Name	J	J error	H	H error	K	K error
tau141	14.521	0.027	130839	0.030	13.013	0.021
tau105	14.917	0.032	13.004	0.011	11.828	0.005
tau120	14.159	0.018	12.227	0.006	11.015	0.003
tau48	16.955	0.194	13.125	0.193	15.715	0.168
tau165	17.288	0.257	16.304	0.224	15.946	0.207
tau52	13.506	0.009	12.759	0.009	12.336	0.008
tau123	16.212	0.087	13.680	0.017	12.627	0.008
tau8	14.729	0.027	14.097	0.031	12.989	0.018
tau19	11.575	0.012	10.217	0.012	9.673	0.012
tau86	15.802	0.054	15.340	0.077	14.875	0.013
tau108	16.133	0.062	14.443	0.029	13.589	0.022
tau126	18.099	0.410	17.147	0.369	16.600	0.313
tau136	17.139	0.151	16.646	0.221	16.037	0.181
tau124	18.102	0.345	17.296	0.340	16.817	0.354
tau15	14.758	0.033	13.264	0.017	12.297	0.010
tau92	16.129	0.053	14.616	0.028	13.781	0.024
tau14	14.585	0.019	13.063	0.010	12.195	0.012
tau31	13.459	0.013	11.883	0.007	11.053	0.011
tau32	14.601	0.019	12.958	0.047	12.145	0.012
tau94	16.801	0.092	15.218	0.047	14.394	0.040
tau 62	16.074	0.068	15.224	0.062		

Table 5.1. The JHK photometry for the Taurus candidates selected for further analysis.

dither pattern). Magnitudes were then determined by using aperture photometry in GAIA. The results obtained are summarised in Table 5.1.

The $I - J$ vs $J - H$ colour-colour diagram is shown in Figure 5.7 for stars with UKIRT data. $J - H$ is approximately constant for M dwarf stars, and then rises and falls again for L dwarfs, as shown in the unreddened sequence for field stars (dotted line). The flat M dwarf line allows the M dwarfs to be dereddened, although the same cannot be done for earlier stars, but these are of less interest here. It is also difficult to deredden early type L dwarfs since the reddening vector is nearly parallel to the sequence. As can be seen from the CMD, several of these objects for which UKIRT infrared data were obtained lie close to the sequence, especially if the reddening is taken into account. If the reddening vector is used to trace the remaining objects, located around $I - J = 5$ $J - H = 1.5$, back to the dereddened sequence, then the majority would lie earlier than M and thus are simply heavily reddened higher mass stars, with the only exception being that one of the objects could be early M class.

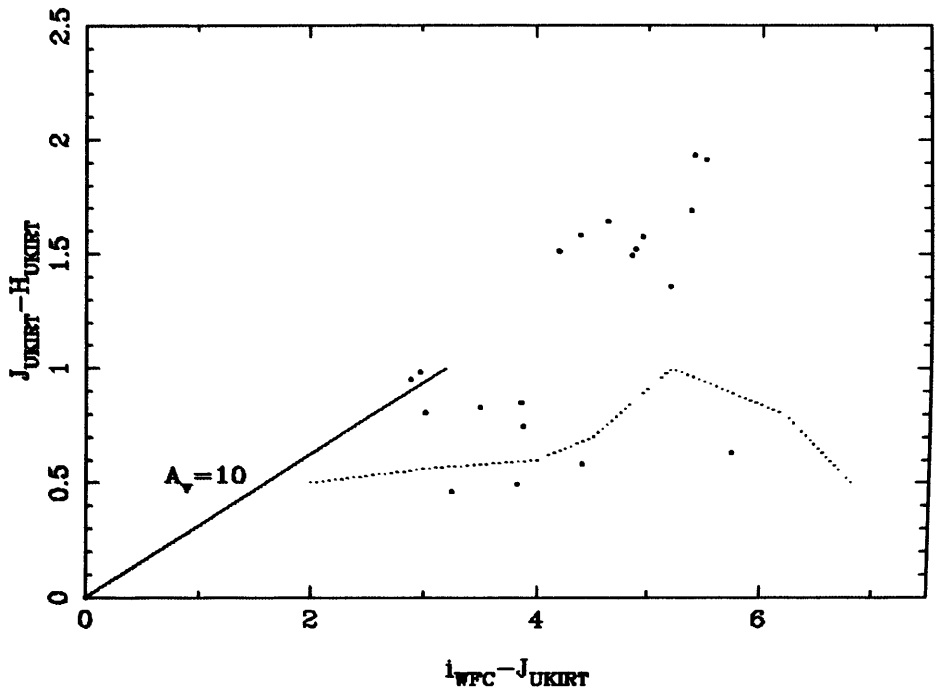

FIGURE 5.7. The $I-J$ vs $J-H$ colour-colour diagram for stars with UKIRT data. The unreddened sequence for field stars is shown as a dotted line.

5.4.3 UIST Spectra

From an initial analysis of the Taurus RIZ photometry (a full description is not included here since the analysis was superseded by that presented in Section 5.3.2) the details of several Taurus brown dwarf candidates were submitted for observation during UIST commisioning time in September 2002, from which spectra for two objects, namely tau115 and tau214, were obtained. Then, following the full analysis of all the photometry, the $J-H$ vs $I-J$ colour-colour diagram was used to select several more objects for follow-up UIST spectroscopy, and observations were carried out in December 2002 using the HK grism on USIT at UKIRT. The data was reduced using the standard ORAC_DR scripts, which automatically produce a sky subtracted, group image containing both a positive and negative spectrum. The specta were then optimally extracted and calibrated in the usual manner using routines available in FIGARO (see Chapters 4 and 6 for more details on spectral extraction procedures).

Figure 5.8 shows the spectra of the six objects for which follow-up UIST HK spectroscopy was obtained. From these spectra it can be seen that two of the objects (tau52 and tau141) look like potential Taurus brown dwarfs due to the distinctive triangular shape of the spectrum, which peaks around 1.65 μm and is formed by the strong H_20 ab-

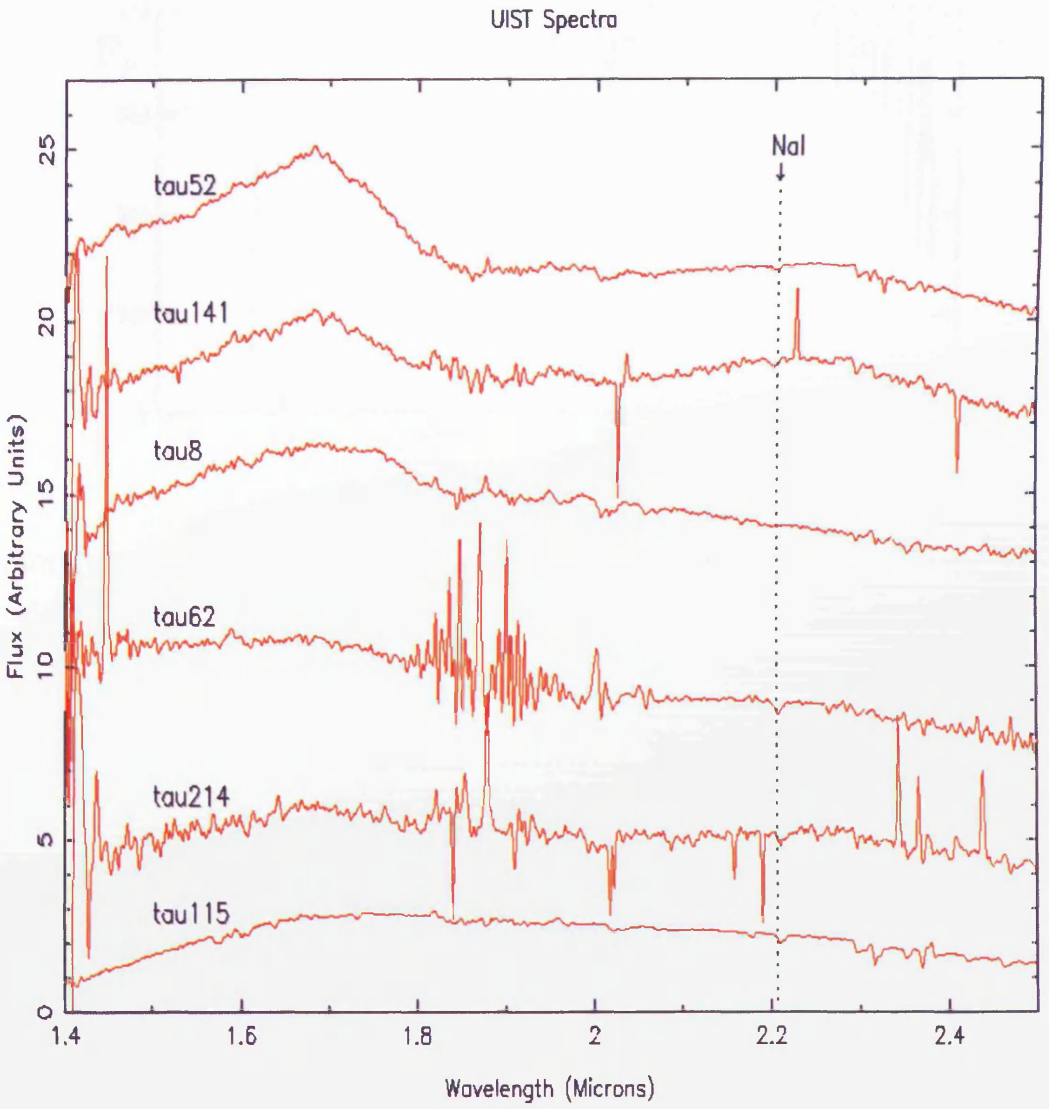

FIGURE 5.8. The HK spectra for the six Taurus objects observed with UIST.

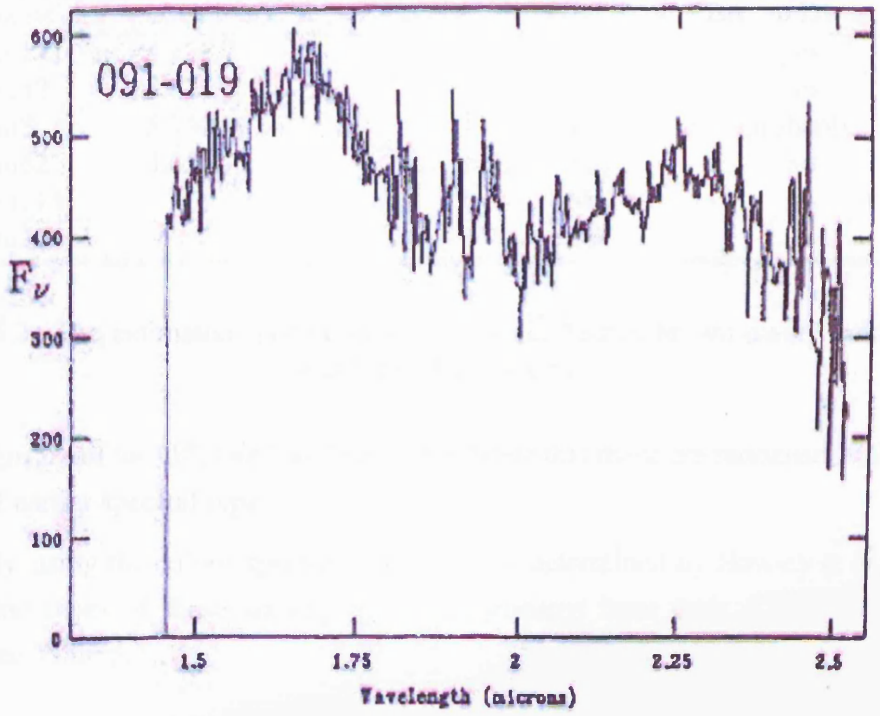

FIGURE 5.9. The spectrum of the Trapezium brown dwarf candidate 091-019, showing the distinctive peak around 1.65 μm. Diagram from Lucas et al. (2001).

sorption bands at either side ($\sim 1.55\mu$m and $\sim 1.7\mu$m). This prominent feature has also been observed in the spectra of brown dwarfs in the Trapezium cluster, and is a signature of very young objects (Lucas et al. 2001). A typical spectrum of a Trapezium brown dwarf candidate is shown in Figure 5.9 for comparison. Tau8 may also show this peak, although it is certainly less obvious than in the other two objects. By fitting theoretical spectral models to their data Lucas et al. (2001) show that this water absorption feature is indicative of a low gravity environment (typically g = 3.5 to 4), and thus it is not surprising that the Taurus brown dwarf spectra display this feature, since the region is still in the early stages of gravitational contraction.

Other gravity sensitive features within the HK waveband include NaI and CO (Lucas et al. 2001). Although the CO bandheads around 2.3 micsp are not clearly distinguishable in any of the six spectra, the NaI absorption line can be easily identified in the spectra of tau62, tau214 and tau115, which makes its absence in the spectra of tau52, tau141 and tau8 all the more prominent. This lack of strong NaI absorption again indicates a low gravity atmosphere, and thus lends further support to these objects being genuine Taurus brown dwarfs.

Name	$I-J$ Colour	$R-I$ Colour	Spectral Type	Brown Dwarf?
tau141	4.298		L0	yes
tau52	3.871		M8	yes
tau8	5.743		L6	probably
tau62	3.856		M8	no
tau115		1.895	M6	no
tau214		3.221	M8	no

Table 5.2. The estimated spectral types of the six Taurus brown dwarf candidates with UIST HK spectra.

The spectra of tau115, tau62 and tau214 indicate that these are reddened background objects of earlier spectral type.

Finally, using the colour-spectral type relations determined by Hawley et al. (2002), the spectral types of these six objects were estimated from their $I-J$ and $R-I$ colours(see Table 5.2).

5.5 Conclusions

R, I and Z band photometry was obtained for 5.65 square degrees of the Taurus Dark Clouds. This data was analysed using three colour-magnitude diagrams, from which 165 potential Taurus brown dwarfs were identified. By using three CMDs instead of just two, the number of brown dwarf candidates found was reduced by approximately 11%. This was therefore a worthwhile step, as it significantly reduced the number of contanimating background objects to be sifted through, especially given the relatively high and variable levels of reddening in the Taurus region.

Of the 165 candidates identified from the CMD analysis, only 21 have follow-up data, and of these only 6 have been identified as potential brown dwarfs; dtau17, dtau31, dtau33, tau8, tau52 and tau141. This implies a success rate of approximately 28 %. If this level of success were maintained in the follow-up work and analysis of the remaining 144 candidates, then around 40 more brown dwarfs could be found within the 5.65 sqaure degrees the Taurus Dark Clouds studied here.

Far optical spectra for seven brown dwarf candidates were obtained with the ESI on the Keck II telescope. Of these seven, three (dtau17, dtau31 and dtau33) show spectral feautures consistent with young, cool, late type M dwarfs, including deep TiO absorption bands and weak Hα emission. When compared against other optical spectra of

brown dwarfs found in Taurus (Martín et al. 2001*a*) those presented here are extremely similar, suggesting that the objects are indeed members of the Taurus Dark Clouds. The weak Hα emission detected in these objects is not enough to unambiguously confirm them as members, since the levels measured are towards the lower end of the range expected for the Taurus region (Martín et al. 2001*a*), but are comparable to the values expected for the field (Martín et al. 1999*a*).

Infrared data from UFTI for 21 objects indicated that at least seven of these objects were located close to the theoretical sequence for field dwarfs in the $I-J$, $J-H$ colour-colour diagram, when reddening was taken into account. Spectra were then obtained for six of these objects with UIST, with three of the objects (tau52, tau141 and tau8) showing spectral features consistent with young, low gravity brown dwarfs, including H_2O absorption bands and weak NaI lines. The identification of these low gravity features is particularly important since they have been shown to be good indicators of both youth and cluster membership for brown dwarfs in star forming regions (Lucas et al. 2001), which suggests that these three objects have a high probability of being genuine Taurus brown dwarfs.

Given that the S/N ratios for both the optical and infrared spectra were relatively high, it seems unlikely that any of these features outlined above have been mis-identified. However, in order to unambiguously determine their brown dwarf status further observations will have to be made, perhaps by calculating the proper motion or by searching for lithium in the spectrum.

From the photometry of the six likely brown dwarf candidates, their spectral types were estimated. dtau17, dtau31 and dtau33 are all M6/M7 class objects, whilst tau52, tau141 and tau8 fall respectively into the M8, L0 and L6 subclasses. For objects with an age of 125 Myrs (such as Pleiads), the substellar limit is found at M6.5 $\pm$ 0.5, but for younger objects this limit moves slightly further into the spectral type subclasses to M7 (Martín, Basri & Zapatero-Osorio 1999). This implies that tau52, tau141 and tau8 are all within the substellar regime and thus could be given brown dwarf status, whilst dtau17, dtau31 and dtau33 all lie on the stellar/substellar boundary and thus require further work before their brown dwarf status can be confirmed.

The NEXTGEN models of Baraffe et al. (2002*b*) suggest that these objects have masses in the range 10 - 20 M_J if an age of 3 Myrs is adopted for the Taurus Dark Clouds region. However, these estimated masses should be treated with caution given the uncertainties associated with theoretical models at very young ages.

Chapter 6

A Study of Brown Dwarfs in the Pleiades

This chapter presents a detailed analysis of the properties of 48 candidate Pleiades brown dwarfs. These candidates have been selected from the four largest optical surveys of the Pleiades carried out to date (see Jameson et al. (2002)). After a brief discussion of the observational data and the analysis procedures, the proper motion of each candidate is determined in order to establish its membership status. The refined list of brown dwarfs is then used to determine the form of the mass function of the Pleiades. In addition, spectroscopic data was obtained for 12 of the 48 candidate Pleiades brown dwarfs. Following an outline of the data aquisition and reduction procedures, the actual spectra are presented and described, and the properties of the spectra are discussed.

6.1 The Pleiades Cluster

The Pleiades cluster is perhaps one of the most ideal areas in which to search for brown dwarfs. Although the cluster is close enough for the faintest members to be easy to observe, at a distance of around 130 pc (Stauffer et al. 1998) it is also far enough away such that surveys do not require large areas of sky to be covered. The Pleiades is also fairly young, with an estimated age of 125 Myrs (Stauffer et al. 1998), which means that the substellar members have not had too long to cool and fade. On the other hand it is not so young that comparison with stellar models is difficult, since these are certainly thought to be untrustworthy for ages less than 10 Myrs, and may be somewhat unreliable for even greater ages (Baraffe et al. 2002*b*). The Pleiades should therefore be an ideal laboratory to test these models.

The low mass and substellar population of the Pleiades is one of the most well studied and well understood of all young, open clusters. The first CCD survey of the Pleiades was carried out by Jameson and Skillen in 1989 (Jameson & Skillen 1989), although the first genuine brown dwarf, Teide 1, was not discovered until 1995 (Rebolo et al. 1995). Since that time many more substellar candidates have been unearthed by the numerous multi-waveband surveys of the cluster, including; R and I (Hambly et al. 1991), I and K (Simons & Becklin 1992), and I and Z (Cossburn et al. 1997). More recent work on the Pleiades brown dwarf population includes I and Z photometry (Moraux et al. 2003*a*), an analysis of the spatial disribution and mass function (Jameson et al. 2002), an investigation into membership status and binarity (Martín et al. 2000), and a large scale I and Z survey (Pinfield et al. 2000).

6.1.1 The Stellar Mass Function

The stellar mass function (MF) describes the number of stars per unit mass over a given mass range, and is usually written as a power-law ($dN/dM \propto M^{-\alpha}$; see Section 3.1). It is an important quantity in astronomy as it gives an insight into the structure and evolution of stellar systems and clusters on both local and Galactic scales, whilst the initial mass function (IMF) provides information on star formation processes. Although the stellar mass function has long been very well defined for $0.4\,M_{\odot} \geq M \geq 50\,M_{\odot}$, with $\alpha \simeq 2.3 - 2.7$ (Salpeter 1955), it is more uncertain at both very high (Rana 1987) and very low masses, and until recently was largely unknown for objects in the very low mass and substellar regime.

The youth of the Pleiades implies that the MF of the cluster would be a reasonably accurate representation of the IMF, and as such makes it a very interesting quantity to determine. In addition, the cluster is believed to be roughly coeval with very little new or recent star formation (Oppenheimer et al. 1997) to distort the current MF away from its initial state. Several estimates for the MF of the Pleiades in the upper substellar mass range ($0.04 - 0.08\,M_{\odot}$) have been determined in recent years ($\alpha \simeq 0.6 \pm 0.15$, Bouvier et al. (1998); $\alpha \simeq 0.7$, Hambly et al. (1999); $\alpha \simeq 0.5 - 1.0$, Martín et al. (2000)), although the MF in the lower substellar/planetary mass range still remains a mystery.

In Jameson et al. (2002) 48 Pleiades brown dwarf candidates were identified on the basis of their $I - K$ colour, the largest magnitude limited sample of the substellar members of the cluster compiled to date. The substellar mass function was then calculated, and found to be slowly rising with $\alpha \simeq 0.41 \pm 0.08$ for $0.035 \leq M \leq 0.3\,M_{\odot}$. How-

ever, since it is unclear whether all contaminating field stars can be identified from the infrared colour-magnitude diagram (CMD), further analysis of this data is required. By also measuring the proper motion of the photometric candidates, genuine Pleiades members can be recognised because the annual movement of cluster members, $\mu_\alpha \cos\delta$ = 19.15 $\pm$ 0.23 mas/yr, μ_δ = -45.72 $\pm$ 0.18 mas/yr (Robichon et al. 1999), is markedly different to that of field stars. Therefore, the list can be refined in order to determine the most stringent constraints on the MF, based on the most reliable brown dwarf candidate list compiled to date.

6.2 Observational Data

The process of identifying candidate brown dwarfs relies upon the results from deep, wide-field surveys. The four largest Pleiades surveys that have been carried out to date are the International Time Project (ITP) survey, the Canada France Hawaii Telescope (CFHT) survey, the Burrell Schmidt (BPL) survey and the INT Wide Field Camera (IWFC) survey (see Table 6.1 for a summary of the key properties of each).

6.2.1 The ITP Survey

The ITP survey (Zapatero-Osorio et al. 1999*b*) was carried out in February and September 1996 on the INT. The data covers an area of $\sim 1\,\mathrm{deg}^2$ in the central region of the Pleiades cluster in the I and Z wavebands. A total of 47 candidates were identified from the I vs $I - Z$ CMD, with I magnitudes down to 22.3, and corresponding masses down to 0.03 $M_\odot$. The survey is complete to $I \sim 21$ and $Z \sim 20.5$, and has limiting magnitudes of 22.2 and 21.5 respectively. Zapatero-Osorio et al. (1997), Martín et al. (1998) and Martín et al. (2000) have acquired further data for several of the candidates, including optical spectroscopy and infrared photometry.

6.2.2 The CFHT Survey

The CFHT survey (Bouvier et al. 1998) was carried out in December 1996 on the CFHT at Mauna Kea. The data covers an area of $\sim 2.5\,\mathrm{deg}^2$ in the R and I wavebands. A total of 26 very low mass (VLM) stars and brown dwarf candidates were identified from the I vs $R - I$ CMD, with I magnitudes down to 20.2, and corresponding masses down to 0.045 $M_\odot$. The survey is complete to $R \sim 23.5$ and $I \sim 22.5$, and has limiting magnitudes

Survey	Wavebands	Area (sq. deg.)	Completeness (I)	Number of brown dwarf candidates
ITP	$I+Z$	1.0	21	47
CFHT	$R+I$	2.5	22.5	26
BPL	$I+Z$	6.25	19.5	30
IWFC	$I+Z$	1.1	22.0	23

Table 6.1. A summary of the key parameters for each of the surveys used to select candidate Pleiades brown dwarfs.

of 25.0 and 23.3 respectively. By calculating the proper motions of the 26 candidates, Moraux et al. (2001) show that only 18 are actual cluster members, and that of these only 11 are substellar. We note that two of the substellar candidates are duplicated in the ITP survey.

6.2.3 The BPL Survey

The BPL survey (Pinfield et al. 2000) was carried out in December 1996 on the Burrell Schmidt telescope at Kitt Peak. The data covers an area of $\sim 6.25\,\mathrm{deg}^2$ in the I and Z wavebands. The survey is complete to $\mathrm{I} \sim 19.5$. Using a combination of follow-up K band photometry and, for the brighter candidates, proper motions, the survey unearthed 309 VLM stellar candidates, of which 156 are new, and 30 brown dwarf candidates, of which 13 are new. However, of these 13 new brown dwarf candidates, 3 have been shown to be non-members due to a lack of lithium absorption (Martín et al. 2000) and infrared data inconsistant with cluster membership (Pinfield et al. 2003).

6.2.4 The IWFC Survey

The IWFC survey (Dobbie et al. 2002*b*) was carried out in December 1998 on the INT. The data covers an area of 1.1 deg^2 in the I and Z wavbands. The survey is complete to $I \sim 22$. A total of 23 potential low mass cluster members were identified from the I vs $I-Z$ CMD and follow-up K band photometry. 15 of these candidates are not duplicated in the ITP, CFHT and BPL surveys. The faintest brown dwarf candidate in this survey, which has an I magnitude of 21.8 and an estimated mass of 0.03 $\mathrm{M}_{\odot}$, may be the coolest substellar Pleiades member identified to date.

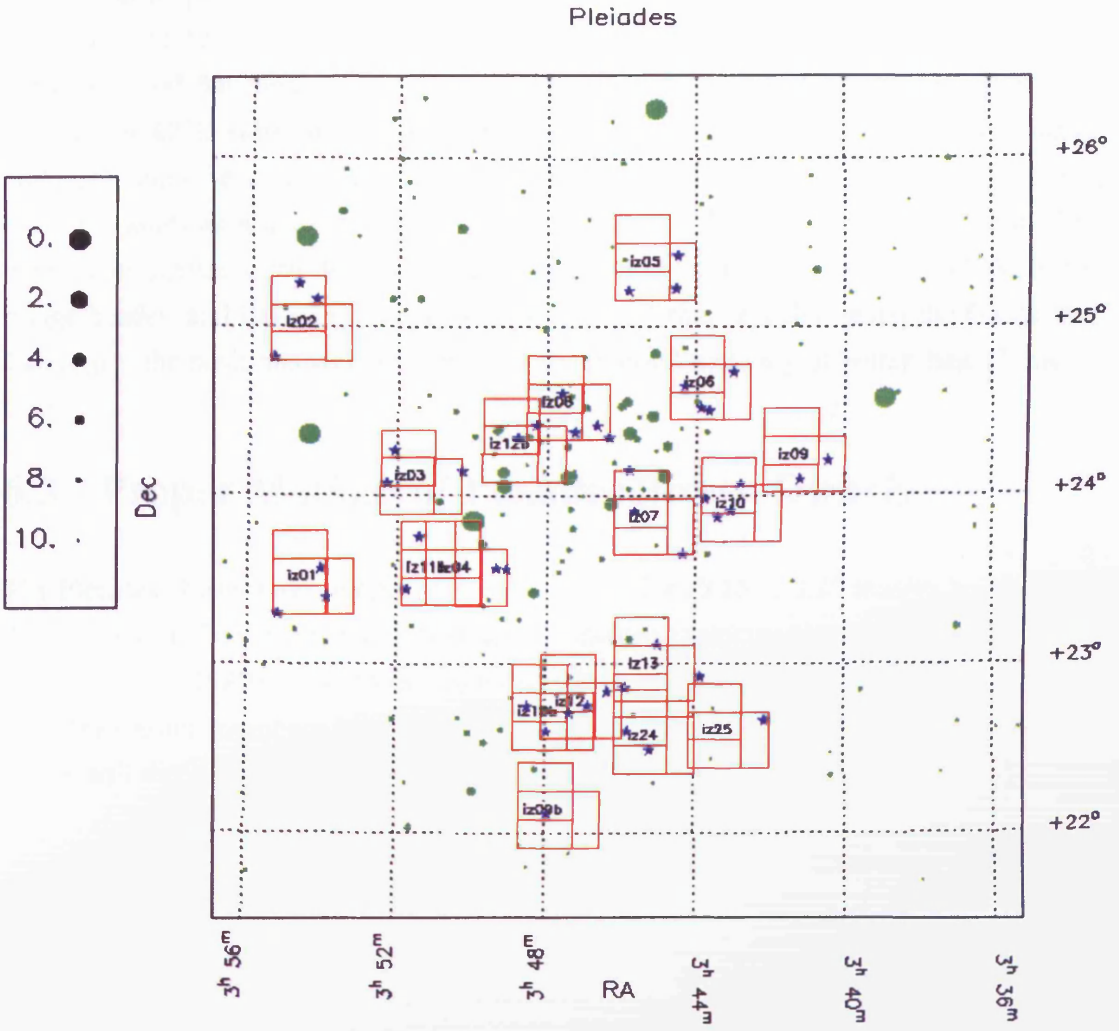

FIGURE 6.1. The fields observed in the Pleiades cluster with the WFC. The fields are shown as red boxes, the brown dwarf candidates as blue stars and the brighter background stars as green dots.

6.2.5 New Pleiades Observations

In order to calculate the proper motions of the brown dwarf candidates identified in the four surveys outlined above, two sets of images, separated in time by a few years, are required. We therefore obtained deep I and Z band images of all of the brown dwarf candidates in February 2002. The images were observed using the INT and the WFC, with the fields being carefully selected to minimise the number of pointings required to cover all of the brown dwarf candidates (see Figure 6.1).

The images were reduced at the Institute of Astronomy, Cambridge, using the WFC

data reduction pipeline (Irwin & Lewis 2001). To summarise the data reduction process, the data were first subject to bias level subtraction, before the application of linearity correction and flat-fielding. To remove the effects of interference between night sky lines in the CCD substrate, fringe maps were constructed for both photometric bands. Although some second order fringe patterns were still present in the Z band images, since the analysis was positional and not photometric these were not a problem. The object coordinates were determined using the world coordinates system (WCS) in the image header, and have an internal accuracy of 0.1″ rms. Finally, using the Guide Star Catalogue, the positions were calibrated to an external accuracy of better than 1″ rms.

6.3 Proper Motions of Pleiades Brown Dwarfs

The Pleiades cluster has a proper motion of $\mu_\alpha \cos\delta = 19.15 \pm 0.23$ mas/yr, μ_δ = -45.72 $\pm$ 0.18 mas/yr (Robichon et al. 1999), and an intrinsic velocity dispersion of $\sim$ 1 mas/yr (van Leeuwen 1980). Due to this motion, which is distinct to that of field stars, true Pleiades cluster members can be easily recognised and thus their stellar or substellar nature will directly follow from their photometric properties.

6.3.1 Coordinate Calibration

The images from the ITP, CFHT and BPL surveys did not have World Coordinate System (WCS, or standard equatorial) coordinates, and therefore needed to be calibrated. This was done using GAIA (Graphical Astronomy and Image Analysis tool), which is an image display and analysis tool developed as part of the VLT project at ESO (star-www.dur.ac.uk/ pdraper/gaia). Firstly, an approximate calibration was applied by cross-referencing the x and y positions of a few stars (typically four or five) in the uncalibrated image with the RA and DEC of the same stars from an image with a known calibration (the Digital Sky Survey, DSS). These positions were selected using the mouse and then *centroided* to improve the accuracy, before the fit was applied. The initial calibration was then tweaked by using all the stars from the United States Naval Observatory (USNO) catalogue in the field of the original image and matching up their RA and DEC postions with the x and y positions of the original objects. The positions were again *centroided*, the fit applied and the rms error of the fit noted - this was typically better than 2 pixels. This process is solely a means of pairing up the correct stars for the transformation, see below.

6.3.2 Astrometric Analysis

The astrometric analysis was performed on the I band images from the two epochs, and the main principles behind the calculations are as follows. Firstly, the x and y pixel coordinates of the brown dwarf candidate are measured on both images using the RIMCUR package in IRAF. These cursor defined positions are then refined with the *centroid* option in the CENTER package. On the same images, positions are also measured for around 25 reference background stars, covering as large an area of sky as possible, depending upon the overlap between the two fields of the two different epochs. All of the x and y positions are then converted into RA and DEC, again using RIMCUR, and are cross correlated to ensure that the pairs of coordinates are correctly matched. Several routines from the STARLINK SLALIB libraries were then used to calculate the spatial transformation between the two sets of x and y coordinates and the corresponding rms error. This was an iterative process designed to increase the accuracy of the coordinate transformation by rejecting objects with extremely anomalous motions, and then recalculating the transformation until it reached convergence (N. Hambly, private communication). It should be noted that a true member of the Pleiades would be rejected during the iteration process as its large proper motion would be viewed as anomolous when compared to that of the reference stars.

The transforamtion procedure enabled the positions of the objects from both epochs to be compared in the same frame of reference, which eliminated any systematic offsets, and allowed the absolute change in postion over time to be measured. Finally, the transformed x and y coordinates were converted into RA and DEC (again using RIMCUR), and the proper motion of the object (in arcsecs) was calculated by:

$$\mu_\alpha = 15(RA_2 - RA_1)\cos\delta/\Delta t \tag{6.1}$$

and

$$\mu_\delta = (DEC_2 - DEC_1)/\Delta t, \tag{6.2}$$

where RA_1 and DEC_1 are the right ascension and declination of the object in the first epoch image, RA_2 and DEC_2 are the right ascension and declination of the object in the second epoch image (transformed to the same reference frame as the first epoch) and Δt is the time interval between the two epochs. In Equation 6.1, the $\cos\delta$ factor is needed because the objects are above the equator, whilst the factor of 15 arises due to the conversion of hours into degrees. For the two sets of images obtained with the WFC Δt

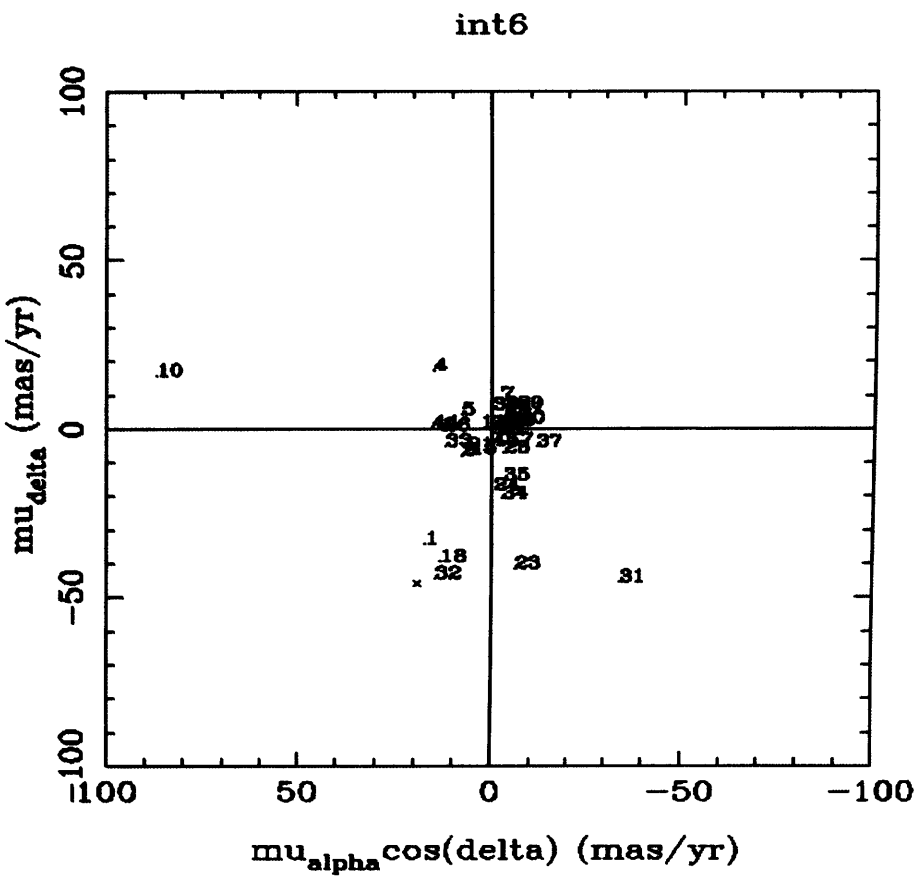

FIGURE 6.2. An example vector point diagram showing the typical distribution of stars after the astrometric analysis. The proper motion of the Pleiades is marked with a cross.

= 3.2 years, whilst for the ITP/WFC, CFHT/WFC and BLP/WFC data Δt = 5.4, 5.2 and 5.2 years respectively.

Since most of the distant background stars, which were used as reference points in the proper motion analysis, would not be expected to have a detectable motion over such short time periods, they define the origin in the vector point diagram, as illustrated in Figure 6.2. In this example vector point diagram, the quoted proper motion of the Pleiades cluster ($\mu_\alpha \cos\delta$ = 19.15 mas/yr, μ_δ = -45.72 mas/yr, Robichon et al. (1999)) is marked with a cross, the brown dwarf candidate being analysed (in this case INT-PL-IZ-6) is labelled 1, and the remaining numbered points are the reference background stars (the numbers merely indicate the order in which the reference points were selected and have no special significance). It can clearly be seen that the majority of the reference background stars are indeed clustered around the origin, as expected, with the only exceptions

being objects 1, 4, 10, 18, 23, 31 and 32. Objects 1, 18 and 32 all look to have a high probability of cluster membership, with 1 being the brown dwarf candidate, and the others most likely being brighter stellar members. The four remaining stars have a wider distribution, and could possibly be halo objects.

The error for each component of the proper motion is calculated from the error in the x or y position for each epoch, via:

$$error = \sqrt{(P_1^2 + P_2^2)}, \tag{6.3}$$

where P_1 is the error in the x or y position of the object in the first epoch image and P_2 is the error in the x or y position of the object in the second epoch image. The error is then converted into the appropriate units using the pixel scale of the detector, which is 0.333″, 0.615″, 0.21″ and 2.0″ per pixel for the INT, ITP, CHFT and BPL images respectively. The errors in x and y do not necessarily correspond to errors in RA and DEC respectively, as this depends upon the orientation of the chip. In general, the errors were smallest for the objects observed with the WFC for both epochs, as these had a consistent pixel scale and were both calibrated in the WCS scheme. For those objects which had images from two data sets (i.e. ITP, CFHT or BPL for epoch 1 and WFC for epoch 2), the errors were larger due to varying pixel scales between the images and different positional calibration methods.

Although in theory the BPL images appeared to be suitable for this analysis, despite their large pixel scale, in practice this pixel scale was too large and therefore prevented the calculation of accurate proper motions using the method outlined above. In order to overcome this problem, infrared data from UFTI was used. Although the field of view of UFTI, at 15″, is much smaller than the field of view of any of the other instruments listed above, this drawback is offset by the fact that the pixel scale is much finer.

For the first epoch images, data from Pinfield et al. (2003) was used, which provided J and H band images, observed in January 2000, of six BPL objects: BPL163, BPL327, BPL316, BPL240, BPL81 and BPL306. Second epoch images were obtained in February 2004 during UFTI service time, giving a time interval of 4.1 years. Each image typically contained four or five stars, including the brown dwarf candidate. In order to calculate the proper motion of an object from an UFTI image, the centre of each object was determined using the CENTER routine in IRAF. Using the first epoch image the distance in pixels between each object and the brown dwarf candidate was calculated, and then these distances were used to predict the pixel coorinates of the brown dwarf candidate in the second epoch image. The difference between the observed and predicted positions gave

the proper motion of the candidate, given that the pixel scale and time interval between epochs was known. This method actually resulted in very accurate measurements due to the fine pixel scale.

6.4 Proper Motion Results

Of the 48 Pleiades brown dwarf candidates listed in Jameson et al. (2002), 43 have had their proper motion calculated in this work. The remaining five proper motions were not calculted because good quality images from two different epochs were not available. It should be noted that although calculations for the CFHT objects were made in this work, and were in good agreement with those determined by Moraux et al. (2001), the values given by Moraux et al. (2001) are more accurate and are therefore quoted here instead.

The results of the proper motion calculations are shown in Table 6.2, and are illustrated in Figure 6.3. In order to determine which objects are Pleaides members, a 2σ error circle was drawn around the actual value of the proper motion, with all objects lying within this circle being deemed members. Given that the typical error on the calculated proper motion was less than 15 mas, this error circle had a radius of 30 mas. Although no explicit calculation of the proper motion of PPL15 and BPL137 has been made in this work, previous measurements have indicated a strong likelihood of cluster membership and, therefore, they are included here as definite members. PPL15 has been detected in several brown dwarf surveys (Basri, Marcy & Graham (1996), Hambly et al. (1999)), and also has a lithium absorption level consistent with that of a Pleiades brown dwarf (Basri et al. 1996). BPL137 (or Teide1) is a particularly well documented brown dwarf, being one of the first to be discovered, and has been confirmed as a brown dwarf via the litium test (Rebolo et al. 1996) and as a Pleiades member via its proper motion (Rebolo et al. 1995). From the results it can be seen that most (31 out of 48) of the objects have a proper motion which is consistent with the true motion of the Pleiades, and these objects can therefore be assumed to be genuine substellar members. These objects are marked 'yes' in Table 6.2, and are shown as black dots in Figure 6.3. The membership status of the remianing objects was determined on an individual basis, depending upon the errors associated with the proper motion calculation and any other membership evidence from previous work.

Name	Other	$\mu_\alpha \cos\delta$ (mas/yr)	μ_δ (mas/yr)	Member	Ref.
BPL163		13.17 ± 0.28	-57.85 ± 0.28	yes	
INT-PL-IZ-6	BPL58	16.53 ± 7.56	-33.35 ± 8.66	yes	
INT-PL-IZ-42		0.38 ± 14.43	-46.25 ± 6.94	yes	
INT-PL-IZ-60		5.16 ± 9.60	-45.00 ± 10.59	yes	
BPL327		-20.25 ± 0.28	-49.76 ± 0.28	?	H,P
Roque47		7.89 ± 7.19	-60.09 ± 14.61	yes	
INT-PL-IZ-37	Roque17, BPL142	-9.57 ± 12.75	-11.45 ± 7.85	no	
Roque15	PPL1	-21.84 ± 33.19	-50.17 ± 33.47	yes?	S
BPL316		-32.51 ± 0.28	-59.93 ± 0.28	?	P
INT-PL-IZ-43		-2.69 ± 6.06	-37.88 ± 8.69	yes	
Roque14	BPL108	15.93 ± 14.82	-25.76 ± 15.44	yes	
INT-PL-IZ-44	BPL78	-0.88 ± 9.92	-52.75 ± 9.66	yes	
BPL240		6.15 ± 0.28	-56.88 ± 0.28	yes	
BPL81		-20.75 ± 0.28	-10.06 ± 0.28	no	
Roque12	BPL172	-16.34 ± 24.92	-24.95 ± 18.19	yes?	
INT-PL-IZ-29	BPL45	17.36 ± 11.77	-38.01 ± 10.19	yes	
BPL306		3.69 ± 0.28	-37.10 ± 0.28	yes	
INT-PL-IZ-33		-26.18 ± 11.57	-30.89 ± 9.45	no	
Roque9	BPL100	-6.62 ± 15.78	-51.05 ± 13.82	yes	
Roque8		-0.15 ± 10.59	-36.59 ± 7.62	yes	
INT-PL-IZ-48		-12.18 ± 16.86	-35.86 ± 12.36	yes?	
INT-PL-IZ-76		-18.6 ± 17.76	4.69 ± 18.41	no	
INT-PL-IZ-55		-19.23 ± 12.33	14.4 ± 15.43	no	
Roque5		29.32 ± 30.44	-35.71 ± 27.02	yes	
INT-PL-IZ-25		26.73 ± 12.12	-41.00 ± 7.88	yes	
Roque36		-7.76 ± 31.44	-7.19 ± 23.10	yes?	
Roque4	BPL66	-7.59 ± 24.79	-26.53 ± 16.57	yes?	
INT-PL-IZ-20		-1.11 ± 13.16	-32.02 ± 9.24	yes	
Roque30		-4.59 ± 24.55	-61.27 ± 14.72	yes	
INT-PL-IZ-84		5.74 ± 6.36	-34.79 ± 6.33	yes	
INT-PL-IZ-81		37.09 ± 10.21	-62.54 ± 10.72	yes	
INT-PL-IZ-69		79.78 ± 23.55	-44.16 ± 18.87	yes?	
CFHT-PL-10		28.6 ± 8.1	-30.0 ± 8.3	yes	M
CFHT-PL-11	Roque16,BPL152	25.4 ± 8.0	-45.4 ± 7.8	yes	M

CFHT-PL-12	BPL294	36.2 ± 7.6	-43.9 ± 7.6	yes	M
CFHT-PL-13	BPL254, Teide2	11.8 ± 7.9	-50.1 ± 7.6	yes	M
CFHT-PL-15		66.5 ± 8.1	-54.1 ± 8.1	no	M
CFHT-PL-16		21.7 ± 7.8	-30.8 ± 7.4	yes	M
CFHT-PL-17	BPL49	30.8 ± 8.0	-47.9 ± 0.28	yes	M
CFHT-PL-21	BPL235, Calar3	23.5 ± 7.6	-34.8 ± 7.6	yes	M
CFHT-PL-23		15.9 ± 7.8	-50.2 ± 7.5	yes	M
CFHT-PL-24	Roque7,BPL62	24.4 ± 7.9	-34.9 ± 7.9	yes	M
CFHT-PL-25	BPL303	25.6 ± 7.3	-44.7 ± 7.4	yes	M
PPL15		No data	No data	yes	B,H
BPL137	Teide1	No data	No data	yes	R1,R2
Roque13	BPL79	No data	No data	?	
Roque33		No data	No data	?	
Roque25		No data	No data	?	

Table 6.2: Proper motions for the compilation of Pleiades brown dwarfs from the ITP, CFHT, BPL and IWFC surveys. The first section of the table gives the results of the calculations made in this work, whilst the second section summarises the measurements made by others. 'yes' indicates definite Pleiades membership, 'yes?' indicates likely members of the cluster, '?' indicates unknown membership status and 'no' indicates definite non-members. The references given in the table refer to membership evidence and proper motion measurements made by others, and are denoted by M: Moraux et al. (2001), H: Hambly et al. (1999), P: Pinfield et al. (2000), B: Basri, Marcy & Graham (1996), R1: Rebolo et al. (1995), R2: Rebolo et al. (1996) and S: Stauffer et al. (1998).

At first glance Roque15, Roque12, INT-PL-IZ-48, Roque36, Roque4 and INT-PL-IZ-69 do not seem to have the expected proper motion, particularly in the RA component. However, the proper motion values calculated for each of these objects has an error which is on average larger than than the errors calculated for the other objects, and when this is taken into account it is certainly reasonable to assume that these six objects are likely members of the cluster, since they then fall within the 2σ error circle. In addition, three of the Roque objects (15, 12, and 4) have been identified as good brown dwarf candidates

in other surveys (Stauffer et al. (1998), Pinfield et al. (2000)), which provides further evidence for their inclusion as genuine Pleiades members. These objects are marked 'yes?' in Table 6.2 and are shown as red dots in Figure 6.3. It should be noted that in the second epoch image of INT-PL-IZ-69 a pixel hotspot was located close to the brown dwarf candidate, and, therefore, that this result could be misleading.

Six objects have proper motions which are very different to that expected (INT-PL-IZ-37, CFHT-PL-15, BPL81, INT-PL-IZ-33, INT-PL-IZ-76 and INT-PL-IZ-55), and so can be ruled out as Pleiades members. These objects are marked 'no' in Table 6.2, and are shown as blue dots in Figure 6.3. It should be noted that the image of INT-PL-IZ-37 was located on the edge of the CCD, and so the measurements for this object may be somewhat inaccurate. For five of these objects this calculation of their proper motion is the first to be made, but Moraux et al. (2001) measured the proper motion of CFHT-PL-15 and counted it as a genuine member of the Pleiades, despite the fact that its proper motion was inconsistent with that of the cluster, on the grounds that it was in a binary system and thus its motion was distorted. However, this argument can be discounted by considering the following possible scenarios.

If CFHT-PL-15 was an unresolved, equal mass binary system then the image would be elliptic and rotate, but the binary motion would not affect the proper motion. If on the other hand CFHT-PL-15 was in a binary system with an extreme mass ratio, say 10:1, the proper motion will again be unaffected since the secondary will be invisible but the primary will be very close to the centre of mass. The worst case scenario is therefore likely to be if the mass ratio is about 2:1.

Also, since close binaries move fast and make many orbits of small amplitude, whereas wide binaries move slowly but with larger amplitude, the scenario which is most likely to distort a proper motion measurement is when the epoch difference equals half the binary orbital period. Thus assuming a 2:1 ratio and $I \simeq 18$ we have $m_1 = 0.05\,M_\odot$ and $m_2 = 0.025\,M_\odot$, and given an epoch of 5.2 years, the semimajor axis of the binary can be calculated from Kepler's third law:

$$a^3 = (m_1 + m_2)P^2. \tag{6.4}$$

This calculation gives a value of a = 2.01 AU, which is equivalent to 15 mas at 130 pc. Furthermore, since the primary moves only 1/3 of the semimajor axis, ie 5 mas, then clearly the binary motion is trivial when compared to the proper motion (5.2 × 50 mas = 260 mas). Therefore this new calculation is consistent with CFHT-PL-15 not being a member of the Pleiades.

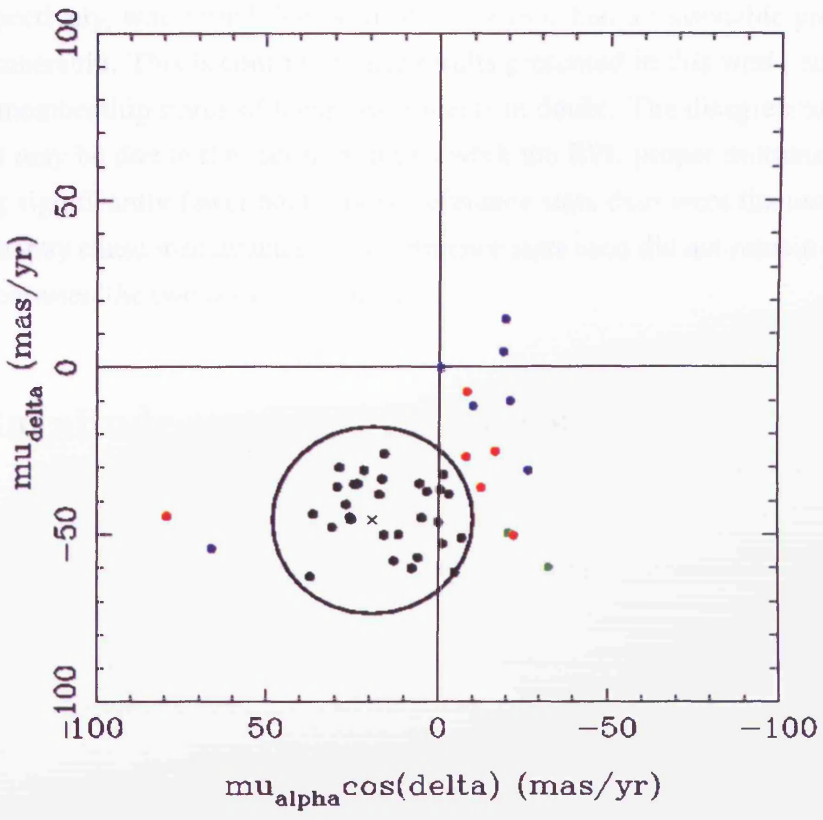

FIGURE 6.3. The spatial distribution of the proper motions calculated. The definite (yes) Pleiades members are shown in black, the likely ('yes?') members are shown in red, the candidates with questionable (?) membership properties are shown in green and the definite non-members (no) are shown in blue. The proper motion of the cluster ($\mu_\alpha \cos\delta$ = 19.15 mas/yr, μ_δ = -45.72 mas/yr) is shown as a black cross, and the 2σ error circle is shown as a black circle.

This leaves five candidates whose membership of the Pleiades remains in question - BPL327, BPL316, Roque13, Roque33 and Roque25. These objects are marked '?' in Table 6.2, and are shown as green dots in Figure 6.3. Of these five, the three Roque objects do not have here any data from which to make a proper motion calculation, and nor do they have any other previous proper motion measurements which can be referred to, and so their membership status remains unclear. The proper motions of BPL327 and BPL316 have been measured previously by Hambly et al. (1999) and Pinfield et al. (2000) respectively, who found that both of the objects had a reasonable probability of cluster membership. This is contrary to the results presented in this work, and therefore leaves the membership status of these two objects in doubt. The disagreement between these reults may be due to the fact that in this work the BPL proper motions were measured using significantly fewer background reference stars than were the rest of the objects, which may cause inaccuracies if the reference stars used did not remain completely stationary between the two observed epochs.

6.5 Magnitude and Mass Estimates

The photometric properties of all of the candidates are given in Table 6.3. The candidates which have been shown to be definite non-members of the cluster, or which have questionable membership properties, are shown in italics. The I_C and K magnitudes have been taken from Jameson et al. (2002) and references therein. Also included in this table are the effective temperatures and masses as derived from the NEXTGEN models of Baraffe et al. (1998). After transforming the model I_C magnitudes to the appropriate distance modulus, the data points for I_C against effective temperature (T_{eff}) and I_C against mass (M) were plotted. The values of T_{eff} and M were then estimated by interpolating between the data points. The derived effective temperatures range from 2952 K to 1855 K whilst the masses range from 0.087 $M_\odot$ to 0.031 $M_\odot$. Assigning exact errors to these values is difficult given that the uncertainties associated with the theoretical models are hard to quantify, but if the photometry is accurate to 5%, then this corresponds approximately to errors in T_{eff} and M of $\pm$ 200 K and $\pm$ 0.015 $M_\odot$ respectively. Assuming that the stellar/substellar boundary is defined by the minimum hydrogen burning mass at 0.075 $M_\odot$ (Baraffe et al. 2002*b*), and taking into account the above errors, these masses indicate that all of the objects are likely to be substellar.

Name	I_c	K	T_{eff} (K)	M ($M_\odot$)
CFHT-PL-10	17.82	14.49	2807	0.076
BPL163	17.83	14.53	2787	0.073
INT-PL-IZ-6	17.83	14.53	2787	0.073
INT-PL-IZ-42	17.84	14.36	2872	0.082
CFHT-PL-11	17.91	14.62	2742	0.069
INT-PL-IZ-60	17.99	14.51	2797	0.074
CFHT-PL-12	18.00	14.20	2952	0.087
CFHT-PL-13	18.02	14.54	2782	0.072
BPL327	*18.07*	*14.60*	*2752*	*0.070*
Roque47	18.12	14.67	2717	0.068
INT-PL-IZ-37	*18.16*	*14.36*	*2872*	*0.082*
Roque15	18.21	14.34	2882	0.083
PPL15	18.24	14.41	2874	0.081
BPL316	*18.30*	*14.93*	*2586*	*0.059*
INT-PL-IZ-43	18.41	14.70	2702	0.065
CFHT-PL-15	*18.62*	*14.93*	*2586*	*0.059*
Roque14	18.64	14.47	2817	0.078
CFHT-PL-16	18.66	14.50	2802	0.074
INT-PL-IZ-44	18.67	15.01	2546	0.056
Roque13	*18.67*	*14.56*	*2772*	*0.071*
BPL240	18.75	15.11	2496	0.054
BPL81	*18.79*	*14.98*	*2561*	*0.057*
CFHT-PL-17	18.80	15.07	2516	0.055
Roque12	18.86	14.97	2566	0.058
INT-PL-IZ-29	18.87	14.93	2586	0.059
CFHT-PL-21	19.00	14.91	2596	0.060
BPL306	19.09	15.15	2476	0.052
BPL137	19.22	15.08	2511	0.055
INT-PL-IZ-33	*19.23*	*15.10*	*2501*	*0.054*
CFHTPL-23	19.33	15.25	2426	0.050
Roque9	19.43	15.22	2441	0.051
CFHT-PL-24	19.50	15.47	2315	0.046
Roque8	19.55	15.57	2265	0.044
CFHT-PL-25	19.69	15.47	2315	0.046
INT-PL-IZ-48	19.93	15.54	2280	0.044

INT-PL-IZ-76	*19.96*	*15.32*	*2391*	*0.048*
INT-PL-IZ-55	*20.04*	*15.78*	*2162*	*0.040*
Roque5	20.19	15.74	2180	0.041
INT-PL-IZ-25	20.25	15.52	2290	0.045
Roque36	20.25	16.09	2031	0.037
Roque4	20.25	15.26	2421	0.050
Roque33	*20.44*	*16.02*	*2061*	*0.038*
INT-PL-IZ-20	20.47	15.67	2215	0.042
Roque30	20.82	16.14	2010	0.036
INT-PL-IZ-84	21.12	16.22	1977	0.035
Roque25	*21.80*	*16.31*	*1939*	*0.034*
INT-PL-IZ-81	21.87	16.32	1935	0.033
INT-PL-IZ-69	22.46	16.51	1855	0.031

Table 6.3: The photometric properties for the brown dwarf candidates, with definite non-members (no) and questionable members (?) shown in italics. The effective temperatures and masses are derived from the NEXTGEN models of Baraffe et al. (1998).

The I_C vs $I_C - K$ CMD for the candidates is illustrated in Figure 6.4. As in the previous diagram, definite Pleiades members are shown in black, 'yes?' members are shown in red, candidates with questionable (?) membership properties are shown in green and the definite non-members are shown in blue. The 125 Myr NEXTGEN model of Baraffe et al. (1998) is shown as a dashed line and the 120 Myr DUSTY model of Chabrier et al. (2000) is shown as a dotted line. Since these objects were selected on the basis of the NEXTGEN model (Jameson et al. 2002), the candidates follow the isochrone quite closely until $\sim I_C - K = 4.0$. Beyond this point the candidates are all slightly fainter than the NEXTGEN model predicts, but from $\sim I_C - K = 4.5$ they begin to follow the DUSTY isochrone very closely. This pattern of agreement between the two models and the observational data is as expected, since only the DUSTY models deal with the treatment of dust in the atmosphere, which becomes important as the brown dwarfs get fainter and cooler. Two parts of the binary sequence can also be seen offset above the main sequence around $I_C - K = 4$ and $I_C - K = 4.75$.

The mass distribution of the brown dwarf candidates is illustrated in Figure 6.5, along with $\sqrt{n}$ error bars. Due to small number statistics, few definite conclusions can be drawn from this diagram regarding the behaviour of the mass function. However, in

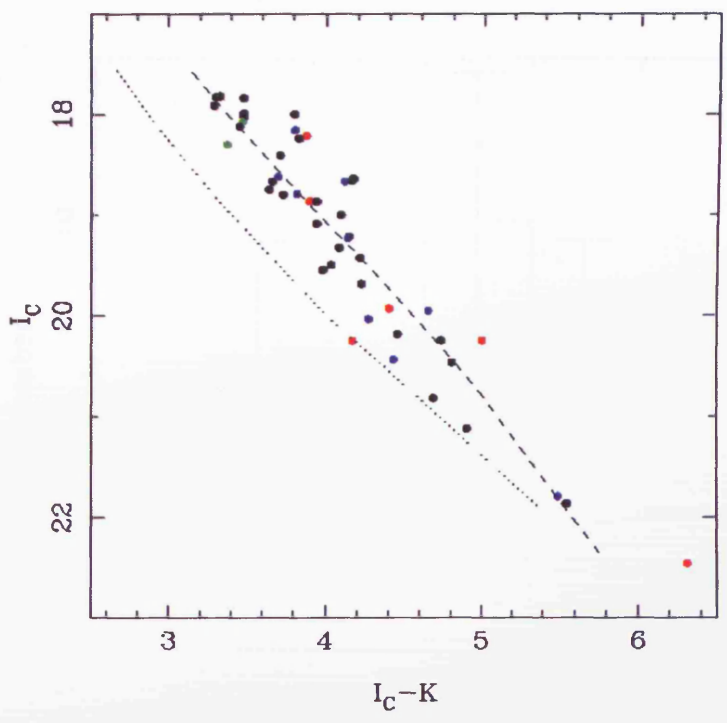

FIGURE 6.4. The I_C vs. I_C-K CMD for the candidates. The definite (yes) Pleiades members are shown in black, the likely ('yes?') members are shown in red, the candidates with questionable (?) membership properties are shown in green and the definite non-members (no) are shown in blue. The 125 Myr NEXTGEN model of Baraffe et al. (1998) is shown as a dashed line and the 120 Myr DUSTY model of Chabrier et al. (2000) is shown as a dotted line.

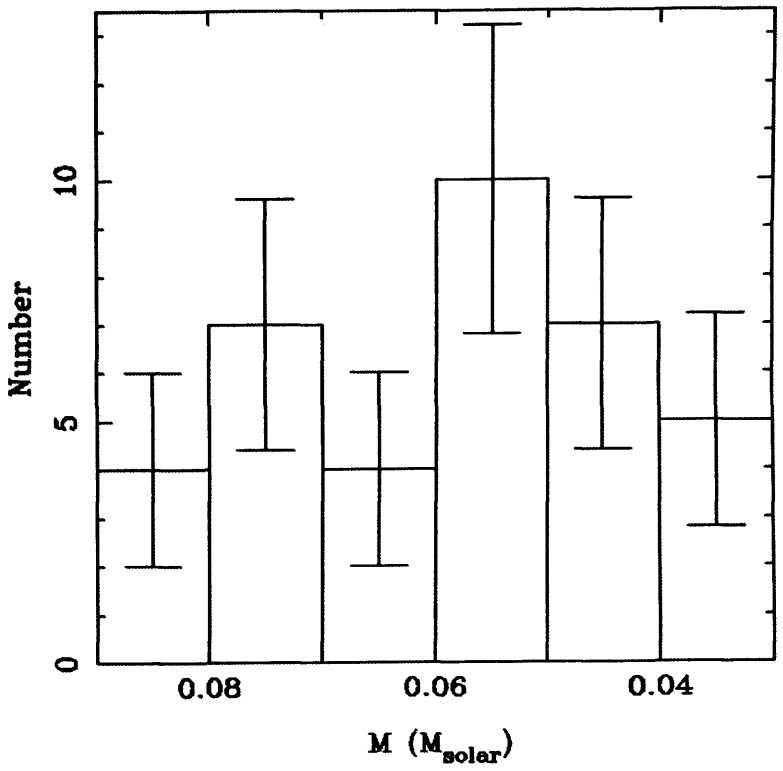

FIGURE 6.5. The observed mass distribution of the Pleiades from the substellar boundary ($0.08_{\odot}$) down to $0.03_{\odot}$.

Name	RA	DEC	$I-K$	Spectral Type
CFHT-PL-10	3 44 32.30	25 25 18.2	3.33	M6
Roque47	3 49 04.80	23 33 40.0	3.45	M7
INT-PL-IZ-43	3 46 23.68	22 50 17.5	3.71	M7.5
CFHT-PL-15	3 55 12.50	23 17 38.0	3.69	M7.5
CFHT-PL-17	3 43 00.10	24 43 52.2	3.73	M7.5
BPL306	3 54 15.22	25 09 51.4	3.94	M8
Roque7	3 43 40.30	24 30 11.0	4.03	M8
INT-PL-IZ-55	3 43 52.04	22 55 24.9	4.26	M8.5
INT-PL-IZ-25	3 43 03.83	23 54 19.7	4.73	L1
Roque30	3 50 16.00	24 08 35.0	4.68	L1
Roque25	3 48 30.60	22 44 50.0	5.49	L3
INT-PL-IZ-69	3 45 14.48	22 29 29.3	5.95	L5

Table 6.4. The names and coordinates of the 12 candidate Pleiades brown dwarfs chosen for spectroscopic follow-up work, along with the $I-K$ colour and the estimated spectral type according to the relations of Kirkpatrick et al. 1999.

general terms the distribution does not rule out the possibilty of a flat or slowly rising MF, and as such does not contradict the expected form of the Pleiades MF (see Section 3.1.3). The distribution may also indicate a small deficit of brown dwarfs in the 0.07-0.06 $M_{\odot}$ mass bin, which corresponds to the expected location of the missing M dwarfs at 0.66 $M_{\odot}$ (Dobbie et al. 2002*c*), although given the large errors involved this may not be a true feature. Finally, the distribution appears to drop away for $M < 0.05\,M_{\odot}$, which is likely due to incompleteness in the survey. Thus the exact form of the MF below $\sim$ 0.05 $M_{\odot}$, and into the planetary mass regime, is still largely undetermined.

6.6 Spectra of Pleiades Brown Dwarfs

Based on the results from the proper motion study of 48 candidate Pleiades brown dwarfs (see Section 6.4), the objects listed in Table 6.4 were selected for follow-up spectroscopic observations. These objects were selected in order to obtain sample spectra across the entire magnitude range covered by the 48 objects, and to further clarify their brown dwarf status. In particular, Roque25 was chosen since no data was available for the proper motion analysis; INT-PL-IZ-69 was chosen since the proper motion analysis was not conclusive, and as the faintest object identified it is particularly interesting; whilst INT-PL-IZ-55 was selected to verify that the 'non-member' results were correct.

6.6.1 Observations and Data Analysis

Spectroscopic observations of the 12 candidate Pleiades brown dwarfs were made by S. Hodgkin on the nights 26-28 December 2002 at UKIRT. The observations primarily made use of the UIST HK grism, although data using the IJ grism was also obtained for four of the targets. Unfortunately the weather conditions during this observation period were quite poor.

The raw data were reduced using the standard routines available with ORAC_DR. Firstly, the *array_tests* recipe was used to generate the bad pixel mask and read-noise measurements required, follwed by the *point_source* recipe which produced a flat-fielded, co-added group image for each object. The spectral extraction was carried out using routines from the STARLINK package FIGARO. After optimally extracting both the positive and negative traces from the group image, and adding these together, each spectrum was de-rippled and then cross-correlated with the standard in order to match up the atmospheric absorption lines. Finally, the spectra were calibrated in terms of both wavelength and flux, and then smoothed and plotted.

However, since the objects were viewed through intermittent thin cloud, the atmospheric water vapour is likely to have varied and this will have affected the flux calibration, particularly between the atmospheric windows. In addition, the signal-to-noise ratio of the spectra is much worse than we had hoped. Although spectra were obtained for four objects (CFHT-PL-10, Roque47, CFHT-PL-15 and BPL306) with the IJ grism, the poor weather conditions combined with the poor performance of the grism below 1 μm resulted in very low quality spectra. Therefore, these spectra have not been included in this thesis.

6.7 Spectroscopic Results

The HK spectra observed for each of the objects listed in Table 6.4 are shown in Figures 6.6 and 6.7. By calculating the $I - K$ colour for each of these objects, their spectral types were estimated using the colour-spectral type relations of Kirkpatrick et al. (1999). These estimates are included in the final column of Table 6.4.

The majority of the spectra show clear H_2O absorption bands around 1.8-2.0μm and 2.4μm, which give rise to the two characteritic 'bumps' visible at 1.7 μm and 2.2 μm. However, in the spectra of the fainter candidates (such as Roque30, Roque25 and INT-PL-IZ-69) the bands become more difficult to distinguish from the noise. The only ex-

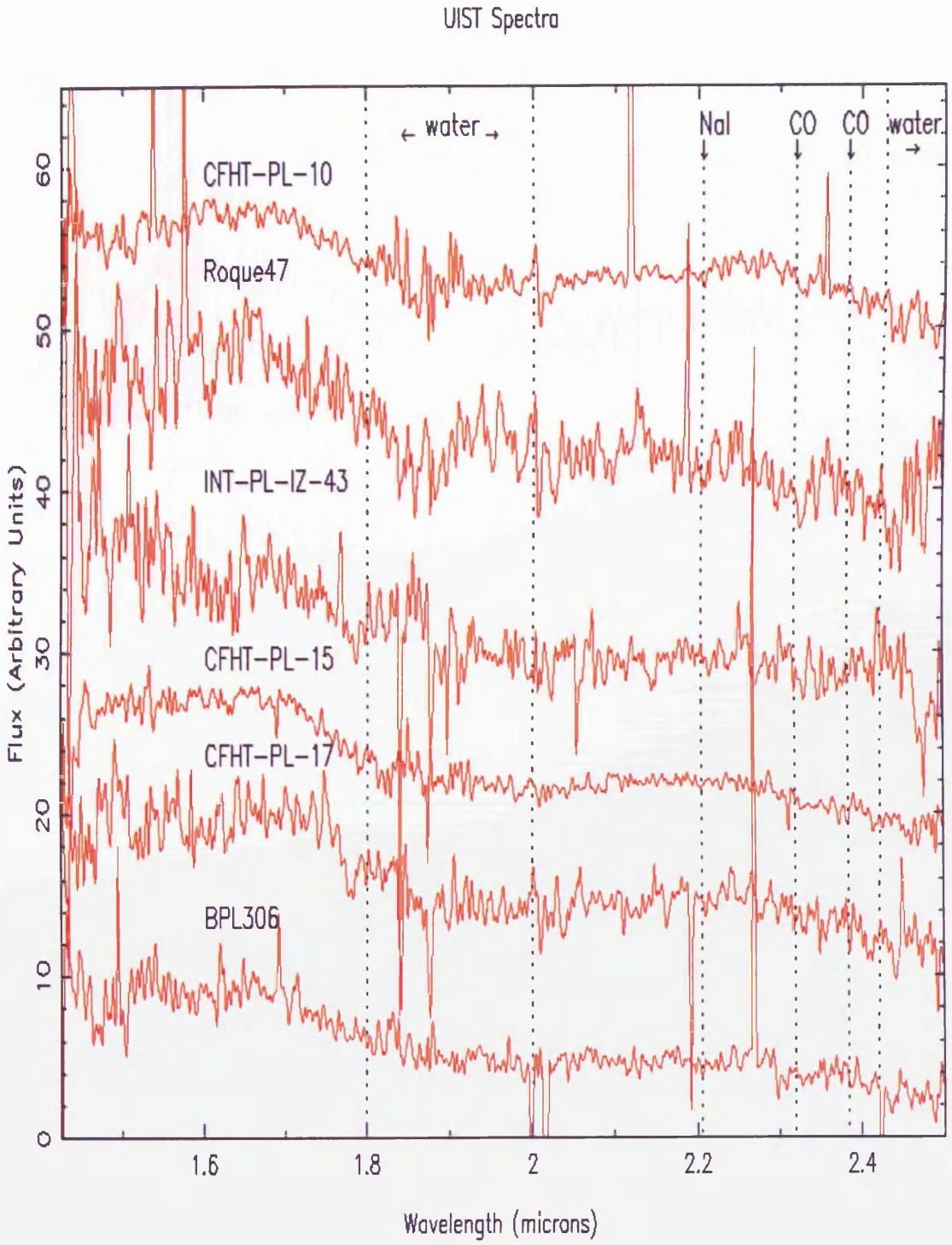

FIGURE 6.6. The UIST HK spectra for the first six objects listed in Table 6.4.

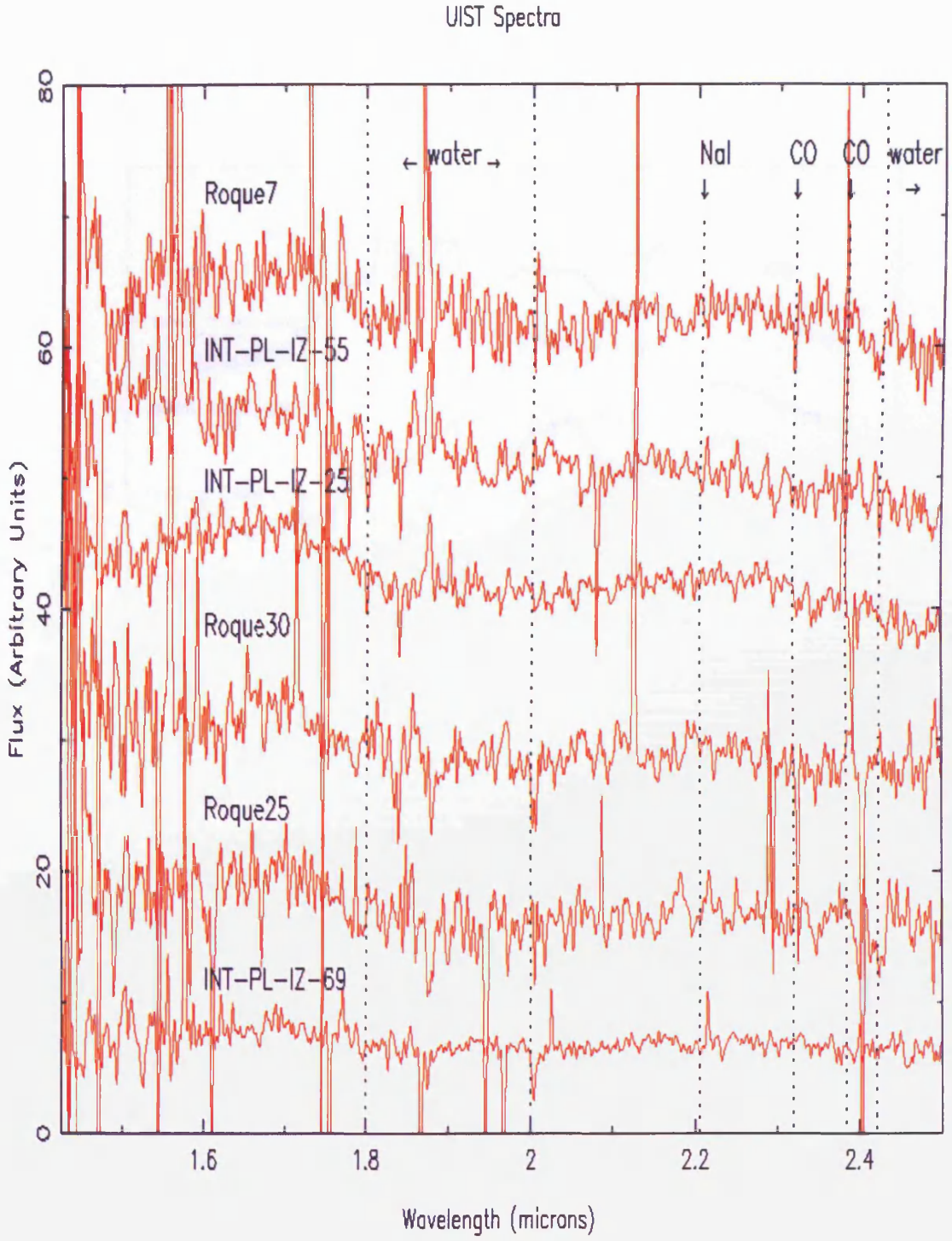

FIGURE 6.7. The UIST HK spectra for the last six objects listed in Table 6.4.

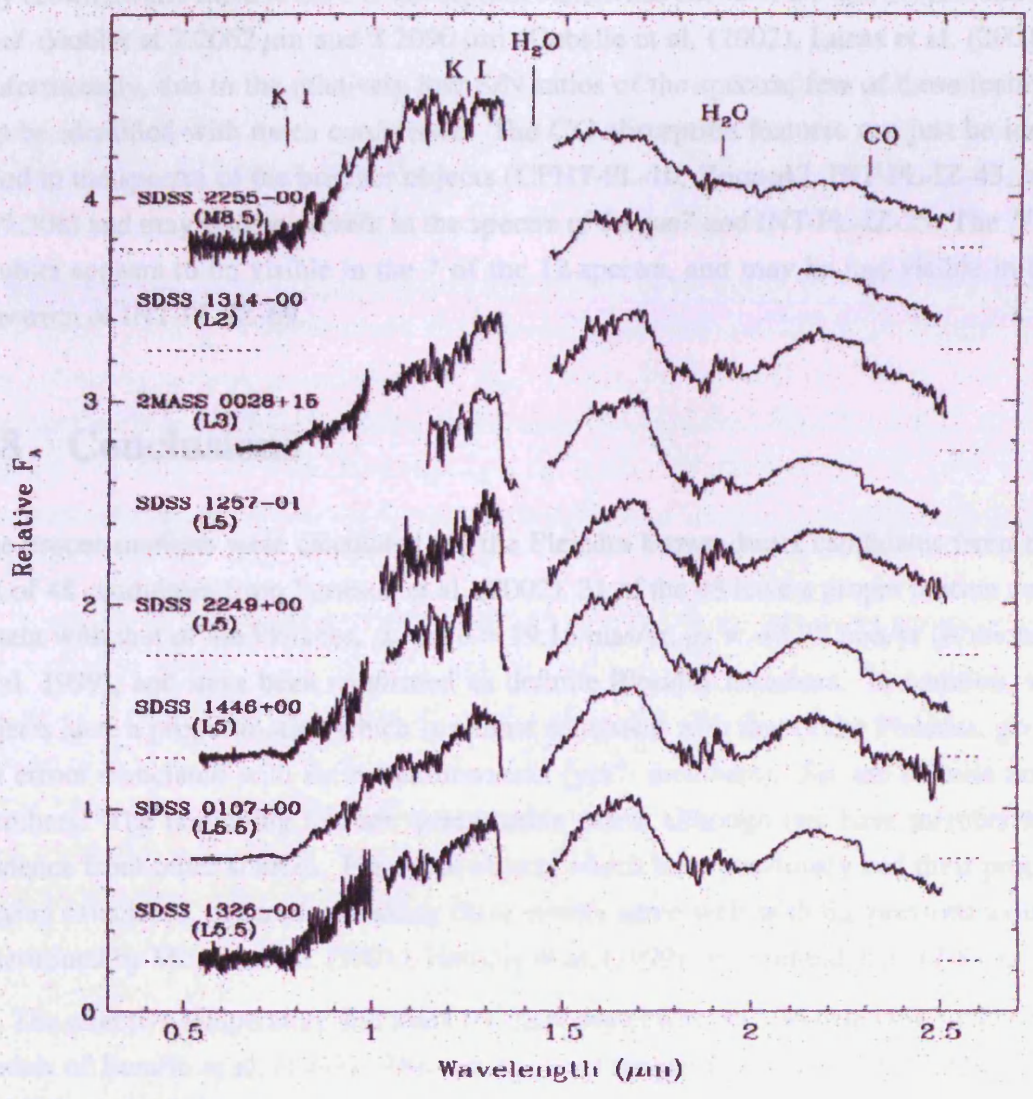

FIGURE 6.8. Example late M and ealy L standard spectra from the classification scheme of Geballe et al. (2002).

ceptions to this are INT-PL-IZ-55, whose spectrum shows no evidence for the water vapour bands, and INT-PL-IZ-43, whose spectrum could possibly contain the bands. Example late M and ealy L standard spectra from the classification scheme of Geballe et al. (2002) are shown for comparison in Figure 6.8.

The other key spectral features in this waveband which are used to identify and classify brown dwarfs include the CO absorption bandheads between 2.3 and 2.4 μm and the NaI doublet at 2.2062 μm and 2.2090 μm (Geballe et al. (2002), Lucas et al. (2001)). Unfortunately, due to the relatively low S/N ratios of the spectra, few of these features can be identified with much confidence. The CO absorption features can just be identified in the spectra of the brighter objects (CFHT-PL-10, Roque47, INT-PL-IZ-43, and BPL306) and may also be present in the spectra of Roque7 and INT-PL-IZ-25. The NaI doublet appears to be visible in the 7 of the 12 spectra, and may be just visible in the spectrum of INT-PL-IZ-69.

6.8 Conclusions

The proper motions were calculated for the Pleiades brown dwarf candidates from the list of 48 candidates from Jameson et al. (2002). 31 of the 48 have a proper motion consistent with that of the Pleiades, $\mu_\alpha \cos\delta$ = 19.15 mas/yr, μ_δ = -45.72 mas/yr (Robichon et al. 1999), and have been confirmed as definite Pleiades members. In addition, six objects have a proper motion which is almost consistent with that of the Pleiades, given the errors associated with their measurements (yes? members). Six are definite non-members. The remaining five are questionable cases, although two have membership evidence from other sources. For those objects which have previously had their proper motion calculated, generally speaking these results agree well with the previous values determined by Moraux et al. (2001), Hambly et al. (1999) and Pinfield et al. (2000).

The effective temperature and mass for each object was derived using the NEXTGEN models of Baraffe et al. (1998). The values found ranged from 2952 K to 1855 K, and 0.087$M_\odot$ to 0.031$M_\odot$ respectively, which given the estimated errors ($\pm$ 0.015 $M_\odot$) and the uncertainties associated with the theoretical models confirms them all as substellar. We have also plotted the I_C vs $I_C - K$ CMD for the candidates, which clearly illustrates the cluster sequence, and part of the binary sequence. The diagram also highlights the differences between the NEXTGEN (Baraffe et al. 1998) and DUSTY (Chabrier et al. 2000) models. For the brightest objects there is good agreement with the NEXTGEN model, whereas for the fainest objects the agreement is better with the DUSTY model. However,

in the region between these two extremes there is little agreement with either model which indicates that there is still much work to be done in the area of brown dwarf evolutionary models.

From the plot of the mass distribution (Figure 6.5), little can be concluded for certain due to the effects of small number statistics. However, the distribution does not preclude a flat or slowly rising mass function, and thus does not contradict any previous estimate of the Pleiades IMF (Jameson et al. (2002), Martín et al. (2000), Bouvier et al. (1998)). In order to constrain the form of the IMF further more brown dwarfs need to be identified within the Pleiades so as to increase the number statistics. In addition, evidence for the missing M dwarfs (Dobbie et al. 2002*c*) is illustrated by the apparent deficit of brown dwarfs between 0.06 and 0.07 $M_{\odot}$.

Spectra in the HK waveband were obtained for 12 of the candidates listed in Jameson et al. (2002). Many of these spectra display absorption features which are typical of M and L dwarfs, such as the presence of H_2O bands and CO and NaI lines, and thus confirm the status of genuine brown dwarf members identified from the proper motion analysis. It should be noted that although the quality of these spectra is poor, when compared to standard benchmark spectra such as those of Geballe et al. (2002), the broad spectral properties can be readily identified.

In particular, the spectrum of INT-PL-IZ-43 does not show clear water vapour bands, but may show evidence for the NaI doublet, which when combined with its proper motion consistent with that of the Pleiades allows this object to still be considered a member of the cluster. The spectrum of INT-PL-IZ-55 does not show any evidence of any of the typical brown dwarf features, which re-confirms its status as a non-member. In addition, this null result suggests that the proper motion method used in this analysis is indeed a reliable indicator of membership status. Finally, the spectrum of CFHT-PL-15 looks like that of a brown dwarf , but it has been ruled out as being a member of the Pleiades on the basis of its proper motion, in contrast to the previous proper motion calculation of Moraux et al. (2001). Therefore, this object is most likely a field brown dwarf. This indicates that spectroscopy is not a fail-safe method for which to confirm Pleiades brown dwarfs.

Finally, the spectral types were estimated for these 12 objects, and were found to lie between M6 and L3 (see Table 6.4). These results indicate that all of these objects are substellar in nature, given that the stellar/substellar limit lies at a spectral type of M6.5 $\pm$ 0.5 for the age of the Pleiades (Martín, Basri & Zapatero-Osorio 1999). The only exception to this is INT-PL-IZ-55, which does not appear to be either a member of the cluster or a brown dwarf, and therefore must be some type of contaminating background

object, such as a distant, reddened galaxy. Overall, the analysis of these 12 spectra has not changed the membership status for any of the objects, and thus the results as revealed by the proper motion study remain unchanged.

Chapter 7

A Large Scale Survey of the Hyades

This chapter presents the results of an $\sim$ 800 square degree survey of the Hyades cluster, using data obtained from online catalogues. Firstly, data from the United States Naval Office (USNO) B1.0 arhcive were rigorously searched for candidates with a proper motion consistent with that of the Hyades. The J, H and K magnitudes for these candidates were then retrieved from the 2MASS data archive, and a photometric selection procedure was carried out. The same procedure was also applied to a *control cluster*, a hypothetical cluster with a proper motion in the opposite direction to the Hyades, to allow the level of contamination from background stars to be estimated. Finally, the kinematic properties of the cluster were investigated.

7.1 The Hyades Cluster

Of all the stellar clusters that have been studied in recent years in the search for brown dwarfs, the Hyades is one of the closest, at a distance of only 46.3 pc (Perryman et al. 1998), and also one of the oldest, with an age of around 625 Myrs (Perryman et al. 1998), although estimates for the age of the cluster vary between 500 Myrs and 900 Myrs. These two factors make it quite difficult to search for brown dwarfs in the Hyades, due to the large area of sky covered by the cluster, and the fact that any brown dwarfs in the cluster will have had time to cool significantly and, therefore, be very faint. Thus surveys have to find a happy medium between covering a sufficiently large area of the cluster and observing to a satisfactory depth.

Despite these difficulties, the Hyades is a fairly well studied cluster, with several relatively small scale surveys concentrating on identifying the low mass and substellar

members of the cluster having been carried out: (Reid 1993); (Gizis et al. 1999); (Dobbie et al. 2002*a*). However, the cluster has yielded few low mass members, and no bone fide substellar members have been identified to date. The precise reason for this apparent deficit of low mass members, when compared to other clusters such as the Pleiades and σ Orionis, is still under debate.

To date there has not been a systematic survey of the entire cluster, out to the tidal radius ($r_t \sim 10$ - 10.5 pc (Perryman et al. 1998)), with the aim of accurately describing its low mass population.

7.2 Data Acquisition and Analysis

All of the data used in this work on the Hyades was obtained from online archives, namely the United States Naval Office (USNO) B1.0 database containing the results of the two Palomar Sky Surveys, and the NASA Infra-Red Science Archive containing the results of the Two Micron All Sky Survey.

7.2.1 The Palomar Sky Surveys

The Palomar Sky Surveys were carried out on the 48 inch (1.2 m) Oschin Schmidt Telescope, which is located on Palomar Mountain in California at an altitude of 1700 m. The telescope has a 72 inch primary mirror, and a correcting plate with a clear aperture of 49.5 inches. The telescope utilises a mirror plus corrector plate to create a large field of view (6.6 square degrees), and this set-up allows large areas of sky to be observed at one time, making the telescope particularly suited for all-sky surveys.

The first Palomar Observatory Sky Survey (POSS I) was carried out during the 1950's, and obtained photographic data in both the red and blue wavebands by using Kodak 103a-E and 103a-O emulsions on the plates. Each Schmidt plate measured 14 inches, and the entire northern celestial hemisphere, and part of the southern celestial hemisphere to a declination limit of -33°, was able to be covered using only 935 plate pairs. For a detailed description of POSS I see Minkowski & Abell (1963).

The next 20 years saw many technological advances, and in the late 1970's the UK Schmidt Telescope carried out a survey of the southern sky. In order to complement this survey, the second Palomar Observatory Sky Survey (POSS II) was begun in the late 1980's, after the Oschin telescope had received several upgrades. POSS II photographed the sky in three wavebands: in blue using a IIIa-J emulsion, in red using a IIIa-F emulsion

and in the near infrared using a IV-N emulsion. Since other surveys covered the entire southern celestial hemisphere, POSS II was confined to the northern hemisphere and was thus able to be completed using 897 fields. For a complete description of POSS II see Reid et al. (1991).

When taken together the POSS I and POSS II data sets enable changes in the sky over a period of 30 years to be observed. In recent years both sets of data have been digitized and made available on the internet.

7.2.2 USNO B1.0 Data

Data from both POSS I and POSS II were retrieved from the USNO-B1.0 catalogue for 208 2° × 2° fields (the maximum field size for catalogue searches), which covered the entire Hyades cluster out to the tidal radius. The fields were arranged on a radial grid pattern, beginning near the bright stars of the Hyades constellation at the centre of the cluster ($04^h\ 26^m\ 54^s$, +15° 52′ 00″). This area of sky covered 38 of the original POSS II plates (see Figure 7.1). Each field contained around 40,000 objects, giving around 8,000,000 objects detected in total over the entire survey. The key data obtained for each object included equatorial coordinates, proper motion components in RA and DEC, and B, R and I magnitudes, along with the corresponding error for each value.

7.2.3 The Two Micron All Sky Survey

The last large scale near infrared survey of the entire sky was conducted by G. Neugebauer and R. B. Leighton in 1969 (Neugebauer & Leighton 1969). Since that time there have been vast improvements in infrared detector technology and so the Two Micron All Sky Survey (2MASS) project was begun in 1997 to provide a new infrared, all-sky database with a much greater level of sensitivity and accuracy. The survey was carried out using two highly automated telescopes: one located at Mount Hopkins in Arizona, and the other locted at CTIO in Chile. Each telescope had a 1.3 m mirror and used a three-channel detector, with each channel containing a 256x256 $HgCdTe$ infrared array. This set-up allowed observations at J, H and K_s (see Figure 7.2 for the filter transmission profiles) to be made simultaneously using dichroic mirrors. The survey was completed in February 2001, and the final all-sky data release was made in late 2002.

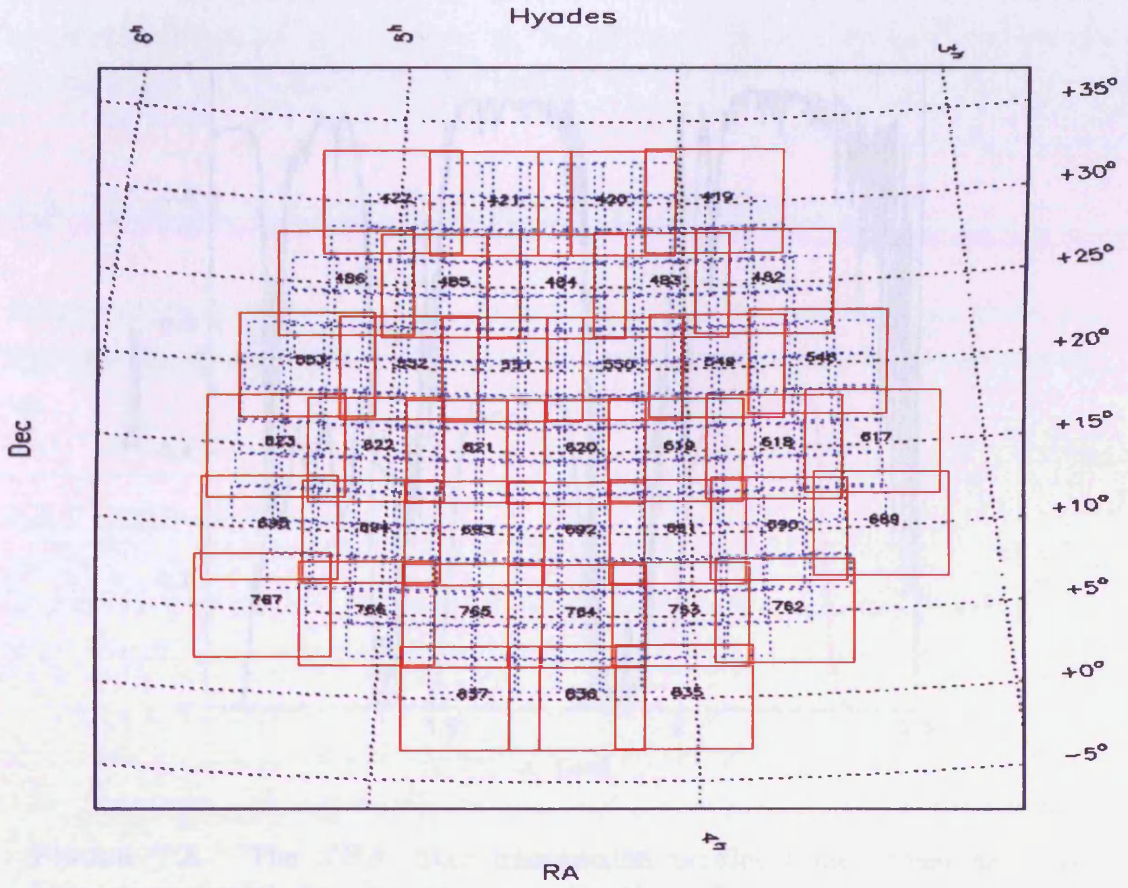

FIGURE 7.1. The fields extracted from the USNO-B1.0 archive. The 208 2° × 2° catalogue fields are shown by dotted blue boxes, whilst the fields covered by the original POSS II plates are shown as solid red boxes.

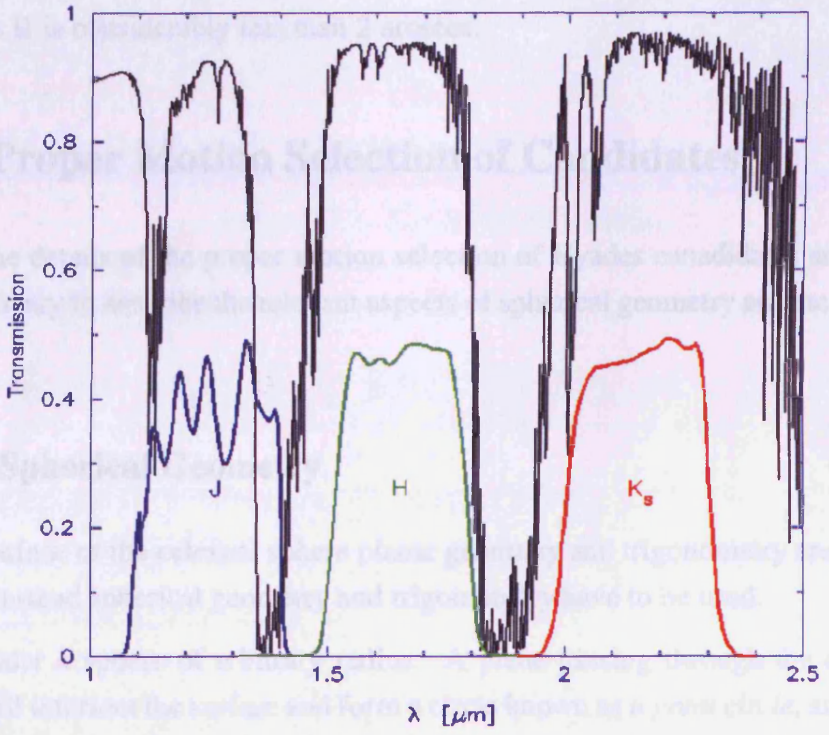

FIGURE 7.2. The JHK filter transmission profiles (blue, green and red lines respectively) for 2MASS as a function of wavelength through the 2MASS optical path, which includes the telescope mirror reflectivity, dewar window, anti-reflection coating, dichroics, filters and the NICMOS detector QE. Model atmospheric transmission is shown in black. Image from www.ipac.caltech.edu/2mass/releases/second/doc/figures/secvi3f1.gif.

7.2.4 2MASS Data

Using the Gator interface provided by the NASA Infra-Red Science Archive, the coordinate tables of the proper motion selected candidates (see following section) for both the Hyades cluster and the control cluster were uploaded to the database in order to retrieve the J, H and K magnitudes. Each object was cross-matched with the catalogue sources to within a radius of 2 arcsecs, which is a large enough radius to overcome any positional errors, but which is also small enough to minimise double-up matches. It should be noted here that the Hyades proper motion difference between the epochs of 2MASS and POSS II is considerably less than 2 arcsecs.

7.3 Proper Motion Selection of Candidates

Before the details of the proper motion selection of Hyades canadidates are given, it is first necessary to describe the relevant aspects of spherical geometry and stellar kinematics.

7.3.1 Spherical Geometry

On the surface of the celestial sphere planar geometry and trigonometry are not applicable, and instead spherical geometry and trigonometry have to be used.

Consider a sphere of arbitrary radius. A plane passing through the centre of the sphere will intersect the surface and form a circle known as a *great circle*, and the arcs of three such circles will form a *spherical triangle*, as shown in Figure 7.3. The following formulae can be applied to spherical triangles:-

The Cosine Rule

$$\cos a = \cos b \cos c + \sin b \sin c \cos A. \tag{7.1}$$

The Sine Rule

$$\frac{\sin a}{\sin A} = \frac{\sin b}{\sin B} = \frac{\sin c}{\sin C}. \tag{7.2}$$

The Four Parts Formulae

$$\cos a \cos B = \sin a \cot c - \sin B \cot C. \tag{7.3}$$

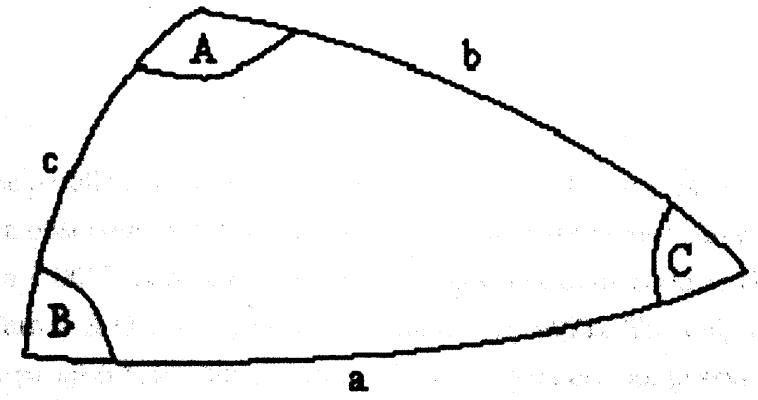

FIGURE 7.3. The spherical triangle.

The Cosine Angle Formula

$$\cos a = \frac{\cos A + \cos B \cos C}{\sin B \sin C}. \tag{7.4}$$

Information collected from Carroll & Ostlie (1996).

7.3.2 Stellar Kinematics

Stellar kinematics is the study of the motion of stars. When observed from Earth, a star can have both an apparent and an intrinsic motion, depending upon its distance. Stars which are gravitationally associated in a cluster also have a distinct group motion.

Stellar Parallax

For nearby stars the motion of the Earth about the Sun creates an apparent stellar motion known as *parallax*, whereby such stars exhibit a small elliptical motion relative to the stationary background of more distant stars. This motion allows the distance to the star to be calculated by using triangulation; the angular distance to the star is measured at least three times, separated by 6 month intervals, creating a baseline equal to the diameter of the orbit of the Earth. The third measurement is needed to remove the proper motion of the object (see next section). In practice, parallax measurements should be made

approximately monthly, except when obscured by the Sun. The distance in parsecs, d, to a nearby star is given by:

$$d = \frac{1}{p''}, \tag{7.5}$$

where p'' is the parallax angle measured in acrsecs. Parallax angles are always less than $1''$. Even when observed from telescopes in orbit, parallax angles can only be measured to greater than $0.001''$, corresponding to distances less than 1000 pc (information collected from Carroll & Ostlie (1996) and Zeilik et al. (1992)). The only exception to this is when maser parallaxes are measureded, allowing distances out to several kpc to be determined. For example, the distance to UX Cygni (Kurayama, Sasao & Kobayash 2005) and IC 133, in the galaxy M33 (Argon et al. 2004), have both been found using this method.

Intrinsic Motion

Because all stars in the Galaxy are in orbit around the galactic centre, they have an intrinsic space velocity. When observed from Earth, this motion has two components: a radial velocity along the line of sight and a transverse velocity along the celestial sphere. The radial velocity can be determined by measuring the Doppler shifts of spectral lines, whilst the transverse velocity can be measured by making two observations of the star, separated by a time interval of several years.

The transverse velocity, v_t, appears as a slow, angular change in the star's equatorial coordinates, and is known as the *proper motion.* It can be split into RA and DEC components on the celestial sphere. The star's proper motion, μ, is related to its transverse motion by:

$$\mu = \frac{v_t}{4.74d}\, arcsec/year. \tag{7.6}$$

where v_t is measured in km/s, and d is the distance to the star, measured in parsces. Information collected from Carroll & Ostlie (1996).

The Moving Cluster Method

By studying the motions of stars in stellar clusters the distance to the cluster can be determined by using a method known as the *moving cluster method.* The stars in a stellar

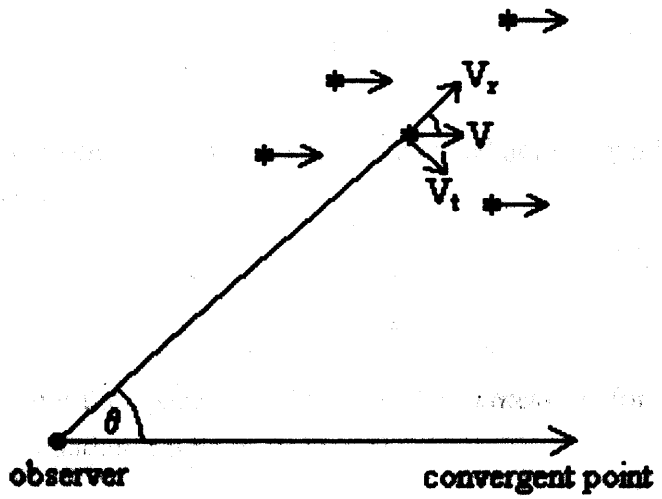

FIGURE 7.4. The geometry of the moving cluster method.

cluster are gravitaionally bound to one another, and so move through space together, with a single bulk velocity. If the change in postion over time is measured for numerous members of a cluster, then the direction of motion of the cluster can be determined. The proper motions of the stars give the appearance that they are all heading towards a single point in space, known as the *convergent point.*

Consider the geometry illustrated in Figure 7.4. The angle, θ, between the cluster and the convergent point is the same as the angle between the line of sight to the cluster and the space velocity of the star. If the space velocity is v, then the transverse and radial velocities are given by:

$$v_t = v \sin\theta \tag{7.7}$$

and

$$v_r = v \cos\theta. \tag{7.8}$$

The two components are related by:

$$v_t = v_r \tan\theta. \tag{7.9}$$

Combining Equation 7.7 with the relationship between a star's tranverse velocity and its proper motion (Equation ??) allows the distance to the star to be calculated:

$$d = \frac{v \sin\theta}{\mu}. \tag{7.10}$$

When d, v and μ are given in their more commonly used units of pc, km/s and arcsec/yr, this equation becomes:

$$d = \frac{v \sin\theta}{4.74\mu''}. \tag{7.11}$$

Finally, by substituting the space velocity with the expression for the radial velocity (Equation 7.8), this equation can be re-written as:

$$d = \frac{v_r \tan\theta}{4.74\mu''}, \tag{7.12}$$

and since v_r, θ and μ'' are all measurable quantities the distance for any star in the cluster can be found. However, once v has been determined for the cluster, Equation 7.11 is a quick way to find the distance of each cluster member. Information collected from Carroll & Ostlie (1996).

7.3.3 Proper Motion Selection Procedure

The proper motion of the Hyades cluster is very large compared to that of other stars, with an average annual proper motion of ~ 110 mas/yr (Reid 1993), and so cluster members are easily recognisable. This fact was utilised in the first step of the proper motion selection process, where potential members were selected on the basis of their position in the proper motion (PM) diagram (see Figure 7.5). If an object lay within the red box, then it was selected as a potential cluster member.

The boundary of this box was calculated by considering the extreme values of the direction and magnitude of the proper motion of the cluster. By using spherical trigonometry (Equations 7.1 and 7.4), and assuming that the cluster ranges in declination between 1.5° and 31.5°, the direction of the proper motion was found to lie between 75.17° (southern tip) and 120.76° (northern tip). By using Equation 7.11 and assuming the cluster lies at a distance between 32 and 60 pc the proper motion of the cluster was found to range between 98 and 184 mas/yr in the direction of the northern tip and between 87

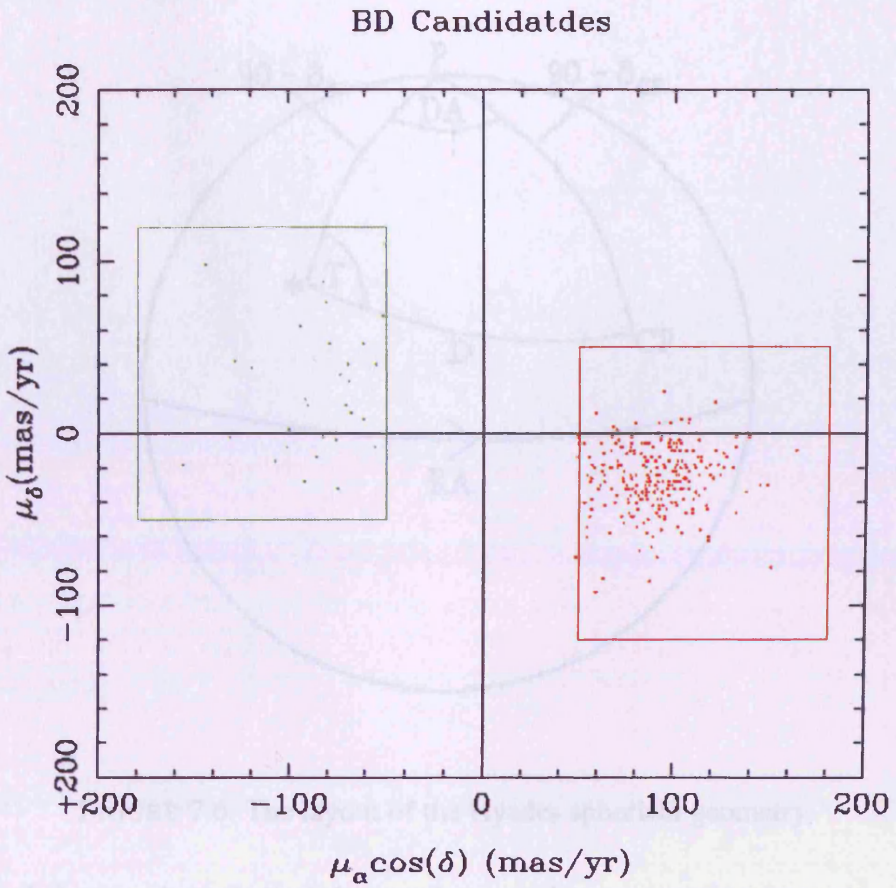

FIGURE 7.5. The proper motion regions used for the initial selection of cluster members in the Hyades (red box) and the control cluster (green box).

and 164 mas/yr in the direction of the southern tip. These extreme ranges defined a segment in the proper motion diagram which was then generously bounded by a rectangle covering $+50 \leq \mu_\alpha \leq +180$ and $+45 \geq \mu_\delta \geq -120$ so as to account for any objects with significant observational errors. Obviously if genuine Hyades members with properties beyond those stated here in the assumptions do exist then they are likely to be excluded from this analysis and thus may create a slight bias in the results. However, the generosity of the initial assumptions, and the extra allowance created by the use of the rectangular box rather than just the calculated segment, should avoid any systematic exclusions from the selection process.

This initial selection procedure reduced the number of objects to around 50,000. In order to determine the level of contamination from reddened background field stars in our survey, we also selected objects which had a proper motion in exactly the opposite direction to that of the Hyades (green box in Figure 7.5). This group of objects became

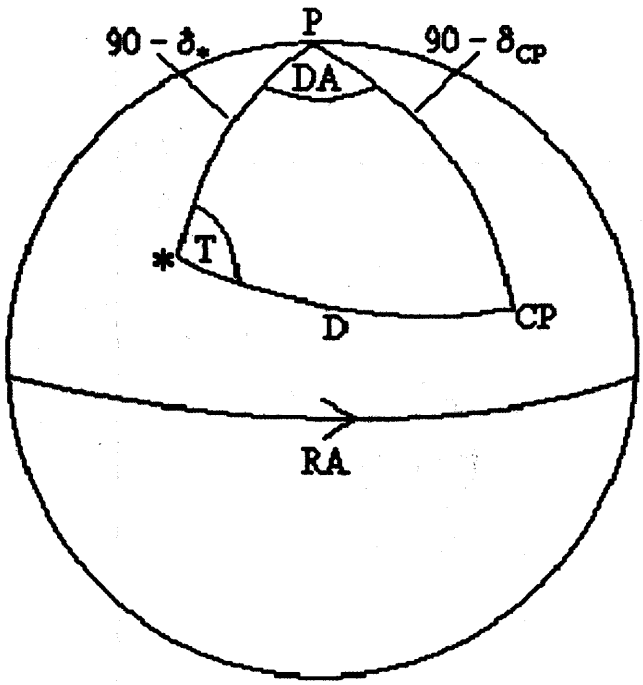

FIGURE 7.6. The layout of the Hyades spherical geometry.

our *control cluster*, a hypothetical cluster of stars with proper motion properties opposite to those of the Hyades, but the same convergent point ($\alpha_{cp} = 94.2°$ and $\delta_{cp} = 7.6°$ (Hanson 1975)).

Since the Hyades covers a large area of sky and all the proper motion vectors point to the convergent point, each member has its own proper motion direction. Thus the list of candidates was further refined by comparing the observed direction of the proper motion with the calculated direction. Using the cosine rule (Equation 7.1) from spherical trigonometry the direction of the proper motion, T, measured East from North, of an object with coordinates $\alpha_\star$ and $\delta_\star$, can be calculated (see Figure 7.6):

$$\cos T = \frac{\sin \delta_{cp} - \sin \delta_\star \cos D}{\cos \delta_\star \sin D}, \tag{7.13}$$

where D is the angular distance of the star from the convergent point, given by:

$$\cos D = \sin \delta_\star \sin \delta_{cp} + \cos \delta_\star \cos \delta_{cp} \cos DA, \tag{7.14}$$

and the angle DA is given by:

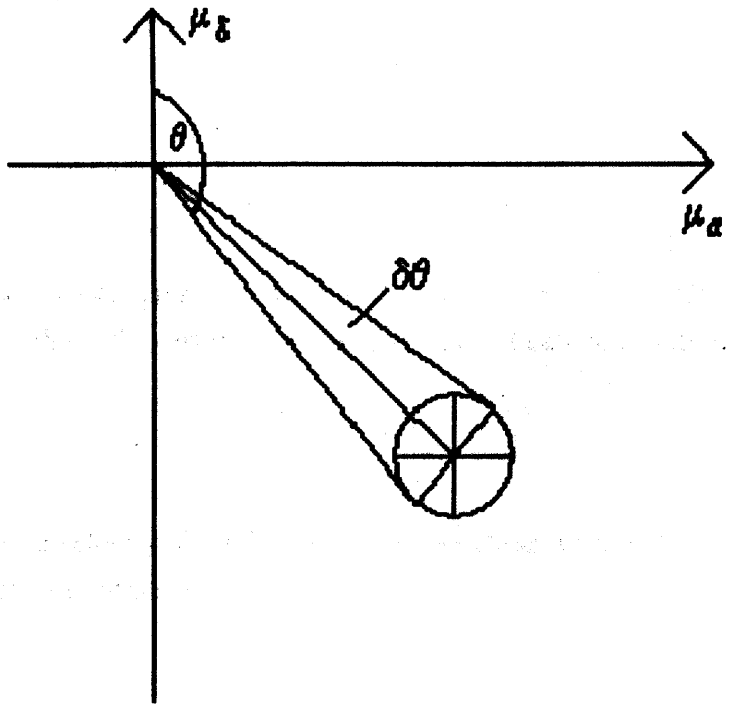

FIGURE 7.7. An illustration of the error, dθ, associated with the observed direction of the proper motion, θ.

$$DA = \alpha_{cp} - \alpha_{\star}. \tag{7.15}$$

The observed direction of the proper motion of an object, θ, can be calculated from:

$$\theta = \tan^{-1}\left(\frac{\mu_\alpha}{\mu_\delta}\right), \tag{7.16}$$

where μ_α and μ_δ are the right ascension and declination components of the proper motion respectively. The error, dθ, associated with this observed angle can be found using:

$$d\theta = \frac{3(\Delta\alpha^2 + \Delta\delta^2)^{1/2}}{(\mu_\alpha^2 + \mu_\delta^2)^{1/2}}, \tag{7.17}$$

where $\Delta\alpha$ and $\Delta\delta$ are the errors in the proper motion (see Figure 7.7). The factor of 3 is included to avoid losing any potential members (3σ includes 97% of normal distribution).

Once these calculations had been performed, candidates were selected if, and only if, the following selection criteria were satisfied for the actual Hyades members and the

control cluster members respectively:

$$\theta - d\theta \leq T \leq \theta + d\theta. \tag{7.18}$$

$$\theta - d\theta \leq T + \pi \leq \theta + d\theta. \tag{7.19}$$

Since the space velocity, relative to the Sun, is well known for the Hyades (v=46.7 km/s, (Detweiler et al. 1984)), the distance to any given object can be calculated by:

$$d = \frac{v \sin D}{4.74\mu}, \tag{7.20}$$

where v is the space velocity of the Hyades, D is as defined in Equation 7.14 and μ is the total proper motion of the object, given by:

$$\mu = \sqrt{\mu_\alpha^2 + \mu_\delta^2}. \tag{7.21}$$

Finally, potential Hyades and control cluster members were selected if they lay at an appropriate distance, i.e. if the following criterion was satisfied:

$$32\,pc \leq d \leq 60\,pc. \tag{7.22}$$

These distances were chosen given that the cluster lies at a distance of 46 pc and has a tidal radius of 10 pc. A further 4 pc was included to cover any errors.

This proper motion selection procedure reduced the number of candidates to around 13,000. All of the above steps were also carried out on the objects in the control cluster, so that the two groups could be compared fairly.

7.4 Photometric Selection of Candidates

Following the cross-correlation of the proper motion selected candidates with the 2MASS database, the number of candidates was reduced further still, down to about 2,000, since the vast majority of the objects from the initial selection were too faint and blue to be detected in the infrared by 2MASS .

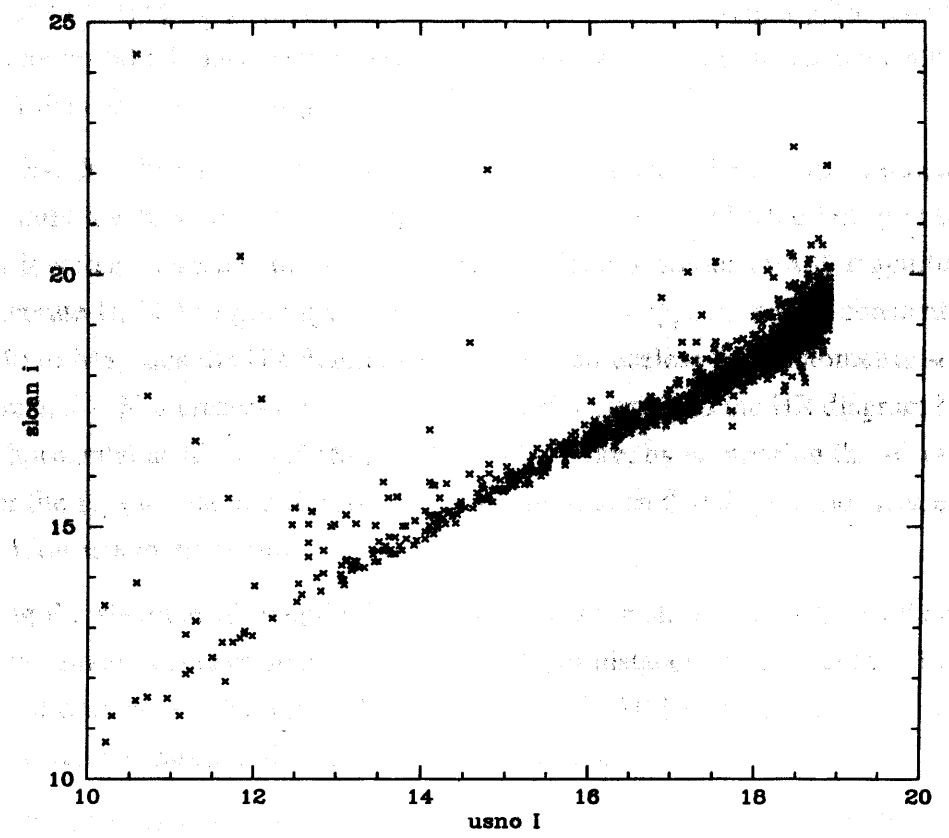

FIGURE 7.8. A comparison of USNO and SDSS I magnitudes. Diagram by S. Casewell (private communication).

Using the photometric data collected from POSS I , POSS II and 2MASS , several colour-magnitude diagrams (CMDs) were plotted. From these plots the candidate list was refined further through the rejection of objects which did not lie on or near the Hyades cluster sequence. It should be pointed out that, although the USNO proper motions are acurate, the photometry is quite poor, especially towards fainter magnitudes. This point is illustrated in Figure 7.8, which compares the USNO and SDSS magnitudes for a test area of sky. For relatively bright I magnitudes (≤ 13), the correlation between USNO and SDSS magnitudes is good, but towards fainter magnitudes this correlation becomes much weaker, with USNO magnitudes of $I \sim 16$ and above having an error of ± 0.5, or worse, when compared to the SDSS magnitudes.

The K vs $B-K$, K vs $R-K$, K vs $I-K$ and K vs $J-K$ colour-magnitude diagrams, and the $H-K$ vs $J-H$ colour-colour diagram are shown in Figures 7.9, 7.11, 7.13, 7.15 and 7.17, along with the same CMDs of the control cluster for comparison

(Figures 7.10, 7.12, 7.14, 7.16 and 7.18). In these plots K is used as the ordinate, since being a 2MASS magnitude it is more accurate than the POSS magnitudes. The red dots are candidates which have been selected as Hyades or control cluster members, whilst the black dots are background stars.

The Hyades cluster main sequence (red dots) can clearly be identified on each plot. At first sight the K vs $J-K$ (see Figure 7.15) plot seems to be the best plot to use to identify low mass stars and brown dwarfs since it uses accurate 2MASS magnitudes and no inaccurate USNO magnitudes. However, $J-K$ is approximately constant at 0.95 from M0 to M8, thus the HR diagram is vertical and useless for photometric selection. In contrast, $J-K$ increases rapidly in the L dwarf regime, and the HR diagram becomes almost horizontal at $K \sim 14.5$ ($M_K = 11.2$). Therefore, by comparing the K vs $J-K$ plots for the Hyades and the control cluster it can be seen that there is no clear evidence for any L dwarfs in the Hyades.

Using the absolute K magnitude from the known distance of each member should reduce the main sequence scatter due to the depth-distance effect (depth ± 10 pc at a distance of only 46 pc). However, the poor B, R and I USNO magnitudes result in poor colours which increase the scatter of the main sequence.

The clearest separation between the Hyades members and the field stars/spurious objects is in the K vs $R-K$ diagram (see Figure 7.11). Hyades members are selected to be those which lie above the clear gap in this diagram. The candidates are then plotted as red dots in this, and the other CMDs, which confirm the membership selection. This selection procedure reduced the number of candidates to 260.

The K vs $I-K$ CMD (see Figure 7.13) is the most sensitive to low mass objects, since $I-K$ is the longest colour that can be determine from the available photometry, at which significant flux levels can be measured (the blackbody function of a brown dwarf peaks in the infrared regime, therefore little energy is emitted in the B and R wavebands and the brown dwarf may not be detectable). From this CMD the clear end to the Hyades sequence is very evident (at around $I-K=4$), as it can be seen that the locus of points of main-sequence objects (red dots) does not meet the band of spurious objects (black dots). The end of the sequence is also not limited by the 2MASS K or USNO I magnitude limits. Thus it is clear that there are no very low mass Hyads.

Prior to this work, the most substantial and comprehensive list of Hyades members was compiled by Reid (1993). This list contained all of the previously known main-sequence members and all of the low mass members identified from the 110 square degrees surveyed, complete to $V=19$. Therefore, in order to produce a complete list of

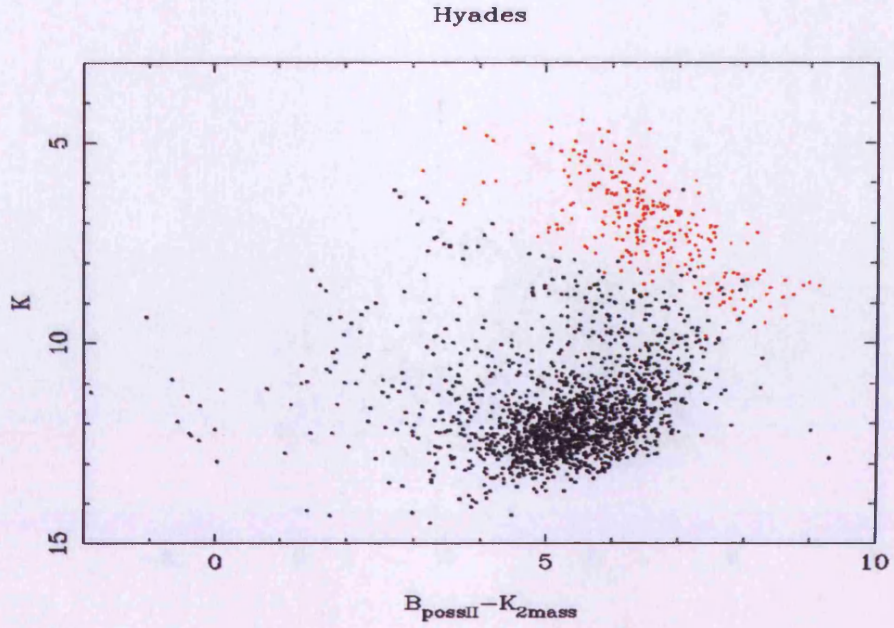

FIGURE 7.9. The K (absolute) vs $B-K$ CMD for the Hyades candidates identified from the proper motion selection. Photometrically selected members are shown as red dots, whilst background stars are shown as black dots.

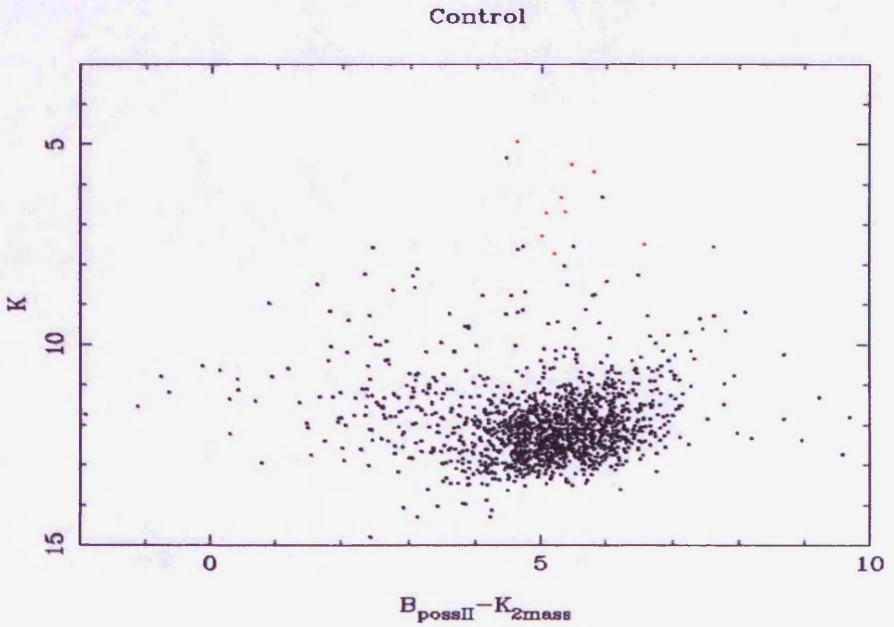

FIGURE 7.10. The K (absolute) vs $B-K$ CMD for the control cluster candidates identified from the proper motion selection. Photometrically selected members are shown as red dots, whilst background stars are shown as black dots.

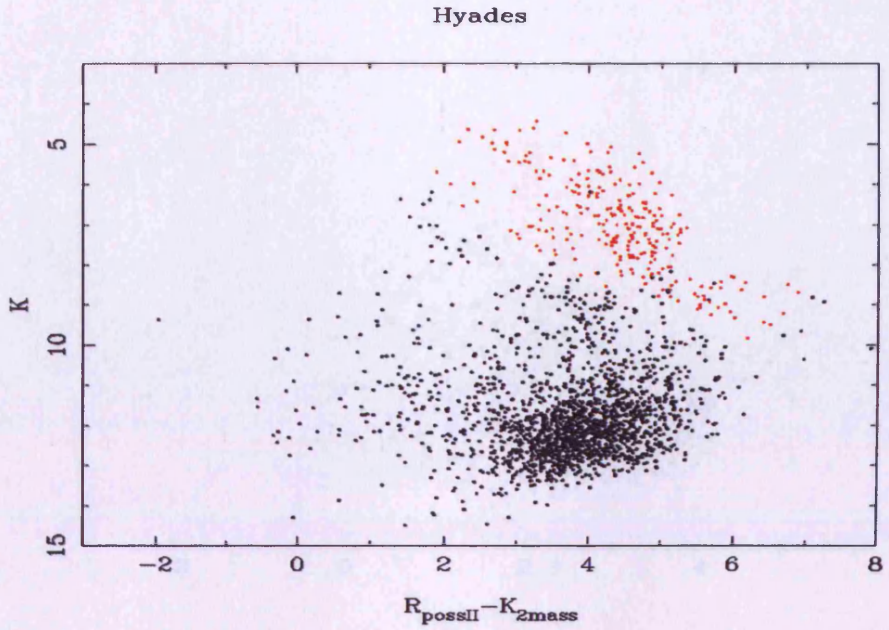

FIGURE 7.11. The K (absolute) vs $R-K$ CMD for the Hyades candidates identified from the proper motion selection. Photometrically selected members are shown as red dots, whilst background stars are shown as black dots.

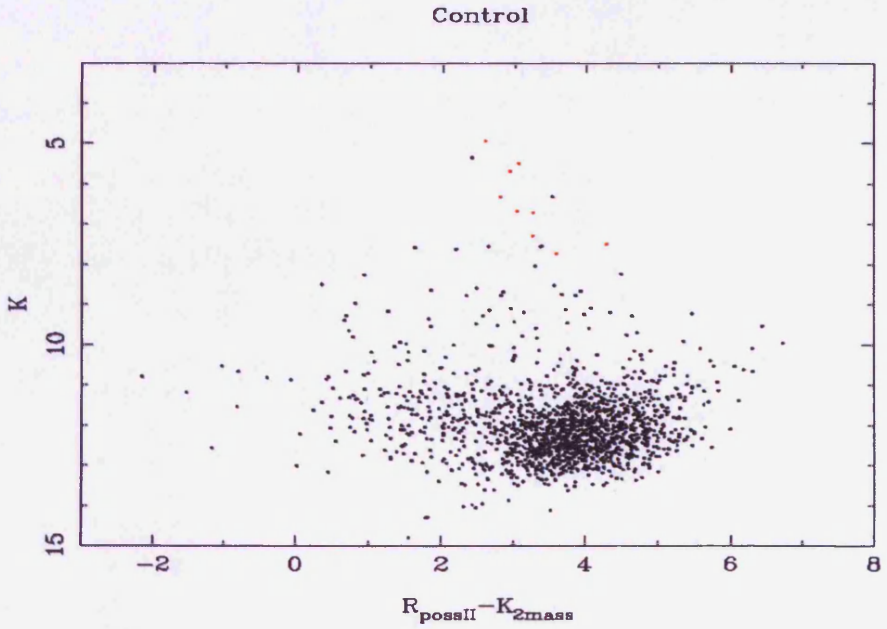

FIGURE 7.12. The K (absolute) vs $R-K$ CMD for the control cluster candidates identified from the proper motion selection. Photometrically selected members are shown as red dots, whilst background stars are shown as black dots.

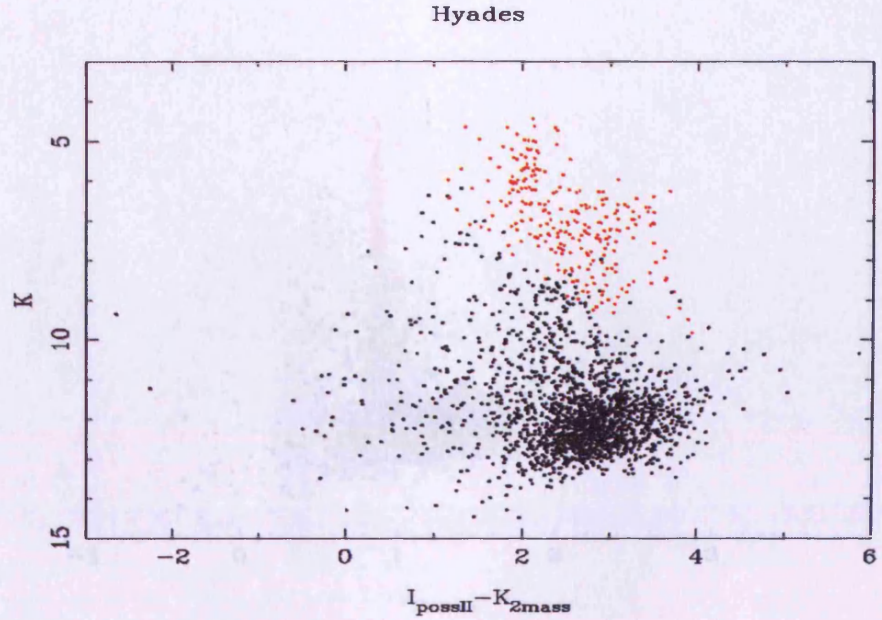

FIGURE 7.13. The K (absolute) vs $I - K$ CMD for the Hyades candidates identified from the proper motion selection. Photometrically selected members are shown as red dots, whilst background stars are shown as black dots.

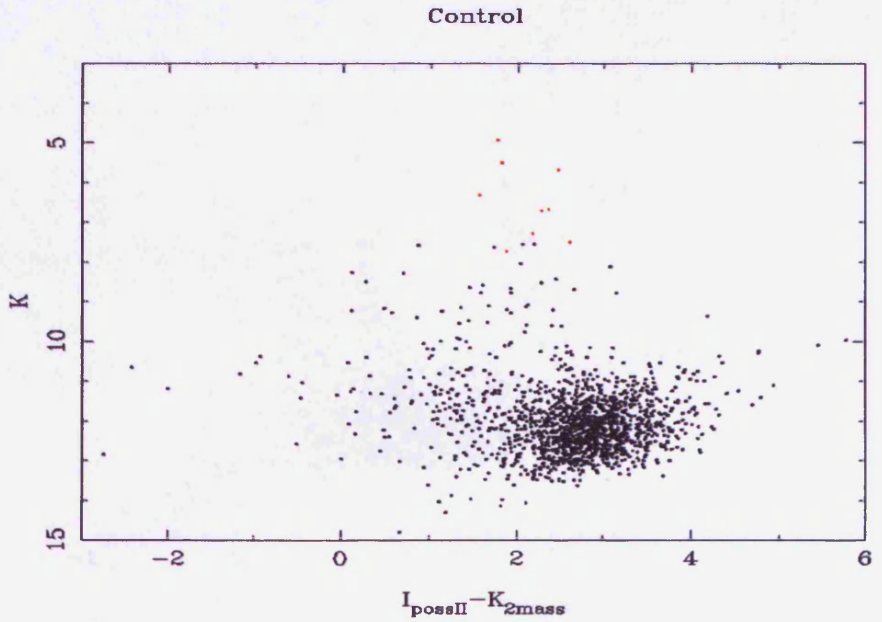

FIGURE 7.14. The K (absolute) vs $I - K$ CMD for the control cluster candidates identified from the proper motion selection. Photometrically selected members are shown as red dots, whilst background stars are shown as black dots.

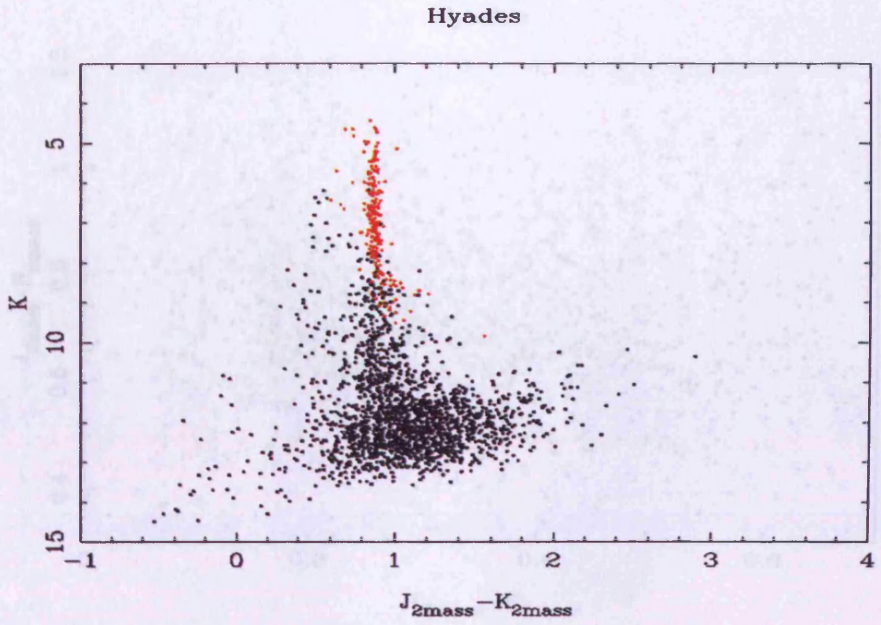

FIGURE 7.15. The K (absolute) vs $J-K$ CMD for the Hyades candidates identified from the proper motion selection. Photometrically selected members are shown as red dots, whilst background stars are shown as black dots.

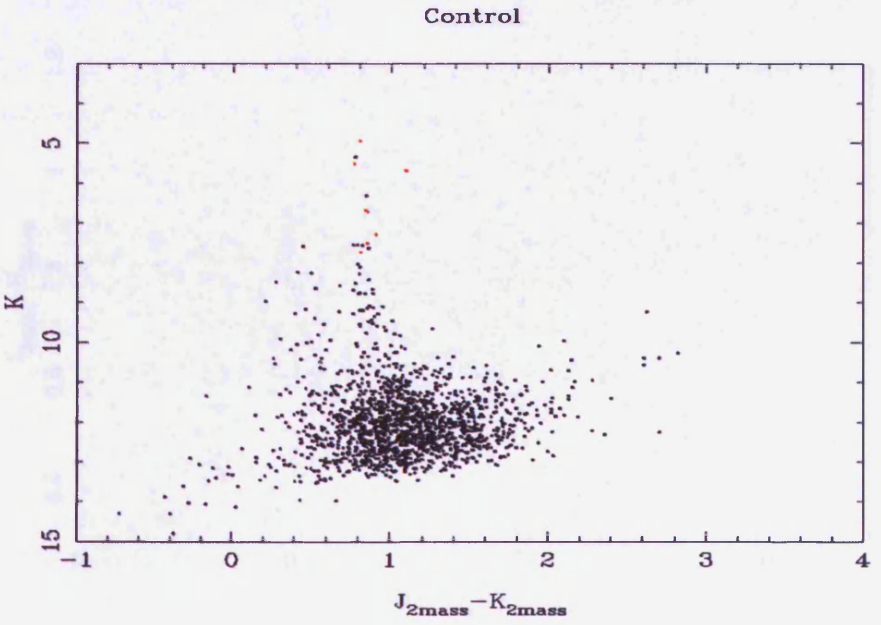

FIGURE 7.16. The K (absolute) vs $J-K$ CMD for the control cluster candidates identified from the proper motion selection. Photometrically selected members are shown as red dots, whilst background stars are shown as black dots.

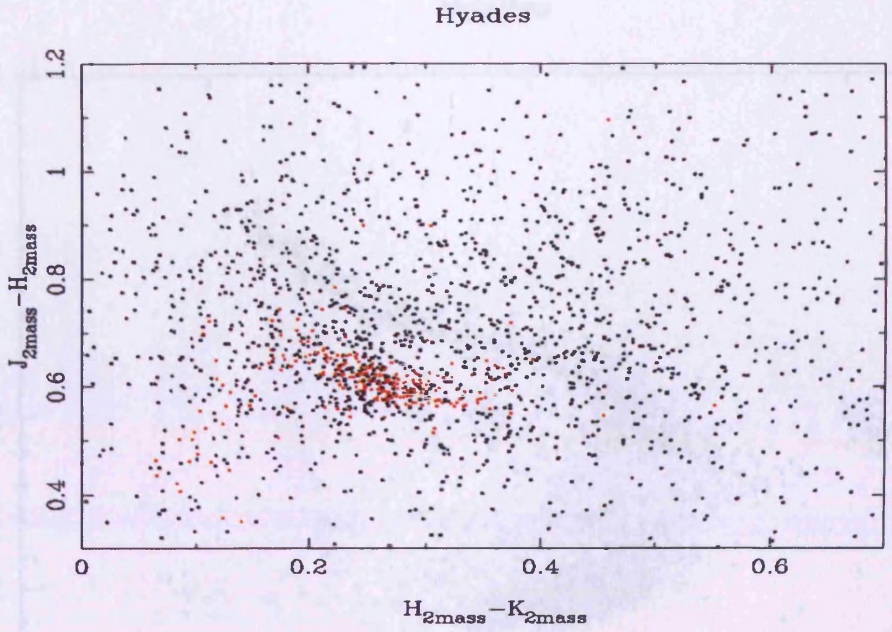

FIGURE 7.17. The $J-H$, $H-K$ colour-colour diagram for the Hyades candidates identified from the proper motion selection. Photometrically selected members are shown as red dots, whilst background stars are shown as black dots.

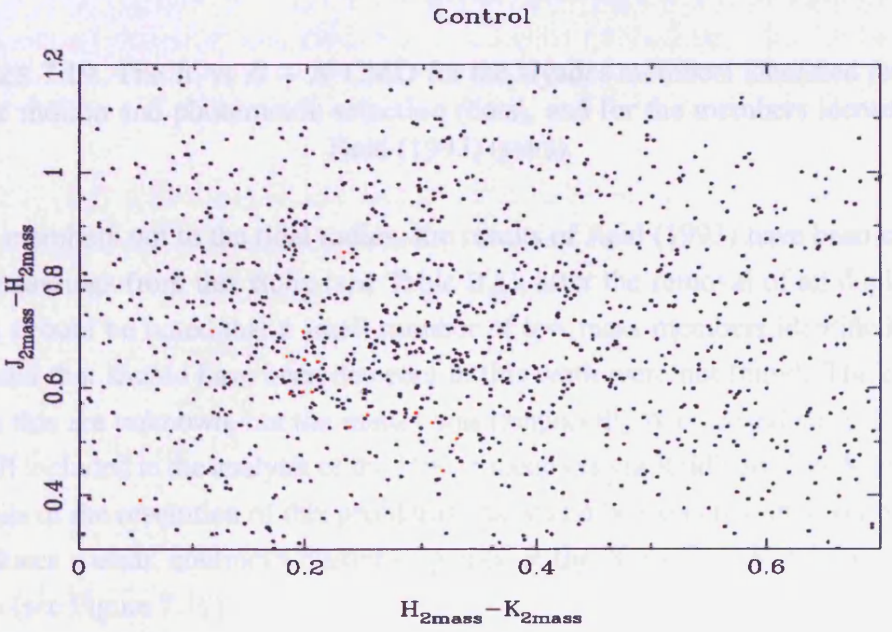

FIGURE 7.18. The $J-H$, $H-K$ colour-colour diagram for the control cluster candidates identified from the proper motion selection. Photometrically selected members are shown as red dots, whilst background stars are shown as black dots.

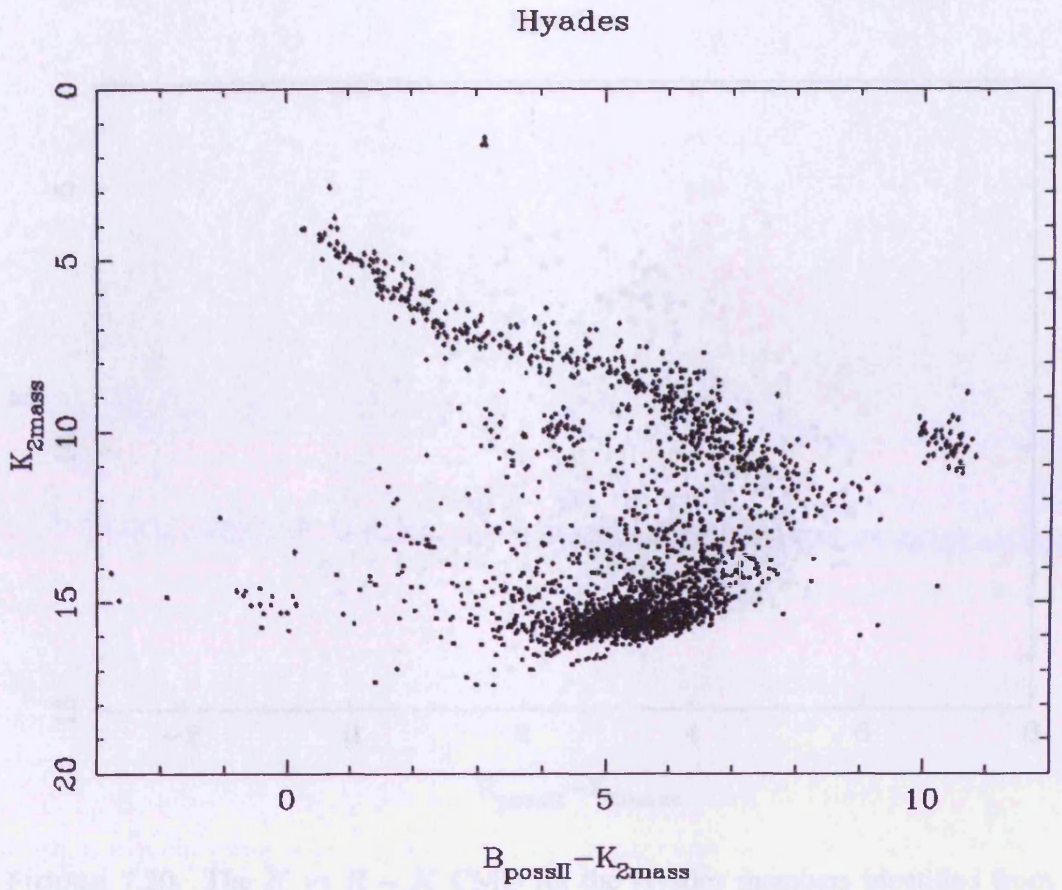

FIGURE 7.19. The K vs $B-K$ CMD for the Hyades members identified from the proper motion and photometric selection (dots), and for the members identified by Reid (1993) (stars).

Haydes members out to the tidal radius, the results of Reid (1993) have been combined with the findings from this study (see Table B.1), after the removal of all duplicate objects. It should be noted that a small number of low mass members identified by Reid (1993) and that should have been detected in this work were not found. The exact reasons for this are unknown, but the matter was temporarily overlooked since the objects were still included in the analysis of the cluster members via Reid's list (see Section 9.3.2 for details of the resolution of this problem). As would be expected, this combined data set produces a clear, continous cluster sequence in the K vs $B-K$ colour-magnitude diagram (see Figure 7.19).

From the K vs $R-K$ colour magnitude diagram (see Figure 7.20), two distinct distributions can be identified: the largest, and most obvious group is of course the Hyades main sequence (red dots), but slightly below and to the left of this sequence is a smaller

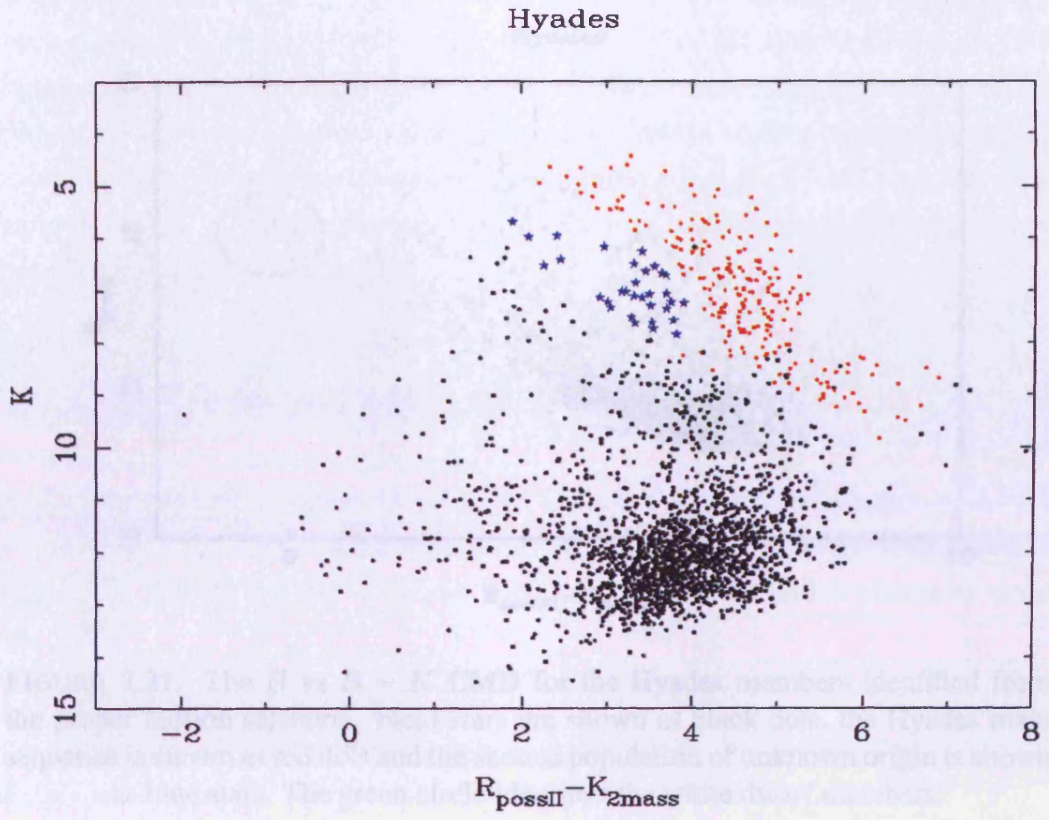

FIGURE 7.20. The K vs $R - K$ CMD for the Hyades members identified from the proper motion selection. Field stars are shown as black dots, the Hyades main sequence is shown as red dots and the second population of unknown origin is shown as blue stars.

group of objects with similar photometric properties (blue stars). In addition, a small population of 10 objects can be identified from the field stars at around $B - K = 0$, $B = 15$ on the B vs $B - K$ CMD (see green circle in Figure 7.21).

With reference to a standard Hertzsprung-Russell diagram, the group of objects located around $B - K = 0$, $B = 15$ can easily be identified as white dwarfs, and checking the coordinates of these objects with those of the known Hyades white dwarfs confirms that this is indeed the case. In fact, it appears that 2 new Hyades white dwarfs may have been discovered here, since only 8 of the 10 objects can be accounted for by the previously known objects. However, it is possible that these remaining two objects are simply background contamination objects, as the same plot for the control cluster shows a small number of objects in this area (see Figure 7.22).

The cluster of objects lying below the Hyades main sequence is more difficult to explain. When compared with the same area on the control cluster B vs $B - K$ colour-

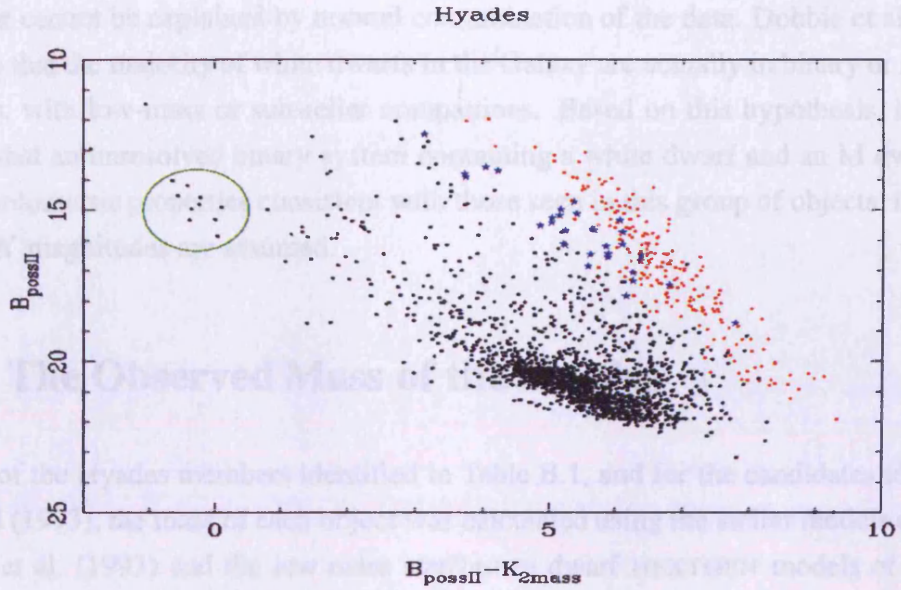

FIGURE 7.21. The B vs $B - K$ CMD for the Hyades members identified from the proper motion selection. Field stars are shown as black dots, the Hyades main sequence is shown as red dots and the second population of unknown origin is shown as blue stars. The green circle identifies the white dwarf members.

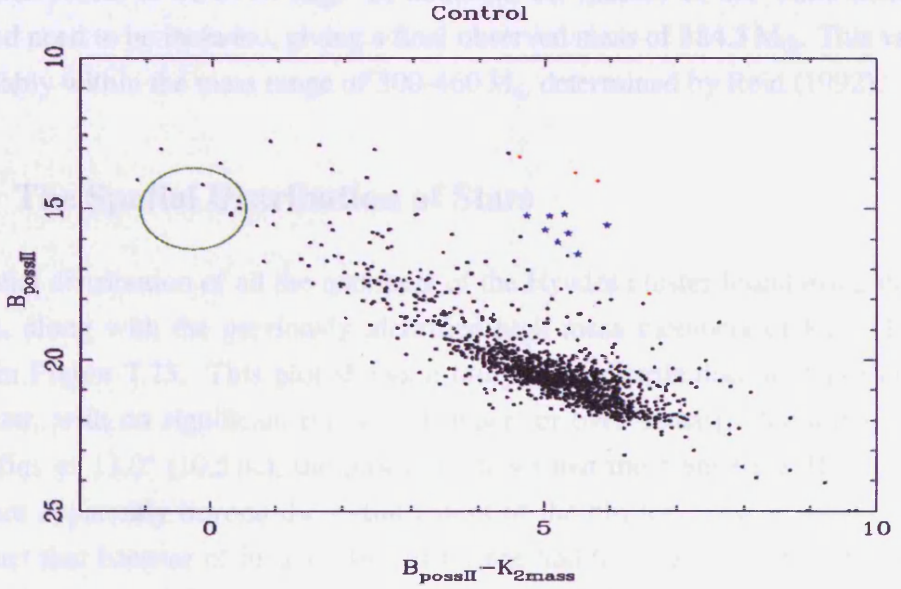

FIGURE 7.22. The B vs $B - K$ CMD for the control cluster members identified from the proper motion selection. The symbols have the same meanings as in Figure 7.21.

magnitude diagram (see Figure 7.22), there is definitely an over-density of objects in this area that cannot be explained by normal contamination of the data. Dobbie et al. (2005) propose that the majority of white dwarfs in the Galaxy are actually in binary or multiple systems, with low-mass or substellar companions. Based on this hypothesis, it can be shown that an unresolved binary system containing a white dwarf and an M dwarf will have photometric properties consistent with those seen in this group of objects, if typical B and K magnitudes are assumed.

7.5 The Observed Mass of the Hyades

For all of the Hyades members identified in Table B.1, and for the candidates identified by Reid (1993), the mass of each object was calculated using the stellar models of Charbonnel et al. (1993) and the low mass star/brown dwarf NEXTGEN models of Baraffe et al. (1998).

For the candidates identified by Reid (1993), the mass was calculated using the V band magnitude, whilst for the candidates identified from the Palomar and 2MASS data, the mass was calculated from the absolute K-band magnitude.

These masses were then summed to give the total observed mass of the Hyades, which was found to be 377.7 $M_{\odot}$. In addition, the masses of the white dwarfs also identified need to be included, giving a final observed mass of 384.3 $M_{\odot}$. This value lies comfortably within the mass range of 300-460 $M_{\odot}$ determined by Reid (1992).

7.5.1 The Spatial Distribution of Stars

The spatial distribution of all the members of the Hyades cluster found using the above analysis, along with the previously identified high mass members of Reid (1993), is shown in Figure 7.23. This plot shows a fairly even distribution of stars throughout the cluster, with no significant regions of under- or over-density. Assuming a cluster tidal radius of 13.0° (10.5 pc), the plot also shows that there are some Hyades objects which are apparently beyond the radial extent of the cluster. This is most likely due to the fact that because of its age, the cluster has had time to travel the circumference of the Galaxy several times, and will therefore have undergone numerous gravitational interactions which have tidally stripped some of the stars from the cluster. Low mass stars will also evaporate from the cluster as they gain energy through interactions with the higher mass cluster members. Despite the fact that these stars or no longer strictly

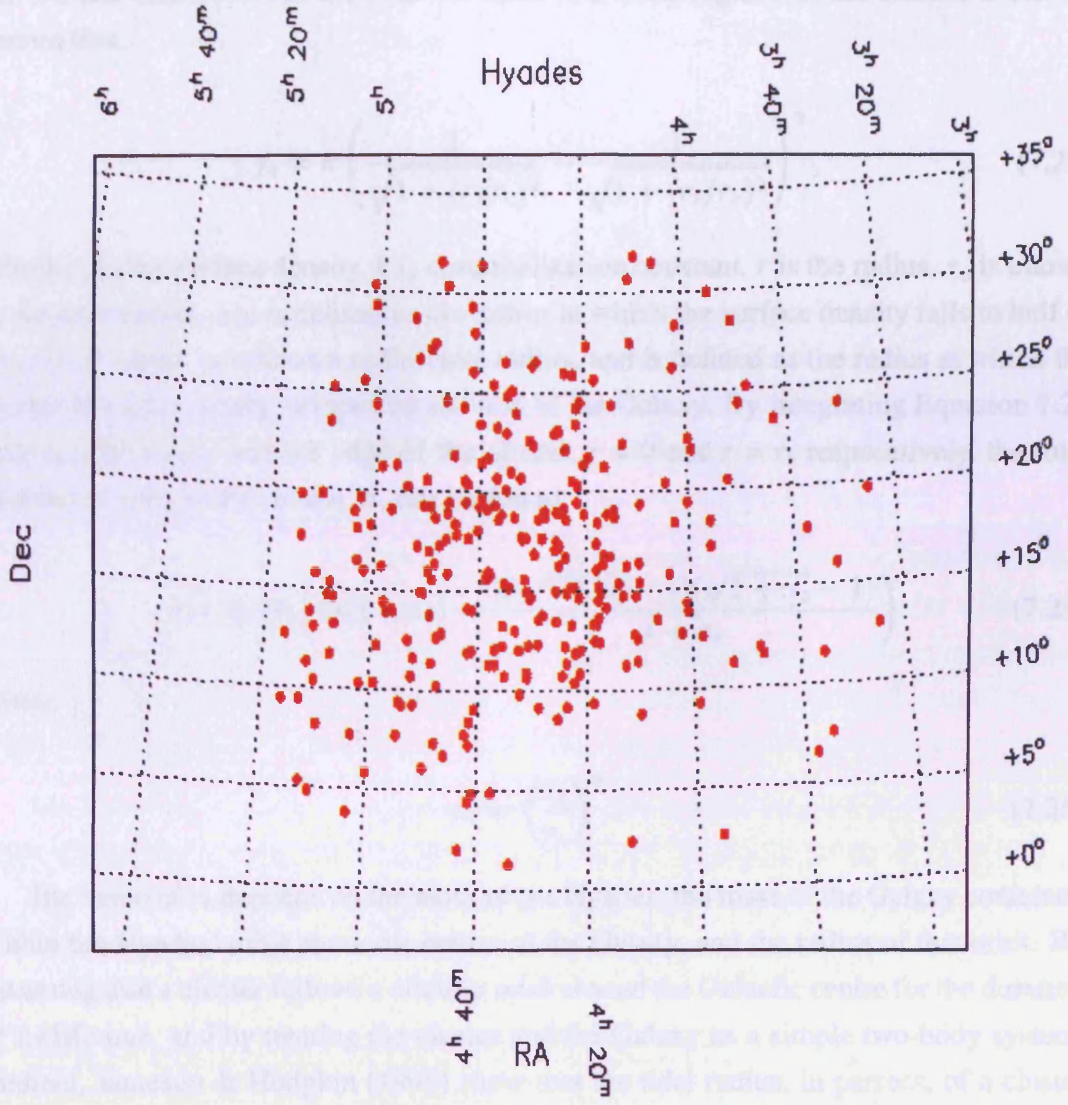

FIGURE 7.23. The spatial distribution of the Hyaeds members identified from both the proper motion selection and the photometric analysis.

bound to the cluster, they still retain many cluster properties, and in particular still have a motion which is consistent with that of the cluster.

7.5.2 The Density Distribution

In order to determine the density distribution of the Hyades, the density functions of King (1962) were used. These equations model the behaviour of the surface density distribution in globular clusters which have not undergone core collapse. By considering

the surface distribution in the both the inner and outer regions of the cluster, it can be shown that:

$$f_s = k\left(\frac{1}{\sqrt{1+(r/r_c)^2}} - \frac{1}{\sqrt{1+(r_t/r_c)^2}}\right)^2, \tag{7.23}$$

where f_s is the surface density, k is a normalization constant, r is the radius. r_c is known as the core radius, and is defined as the radius at which the surface density falls to half of its central value. r_t is known as the tidal radius, and is defined as the radius at which the cluster becomes tidally stripped by the rest of the Galaxy. By integrating Equation 7.23 between the centre and the edge of the cluster, $r = 0$ and $r = r_t$ respecetively, the total number of stars in the cluster, n, can be found:

$$n = \pi r_c^2 k\left(\ln(1+x_t) - \frac{(3\sqrt{1+x_t}-1)(\sqrt{1+x_t}-1)}{1+x_t}\right) \tag{7.24}$$

where

$$x_t = \left(\frac{r_t}{r_c}\right)^2. \tag{7.25}$$

The value of r_t depends on the mass of the Hyades, the mass of the Galaxy contained within the Hyades' orbit about the centre of the Galaxy, and the radius of this orbit. By assuming that a cluster follows a circular orbit around the Galactic centre for the duration of its lifetime, and by treating the cluster and the Galaxy as a simple two-body system, Pinfield, Jameson & Hodgkin (1998) show that the tidal radius, in parsecs, of a cluster near the sun, can be approximated by:

$$r_t = 1.46 M_c^{1/3}, \tag{7.26}$$

where M_c is the total mass of the cluster, measured in solar masses. Using the value of 384.3 $M_\odot$ calculated earlier for the total mass of the cluster, the tidal radius of the Hyades is located at 10.6 pc.

Bin	Mass Range ($M_\odot$)	Number of stars	Average mass ($M_\odot$)
1	< 0.6	343	0.272
2	0.6 - 1	162	0.729
3	> 1.0	111	1.499

Table 7.1. The mass bins used for the Hyades members.

7.5.3 The Observed Hyades Spatial Distribution

In order to make Equation 7.23 viable for use in the Hyades cluster, the cluster members were binned into three mass bins: $< 0.6\,M_\odot$, $0.6 < M < 1\,M_\odot$ and $> 1\,M_\odot$. The number of stars and the average mass of the stars in each bin are shown in Table 7.1.

The cluster was then partitioned into a central circle surrounded by annuli of 1 pc, and the number of stars in each region and mass bin was counted. Thus for each mass bin it is possible to plot the cumulative distribution of stars against radius, r (see Figures 7.24, 7.26 and 7.28), and also the surface number density, f_s, against radius (see Figures 7.25, 7.27 and 7.29).

For mass bins 1 and 2 the cumulative distribution is well behaved and asymtotes to a finite number, whereas bin 3 is slightly discrepant. It should be noted that with all the cumulative distributions the final number is not reached until after the tidal radius of 10.6 pc. This is no doubt due to including some members that have technically escaped the cluster.

It was not therefore surprising that the spatial distribution could not be fitted by forcing $r_t = 10.6$. The best fit to the spatial distribution was found by allowing r_t to be a free parameter. From the spatial fit the χ^2 statistic can be minimized by using a FORTRAN routine called *dx_srchmin* (by R. Willingale, private communication) in order to obtain r_c, k and r_t. The values found for r_c and k are given in Table 7.2, but the values for r_t are not included since they were unrealistic. The best-fitting form of Equation 7.23 for each mass bin is shown in Figures 7.25, 7.27 and 7.29. The errors shown on the surface density plots are $\pm(100\sqrt{N}/N)$ per cent. As expected for a relaxed cluster, r_c increases with decreasing mass.

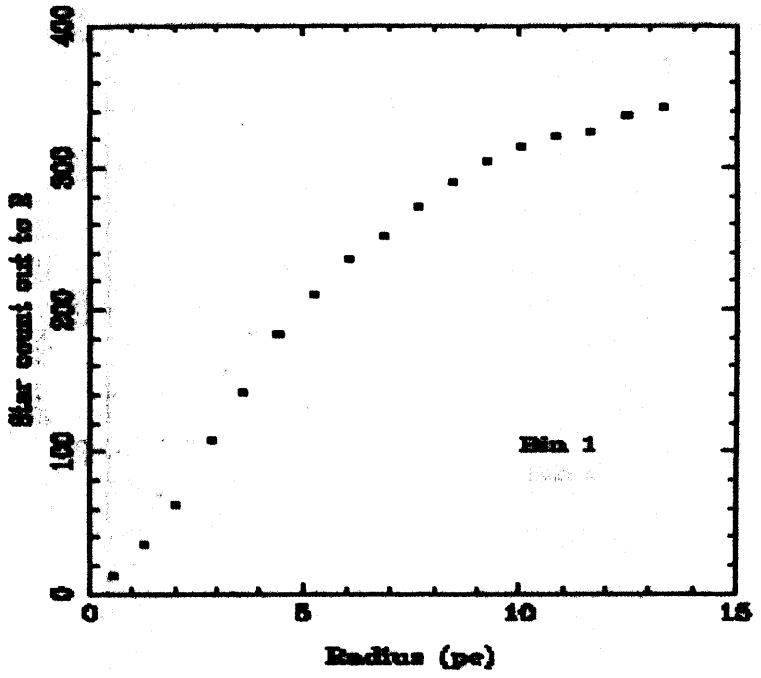

FIGURE 7.24. The cumulative number of stars, as a function of radial distance, for the $< 0.6\,M_{\odot}$ mass bin.

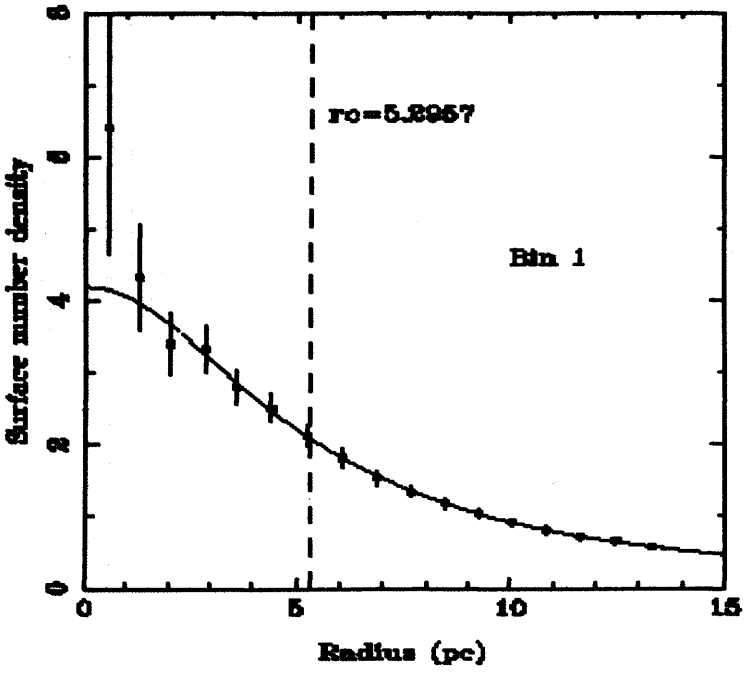

FIGURE 7.25. The surface number density, as a function of radial distance, for the < 0.6 mass $M_{\odot}$ bin.

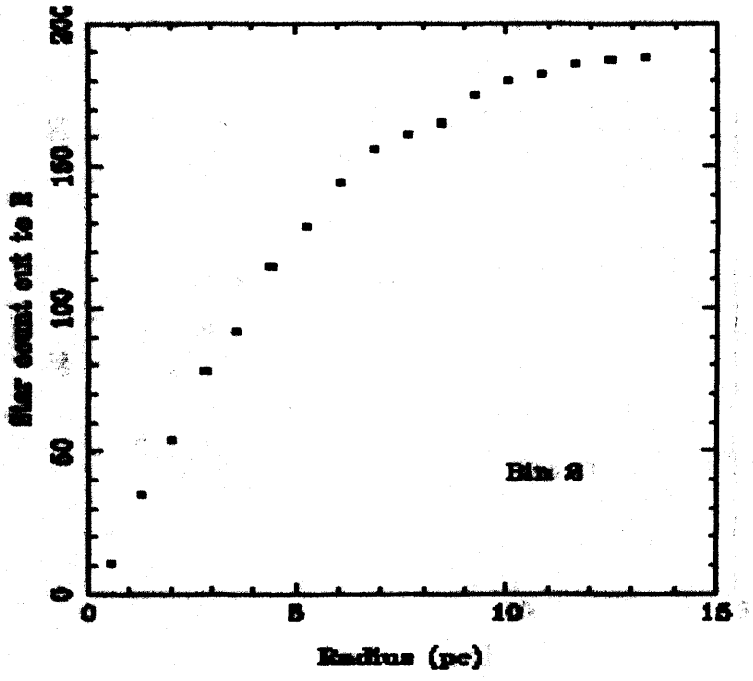

FIGURE 7.26. The cumulative number of stars, as a function of radial distance, for the 0.6 - 1 $M_{\odot}$ mass bin.

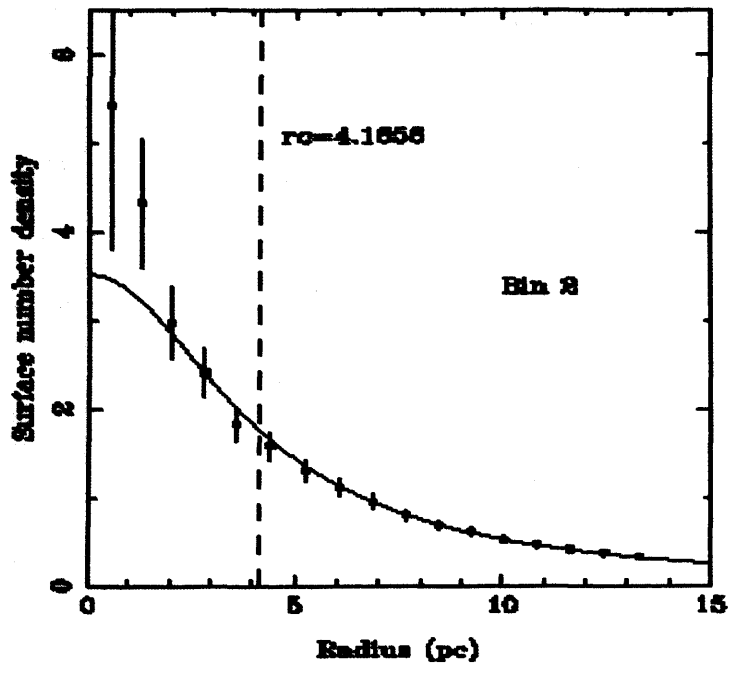

FIGURE 7.27. The surface number density, as a function of radial distance, for the 0.6 - 1 $M_{\odot}$ mass bin.

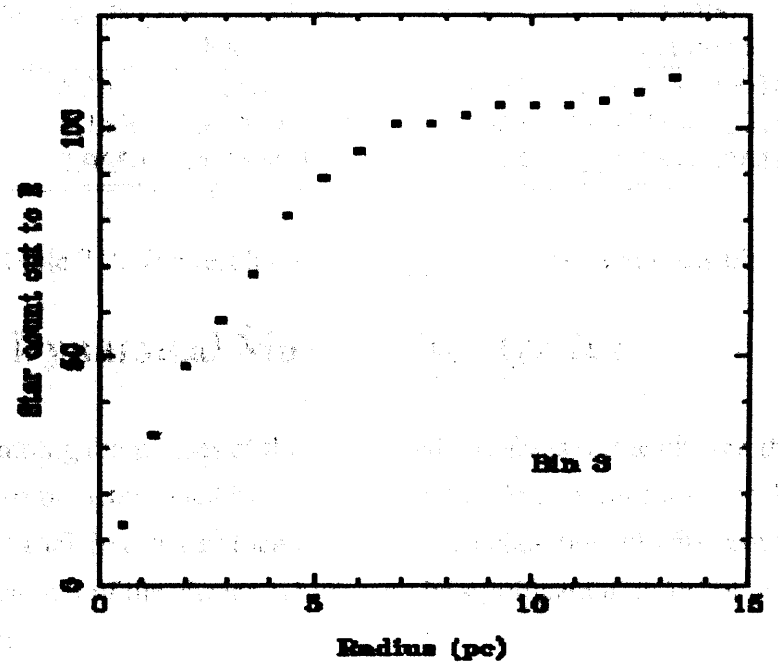

FIGURE 7.28. The cumulative number of stars, as a function of radial distance, for the $> 1\,M_{\odot}$ mass bin.

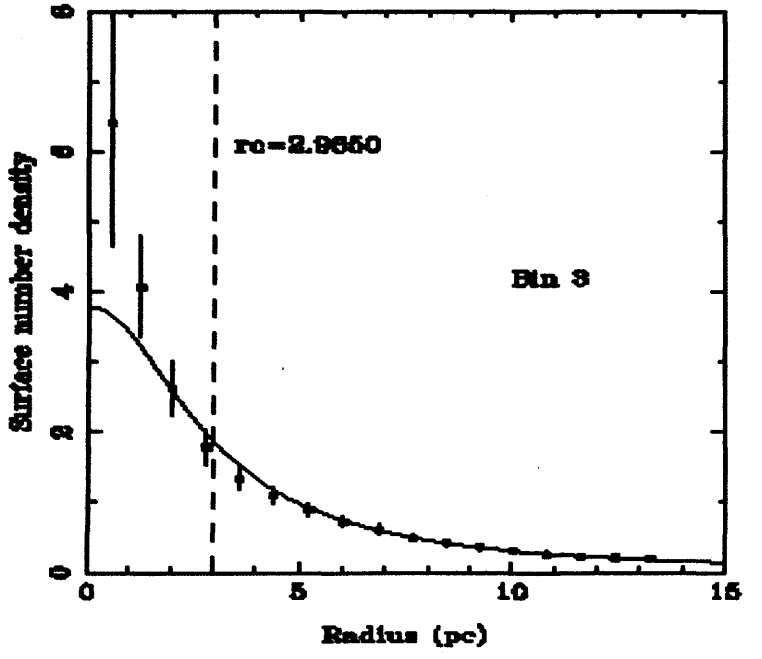

FIGURE 7.29. The surface number density, as a function of radial distance, for the $> 1\,M_{\odot}$ mass bin.

Bin	r_c (pc)	r_c limits (68% confidence)	k	k limits (68% confidence)
1	5.2957	[4.8880-5.7484]	4.1961	[3.7441-4.6963]
2	4.1656	[3.7379-4.6469]	3.5086	[2.9735-4.1374]
3	2.9650	[2.5524-3.4438]	3.7874	[2.9705-4.8264]

Table 7.2. The results of the King profile fits each mass bin.

7.6 The Dynamical Mass of the Hyades

As well as summing the masses of the individual members of the cluster, the mass of the Hyades can also be determined by using the spatial density profiles calculated for each mass bin. The virial theorm can then be used to calculate the velocity required to escape the gravitational pull of the cluster, which may be significant in terms of retaining brown dwarf members.

7.6.1 Deprojection

Equation 7.23 can also be deprojected to give the spatial density of stars, $\phi(r)$:

$$\phi(r) = \frac{k}{\pi r_c^2 (1 + (r_t/r_c)^2)^{3/2}} \frac{1}{z^2} \left(\frac{1}{z} \cos^{-1} z - \sqrt{1 - z^2} \right) \tag{7.27}$$

where

$$z = \sqrt{\frac{1 + (r/r_c)^2}{1 + (r_t/r_c)^2}}. \tag{7.28}$$

Using these equations the deprojected density profiles were calculated for each mass bin, and these were added together to find the total density profile for the cluster (see Figure 7.30). It can be seen that the highest mass bin (bin 3, shown as a blue curve) contributes towards almost half of the central density, with the lower two mass bins (red curve for bin 1, green curve for bin 2) contributing almost equal amounts. The total density profile was then numerically integrated in order to determine the mass of the cluster as a function of radial distance, as shown in Figure 7.31, giving the total mass of the cluster to be 383.567$M_\odot$. This figure agrees well with the value of the observed total mass of the cluster calculated earlier (384.3 $M_\odot$).

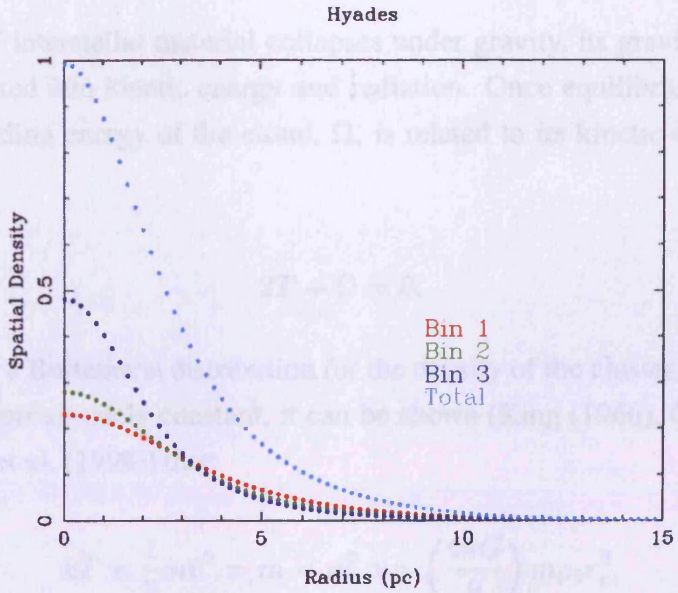

FIGURE 7.30. The density distribution of the Hyades members as a function of radial distance. Individual profiles for each of the mass bins are plotted as red, green and blue curves (bin 1, bin 2 and bin 3 respectively), whilst the total density profile is plotted as a turquoise curve.

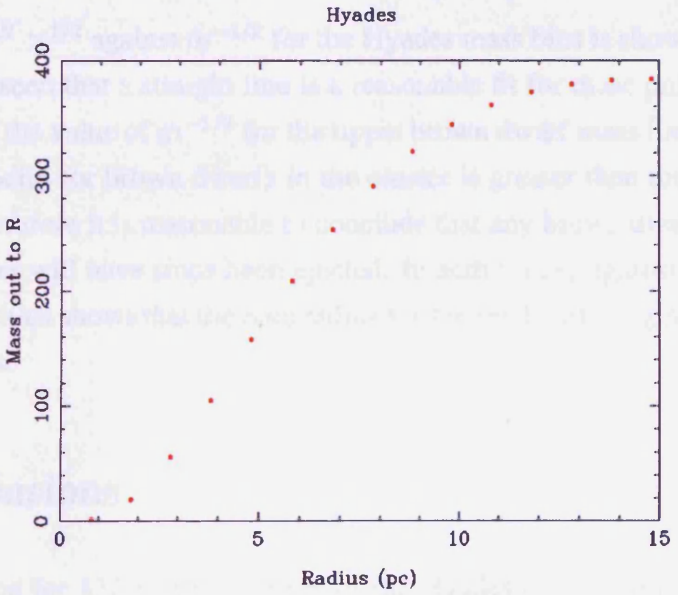

FIGURE 7.31. The mass distribution of the Hyades members as a function of radial distance.

7.6.2 The Virial Theorem

When a cloud of interstellar material collapses under gravity, its gravitational potential energy is converted into kinetic energy and radiation. Once equilibrium is reached the gravitational binding energy of the cloud, Ω, is related to its kinetic energy, T, by the virial theorem:

$$2T + \Omega = 0. \tag{7.29}$$

By assuming a Boltzmann distribution for the density of the cluster, and that the central density is approximately constant, it can be shown (King (1966), Costa & Freeman (1976), Pinfield et al. (1998)) that:

$$kT = \frac{1}{3}m\bar{v}^2 = m < \sigma^2 >= \left(\frac{4\pi G}{9}\right) m\rho_0 r_c^2, \tag{7.30}$$

where kT is the typical energy associated with the cluster stars, m is the mass of the stars being considered (ie. the average mass of the stars in a particular mass bin), v^2 is the mean square velocity of the stars in a particular bin, $< \sigma^2 >$ is the velocity dispersion, ρ_0 is the central density of the cluster and r_c is the core radius for a particular bin. If equipartition of energy has occurred in the Hyades, then $m < \sigma^2 >$ should be constant and therefore $r_c \propto m^{-1/2}$ since $r_c \propto < \sigma^2 >^{1/2}$.

A plot of $< \sigma^2 >^{1/2}$ against $m^{-1/2}$ for the Hyades mass bins is shown in Figure 7.32. It can clearly be seen that a straight line is a reasonable fit for these points. By extrapolating this line to the value of $m^{-1/2}$ for the upper brown dwarf mass limit of 0.08 $M_\odot$ we find that the velocity for brown dwarfs in the cluster is greater than the escape velocity of the cluster, therefore it is reasonable to conclude that any brown dwarfs formed at the birth of the cluster will have since been ejected. In addition, r_c against $m^{-1/2}$ is plotted in Figure 7.33, which shows that the core radius for brown dwarfs is approximately equal to the tidal radius.

7.7 Conclusions

Data was obtained for 832 square degrees of the Hyades cluster from the USNO B1.0 catalogue, and analysed in terms of proper motion, from which potential cluster members were selected. Infrared data from 2MASS was also obtained for the potential members. These objects were then analysed using colour-magnitude diagrams in order to select

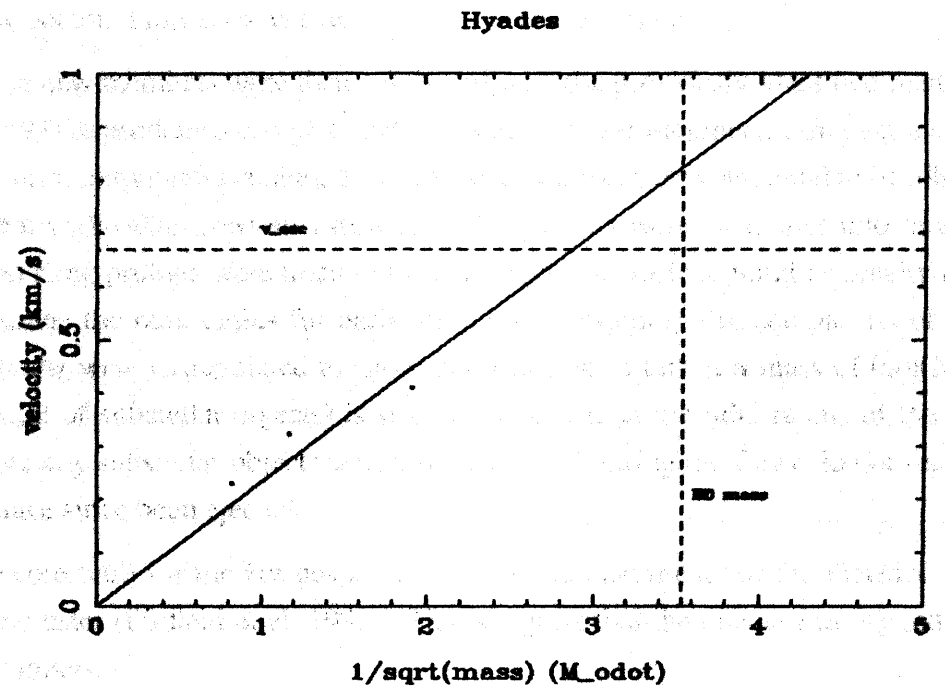

FIGURE 7.32. The $< \sigma^2 >^{1/2}$ against $m^{-1/2}$ plot for the Hyades mass bins.

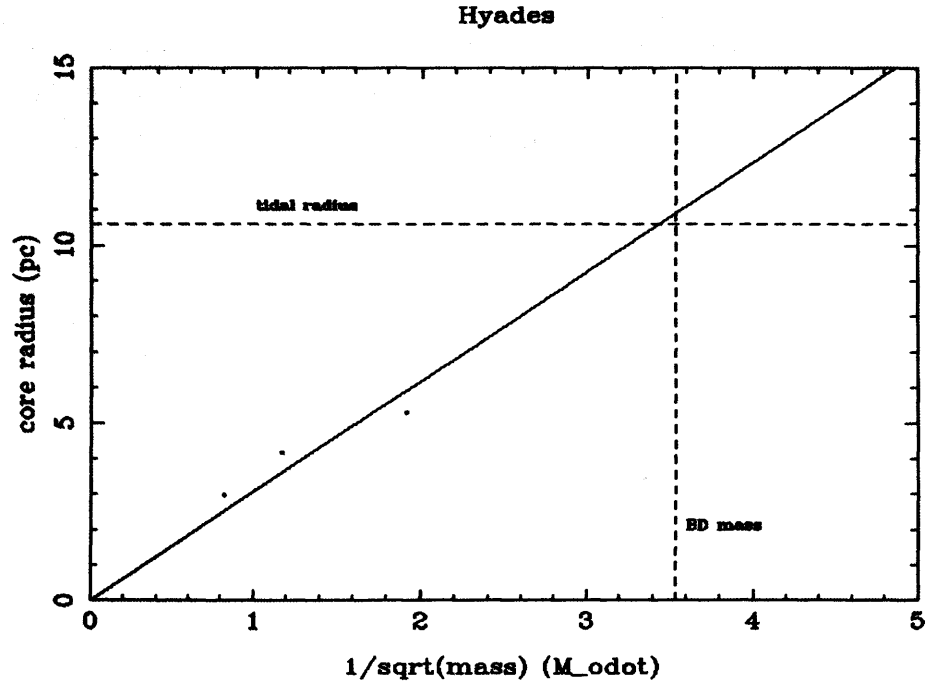

FIGURE 7.33. The r_c against $m^{-1/2}$ plot for the Hyades mass bins.

those objects which had photometry consistent with the cluster. Through this analysis 260 new potential low mass cluster members were identified.

These new members were then combined with the previously identified members of Reid (1993) to produce a complete list of Hyades cluster members. After estimating the mass of each individual member, the total mass of the cluster was found to be 384.3 $M_{\odot}$, consistent with other previous estimates. The objects were then split into three mass bins, and King profiles were fitted to the radial plots of surface number density in order to determine the core radius for each mass bin. Assuming the equipartion of energy, these results were extrapolated to show that the core radius at a mass of 0.08 $M_{\odot}$ (the upper limit of substellar objects) is slightly greater than the tidal radius of the cluster. Therefore any substellar objects which were created during the formation of the cluster would have since been ejected.

The core radii for the Hyades are (now) greater than those for the Pleiades, a more massive cluster (Pinfield et al. 1998). This suggests that the cluster has expanded as it loses members.

Natural evaporation (low mass stars attaining the escape velocity through collisions, leading to equipartition of energy) removes a larger energy fraction than mass fraction, and so the cluster will tend to contract. On the other hand, tidal interactions will heat and expand the cluster.

Thus it is reasonable to conclude that the Hyades is being destroyed by tidal interactions rather than by 'evaporation'. The Hyades has orbited the Galaxy three times, giving it plenty of opportunity to 'bump' into other objects.

Chapter 8

Conclusions and Further Work

This final chapter summarises all of the work undertaken during the course of this PhD. The main results and conclusions for each of the three science chapters are outlined, along with suggestions and ideas to further develop and extend the work presented. Finally, all of the work is drawn together and its significance within the wider field of brown dwarf research is assessed.

8.1 Chapter 6 - Brown Dwarfs in the Taurus Dark Clouds

This chapter presents the results of a deep, large scale survey of the Taurus Dark Clouds. The survey was concentrated on four regions which have previously been identified as active areas of star formation, with the aim of identifying young, very low mass brown dwarfs. Photometry in the R, I and Z wavebands was obtained for all four regions. From this data the most promising brown dwarf candidates were identified using colour-magnitude diagrams. These candidates were followed-up by collecting infrared and spectroscopic data.

8.1.1 Conclusions

From the analysis of the RIZ photometry obtained for the Taurus Dark Clouds, 165 potential brown dwarf candidates were identified. The selection process used to determine these candidates included the use of three selection critieria from three different CMDs. This proved to be an effective method of selection as the number of candidates was then 11% lower than when just two criteria and CMDs were used.

Follow-up infrared photometry was obtained for 21 of the faintest and reddest of the candidates, with at least seven of these lying close to the field dwarf sequence in the $I-J$ vs $J-H$ colour-colour diagram. Spectra of six of these objects revealed two, or possibly three, to be definite brown dwarfs, due to the presence of gravity sensitive H_2O absorption features and weak NaI lines. Additional spectra of seven other candidates revealed three more late-type M dwarfs, given the presence of deep TiO absorption and weak Hα emission. The masses of these objects are in the range 10 - 20 M_J. Although the evidence gathered so far looks promising, further observations are required to confirm the status of these 6 new brown dwarfs.

Overall, a brown dwarf identification success rate of approximately 28 % was achieved, implying that up to 40 more brown dwarfs could be identified in the Taurus Dark Clouds.

8.1.2 Further Work

In order to develop the work carried out so far in Taurus, further analysis of the selected brown dwarf candidates is required so as to eliminate any contaminating objects. This could be done by obtaining follow-up infrared photometry, perhaps from 2MASS, and/or by obtaining additional optical or infrared spectra. By compiling a comprehensive list of members it will be possible to determine accurately the form of the IMF for the region. Obviously the accuracy of the IMF would increase if more members of the cluster were identified, either from new far optical surveys or from archive catalogue data from all-sky surveys (both old and new). In addition, the work of Hartmann et al. (1991) indicates that new potential Taurus brown dwarfs could be found from proper motion surveys of the region, as genuine members appear to have a small but distinct proper motion ($\mu_\alpha \sim -20$ mas/yr, $\mu_\delta \sim +10$ mas/yr).

8.2 Chapter 7 - A Study of Brown Dwarfs in the Pleiades

This chapter presents the results of a comprehensive study of the proper motions of brown dwarfs in the Pleiades. The objects studied were identified from the most complete sample to date of low mass and brown dwarf members of the Pleiades, compiled by Jameson et al. (2002). The proper motion for each object was calculated using a pair of images taken at two different epochs, and then checked for consistency with the known motion of the cluster. Theoretical evolutionary models were then used to estimate the

mass of the definite members, and the substellar IMF was calculated. In addition, spectra for 12 of the brown dwarf candidates were obtained.

8.2.1 Conclusions

A thorough analysis of the proper motions of 48 brown dwarf candidates in the Pleiades revealed that 31 of these are genuine cluster members. A further six are highly likely to be members, whilst another six are found to be definite non-members. The membership status of the final five objects still remains uncertain. Masses in the range $0.087\,M_{\odot}$ to $0.031\,M_{\odot}$ were derived for each object using the NEXTGEN models of Baraffe et al. (1998). Although limited somewhat by low number statistics, the shape of the mass distribution of the cluster was found not to contradict the expectation of the Pleiades IMF being flat or slowly rising. The distribution may also show evidence for the missing M dwarfs (Dobbie et al. 2002*c*).

HK spectra of 12 of the brown dwarfs confirm their status as determined from the proper motion study. Although for many of the objects the spectra are of poor quality, the spectra of the confirmed brown dwarfs show the expected H_2O absorption features, and the brightest may even display NaI and/or CO features. The estimated spectral types are also consistent with these members being substellar.

8.2.2 Further Work

Although the Pleiades is one of the most studied stellar clusters in the Galaxy it is still worthwhile to carry out further work on the cluster in order to develop a deeper understanding of the theory of brown dwarfs, and to enable the accurate comparison of observation with theory. By observing the cluster to deeper magnitudes, more brown dwarf candidates are likely to be discovered, which will help to further increase the accuracy of evolutionary and atmospheric models, and to further refine the form of the IMF and our understanding of star formation processes. These increased sensitivity observations will easily be achieved with the UKIDSS Galactic Cluster Survey (GCS), and still deeper observations could be made with the WFCAM at UKIRT.

8.3 Chapter 8 - A Large Scale Survey of the Hyades

This chapter presents the results of an extremely large survey of the Hyades cluster using data from the USNO and 2MASS archives. Data covering an area of over 800 square degrees was obtained from the USNO B1.0 online database, to ensure complete coverage of the entire cluster out to, and beyond, the tidal radius. The data was analysed to select candidates with a proper motion consistent with that of the Hyades, and 2MASS infrared photometry was then obtained for these objects. Following photometric selection, the remaining candidates were used to calculate the core radius of the cluster, and hence the velocity required for a brown dwarf to escape from the cluster was determined.

8.3.1 Conclusions

Through the proper motion and photometric selection procedures carried out on the USNO B1.0 and 2MASS data, 260 new potential low mass members of the Hyades were identified. Combining these objects with those identified previously by Reid (1993), and calculating the mass for each member results in a total cluster mass of 384.3 $M_{\odot}$.

The core radius at three different mass intervals was determined by calculating the King profile for each mass bin, and extrapolation of these results down to the brown dwarf mass limit indicates that the core radius for brown dwarfs is greater than the tidal radius of the cluster, and therefore any substellar members will have been ejected. When compared to the Pleiades, it appears that the Hyades is expanding as it looses members, which in turn suggests that the cluster is being destroyed by tidal interactions rather than by natural evaporation.

8.3.2 Further Work

The first step in continuing the work conducted on the Hyades would be to identify why some candidates identified by Reid (1993) are not duplicated in this analysis. Indeed, work has already been done on this problem, and it has been found that some of the members were excluded because their proper motion errors were underestimated. The missing objects were found to have proper motion errors of zero (USNO errors are quantized in units of 1 mas and can genuinely be zero when measured as less than 0.5 mas), and thus were rejected during the original selection procedures. After taking this factor into account, a re-analysis of the kinematic properties of the Hyades results in a slightly

different value being obtained for the escape velocity of the cluster, but the main conclusion that any brown dwarfs would have been ejected from the cluster remains valid (Osborne, Casewell & Jameson 2005).

Another obvious piece of follow-up work would be to obtain further photometry and/or spectra for the objects identified from the B, $B - K$ CMD as probable white dwarf/brown dwarf binaries in order to unambiguously determine their status. In addition, the same could be done for the two possible new white dwarfs found.

Despite the fact that the work presented in this thesis, and other previous work, indicates a deficit of brown dwarfs in the Hyades, it would be interesting to try and find the missing members of the cluster. This could be done by applying the method used by Bannister and Jameson (private communication) to identify members of the Ursa Major cluster. In this work, the authors conducted a proper motion search of the archives of known 'field' L and T dwarfs found by 2MASS and DENIS. It was found that some of the brown dwarfs previously assumed to be 'in the field' were actually members of the Ursa Major cluster. Therefore it is reasonable to assume that some of the other previously identified field brown dwarfs may be escaped members of the Hyades.

8.4 Overall Summary

The work carried out during the course of this PhD and presented in this thesis has aimed to further the knowledge of the properties of brown dwarfs in the Taurus star forming region and the Pleiades and Hyades stellar clusters. Overall, this aim has been achieved: six new brown dwarfs have been found in the Taurus Dark Clouds; many of the known brown dwarfs in the Pleiades have had their membership status confirmed via proper motion calculations; and the Hyades cluster has been thoroughly, albeit unsuccessfully, searched for brown dwarf members.

In terms of the work done in Taurus, the discovery of six likely brown dwarfs is of fairly high significance given that only around 20 others have been identified in the area to date (see Section 5.2 for more details). Although alone these six new brown dwarfs are not enough to calculate the IMF for the Taurus Dark Clouds, if combined with the other known members then this quantity could be estimated, and the errors associated with previous calculations could be reduced (see Briceño et al. (2002), Luhman (2000)). Given a more accurate IMF, it would then be interesting to see whether or not some of the differences (such as the slightly narrower and more pronounced peak) between the Taurus IMF and that of other star formation regions remain (Luhman et al. 2000). When

comparing the spectra of these six brown dwarfs to those of other Taurus candidates (Martín et al. 2001*a*) there are, as would be expected, many similarities. The spectra also display many similar features to those of other star forming regions, such as σ Orionis (Béjar et al. 1999) and Trapezium (Lucas et al. 2001) (see Section 2.4.6 for more details on these clusters). The presence and similarity of gravity sensitive features such as H_2O absorption around 1.65 μm and weak NaI lines in all the spectra suggests that these star forming areas are experiencing virtually the same physical processes, and therefore that there is likely to be only one main mechanism for star formation. In addition, although it has been shown previously that using two CMDs is an efficient method for identifying brown dwarfs (Zapatero-Osorio et al. 1999*b*), we show here that the use of three CMDs may be better still, since it can reduce the number of contaminants by a further 11 %.

Although the Pleiades is perhaps the most well studied stellar cluster in terms of its brown dwarf population, the work done in this thesis is still of some significance. For the majority of the 48 brown dwarfs listed in Jameson et al. (2002), the proper motion is calculated for the first time in this work, and thus it is the first time that these objects have been absolutely confirmed as Pleiades members. This is important since a photometric analysis alone is not sufficient in removing all of the contaminating field objects, and some non-members were actually identified. Comparison of the observed photometric data with the theoretical evoloutionary models of Baraffe et al. (1998) and Chabrier et al. (2000) show that ideally the properties of these two different models need to be combined in order to produce a single model which agrees with observation across the entire magnitude range. In terms of the mass function, the results presented here are not definitive due to small number statistics, but they do not rule out any of the previous estimates made of the Pleiades IMF (see for example Bouvier et al. (1998), Hambly et al. (1999) and Martín et al. (2000)). Therefore it can still be said that the Pleaides IMF is expected to be slowly rising across the substellar boundary.

Perhaps the most significant contribution to brown dwarf research to have been made by the work done during the course of this PhD is that done on the Hyades stellar cluster. After an extremely thorough survey of the entire cluster out to the tidal radius, no brown dwarfs were identified from the proper motion and photometric selections. This null result is important for several reasons:

- Firstly, although it has been suggested that the Hyades would have a deficit of brown dwarfs, this is the first time that the entire cluster has been searched in order to verify this hypothesis.
- Secondly, the result may have implications for the longer term evolution of other stellar clusters, such as the Pleiades. For instance, if the Pleiades is an earlier form of the Hyades

and will follow a similar evolutionary path over the next 500 Myrs, then the Pleiades may be destined to lose its currently large substellar population (see for example the large number of brown dwarfs found in surveys by Bouvier et al. (1998), Zapatero-Osorio et al. (1999*b*) Pinfield et al. (2000) and Dobbie et al. (2002*b*)). However, it should be noted that not all older open clusters have a deficit of brown dwarfs , for example Praesepe (at an age of 700 Myrs) has a small but significant brown dwarf population (see Section 2.4.6) for more details.

• Finally, whilst there is some evidence to suggest that star formation regions and young open clusters can be descibed using the same MF in the substellar region (Luhman et al. 2000), it seems unlikely that the same can apply to the Hyades given its lack of brown dwarfs.

Appendix A

Taurus Candidates

Listed in Table A.1 are the candidates identified from the RIZ photometric selection as outlined in Chapter 5. The magnitudes are in the WFC filter system.

Name	RA	DEC	I	Z	R	R-Z
taucand141	4 33 42.920	25 26 47.290	18.8190	16.6320	22.1470	5.5150
taucand105	4 32 5.030	24 31 9.540	20.4170	18.2030	23.6430	5.4400
taucand120	4 32 29.480	24 23 13.090	19.5570	17.4320	22.7020	5.2700
taucand48	4 16 56.810	29 13 33.660	20.4500	18.7850	24.0130	5.2280
taucand165	4 30 28.770	19 0 10.240	20.2570	18.6780	23.7890	5.1110
taucand52	4 31 19.080	23 35 4.840	17.3770	15.5010	20.5930	5.0920
taucand123	4 31 46.980	24 24 56.380	20.8570	18.9480	24.0370	5.0890
taucand122	4 32 8.590	24 22 13.180	20.7830	18.9230	24.0040	5.0810
taucand76	4 31 18.980	24 30 21.230	20.7820	19.0750	24.1090	5.0340
taucand33	4 19 23.350	27 26 49.700	19.8670	18.1240	23.1410	5.0170
taucand8	4 17 38.890	27 46 22.980	20.4720	18.5970	23.5690	4.9720
taucand19	4 18 17.400	27 31 36.740	16.7580	14.7450	19.6870	4.9420
taucand135	4 36 14.710	24 43 21.240	20.0130	18.2440	23.1730	4.9290
taucand86	4 32 21.550	24 11 22.030	19.0540	17.3880	22.2820	4.8940
taucand108	4 31 41.990	24 31 27.180	21.5040	18.8880	23.7240	4.8360
taucand107	4 31 41.950	24 31 26.900	21.4260	18.8880	23.7240	4.8360
taucand126	4 33 11.200	24 45 40.680	20.9920	19.2600	24.0920	4.8320
taucand136	4 35 57.510	24 40 55.120	20.9600	19.1010	23.9270	4.8260
taucand124	4 34 14.040	24 50 28.330	21.1210	19.4820	24.2760	4.7940
taucand15	4 17 28.510	27 41 46.750	19.6020	17.6370	22.3910	4.7540
taucand92	4 30 44.550	24 12 17.440	20.3240	18.5180	23.2630	4.7450

taucand14	4 17 47.030	27 34 59.570	19.4580	17.4380	22.1310	4.6930
taucand31	4 18 46.100	27 18 48.520	18.3980	16.4420	21.1090	4.6670
taucand32	4 19 25.460	27 18 17.750	19.2270	17.3390	22.0030	4.6640
taucand94	4 30 43.790	24 11 28.110	21.1830	19.3320	23.9540	4.6220
taucand16	4 17 29.800	27 43 26.840	19.9090	18.0250	22.6310	4.6060
taucand62	4 29 49.110	24 23 8.340	19.9300	18.2420	22.8370	4.5950
taucand40	4 16 54.830	28 57 7.600	21.2260	19.6090	24.2040	4.5950
taucand72	4 29 46.500	24 31 49.300	16.8960	14.9420	19.5290	4.5870
taucand4	4 17 39.360	27 48 14.220	18.1020	16.3030	20.8730	4.5700
taucand74	4 29 43.150	24 32 15.530	19.7920	17.8160	22.3560	4.5400
taucand87	4 32 34.180	24 9 36.400	20.3140	18.6720	23.2070	4.5350
taucand53	4 31 6.690	23 38 30.880	20.0950	18.5720	23.0810	4.5090
taucand7	4 17 40.070	27 49 28.310	20.0940	18.5180	23.0030	4.4850
taucand9	4 17 31.350	27 54 2.020	20.9180	19.2310	23.7160	4.4850
taucand147	4 35 7.600	25 37 47.850	19.4090	17.7400	22.2190	4.4790
taucand132	4 35 5.670	24 48 37.950	20.5190	18.9970	23.4560	4.4590
taucand46	4 16 28.960	28 45 52.860	19.0440	17.1880	21.6410	4.4530
taucand106	4 31 58.690	24 27 10.060	20.5030	18.8230	23.2650	4.4420
taucand38	4 16 39.110	28 58 49.500	15.9620	14.4360	18.8650	4.4290
taucand91	4 30 49.370	24 9 46.200	20.0440	18.3860	22.8100	4.4240
taucand63	4 29 40.880	24 25 29.740	21.0990	19.4500	23.8720	4.4220
taucand47	4 17 30.090	28 51 31.000	21.2040	19.5970	24.0010	4.4040
taucand121	4 32 38.110	24 13 52.430	20.2270	18.5320	22.9310	4.3990
taucand6	4 17 32.340	27 51 56.140	19.2720	17.5920	21.9800	4.3880
taucand137	4 36 13.070	24 43 44.920	21.7660	20.0440	24.4140	4.3700
taucand68	4 29 35.870	24 27 2.480	20.7020	18.9690	23.3100	4.3410
taucand37	4 15 37.010	28 35 20.090	21.0200	19.4090	23.7450	4.3360
taucand88	4 31 15.810	24 11 49.480	20.4100	18.8420	23.1760	4.3340
taucand130	4 33 58.120	25 1 2.770	19.6580	18.1910	22.5250	4.3340
taucand93	4 30 58.620	24 15 40.000	20.6260	18.9120	23.2450	4.3330
taucand163	4 30 56.120	18 42 9.420	18.5170	17.1810	21.5000	4.3190
taucand152	4 35 14.550	25 27 10.010	19.6770	18.1360	22.4240	4.2880
taucand129	4 35 9.710	25 1 44.410	19.0090	17.5980	21.8840	4.2860
taucand156	4 35 9.720	25 1 44.440	19.0310	17.5840	21.8650	4.2810
taucand119	4 32 14.750	24 15 19.500	19.5410	18.0340	22.2930	4.2590
taucand90	4 30 53.540	24 3 49.550	19.6780	18.1230	22.3810	4.2580
taucand23	4 18 4.650	27 30 0.880	17.8170	16.0930	20.3360	4.2430

taucand75	4 29 50.200	24 31 56.350	19.8810	18.1170	22.3400	4.2230
taucand104	4 32 4.800	24 34 1.600	19.8880	18.2060	22.4270	4.2210
taucand51	4 17 31.820	28 49 44.730	18.1160	16.6150	20.8280	4.2130
taucand69	4 29 51.610	24 44 58.070	18.7490	17.2630	21.4730	4.2100
taucand67	4 28 59.640	24 25 49.920	19.5010	17.9210	22.1300	4.2090
taucand145	4 35 15.630	25 36 48.360	18.3720	16.8040	20.9810	4.1770
taucand164	4 30 5.660	18 37 40.760	18.6090	17.1800	21.3540	4.1740
taucand45	4 17 31.810	28 49 44.760	18.1280	16.6670	20.8210	4.1540
taucand13	4 18 2.740	27 35 4.860	18.0020	16.3050	20.4430	4.1380
taucand61	4 31 4.380	24 27 34.700	18.7020	16.9440	21.0610	4.1170
taucand100	4 32 32.960	24 28 21.000	18.2990	16.7690	20.8840	4.1150
taucand36	4 15 23.080	28 48 19.890	17.4840	15.7020	19.8160	4.1140
taucand102	4 31 4.350	24 27 34.630	18.6970	16.9830	21.0880	4.1050
taucand103	4 32 32.530	24 25 32.520	19.2200	17.5070	21.5840	4.0770
taucand117	4 32 18.750	24 24 24.650	18.4960	17.0660	21.1220	4.0560
taucand116	4 31 59.230	24 23 19.310	18.2290	16.8010	20.8530	4.0520
taucand24	4 18 2.760	27 35 4.620	18.0900	16.4270	20.4550	4.0280
taucand84	4 31 27.640	24 13 9.590	18.6220	17.2280	21.2190	3.9910
taucand55	4 31 54.020	23 58 48.680	18.6660	17.3150	21.3050	3.9900
taucand25	4 18 8.280	27 38 10.900	18.4520	16.8180	20.8060	3.9880
taucand161	4 30 5.660	18 37 40.850	18.6330	17.2550	21.2400	3.9850
taucand59	4 29 49.340	24 23 8.600	18.5910	17.1060	21.0860	3.9800
taucand60	4 30 41.400	24 29 14.300	18.6250	17.1070	21.0850	3.9780
taucand114	4 32 12.700	24 21 17.370	17.5260	16.0230	19.9910	3.9680
taucand131	4 36 25.580	24 49 27.740	18.4060	17.0750	21.0290	3.9540
taucand146	4 35 17.830	25 34 11.450	18.9350	17.3710	21.3230	3.9520
taucand5	4 17 46.150	27 54 27.180	18.8530	17.2550	21.1980	3.9430
taucand58	4 31 5.550	24 25 45.370	17.7660	16.2550	20.1910	3.9360
taucand118	4 31 33.250	24 19 1.490	18.6320	17.1840	21.1190	3.9350
taucand101	4 32 27.710	24 28 11.120	18.3860	16.9540	20.8850	3.9310
taucand29	4 19 8.500	27 17 9.660	17.5430	15.9480	19.8770	3.9290
taucand157	4 37 4.660	25 18 33.030	17.5360	16.1950	20.1240	3.9290
taucand158	4 36 36.440	25 18 1.710	18.6140	17.2630	21.1870	3.9240
taucand97	4 31 5.530	24 25 45.310	17.7750	16.2900	20.2000	3.9100
taucand85	4 32 6.350	24 8 15.060	18.7170	17.3550	21.2460	3.8910
taucand160	4 29 43.760	18 15 36.420	18.3490	17.0110	20.8940	3.8830
taucand66	4 29 28.170	24 23 10.190	18.7090	17.2830	21.1660	3.8830

taucand56	4 30 58.450	24 5 8.500	18.7480	17.3890	21.2130	3.8240
taucand50	4 17 33.520	29 6 5.830	17.1830	15.9550	19.7790	3.8240
taucand162	4 31 12.550	18 40 2.540	16.5700	15.3070	19.1110	3.8040
taucand39	4 17 33.510	29 6 5.860	17.2040	15.9620	19.7640	3.8020
taucand128	4 33 49.740	25 6 46.020	18.6060	17.2480	21.0450	3.7970
taucand35	4 15 29.540	28 53 15.590	16.9810	15.6560	19.4220	3.7660
taucand3	4 17 40.500	27 51 48.040	17.8840	16.5850	20.2920	3.7070
taucand154	4 36 54.850	24 55 50.310	17.8840	16.5900	20.2890	3.6990
taucand99	4 32 39.470	24 27 4.610	18.2160	16.6710	20.3680	3.6970
taucand151	4 35 47.840	25 28 51.440	18.4830	17.0800	20.7750	3.6950
taucand57	4 30 19.550	24 27 36.750	17.6480	16.1010	19.7770	3.6760
taucand22	4 18 27.310	27 29 6.640	17.7970	16.2460	19.9140	3.6680
taucand149	4 35 32.010	25 29 14.940	17.5300	16.1150	19.7800	3.6650
taucand83	4 32 0.030	24 6 34.580	18.3580	17.0310	20.6910	3.6600
taucand82	4 31 38.320	24 8 1.720	18.2460	16.9330	20.5750	3.6420
taucand44	4 17 4.510	28 46 23.710	17.8530	16.5080	20.1240	3.6160
taucand98	4 31 39.930	24 25 50.630	17.8320	16.4780	20.0880	3.6100
taucand12	4 17 9.560	27 38 49.680	17.6980	16.4270	19.9840	3.5570
taucand140	4 34 3.240	25 27 49.220	17.8750	16.4890	20.0190	3.5300
taucand159	4 29 34.100	18 25 35.850	17.0630	15.8310	19.3580	3.5270
taucand73	4 30 17.710	24 31 41.350	17.4710	16.0820	19.6050	3.5230
taucand155	4 35 9.150	24 59 23.190	17.6150	16.3630	19.8840	3.5210
taucand150	4 35 51.910	25 24 51.960	17.8700	16.5070	20.0240	3.5170
taucand113	4 32 7.980	24 15 30.030	16.9890	15.5820	19.0940	3.5120
taucand30	4 19 21.890	27 19 13.900	18.0280	16.6280	20.1280	3.5000
taucand153	4 36 49.350	24 54 32.060	16.0820	14.8670	18.3520	3.4850
taucand134	4 36 31.300	24 35 53.600	16.7040	15.5400	19.0140	3.4740
taucand65	4 29 26.680	24 23 33.120	17.0280	15.7600	19.1360	3.3760
taucand54	4 31 32.030	24 4 18.840	15.9430	14.8280	18.1680	3.3400
taucand79	4 31 32.040	24 4 18.830	15.9960	14.8550	18.1900	3.3350
taucand81	4 31 43.580	24 9 20.180	16.8520	15.6420	18.9620	3.3200
taucand115	4 31 47.020	24 22 0.370	17.5990	16.2220	19.4940	3.2720
taucand89	4 30 13.420	24 18 39.610	16.7180	15.5540	18.8050	3.2510
taucand20	4 18 8.440	27 38 21.960	17.1350	15.7970	19.0320	3.2350
taucand144	4 35 28.060	25 36 13.850	17.2600	15.9570	19.1560	3.1990
taucand21	4 18 9.440	27 39 19.660	17.2730	15.9450	19.1420	3.1970
taucand110	4 32 4.350	24 13 54.580	16.1530	14.8050	17.9950	3.1900

taucand112	4 32 35.470	24 15 18.660	16.9090	15.6160	18.7870	3.1710
taucand11	4 17 34.600	27 44 13.130	17.3020	15.9780	19.1480	3.1700
taucand64	4 29 34.500	24 26 30.120	16.9440	15.6100	18.7490	3.1390
taucand28	4 18 55.080	27 20 16.760	16.4200	15.1430	18.2680	3.1250
taucand111	4 31 41.500	24 17 18.920	16.5750	15.2730	18.3970	3.1240
taucand77	4 32 4.570	24 12 42.230	15.6470	14.3830	17.5030	3.1200
taucand2	4 17 43.650	27 52 8.020	16.9290	15.7280	18.8470	3.1190
taucand138	4 35 37.020	25 15 44.590	16.9280	15.6940	18.8130	3.1190
taucand17	4 17 54.180	27 31 43.730	15.9570	14.6630	17.7480	3.0850
taucand127	4 34 6.150	25 4 28.600	16.4920	15.2540	18.2890	3.0350
taucand96	4 31 57.820	24 36 10.990	16.5750	15.3190	18.3360	3.0170
taucand43	4 17 45.640	28 46 14.430	16.4210	15.2800	18.2850	3.0050
taucand18	4 18 5.490	27 38 13.120	16.7520	15.5230	18.4920	2.9690
taucand143	4 34 26.770	25 32 46.250	16.5210	15.2850	18.2500	2.9650
taucand49	4 17 34.840	28 48 16.910	15.8620	14.6850	17.6310	2.9460
taucand95	4 32 0.430	24 34 47.080	16.4300	15.2190	18.1470	2.9280
taucand78	4 32 23.900	24 10 33.500	15.6830	14.5050	17.4190	2.9140
taucand133	4 36 2.450	24 43 9.340	16.5360	15.3490	18.2620	2.9130
taucand109	4 32 7.970	24 16 28.150	16.0060	14.8020	17.6950	2.8930
taucand1	4 17 41.230	27 45 44.440	16.4420	15.2780	18.1570	2.8790
taucand34	4 16 6.010	28 48 59.220	16.1780	15.0150	17.8870	2.8720
taucand70	4 29 59.680	24 35 18.770	15.5980	14.4910	17.3380	2.8470
taucand27	4 18 46.330	27 21 42.310	15.6330	14.4730	17.2860	2.8130
taucand148	4 35 10.620	25 27 43.300	16.0550	14.9410	17.7540	2.8130
taucand41	4 17 34.830	28 48 16.940	15.8800	14.7390	17.5360	2.7970
taucand139	4 33 50.610	25 24 7.610	16.1290	15.0160	17.8110	2.7950
taucand125	4 32 52.800	24 47 33.940	16.1090	14.9720	17.7310	2.7590
taucand80	4 32 14.100	24 7 36.770	16.0350	14.9190	17.6680	2.7490
taucand142	4 34 51.340	25 40 4.630	16.0000	14.8870	17.6240	2.7370
taucand71	4 31 9.490	24 35 24.180	15.9900	14.8930	17.6030	2.7100
taucand42	4 16 59.540	28 55 25.460	15.9050	14.7960	17.5040	2.7080
taucand26	4 18 47.340	27 21 29.290	15.5630	14.4650	17.1710	2.7060
taucand10	4 17 54.950	27 38 40.510	16.0090	14.8840	17.5770	2.693

Table A.1: The potential brown dwarf candidates identified in the Taurus Dark Clouds.

Appendix B

Hyades Candidates

Listed in Table B.1 are the candidates identified from the proper motion and photometric selections as outlined in Chapter 7. Each candidate has three rows of data: row 1 gives the physical data, including position, proper motion (in mas/yr), mass (in $M_{\odot}$) and distance (in pc); row 2 gives the POSS I and POSS II magnitudes; row 3 gives the 2MASS magnitudes.

ID	RA	DEC	μ_α	μ_δ	mass	dist
	B1	B2	R1	R2	I	
	J	H	K			
5262	4 32 37.825	9 51 6.700	102	-8	0.752704	41.9597
	13.5600	13.0700	10.7000	10.8000	9.6500	
	8.3860	7.7410	7.5410			
9432	5 11 9.693	15 48 57.500	56	-24	0.721261	50.0536
	13.7200	13.1600	0.0000	11.3200	10.2300	
	8.9740	8.2770	8.1020			
3703	4 51 49.166	17 16 25.540	66	-28	0.714582	53.3864
	13.2700	12.0300	10.6700	10.6000	9.6200	
	9.0150	8.4310	8.2790			
909	4 27 56.760	19 3 38.850	80	-32	0.713240	55.0756
	13.3800	14.1400	10.6500	11.0300	10.1700	
	9.0450	8.4800	8.3540			
116	4 28 28.781	17 41 45.150	106	-42	0.712497	40.8834
	14.2400	14.2500	11.3000	10.7400	10.0800	
	8.5920	7.9560	7.7110			
4293	4 33 23.758	23 59 27.030	94	-50	0.699905	45.8300

	14.0400	13.9500	11.3900	11.7000	10.4200	
	8.9140	8.2420	8.0280			
2353	4 24 7.425	22 7 7.840	114	-46	0.681392	40.9913
	12.5100	11.9700	10.2900	10.4000	9.8100	
	8.6270	8.0660	7.8860			
8947	5 10 24.435	10 25 4.800	50	-6	0.658972	55.9932
	12.6900	12.8600	10.6500	10.8800	10.1800	
	9.4920	8.8470	8.6830			
3558	4 51 2.419	14 58 16.500	88	-32	0.654808	39.8576
	13.2000	13.4000	10.7000	10.8100	9.9800	
	8.7960	8.1450	7.9670			
184	4 31 29.060	17 43 7.410	102	6	0.652544	44.6187
	0.0000	14.0500	0.0000	10.8700	10.2800	
	9.0600	8.3900	8.2240			
5217	4 23 50.705	9 12 19.580	104	-6	0.649806	44.3639
	14.3100	14.4600	12.3500	12.1900	10.3400	
	9.1170	8.4810	8.2260			
1315	4 18 47.019	13 21 58.690	106	-16	0.644699	45.3332
	13.6800	13.3600	11.0400	11.1500	10.4400	
	9.1210	8.4810	8.3000			
350	4 25 13.541	17 16 5.540	106	-28	0.632540	43.3706
	15.6400	14.2900	12.7800	12.5500	10.6500	
	9.1490	8.4810	8.2680			
526	4 31 44.827	15 37 46.050	108	-32	0.622704	39.5969
	13.7100	12.9000	11.0300	10.8000	9.8900	
	9.1300	8.3450	8.1220			
1304	4 17 47.679	13 39 42.360	104	-16	0.612772	46.5842
	14.3200	13.9300	11.3800	12.5300	10.5700	
	9.4050	8.7200	8.5270			
1051	4 25 14.549	18 58 24.910	92	-28	0.609948	50.2430
	14.9800	14.9000	12.5900	12.9500	10.7900	
	9.5940	8.9580	8.7060			
1650	4 48 30.612	16 23 19.020	78	-30	0.609853	46.5995
	14.6000	13.7500	11.3500	11.3600	10.4100	
	9.4150	8.7730	8.5430			
563	4 34 39.942	15 12 32.660	104	-28	0.608345	40.2909
	14.4400	13.8200	11.9100	11.4000	10.2900	

	9.0420	8.4100	8.2350			
1818	4 42 30.289	20 27 11.530	88	-38	0.603477	45.3424
	15.3300	15.2900	12.8400	13.1900	10.6700	
	9.3960	8.7720	8.5170			
4395	4 25 20.026	23 6 31.260	90	-38	0.593563	51.8229
	14.6600	14.3400	11.4400	11.9700	11.0300	
	9.7310	9.1060	8.8590			
5211	4 22 30.037	10 26 4.750	102	-6	0.584278	45.7927
	14.7300	14.2100	12.1800	12.1000	10.6100	
	9.5110	8.8470	8.6390			
1555	4 41 27.817	14 4 34.110	86	-18	0.573012	46.0885
	15.4200	14.8400	12.6600	12.3500	10.7400	
	9.5760	8.9380	8.7120			
15043	3 37 33.880	17 51 0.670	166	-24	0.569558	37.8081
	15.2600	14.6900	12.6900	12.0800	10.1900	
	9.1860	8.5640	8.3000			
15042	3 37 33.357	17 51 14.390	172	-26	0.567651	36.4565
	14.6000	13.9700	11.3400	11.3300	9.8500	
	9.1000	8.4740	8.2310			
324	4 23 59.131	16 43 17.700	110	-26	0.565820	42.2539
	14.5800	13.9000	11.9200	11.4300	10.6900	
	9.4210	8.7870	8.5610			
3133	4 41 28.754	12 0 33.720	86	-14	0.562179	45.7770
	14.9500	14.5400	12.4400	11.9100	10.6800	
	9.6130	8.9810	8.7540			
431	4 23 50.352	14 55 17.510	116	-24	0.561817	39.8352
	15.4400	14.6400	12.7000	13.1800	10.9900	
	9.2930	8.7180	8.4540			
3264	4 52 23.866	10 43 9.910	76	-12	0.560845	46.0097
	0.0000	14.2900	11.7600	11.7900	10.7000	
	9.6330	8.9730	8.7720			
784	4 36 4.172	18 53 19.000	90	-32	0.539443	46.7227
	15.5200	15.6700	12.9300	13.5300	10.9600	
	9.7720	9.1480	8.9180			
917	4 29 1.000	18 40 25.360	108	-28	0.539159	42.0350
	0.0000	15.4600	0.0000	12.9600	10.8200	
	9.5710	8.9470	8.6900			

2156	4 39 55.898	21 29 39.740	72	-32	0.526449	57.1178
	15.2300	15.6900	12.4400	13.5200	11.1400	
	10.3170	9.6120	9.4230			
7273	3 49 43.177	24 19 5.080	128	-44	0.525713	45.7297
	15.8400	14.7800	12.8200	12.9200	10.6700	
	9.8050	9.2250	8.9440			
3139	4 42 4.531	11 55 13.790	80	-10	0.522376	49.1663
	15.4800	14.9700	12.8300	12.4800	11.1400	
	9.9880	9.3650	9.1190			
155	4 29 55.739	16 54 50.670	112	-28	0.522094	39.6421
	14.9100	14.9600	12.1800	11.9100	10.7100	
	9.5240	8.9010	8.6530			
1353	4 22 59.901	13 18 58.570	90	-14	0.517840	51.6697
	15.6300	14.8800	13.1200	13.5300	11.4000	
	10.1220	9.4670	9.2510			
2289	4 19 29.761	21 45 14.180	96	-34	0.515566	50.7006
	14.6400	14.4700	12.4900	13.3500	11.2200	
	10.1060	9.4420	9.2220			
7062	4 2 25.469	26 11 37.020	102	-42	0.515359	53.6783
	12.9800	12.4800	11.1100	11.2400	10.6400	
	9.9790	9.4550	9.3470			
911	4 27 59.207	18 45 32.700	90	-28	0.511849	50.1713
	16.5200	15.7500	13.6500	14.0700	11.4000	
	10.0530	9.4670	9.2190			
2826	4 6 34.621	13 32 56.810	112	-10	0.510162	47.1040
	15.1000	15.0700	12.5100	12.9400	11.0700	
	9.9820	9.2580	9.0910			
1151	4 17 50.630	18 28 30.890	110	-26	0.507764	44.7400
	15.3900	15.1000	12.7800	13.1600	11.1000	
	9.8410	9.2460	8.9920			
4746	3 59 14.173	22 2 37.910	142	-46	0.504902	38.9076
	14.2000	14.2000	11.7800	12.1400	10.9500	
	9.5380	8.9140	8.7040			
15657	4 41 46.747	4 26 11.680	78	14	0.488284	50.2308
	14.9600	14.6700	13.2600	13.3100	11.8000	
	10.2050	9.6090	9.3480			
1486	4 33 27.009	13 2 43.670	108	-18	0.488191	39.4163

	15.2000	14.8600	12.7000	12.1300	10.9500	
	9.6830	9.0690	8.8220			
15236	3 35 42.971	11 33 22.240	172	-4	0.482404	36.7128
	15.1300	14.6900	12.5200	12.4400	10.7900	
	9.5590	8.9600	8.6990			
794	4 36 38.930	18 36 56.770	102	-36	0.481593	40.9384
	15.5200	15.3800	12.9700	13.3500	10.8100	
	9.7770	9.1530	8.9400			
802	4 37 21.889	19 21 17.390	88	-34	0.469614	47.1296
	16.6900	16.5500	14.1200	14.2700	11.3400	
	10.1820	9.5720	9.3110			
1310	4 18 8.533	13 19 52.680	102	-10	0.466343	47.6352
	16.1100	15.7600	13.4800	14.3000	12.4300	
	10.2880	9.6980	9.3520			
13503	5 14 33.703	19 46 36.910	52	-38	0.465886	50.7705
	14.9200	13.7100	12.1000	11.8900	10.6400	
	10.2980	9.5990	9.4930			
821	4 38 54.708	19 10 56.110	90	-34	0.464482	45.5698
	16.0500	15.8800	13.6600	13.9400	11.2000	
	10.1630	9.5060	9.2660			
6638	5 3 23.981	25 33 45.530	60	-54	0.461896	51.7170
	13.8400	13.5900	11.7500	11.6300	11.1500	
	10.2890	9.6730	9.5550			
19	4 14 29.823	18 43 48.240	102	-30	0.461550	48.7147
	15.6900	15.5700	13.1600	13.7700	11.5700	
	10.2940	9.7110	9.4270			
842	4 40 12.707	19 17 10.040	96	-38	0.459769	42.1015
	15.7200	15.3000	13.0400	13.6600	10.9700	
	9.9480	9.3630	9.1200			
10610	4 41 27.920	28 0 42.190	82	-100	0.459624	38.5426
	0.0000	14.7100	18.4700	12.7400	10.9300	
	9.7780	9.1530	8.9290			
29	4 16 3.572	18 51 33.220	104	-30	0.454042	47.4212
	15.6600	15.1100	12.9100	13.3900	11.3000	
	10.2470	9.6540	9.4100			
6782	4 35 3.312	24 51 14.690	70	-42	0.453446	59.9693
	16.2900	15.2800	13.7700	13.7700	11.7800	

	10.7900	10.1850	9.9230			
3502	4 56 12.645	13 59 2.960	58	-26	0.449657	54.9951
	0.0000	15.4800	13.4300	13.4300	11.6700	
	10.6150	10.0200	9.7560			
4070	4 43 24.743	24 17 48.110	88	-54	0.447263	44.6331
	15.0800	15.5500	12.9600	13.4400	11.2000	
	10.1910	9.5310	9.3160			
4394	4 25 18.169	23 3 39.060	104	-44	0.433645	44.8144
	15.6200	15.5900	12.7600	13.1500	11.4700	
	10.2640	9.6170	9.4010			
4280	4 30 44.991	22 37 48.330	82	-40	0.432136	53.3238
	16.4500	16.1500	14.0200	13.9600	12.2000	
	10.6240	10.0130	9.7870			
4348	4 21 55.853	23 25 6.000	128	-62	0.428542	36.4629
	14.6300	14.9000	12.1100	12.7700	11.0100	
	9.8850	9.2240	8.9820			
17011	4 5 53.177	31 30 26.810	102	-28	0.427200	58.2839
	0.0000	15.6700	0.0000	12.9600	11.4200	
	10.8300	10.1760	10.0080			
4883	3 55 57.173	18 25 56.330	130	-24	0.426194	43.6928
	15.8200	15.2900	13.8300	13.4100	11.3600	
	10.2300	9.6290	9.3880			
3029	4 30 57.337	12 18 13.720	116	-16	0.421129	37.5012
	16.3200	15.2900	13.3600	12.9300	11.1800	
	9.9450	9.3740	9.0850			
9380	5 7 34.946	14 39 14.220	64	-22	0.420989	45.8867
	16.1900	16.3500	13.2000	13.6200	11.4000	
	10.4160	9.8000	9.5240			
5018	4 0 44.949	13 54 22.720	130	-14	0.419779	42.1026
	16.2000	15.7900	13.4300	13.9300	11.4800	
	10.2600	9.6150	9.3440			
1186	4 12 21.723	16 15 3.430	150	-30	0.419166	33.7442
	15.5300	15.1800	13.0700	13.7600	11.3900	
	9.7360	9.0950	8.8670			
2973	4 24 44.026	10 46 19.610	104	-10	0.415009	44.0199
	16.0300	15.8500	13.3600	13.5600	12.1100	
	10.3040	9.6560	9.4680			

2320	4 22 42.843	20 34 12.550	100	-42	0.413929	46.0671
	17.2400	16.8500	14.4500	14.6900	13.2400	
	10.4580	9.8340	9.5730			
3033	4 31 15.734	10 42 15.480	90	-8	0.412954	48.1820
	17.1100	16.4400	13.9300	13.6600	12.0500	
	10.5350	9.9440	9.6760			
1221	4 16 54.453	16 21 25.000	106	-24	0.411963	46.0839
	16.2400	15.5600	13.0500	14.1000	12.4400	
	10.4340	9.8130	9.5850			
1224	4 17 28.134	14 54 3.930	104	-18	0.411894	46.8456
	15.9400	15.5200	13.3200	14.1600	12.5300	
	10.4710	9.8690	9.6210			
5568	4 59 19.817	10 23 9.520	80	-12	0.411824	40.3077
	15.5300	15.3400	0.0000	12.6900	11.2300	
	10.1860	9.5280	9.2950			
419	4 22 30.520	15 13 12.910	88	-16	0.410679	53.3902
	16.7200	15.9600	14.1500	14.4300	12.5200	
	10.7750	10.1380	9.9120			
5354	4 47 37.115	10 13 58.940	68	-2	0.407095	54.6673
	0.0000	16.7500	13.3000	13.9600	12.3300	
	10.8470	10.2460	9.9840			
7737	3 52 34.314	11 15 38.690	166	-10	0.404473	34.6004
	0.0000	15.0200	0.0000	13.1000	10.8400	
	9.8640	9.2450	9.0060			
1057	4 25 41.819	19 0 47.590	82	-26	0.391142	56.0129
	17.0600	16.4900	14.5800	14.5300	13.6100	
	11.0100	10.3870	10.1300			
1242	4 10 31.945	12 35 5.140	82	-40	0.387084	56.3471
	0.0000	13.9100	0.0000	12.6100	11.3200	
	10.7660	10.2630	10.1670			
1714	4 44 43.749	18 24 29.860	86	-38	0.383215	44.0431
	17.6100	16.0900	14.3500	14.3800	12.9400	
	10.5610	9.9040	9.6550			
3009	4 29 16.235	12 21 37.440	100	-10	0.381891	44.3304
	16.7900	15.9000	13.8700	14.4400	12.6200	
	10.5370	9.9240	9.6770			
8419	4 46 9.189	6 45 0.410	92	6	0.378482	40.8910

	16.5800	16.1100	14.0800	14.2800	12.4200	
	10.3950	9.8170	9.5220			
17583	4 43 16.966	2 0 26.370	86	26	0.372720	44.5132
	15.8700	16.4400	13.6600	14.1600	12.0300	
	10.6380	10.0350	9.7410			
7702	3 47 2.670	11 41 30.470	120	-60	0.372356	44.3046
	15.2200	15.1300	12.9600	13.0300	11.4800	
	10.5400	9.9820	9.7330			
4667	3 59 51.821	22 36 13.510	104	-32	0.370458	53.4255
	15.6600	16.5200	13.6400	13.9800	12.1400	
	11.0210	10.3860	10.1510			
6775	4 34 14.295	25 8 29.260	84	-46	0.369189	51.5945
	14.2800	13.8100	12.3100	12.3300	11.6800	
	10.7420	10.1860	10.0830			
505	4 30 33.884	14 44 53.190	102	-22	0.363927	42.8527
	16.4900	16.4600	13.8400	13.5700	11.8000	
	10.5630	9.9540	9.7120			
2897	4 10 33.954	11 27 34.750	140	0	0.363748	36.6066
	14.8300	14.7300	12.4400	12.9100	11.2200	
	10.2020	9.5980	9.3710			
11624	3 42 53.260	23 26 49.720	172	-50	0.361401	35.4554
	16.6700	15.9100	13.1200	13.7200	11.3400	
	10.2020	9.5450	9.3160			
2295	4 20 29.371	21 22 43.370	92	-38	0.360328	51.3516
	18.0700	16.2800	14.3000	14.6600	12.3100	
	11.0180	10.4100	10.1270			
1520	4 35 48.519	13 17 17.020	92	-16	0.358706	45.3472
	16.9400	16.6700	13.9500	13.8300	11.9400	
	10.7310	10.1080	9.8670			
6937	4 21 0.615	24 31 7.880	104	-50	0.358690	45.7860
	16.2800	16.3900	13.4900	14.1700	12.1300	
	10.7860	10.1290	9.8880			
1228	4 17 55.567	14 32 46.640	100	-16	0.358544	48.5684
	16.6200	16.3700	14.0300	14.7600	12.9200	
	10.8710	10.2760	10.0170			
2130	4 37 5.166	20 43 5.670	78	-28	0.358075	54.7758
	17.5700	17.0000	14.9300	15.0500	13.4300	

	11.1130	10.5230	10.2810			
1202	4 13 52.353	15 21 54.130	120	-20	0.356975	41.7859
	16.4100	16.1600	14.0300	14.6500	12.7700	
	10.5410	9.9750	9.7000			
2965	4 23 59.503	11 22 59.070	88	-6	0.356394	52.5406
	17.2700	16.8600	14.1200	14.5800	12.9100	
	11.0910	10.5220	10.2010			
12402	4 37 44.111	4 54 6.750	96	14	0.355313	42.5355
	16.3600	15.8000	14.1100	13.9900	12.4100	
	10.6200	10.0330	9.7490			
3875	4 50 16.671	20 37 32.660	94	-66	0.352965	35.7632
	0.0000	15.4000	0.0000	13.8000	11.1900	
	10.2810	9.6280	9.3870			
1754	4 47 37.952	17 19 44.760	78	-32	0.349012	47.1736
	15.1000	15.6400	13.0200	13.4500	13.2000	
	10.6920	10.1850	10.0130			
5020	4 0 59.482	14 20 45.170	126	-18	0.348757	43.2497
	16.8700	16.2700	14.1800	14.4000	12.5800	
	10.6930	10.0830	9.8260			
1972	4 42 58.475	20 36 17.530	82	-36	0.347133	48.4775
	17.3800	16.6000	14.5600	14.9000	13.5100	
	10.8920	10.3490	10.0840			
1681	4 42 18.811	17 41 38.490	84	-30	0.345862	46.8956
	17.1300	16.7800	14.5300	14.4500	13.4100	
	10.8600	10.2830	10.0200			
11310	3 50 23.501	28 27 29.010	84	-74	0.342539	56.9290
	0.0000	15.6900	0.0000	14.0900	13.1800	
	11.3340	10.6810	10.4620			
2949	4 21 23.455	10 52 2.400	94	-4	0.342444	50.2125
	17.6900	17.5400	14.5600	15.0000	13.0100	
	11.0490	10.4530	10.1900			
3046	4 32 45.394	12 4 0.080	94	-14	0.340004	45.4477
	17.2700	16.9300	14.1100	13.8700	12.4200	
	10.8460	10.2270	9.9890			
17196	3 25 31.089	19 41 45.580	88	-72	0.337167	59.3060
	16.9000	16.4600	13.9800	14.2600	11.8300	
	11.4490	10.8370	10.5850			

9275	5 10 56.536	13 7 19.360	64	-18	0.336089	43.5823
	16.6100	16.9300	13.9000	14.2100	12.1700	
	10.8000	10.1550	9.9230			
2684	4 2 53.095	18 24 26.460	126	-26	0.334189	43.1403
	17.2400	15.9900	14.0500	14.3800	12.1400	
	10.7700	10.1780	9.9130			
12465	4 49 52.111	6 6 33.680	96	6	0.333598	37.7504
	16.2300	15.8100	13.7700	13.9600	12.2300	
	10.4610	9.8860	9.6270			
1140	4 16 43.289	16 49 20.120	96	-24	0.333366	50.8409
	17.4400	16.8700	14.5800	15.5000	13.3400	
	11.1610	10.5650	10.2750			
1598	4 47 49.659	12 41 29.360	68	-10	0.330578	54.7806
	0.0000	17.4200	14.7000	14.7600	13.0500	
	11.3370	10.7130	10.4550			
3927	4 56 16.653	21 22 1.710	68	-42	0.330516	49.7667
	16.4700	16.7300	14.3300	14.3600	12.8000	
	11.1380	10.5040	10.2470			
2936	4 17 39.695	12 24 53.600	116	-14	0.330408	41.7837
	16.8000	16.4300	14.0900	14.7500	13.1100	
	10.7460	10.1360	9.8680			
1824	4 42 50.929	19 29 13.870	90	-36	0.328789	44.0654
	17.3200	16.9900	14.6200	14.9700	13.4100	
	10.8220	10.2240	9.9940			
8603	4 54 48.813	7 44 20.040	92	0	0.328743	37.1741
	16.4300	16.0900	14.1300	13.6900	11.6000	
	10.4970	9.8730	9.6250			
197	4 32 7.953	17 39 52.210	98	-34	0.327313	43.7096
	17.6000	17.1700	14.5900	14.6100	13.4700	
	10.8980	10.2880	9.9860			
376	4 26 4.301	17 7 14.620	104	-32	0.324587	43.3735
	17.9700	16.4400	14.9800	14.6400	12.2800	
	10.8870	10.2760	9.9870			
4347	4 21 53.090	24 14 25.910	124	-56	0.323016	38.5093
	0.0000	16.7100	0.0000	14.4000	12.3600	
	10.5870	10.0060	9.7390			
1133	4 15 34.834	16 45 44.870	104	-20	0.322376	47.8543

	16.4300	16.4000	13.8400	14.9400	13.2600	
	11.0500	10.4720	10.2150			
8766	5 9 40.460	8 12 50.490	78	-6	0.314333	36.0468
	16.3900	15.7400	13.4500	12.9700	11.3000	
	10.5260	9.9290	9.6530			
202	4 32 23.753	17 45 2.810	108	-32	0.310947	40.2080
	14.7600	15.2900	14.1200	14.1400	13.2300	
	10.7530	10.1610	9.9130			
1227	4 17 51.611	15 13 37.890	98	-20	0.310130	49.3887
	16.8600	16.8200	14.6400	15.2700	13.3100	
	11.2240	10.6380	10.3650			
1314	4 18 42.233	12 30 38.710	108	-10	0.301660	44.6787
	16.9500	16.5800	14.3000	15.0700	13.2800	
	11.0620	10.4800	10.2050			
1710	4 44 28.366	17 51 11.270	70	-20	0.300467	56.5525
	18.1900	17.1300	0.0000	15.3100	13.9800	
	11.5790	10.9880	10.7250			
1162	4 9 57.548	15 25 1.210	100	-28	0.300380	50.2737
	0.0000	17.1900	0.0000	15.6100	13.7000	
	11.3720	10.7360	10.4700			
1593	4 46 52.903	12 53 1.820	92	-16	0.300075	40.7679
	16.6000	16.8900	13.7800	14.1400	12.1000	
	10.8960	10.2750	10.0170			
361	4 25 47.000	17 32 40.660	98	-28	0.298683	46.5799
	18.2500	16.1600	15.2200	14.8100	12.6300	
	11.1890	10.5890	10.3160			
2343	4 23 57.396	22 10 53.780	118	-46	0.295597	39.8587
	17.0000	16.7900	14.0800	14.5800	12.5800	
	10.8670	10.2530	9.9990			
983	4 20 27.619	18 53 50.140	106	-40	0.295597	44.0264
	17.3300	16.2200	14.0000	14.4000	12.1900	
	11.0630	10.4830	10.2150			
2417	4 12 47.346	22 23 27.040	118	-44	0.294950	42.9357
	16.4100	17.2900	13.8900	14.5300	12.1600	
	11.0610	10.4970	10.1650			
13399	5 14 16.159	17 39 49.890	66	-40	0.290596	39.9875
	15.7400	15.1800	13.5200	13.2400	12.5400	

	10.9100	10.2480	10.0410			
6947	4 22 24.217	25 55 5.790	86	-48	0.290326	54.1919
	16.7500	16.5700	13.5000	13.8600	13.3100	
	11.6190	10.8930	10.7030			
4157	4 35 13.179	22 59 20.520	98	-46	0.289688	43.8978
	17.8800	18.2600	14.7600	15.1100	13.1100	
	11.1270	10.5300	10.2500			
2634	4 4 27.019	20 24 30.500	118	-34	0.289433	45.4027
	17.5800	16.6500	14.3700	14.9800	12.7600	
	11.2100	10.5940	10.3250			
1384	4 25 51.644	13 30 9.690	110	-22	0.288852	41.0636
	17.3300	16.4500	14.2400	14.8000	13.0000	
	11.0130	10.4000	10.1110			
730	4 40 28.269	18 5 16.180	118	-36	0.286300	34.5979
	17.5400	17.0000	14.6400	14.8700	13.2300	
	10.6360	10.0270	9.7570			
12659	5 0 11.945	5 51 19.870	70	10	0.284729	45.5835
	17.0900	16.7300	14.6300	14.8800	12.6400	
	11.2360	10.6250	10.3670			
6730	4 41 41.669	26 3 55.650	60	-60	0.284687	56.6411
	0.0000	17.0700	0.0000	14.5200	12.7500	
	11.7640	11.0710	10.8390			
841	4 39 51.585	19 39 34.610	86	-36	0.283666	46.9970
	19.1100	17.9000	15.7400	15.7600	13.9200	
	11.3650	10.7740	10.4410			
8380	4 41 42.989	8 26 20.040	100	-6	0.282578	39.2938
	16.5600	16.1400	14.1200	13.5400	11.4500	
	10.9400	10.3470	10.0600			
3105	4 38 9.470	11 19 5.440	84	-6	0.282146	48.6976
	18.5300	18.0700	14.9500	15.0600	13.2300	
	11.4100	10.8050	10.5290			
954	4 33 42.799	18 45 59.310	110	-38	0.282063	38.9751
	17.6900	16.7200	14.6800	14.9700	13.3200	
	10.9070	10.3210	10.0460			
1655	4 48 59.593	15 36 17.450	90	-30	0.281438	40.4467
	17.7200	17.6600	14.7400	15.1000	12.6400	
	11.0010	10.4180	10.1310			

2255	4 32 29.423	20 44 8.030	78	-26	0.279678	57.0341
	19.3100	18.3400	15.8800	16.1300	14.3300	
	11.7620	11.1920	10.8900			
13980	4 42 8.822	29 20 33.970	94	-76	0.279139	42.1078
	16.0100	15.2600	13.7400	13.5300	12.4300	
	11.1190	10.4340	10.2350			
17508	4 34 21.101	1 19 13.980	74	16	0.275853	57.6200
	15.6700	16.1600	0.0000	13.8400	12.8000	
	11.8160	11.1900	10.9400			
7168	3 47 53.915	25 9 20.930	166	-78	0.273710	34.2328
	15.6500	14.9800	12.7500	13.2200	11.3400	
	10.6830	10.0640	9.8250			
14008	4 46 56.039	30 23 12.490	68	-60	0.272040	55.9743
	18.0200	17.2600	15.2200	15.1000	13.6500	
	11.7390	11.1520	10.9050			
3537	4 57 57.790	14 27 7.370	74	-18	0.270364	45.3211
	0.0000	17.6100	14.6000	15.0600	12.8000	
	11.3040	10.7070	10.4590			
2948	4 21 19.747	12 2 38.370	104	-4	0.268708	45.5656
	18.8100	17.4800	15.0700	15.7200	13.6700	
	11.3610	10.7540	10.4830			
411	4 21 35.090	14 41 42.950	106	-20	0.266981	44.4286
	16.5300	16.8800	14.5200	15.2000	13.4300	
	11.2960	10.6860	10.4410			
381	4 18 12.969	16 5 53.500	98	-18	0.264531	49.7245
	17.6500	17.5300	14.9100	15.7600	13.6900	
	11.5830	10.9700	10.7040			
9016	5 13 5.383	9 27 33.670	62	-6	0.264491	43.2228
	15.2100	15.4200	12.7700	13.3900	12.0100	
	11.1930	10.6350	10.4000			
1291	4 16 25.411	14 10 17.090	134	-20	0.263365	36.6280
	16.8800	16.4900	13.9700	15.0400	13.1100	
	10.9250	10.3210	10.0490			
10297	4 52 17.766	26 41 41.550	70	-84	0.262770	41.8726
	0.0000	16.6900	0.0000	14.0800	12.2700	
	11.1280	10.5690	10.3440			
575	4 35 28.435	15 23 57.240	94	-32	0.261176	43.4810

	18.6000	0.0000	15.6400	0.0000	13.5300	
	11.3200	10.7210	10.4380			
6282	5 4 6.177	19 0 26.570	66	-22	0.260796	50.7831
	0.0000	17.5500	0.0000	15.5300	13.7000	
	11.6750	11.0420	10.7780			
13027	5 16 15.845	9 26 47.930	58	-6	0.260468	43.9555
	16.5400	16.6800	14.1600	14.7000	12.8900	
	11.3510	10.6920	10.4670			
8381	4 41 46.858	7 16 32.730	80	6	0.260376	49.0765
	17.4300	17.4900	15.0100	14.5900	13.1300	
	11.5370	11.0140	10.7070			
3070	4 35 24.649	10 44 52.730	104	-4	0.260166	40.3233
	18.1600	17.7900	14.7800	14.8500	12.9800	
	11.1790	10.5470	10.2820			
1603	4 49 10.555	13 48 41.190	88	-24	0.257218	41.1385
	17.2800	17.2500	14.3200	14.7200	12.8300	
	11.2450	10.6390	10.3480			
6861	4 30 17.023	26 22 26.460	82	-52	0.255418	53.0236
	18.1500	18.0000	15.4400	15.4900	13.6300	
	11.8030	11.1560	10.9130			
2956	4 22 25.270	11 53 25.840	114	-14	0.253268	40.9188
	16.2300	16.2100	13.4900	13.8600	12.7600	
	11.1900	10.5510	10.3670			
591	4 38 10.546	15 49 17.600	94	-24	0.251068	43.6795
	18.1400	17.8000	15.3100	14.8800	12.8100	
	11.3840	10.7900	10.5260			
10262	4 49 57.974	27 12 36.900	102	-72	0.250190	37.5571
	17.4100	16.6700	14.5900	14.7800	12.9500	
	11.0670	10.4960	10.2050			
2798	4 2 4.173	12 48 26.360	104	-54	0.250178	46.4396
	0.0000	15.5200	0.0000	13.6900	12.7400	
	11.5190	10.8630	10.6660			
3102	4 37 14.547	11 19 26.920	84	-12	0.248543	48.7427
	18.4800	17.8800	15.0400	15.1000	13.3100	
	11.6340	11.0670	10.7840			
5240	4 29 5.714	9 10 57.040	78	-2	0.247684	56.6936
	18.8200	18.4400	15.6400	16.2000	13.9600	

	12.0040	11.4150	11.1190			
5971	4 58 38.127	16 13 21.140	60	-20	0.247281	55.7048
	19.3000	18.6200	0.0000	15.8900	13.3800	
	11.9800	11.3200	11.0840			
9389	5 8 15.403	15 22 37.720	54	-6	0.246929	57.5095
	18.1100	16.8900	15.3600	15.2800	13.3500	
	12.0380	11.4640	11.1560			
10744	4 19 43.377	27 20 57.600	132	-76	0.246250	36.1953
	16.1100	16.5100	13.8700	13.8400	12.8200	
	11.0460	10.4290	10.1560			
1938	4 48 34.988	18 43 44.760	82	-32	0.241063	45.7856
	0.0000	17.3100	15.3500	15.6200	13.6800	
	11.5810	10.9960	10.7080			
20	4 14 45.227	19 3 50.460	96	-28	0.240337	51.8491
	18.5000	17.0300	14.8900	15.5200	13.1200	
	11.8820	11.2590	10.9840			
3101	4 37 9.895	12 6 20.160	86	-6	0.240091	48.1882
	18.6900	18.2500	15.1700	15.1500	13.2200	
	11.7140	11.1260	10.8270			
1158	4 18 8.995	17 24 58.490	104	-28	0.238705	46.4600
	17.8000	16.9000	14.7200	15.0500	12.9200	
	11.6470	11.0830	10.7590			
10672	4 29 36.237	26 34 23.510	100	-62	0.238131	44.0486
	18.0000	17.5600	14.9500	15.0000	13.4800	
	11.5640	10.9410	10.6480			
4843	4 0 15.581	19 24 36.560	122	-32	0.237570	44.9585
	17.9600	17.0700	14.7200	15.0100	13.2600	
	11.5790	10.9700	10.6970			
1786	4 49 36.564	17 1 59.400	78	-32	0.237545	46.1500
	18.2600	17.4200	15.4800	15.4000	14.0000	
	11.6520	11.0090	10.7540			
2968	4 24 15.381	12 14 50.530	100	-8	0.235119	46.2355
	18.6100	17.2300	15.0800	15.6000	13.7200	
	11.6320	11.0140	10.7780			
5192	4 18 55.789	9 23 47.010	112	0	0.234468	42.9033
	17.6000	18.0800	14.9200	15.8400	13.4900	
	11.5220	10.8840	10.6210			

8447	4 47 54.053	7 22 14.790	68	4	0.231949	54.2620
	18.0200	18.2900	0.0000	15.3700	13.7900	
	12.0530	11.4600	11.1520			
5480	4 54 37.783	9 24 32.810	78	-8	0.227943	43.7861
	17.5000	17.4800	14.6900	15.2400	12.9700	
	11.5410	11.0260	10.7200			
12798	5 12 16.003	5 22 10.790	52	8	0.227156	52.1912
	18.3500	17.4700	15.3500	15.4000	13.0800	
	12.0010	11.4060	11.1080			
8382	4 42 26.623	7 47 4.130	70	2	0.227016	55.8173
	19.5900	19.2600	0.0000	16.1200	14.1300	
	12.1640	11.5660	11.2550			
10467	4 49 11.301	27 29 56.010	96	-6	0.226676	49.2474
	18.7500	0.0000	0.0000	14.2500	14.0400	
	11.9630	11.2170	10.9860			
1736	4 46 27.137	17 37 36.050	94	-30	0.222565	40.8977
	18.1900	17.8400	14.7600	15.5100	14.1000	
	11.4670	10.8670	10.6180			
450	4 25 50.436	15 0 9.320	104	-22	0.220946	43.7410
	18.3400	17.4100	14.9500	15.8200	13.7400	
	11.6290	11.0490	10.7780			
3843	4 53 56.319	20 17 45.590	64	-32	0.220215	55.4119
	0.0000	16.8700	0.0000	15.0600	13.7200	
	12.1720	11.5480	11.2980			
5468	4 53 56.993	9 15 58.950	94	-2	0.216096	36.7884
	17.4100	17.3100	14.6000	14.9600	12.9100	
	11.3080	10.7420	10.4450			
12774	5 10 31.495	4 52 32.900	62	14	0.215793	44.5224
	16.7400	16.4700	14.1200	14.3700	12.6900	
	11.7500	11.1110	10.8620			
16454	4 48 19.803	31 35 48.900	82	-78	0.214074	45.6562
	17.0000	16.1300	14.2400	14.2400	13.1000	
	11.7720	11.1450	10.9320			
9202	5 7 10.041	13 16 11.210	68	-20	0.210039	43.0113
	18.2200	18.3500	15.3800	15.6900	13.2400	
	11.7560	11.1300	10.8390			
1640	4 46 5.211	15 53 24.260	80	-24	0.208015	47.3652

	18.6200	18.3400	15.5700	15.8100	13.4900	
	11.9220	11.3140	11.0670			
2099	4 34 21.645	21 2 15.020	84	-48	0.207983	48.0401
	17.6900	17.3000	15.0500	15.4400	14.0300	
	11.9640	11.3260	11.0980			
12412	4 40 57.213	4 50 54.570	74	6	0.207529	53.9213
	19.5100	18.1700	15.9100	16.2400	14.0100	
	12.2360	11.6020	11.3530			
996	4 21 38.292	20 18 10.320	124	-42	0.205656	38.3245
	18.9400	17.1200	15.3900	15.3300	12.9500	
	11.5100	10.9010	10.6290			
3530	4 57 27.554	13 56 42.860	72	-16	0.203397	46.7342
	18.1500	17.9800	15.2400	15.6100	13.5300	
	11.9200	11.3400	11.0810			
5142	4 10 4.028	8 47 35.770	108	6	0.202931	47.4197
	17.7100	17.3500	0.0000	14.6400	13.5700	
	11.9640	11.3400	11.1170			
1956	4 49 28.299	19 16 38.650	80	-38	0.201152	45.5816
	18.9400	17.7800	15.5300	15.6300	14.0800	
	11.9290	11.3390	11.0480			
1027	4 23 56.661	18 38 20.170	84	-24	0.199730	55.6231
	19.8000	17.2300	16.4300	16.6200	15.1100	
	12.3530	11.7720	11.4940			
6131	5 0 55.815	18 18 24.680	62	-92	0.199408	32.3035
	16.6600	0.0000	0.0000	15.1700	13.0900	
	11.2130	10.4910	10.3170			
5318	4 40 52.039	9 5 15.450	98	-8	0.197256	40.3898
	18.1500	17.9700	15.1200	15.2400	13.1900	
	11.6960	11.1320	10.8230			
5005	3 58 14.361	12 37 40.840	128	-12	0.196149	43.3428
	18.5500	17.5000	15.4300	15.5800	13.5200	
	11.8450	11.2560	10.9870			
1418	4 28 22.457	13 49 21.390	110	-32	0.195679	39.4826
	18.5700	17.0600	15.2000	15.3400	13.5100	
	11.6700	11.0500	10.7890			
1560	4 42 12.451	14 8 51.400	90	-22	0.194184	43.4376
	18.9700	18.3000	15.3000	15.6600	13.4500	

	11.8890	11.2950	11.0110			
9064	5 7 42.469	11 45 23.880	50	-2	0.191280	59.2758
	18.2900	17.8500	15.4100	15.5100	13.5900	
	12.5650	11.9440	11.7150			
445	4 25 16.523	16 18 8.680	110	-20	0.190653	42.1718
	19.0800	17.7300	15.9600	15.8700	13.9000	
	11.8670	11.2960	10.9820			
3035	4 31 19.551	10 55 25.810	114	-4	0.189998	38.1686
	18.5400	18.2700	15.1200	15.1800	13.5100	
	11.6430	11.0170	10.7720			
1036	4 24 20.934	19 10 50.830	104	-40	0.183568	43.7209
	19.2900	18.3100	16.0400	15.9600	14.7300	
	12.0290	11.4230	11.1330			
2005	4 45 3.739	21 50 37.490	74	-40	0.177914	51.8836
	17.9100	17.8200	15.3200	15.9400	14.3600	
	12.4430	11.8510	11.5650			
2147	4 38 43.383	21 44 14.540	102	-48	0.173302	40.4105
	18.5200	18.1500	15.4500	16.1800	14.5800	
	11.9500	11.3410	11.0730			
427	4 23 1.515	15 13 41.710	114	-18	0.173033	41.2198
	19.3300	17.8800	16.3300	16.1900	14.0100	
	12.0230	11.4190	11.1190			
6169	5 3 32.653	18 8 52.600	64	-30	0.169514	49.2886
	20.1000	18.5100	16.3800	16.5400	14.6000	
	12.4340	11.8580	11.5470			
4456	4 14 50.205	24 22 37.680	102	-38	0.168730	50.1359
	18.7500	18.9400	15.7200	16.3900	14.3600	
	12.4790	11.9030	11.5930			
5699	4 59 3.117	12 15 44.980	88	-16	0.168097	37.1262
	18.2800	18.2200	15.3400	15.5100	13.3400	
	11.8380	11.2250	10.9480			
16805	4 9 36.971	31 50 10.880	100	-68	0.162634	50.4207
	19.2700	18.0500	15.9700	16.1000	14.3100	
	12.4580	11.9130	11.6770			
3815	4 50 42.895	19 18 15.390	88	-38	0.160319	41.7039
	19.2800	18.0400	15.9700	15.8800	14.3000	
	12.1810	11.5740	11.2930			

13836	5 1 58.605	30 22 54.210	54	-114	0.159944	37.5540
	17.9000	17.1900	15.1800	15.1600	14.0200	
	11.9750	11.3540	11.0700			
12035	3 38 7.135	6 34 25.970	172	8	0.159935	36.2936
	18.6700	19.2600	16.1800	15.9400	13.5400	
	11.8930	11.3220	10.9960			
6271	5 3 6.303	19 40 43.640	60	-38	0.158301	50.9806
	19.7700	18.3500	16.6500	16.6000	14.4900	
	12.6620	12.0490	11.7540			
15078	3 32 15.572	16 1 53.950	128	-12	0.156419	50.3365
	18.3300	17.6200	15.4500	15.6200	14.1500	
	12.6170	12.0040	11.7500			
511	4 30 42.604	14 39 41.530	122	-24	0.155622	35.8971
	19.2900	18.8300	15.5000	15.4600	13.5000	
	11.9320	11.3550	11.0260			
9394	5 8 41.138	14 44 39.850	50	-14	0.155355	59.1268
	19.4300	19.8000	16.9200	16.9500	14.6700	
	13.0370	12.4860	12.1130			
5223	4 25 37.219	8 35 28.980	108	8	0.153017	42.0501
	19.9200	19.2700	16.7800	17.3400	14.4500	
	12.3240	11.7290	11.4030			
5418	4 51 57.259	9 16 53.160	98	-6	0.152159	36.0351
	18.5100	18.1900	15.4500	15.8100	13.5500	
	11.9650	11.3430	11.0790			
1167	4 10 40.799	14 44 0.870	122	-18	0.151414	41.9907
	0.0000	19.6100	16.7400	17.3900	14.8600	
	12.3880	11.7950	11.4210			
2909	4 12 49.916	11 14 46.650	134	-2	0.147540	37.6157
	18.4300	18.9000	15.2100	16.6000	14.1500	
	12.1290	11.4950	11.2340			
6163	5 3 18.733	16 30 58.770	58	-28	0.143966	52.4099
	0.0000	20.1700	17.1700	17.1800	14.7900	
	12.9440	12.3260	12.0040			
7705	3 47 31.557	12 1 11.070	134	-8	0.143255	44.1778
	20.0500	19.6600	17.6100	17.4400	14.4300	
	12.6120	12.0140	11.6430			
6901	4 18 13.747	25 39 39.840	102	-48	0.141345	48.2495

	21.1100	20.4500	18.3300	17.9900	15.4900	
	12.8540	12.2300	11.8620			
15935	5 3 19.078	3 50 25.210	78	20	0.140299	39.1425
	18.2900	18.0100	15.7600	16.1800	13.6800	
	12.2790	11.6910	11.4230			
1429	4 29 2.873	13 37 58.820	106	8	0.138016	42.2701
	0.0000	20.5800	0.0000	18.3500	15.2400	
	12.6530	11.9430	11.6240			
6461	5 0 38.941	24 22 58.230	62	-44	0.137507	54.2870
	19.6800	19.5300	17.4200	17.2900	14.7900	
	13.0890	12.5460	12.1750			
16563	4 40 15.725	31 26 6.030	62	-64	0.135557	59.8575
	0.0000	18.8800	0.0000	16.6400	14.9800	
	13.4040	12.7180	12.4170			
1161	4 9 57.108	16 22 41.840	154	-30	0.135525	33.4512
	19.6100	18.7100	16.1700	16.6800	14.4100	
	12.0850	11.4640	11.1540			
3199	4 48 45.981	11 23 8.620	92	-20	0.133419	39.2465
	19.9700	20.4000	17.2400	17.1900	14.9900	
	12.5040	11.8910	11.5340			
14777	3 30 5.093	24 5 28.190	178	-48	0.133011	36.5341
	20.8100	20.5000	18.2000	17.1700	14.1900	
	12.3860	11.7510	11.3850			
5100	3 59 10.175	9 17 2.100	140	-2	0.130835	39.4133
	19.6300	18.8100	16.4000	16.5800	14.5300	
	12.4880	11.8810	11.5850			
517	4 31 16.368	15 0 11.920	104	-24	0.130489	41.7353
	20.2100	20.0800	16.2900	16.8100	14.4300	
	12.6290	12.0700	11.7150			
999	4 21 49.564	19 29 8.800	116	-38	0.130097	40.7187
	20.7100	20.0300	18.0600	17.7500	14.8700	
	12.7110	12.0600	11.6680			
6959	4 24 8.760	25 59 53.780	134	18	0.126266	39.1514
	20.9500	19.2400	18.5100	0.0000	19.0200	
	12.7950	11.8950	11.6480			
2231	4 30 0.476	22 22 30.360	112	-58	0.124601	38.6224
	20.7000	19.4300	17.3400	17.0800	14.7700	

	12.5620	11.9920	11.6480			
1246	4 11 6.404	12 47 48.350	124	-10	0.121637	41.1875
	0.0000	19.2800	17.1100	17.4000	14.5200	
	12.6920	12.1280	11.8420			
16820	4 10 55.530	30 41 46.720	84	-62	0.121541	57.3072
	20.3000	19.8800	17.5600	17.5000	15.4700	
	13.7640	12.8650	12.5610			
2769	4 4 10.745	15 48 22.020	130	-20	0.120985	41.2753
	20.0000	18.3500	17.0800	16.9600	14.5900	
	12.7790	12.2030	11.8590			
1888	4 46 2.698	19 28 6.180	74	-36	0.120785	50.5986
	0.0000	20.6100	17.6300	17.7800	16.0200	
	13.2370	12.6200	12.3050			
9142	5 11 59.396	11 19 41.840	56	-14	0.120211	48.2093
	0.0000	20.9300	18.5200	18.6000	15.3900	
	13.3260	12.7610	12.2110			
602	4 38 58.480	15 39 41.490	88	-20	0.116802	46.5631
	0.0000	20.7600	18.3300	17.7700	15.1000	
	13.1280	12.5500	12.2030			
3509	4 56 22.991	14 6 3.970	72	-20	0.115457	46.7607
	19.9900	19.9900	17.3900	17.4500	14.7400	
	13.1230	12.5360	12.2400			
3080	4 35 51.720	12 15 20.390	74	-8	0.114346	56.5173
	0.0000	20.6300	18.2400	18.3100	15.7500	
	13.6760	13.1290	12.6750			
998	4 21 44.341	20 24 10.660	92	-34	0.112125	51.1752
	20.2300	20.6400	18.8000	18.3600	15.1300	
	13.4940	12.8620	12.5080			
7488	3 52 20.768	20 28 41.270	146	-34	0.111025	39.7454
	0.0000	19.6400	17.2800	17.4900	14.9500	
	12.9130	12.2870	11.9840			
14497	3 54 51.049	29 57 34.370	174	-90	0.108051	32.3726
	20.0400	19.2100	16.9400	17.1200	14.5000	
	12.5090	11.9430	11.6090			
6756	4 46 45.011	24 36 40.370	94	-58	0.107759	41.0903
	0.0000	20.2000	17.8800	17.8900	14.8500	
	13.0790	12.4930	12.1340			

594	4 38 27.689	16 0 11.030	90	-26	0.106697	45.2091
	0.0000	20.7300	18.3500	17.8400	15.4100	
	13.3340	12.6900	12.3680			
4172	4 36 58.126	23 16 38.580	88	-44	0.103994	47.9740
	0.0000	20.3900	18.5500	18.4900	15.4000	
	13.5290	12.9070	12.5680			
772	4 35 13.522	20 8 1.440	90	-30	0.102591	48.1046
	0.0000	21.9200	18.5900	19.2700	16.3900	
	13.7050	12.9860	12.6130			
4215	4 40 10.991	23 25 14.440	100	-44	0.101271	42.4147
	19.9600	20.3300	18.4700	18.0400	15.1700	
	13.3790	12.7300	12.3780			
10944	4 1 39.485	28 19 1.090	116	-62	0.098832	46.1195
	0.0000	21.2300	18.3400	18.6200	15.6600	
	13.5660	12.9860	12.6350			
1891	4 46 9.650	18 57 28.230	84	-34	0.095434	45.5381
	0.0000	20.5900	18.9000	19.1100	16.3700	
	13.7750	13.1210	12.7240			
15433	3 55 48.302	2 37 55.930	134	48	0.093977	40.1383
	0.0000	20.7900	19.2300	18.9900	16.3800	
	13.5040	12.8640	12.5050			
10505	4 35 29.208	26 33 57.820	104	-56	0.086917	42.4950
	0.0000	20.3600	19.0600	19.1300	16.8800	
	14.5160	13.4200	12.9620			

Table B.1: The members of the Hyades identified from the proper motion and photometric selections.

Bibliography

Adams, F. C. & Laughlin, G. (1997), 'A dying Universe: The long term fate and evolution of astrophysical objects', *Rev. Mod. Phys.* **69**, 337.

Ali, B., Forrest, W. J., Stauffer, J. S. & Leggett, S. K. (2000), 'Preliminary results from an ISOCAM based search for brown dwarfs in the Hyades', *A&AS* **32**, 1613.

Allard, F. A. (1990), Model atmospheres for M dwarfs, PhD thesis, University of Heidelberg.

Allard, F. A., Hauschildt, P. H., Alexander, D. R. & Starrfield, S. (1997), 'Model atmospheres of very low mass stars and brown dwarfs', *Ann. Rev. Astron. Astrophys.* **35**, 137.

Argon, A. L., Greenhill, L. J., Moran, J. M., Reid, M. J., Menten, K. M. & Inoue, M. (2004), 'The IC133 water vapour maser in the galaxy M33: A geometric distance', *ApJ* **615**, 702.

Baraffe, I., Chabrier, G., Allard, F. & Hasuchildt, P. H. (1998), 'Evolutionary models for solar metallicity low-mass stars: Mass-magnitude relationships and color-magnitude diagrams', *A&A* **337**, 403.

Baraffe, I., Chabrier, G., Allard, F. & Hasuchildt, P. H. (2002*a*), 'Evolutionary models for low mass stars and brown dwarfs: Uncertainties and limits at very young ages', *A&A* **382**, 563.

Baraffe, I., Chabrier, G., Allard, F. & Hauschildt, P. H. (2002*b*), 'Evolutionary models for low mass stars and brown dwarfs: Uncertainties and limits at very young ages', *A&A* **382**, 563.

Barrados y Navascués, D., Bejar, V. J. S., Mundt, R., Martín, E. L., Rebolo, R., Zapatero-Osorio, M. R. & Bailer-Jones, C. A. L. (2003), 'The σ Orionis substellar population', *A&A* **404**, 171.

Barrados y Navascués, D., Stauffer, J. R., Briceño, C., Patten, B. M., Hambly, N. C. & Adams, J. D. (2001), 'Very low-mass stars and brown dwarfs of the young open cluster IC 2391', *ApJS* **134**, 103.

Barrados y Navascués, D., Stauffer, J. R. & Jayawardhana, R. (2004), 'Spectroscopy of very low mass stars and brown dwarfs in IC 2391: Lithium depletion and Hα emission', *ApJ* **614**, 386.

Barrados y Navascués, D., Stauffer, J. R. & Patten, B. M. (1999), 'The lithium-depletion boundary and the age of the young open cluster IC 2391', *ApJ* **522**, L53.

Barrados y Navascués, D., Zapatero-Osorio, M. R., Martín, E. L., Bejar, V. J. S., Rebolo, R. & Mundt, R. (2002), 'Discovery of a very cool object with extraordinarily strong Hα emission', *A&A* **393**, L85.

Basri, G., Marcy, G. W. & Graham, J. R. (1996), 'Lithium in brown dwarf candidates: The mass and age of the faintest Pleiades stars', *ApJ* **458**, 600.

Bate, M. R., Bonnell, I. A. & Bromm, V. (2002), 'The formation mechanism of brown dwarfs', *MNRAS* **332**, L65.

Beckett, M. G. (1995), 'High resolution infrared imaging', *PhD Thesis, University of Cambridge* .

Becklin, E. E. & Zuckerman, B. (1988), 'A low temperature companion to a white dwarf star', *Nature* **336**, 656.

Bejar, V. J. S., Martín, E. L. & Zapatero-Osorio, M. R. (2001), 'The substellar mass function in σ Orionis', *ApJ* **556**, 830.

Béjar, V. J. S., Zapatero-Osorio, M. R. & Rebolo, R. (1999), 'A search for very low mass stars and brown dwarfs in the young σ Orionis cluster', *ApJ* **521**, 671.

Bouvier, J., Stauffer, J., Martín, E. L., Barrados y Navascués, D., Wallace, B. & Bejar, V. J. S. (1998), 'Brown dwarfs and very low-mass stars in the Pleiades cluster: A deep wide-field imaging survey', *A&A* **336**, 490.

Bouy, H., Brandner, W., Martín, E. L., Delfosse, X., Allard, F., Baraffe, I., Forveille, T. & Demarco, R. (2004*a*), 'A young binary brown dwarf in the R-CrA star forming region', *A&A* **424**, 213.

Bouy, H., Duchêne, G., Köhler, R., Brandner, W., Bouvier, J., Martín, E. L., Ghez, A., Delfosse, X., Forveille, T., Allard, F., Baraffe, I., Basri, G., Close, L. M. & McCabe, C. E. (2004*b*), 'First determination of the dynamical mass of a binary L dwarf', *A&A* **423**, 341.

Briceño, C., Hartmann, L., Stauffer, J. & Martín, E. L. (1998), 'A search for very low mass pre-main-sequence stars in Taurus', *AJ* **115**, 2074.

Briceño, C., Luhman, K. L., Hartmann, L., Stauffer, J. R. & Kirkpatrick, J. D. (2002), 'The initial mass function in the Taurus star-forming region', *ApJ* **580**, 317.

Briggs, K. R. & Pye, J. P. (2001), 'XMM Newton's first look in the Pleiades', *Astronomische Gesellschaft Abstract Series* **18**.

Briggs, K. R. & Pye, J. P. (2004), 'X-ray emission from a brown dwarf in the Pleiades', *MNRAS* **353**, 673.

Bryja, C. (1993), 'The lower end of the Hyades initial mass function', *AAS* **25**, 1385.

Bryja, C., Humphreys, R. M. & Jones, T. J. (1994), 'The lowest mass stars in the Hyades', *AJ* **107**, 246.

Bryja, C., Jones, T. J., Humphreys, R. M., Lawrence, G., Pennington, R. L. & Zumach, W. (1992), 'Candidate brown dwarfs in the Hyades', *ApJ* **388**, L23.

Burgasser, A. J., Geballe, T. R., Leggett, S. K., Kirkpatrick, J. D. & Golimowski, D. A. (2005), 'A unified near infrared spectral classification scheme for T dwarfs', *ApJ* p. in press.

Burgasser, A. J., Kirkpatrick, J. D., Cutri, R. M., McCallon, H., Kopan, G., Gizis, J. E., Liebert, J., Reid, I. N., Brown, M. E., Monet, D. G., Dahn, C. C., Beichman, C. A. & Skrutskie, M. F. (2002*a*), 'Discovery of a brown dwarf companion to Gliese 570ABC: A 2MASS T dwarf significantly cooler than Gliese 229b', *ApJ* **531**, L57.

Burgasser, A. J., Kirkpatrick, J. D., McElwain, M. W., Cutri, R. M., Burgasser, A. J. & Skrutskie, M. F. (2003), 'The 2MASS wide-field T dwarf search. I. Discovery of a bright T dwarf within 10 pc of the Sun', *AJ* **125**, 850.

Burgasser, A. J., Kirrkpatrick, J. D., Brown, M. E., Reid, I. N., Burrows, A., Leibert, J., Matthews, K., Gizis, J. E., Dahn, C. C., Monet, D. G., Cutri, R. M. & Skrutskie, M. F. (2002*b*), 'The spectra of T dwarfs. I. Near infrared data and spectral classification', *ApJ* **564**, 421.

Burgasser, A. J., Liebert, J., Kirkpatrick, J. D. & Gizis, J. E. (2002*c*), 'A search for variability in the active T dwarf 2MASS 1237+6526', *AJ* **123**, 2744.

Burgasser, A. J., Marley, M. S., Ackerman, A. S., Saumon, D., Lodders, K., Dahn, C. C., Harris, H. C. & Kirkpatrick, J. D. (2002*d*), 'Evidence for cloud disruption in the L/T dwarf transition', *ApJ* **571**, 151.

Burgasser, A. J., McElwain, M. W., Cruz, K. C., Tinney, C. G. & Reid, I. N. (2004), 'The 2MASS wide-field T dwarf search. III. Seven new T dwarfs and other cool dwarf discoveries', *AJ* **127**, 2856.

Burgasser, A. J., Wilson, J. C., Kirkpatrick, J. D., Skrutskie, M. F., Colonno, M. R., Enos, A. T., Smith, J. D., Henderson, C. P., Gizis, J. E., Brwon, M. E. & Houck, J. R. (2002*e*), 'Discovery of a bright field methane (T-type) brown dwarf by 2MASS', *AJ* **120**, 1100.

Burrows, A., Hubbard, W. B., Saumon, D. & Lunine, J. I. (1993), 'An expanded set of brown dwarf and very low mass star models', *APJ* **406**, 158.

Burrows, A., Marley, M. S., Hubbard, W. B., Lunine, J. I., Guillot, T., Saumon, D., Freedman, R., Sudarsky, D. & Sharp, C. (1997), 'A nongray theory of extrasolar giant planets and brown dwarfs', *ApJ* **491**, 856.

Burrows, A. & Volobuyev, M. (2003), 'Calculations of the far-wing line profiles of sodium and potassium in the atmospheres of substellar-mass objects', *ApJ* **583**, 985.

Chabrier, G. & Baraffe, I. (1997), 'Structure and evolution of low mass stars', *A&A* **327**, 1039.

Chabrier, G., Baraffe, I., Allard, F. & Hauschildt, P. H. (2000), 'Evolutionary models for very low mass stars and brown dwarfs with dusty atmospheres', *A&A* **542**, 464.

Charbonnel, C., Meynet, G., Maeder, A., Schaller, G. & Schaerer, D. (1993), 'Grids of stellar models. III. From 0.8 to 120 $M_{\odot}$ at Z=0.004', *A&AS* **101**, 415.

Close, L. M., Potter, D., Brandner, W., Lloyd-Hart, M., Liebert, J., Burrows, A. & Siegler, N. (2002*a*), 'Discovery of a 0.15" binary brown dwarf 2MASSJ1426326+155701 with Gemini/Hokupa'a adaptive optics', *ApJ* **566**, 1095.

Close, L. M., Siegler, N., Potter, D., Brandner, W. & Liebert, J. (2002*b*), 'An adaptive optics survey of M8-M9 stars: Discovery of 4 very low mass binaries with at least one system containing a brown dwarf companion', *ApJ* **567**, L53.

Comerón, F., Neuhäuser, R. & Kaas, A. A. (2000), 'Probing the brown dwarf population of the Chamaeleon I star forming region', *A&A* **359**, 269.

Comerón, F., Rieke, G. H. & Neuhäuser, R. (1999), 'Faint members of the Chamaeleon I cloud', *A&A* **343**, 477.

Cossburn, M. R., Hodgkin, S. T., Jameson, R. F. & Pinfield, D. J. (1997), 'Discovery of the lowest mass brown dwarf in the Pleiades', *MNRAS* **288**, L23.

Costa, G. S. D. & Freeman, K. C. (1976), 'The structure and mass function of the globular cluster M3', *ApJ* **206**, 128.

Cruz, K. L., Burgasser, A. J., Reid, I. N. & Liebert, J. (2004), '2MASS J05185995-2828372: Discovery of an unresolved L/T binary', *ApJ* **604**, L61.

Cruz, K. L., Reid, I. N., Liebert, J., Kirkpatrick, J. D. & Lowrance, P. (2003), 'Meeting the cool neighbors. V. A 2MASS-selected sample of ultracool dwarfs', *AJ* **126**, 2421.

D'Antona, F. & Mazzitelli, I. (1997), 'Evolution of low mass stars', *MmSAI* **68**, 807.

Delfosse, X., Tinney, C. G., Forveille, T., Epchtein, N., Bertin, E., Borsenberger, J., Copet, E., de Batz, B., Fouque, P., Kimeswenger, S., Bertre, T. L., Lacombe, F., Rouan, D. & Tiphene, D. (1997), 'Field brown dwarfs found by DENIS', *A&A* **327**, L25.

Delfosse, X., Tinney, C. G., Forveille, T., Epchtein, N., Borsenberger, J., Fouque, P., Kimeswenger, S. & Tiphene, D. (1999), 'Searching for very low mass stars and brown dwarfs with DENIS', *A&AS* **135**, 41.

Detweiler, H. L., Yoss, K. M., Radick, R. R. & Becker, S. A. (1984), 'The radial velocity of the Hyades cluster', *AJ* **89**, 1038.

Dobbie, P. D., Burleigh, M. R., Levan, A. J., Barstow, M. A., Napiwotzki, R., Holberg, J. B., Hubeny, I. & Howell, S. B. (2005), 'A near-infrared spectroscopic search for very-low-mass cool companions to notable DA white dwarfs', *MNRAS* **357**, 1049.

Dobbie, P. D., Kenyon, F., Jameson, R. F., Hodgkin, S. T., Hambly, N. C. & Hawkins, M. R. S. (2002*a*), 'A deep, large area search for very low mass members of the Hyades open cluster', *MNRAS* **329**, 543.

Dobbie, P. D., Kenyon, F., Jameson, R. F., Hodgkin, S. T., Pinfield, D. J. & Osborne, S. L. (2002*b*), 'A deep IZ survey of 1.1 deg^2 of the Pleiades cluster: Three candidate members with M $\leq$ 0.04 M$_\odot$', *MNRAS* **335**, 687.

Dobbie, P. D., Pinfield, D. J., Jameson, R. F. & Hodgkin, S. T. (2002*c*), 'The missing M dwarfs', *MNRAS* **335**, L79.

Endl, M., Hatzes, A. P., Cochran, W. D., McArthur, B., Allende Prieto, C., Paulson, D. B., Guenther, E. & Bedalov, A. (2004), 'HD137510: An oasis in the brown dwarf desert', *ApJ* **611**, 1121.

Epchtein, N. (1997), 'The deep near infrared southern sky survey (denis): Progress status and scientific achievements', *2nd DENIS Euroconference; In the impact of large scale near-ir sky surveys* **ed. F. Garzon et al**, 15.

Fan, X., Knapp, G. R., Strauss, M. A., Gunn, J. E., Lupton, R. H., Ivezic, Z., Rockosi, C. M., Yanny, B., Kent, S., Schneider, D. P., Kirkpatrick, J. D., Annis, J., Bastian, S., Berman, E., Csabai, J. B. I., Federwitz, G. R., Fukugita, M., Gurbani, V. K., Hennessy, G. S., Hindsley, R. B., Ichikawa, T., Lamb, D. Q., Lindenmeyer, C., Mantsch, P. M., McKay, T. A., Munn, J. A., Nash, T., Okamura, S., Pauls, A. G., Pier, J. R., Rechenmacher, R., Rivetta, C. H., Sergey, G., Stoughton, C., Szalay, A. S., Szokoly, G. P., Tucker, D. L. & York, D. G. (2000), 'L dwarfs found in Sloan Digital Sky Survey commissioning imaging data', *AJ* **119**, 928.

Farihi, J. & Christopher, M. (2004), 'A possible brown dwarf companion to the white dwarf GD1400', *AJ* **128**, 1868.

Freed, M., Close, L. M. & Siegler, N. (2002), 'Discovery of a tight brown dwarf companion to the low mass star LHS 2397a', *ApJ* **584**, 453.

Geballe, T. R., Knapp, G. R., Leggett, S. K., Fan, X., Golimowski, D. A., Anderson, S., Brinkmann, J., Csabai, I., Gunn, J. E., Hawley, S. L., Hennessey, G., Henry, T. J., Hill, G. J., Ivezic, R. B. H. Z., Lupton, R. H., McDaniel, A., Munn, J. A., Narayanan, V. K., Peng, E., Pier, J. R., Rockosi, C. M., Schneider, D. P., Smith, J. A., Strauss, M. A., Tsvetanov, Z. I., Uomoto, A. & Zheng, W. (2002), 'Toward spectral classification of L and T dwarfs: Infrared and optical spectroscopy and analysis', *ApJ* **564**, 466.

Gizis, J. E., Kirkpatrick, J. D., Burgasser, A., Reid, I. N., Monet, D. G., Liebert, J. & Wilson, J. C. (2001), 'Substellar companions to main-sequence stars: No brown dwarf desert at wide separations', *ApJ* **551**, L163.

Gizis, J. E., Reid, I. N. & Hawley, S. L. (2002), 'The Palomar/MSU nearby star spectroscopic survey. III. Chromospheric activity, M dwarf ages, and the local star formation history', *AJ* **123**, 3356.

Gizis, J. E., Reid, I. N., Knapp, G. R., Liebert, J., Kirkpatrick, J. D., Koerner, D. W. & Burgasser, A. J. (2003), 'Hubble Space Telescope observations of binary very low mass stars and brown dwarfs', *AJ* **125**, 3302.

Gizis, J. E., Reid, I. N. & Monet, D. G. (1999), 'A 2MASS survey for brown dwarfs towards the Hyades', *AJ* **118**, 997.

Gómez, M., Hartmann, L. W., Kenyon, S. & Hewett, R. (1993), 'On the spatial distribution of pre-main-sequence stars in Taurus', *AJ* **105**, 1927.

Gregorio-Hetem, J. C., Sanzovo, G. C. & Lepine, J. R. D. (1989), 'Erratum - star counts and IRAS sources in southern dark clouds', *A&AS* **79**, 452.

Guenther, E. & Wuchterl, G. (2003), 'Companions of old brown dwarfs and very low mass stars', *A&A* **401**, 677.

Halbwachs, J. L., Arenou, F., Mayor, M., Udry, S. & Queloz, D. (2000), 'Exploring the brown dwarf desert with Hipparcos', *A&A* **355**, 581.

Hall, P. B. (2001), '2MASS 1315309-264951: An L dwarf with strong and variable $H\alpha$ emission', *ApJ* **564**, L89.

Hambly, N. C., Hawkins, M. R. S. & Jameson, R. F. (1991), 'A deep proper motion survey of the Pleiades for low-mass stars and brown dwarfs', *MNRAS* **253**, 1.

Hambly, N. C., Hodgkin, S. T., Cossburn, M. R. & Jameson, R. F. (1999), 'Brown dwarfs in the Pleiades and the initial mass function across the stellar/substellar boundary', *MNRAS* **303**, 835.

Hambly, N. C., Miller, L., MacGillivray, H. T., Herd, J. T. & Cormack, W. A. (1998), 'Precision astrometry with SuperCOSMOS', *MNRAS* **298**, 897.

Hambly, N. C., Steele, I. A., Hawkins, M. R. S. & Jameson, R. F. (1995), 'The very low-mass main sequence in the Galactic cluster Praesepe', *MNRAS* **273**, 505.

Hanson, R. B. (1975), 'A study of the motion, membership, and distance of the Hyades cluster', *AJ* **80**, 379.

Hartmann, L., Stauffer, J. R., Kenyon, S. J. & Jones, B. F. (1991), 'A proper motion survey for pre-main-sequence stars in Taurus-Auriga', *AJ* **101**, 1050.

Hauck, B. (1981), 'The distance modulus of the Hyades, Coma Berenices and Praesepe clusters', *A&A* **99**, 207.

Hawley, S. L., Covey, K. R., Knapp, G. R., Golimowski, D. A., Fan, X., Anderson, S. F., Gunn, J. E., Harris, H. C., Ivezić, Z., Long, G. M., Lupton, R. H., McGehee, P. M., Narayanan, V., Peng, E., Schlegel, D., Schneider, D. P., Spahn, E. Y., Strauss, M. A., Szkody, P., Tsvetanov, Z., Walkowicz, L. M., Brinkmann, J., Harvanek, M., Hennessy, G. S., Kleinman, S. J., Krzesinski, J., Long, D., Neilsen, E. H., Newman, P. R., Nitta, A., Snedden, S. A. & York, D. G. (2002), 'Characterization of M, L and T dwarfs in the Sloan Digital Sky Survey', *AJ* **123**, 3409.

Hayashi, C. & Nakano, T. (1963), 'Evolution of stars of small masses in the pre-main sequence stages', *Prog. Theor. Phys.* **30**, 460.

Hillenbrand, L. A. (1997), 'On the stellar population and star-forming history of the Orion Nebula cluster', *AJ* **113**, 1733.

Hodgkin, S. T. & Jameson, R. F. (2000), The mass function of the Pleiades, *in* 'Stellar Clusters and Associations', Vol. 198 of *ASP Conference Proceedings*, p. 59.

Hubbard, W. B., Burrows, A. & Lunine, J. I. (1990), 'The initial mass function for very low mass stars in the Hyades', *ApJ* **358**, L53.

Irwin, M. J. & Lewis, J. R. (2001), 'INT WFS pipeline processing', *New Astron. Rev.* **45**, 105.

Itoh, Y., Tamura, M. & Gatley, I. (1996), 'A near-infrared survey of the Taurus molecular cloud: Near-infrared luminosity function', *ApJ* **465**, L129.

Itoh, Y., Tamura, M. & Nakajima, T. (1999), 'A near-infrared search for companions around very low luminosity young stellar objects in Taurus', *AJ* **117**, 1471.

Ives, D. J., Tulloch, S. & Churchill, J. (1996), 'INT prime focus mosaic camera', *SPIE* **2654**, 266.

Jameson, R. F., Dobbie, P. D., Hodgkin, S. T. & Pinfield, D. J. (2002), 'Brown dwarfs in the Pleiades: Spatial distribution and mass function', *MNRAS* **335**, 853.

Jameson, R. F. & Skillen, W. J. I. (1989), 'A search for low-mass stars and brown dwarfs in the Pleiades', *MNRAS* **239**, 247.

Jeans, J. H. (1902), *Phil. Trans. Roy. Soc.* **199**, 1.

Joergens, V., Fernández, M., Carpenter, J. M. & Neuhäuser, R. (2003), 'Rotational periods of very young brown dwarfs and very low mass stars in Chamaeleon I', *ApJ* **594**, 571.

Jones, B. F. & Cudworth, K. (1983), 'A proper motion membership study of Praesepe', *AJ* **88**, 215.

Jones, B. F. & Stauffer, J. R. (1991), 'The luminosity function of Praesepe. I - A proper motion and photometric search for candidate members', *AJ* **102**, 1080.

Jones, H. R. A., Miller, L. & Glazebrook, K. (1994), 'A new candidate brown dwarf from an infrared survey', *MNRAS* **270**, L47.

Kendall, T. R., Delfosse, X., Martín, E. L. & Forveille, T. (2004), 'Discovery of very nearby ultracool dwarfs from DENIS', *A&A* **416**, L17.

Kenyon, F. (2001), 'Hyades, Pleiades and Taurus brown dwarfs', *PhD Thesis, University of Leicester* .

King, I. R. (1962), 'The structure of star clusters. I. An empirical density law', *AJ* **67**, 471.

King, I. R. (1966), 'The structure of star clusters. IV. Photoelectric surface photometry in nine globular clusters', *AJ* **71**, 276.

Kirkpatrick, J. D. (2003), '2MASS data mining and the M, L and T dwarf archives', *Brown Dwarfs, IAU Symposium* **211**, 189.

Kirkpatrick, J. D., Reid, I. N., Liebert, J., Cutri, R. M., Nelson, B., Beichman, C. A., Dahn, C. C., Monet, D. G., Gizis, J. E. & Skrutskie, M. F. (1999), 'Dwarfs cooler than 'M': The definition of spectral type 'L' using discoveries from the 2-Micron All-Sky Survey (2MASS)', *ApJ* **519**, 802.

Klein-Wassnik, W. J. (1927), *Publ. Kapteyn Astron. Laboratory* **No. 41**.

Kroupa, P., Aarseth, S. & Hurley, J. (2001), 'The formation of a bound star cluster: From the Orion nebula cluster to the Pleiades', *MNRAS* **321**, 699.

Kumar, S. S. (1963), 'The structure of stars of very low mass', *ApJ* **137**, 1121.

Kurayama, T., Sasao, T. & Kobayash, H. (2005), 'Parallax measurements of the Mira-type star UX Cygni with phase-referencing VLBI', *ApJ* **627**, L49.

Landolt, A. U. (1992), 'UBVRI photometric standard stars in the magnitude range 11.5-16.0 around the celestial equator', *AJ* **104**, 340.

Latham, D. W., Anderson, J., Geary, J. C., Rodrigues, O. & Stefanik, R. P. (1988), 'A fibre feed for precise radial velocity work with the CfA echelle spectrographs', *ASPC* **3**, 269.

Latham, D. W., Stefanik, R. P., Mazeh, T., Mayor, M. & Burki, G. (1989), 'The unseen companion of hd 114762 - A probable brown dwarf', *Nature* **339**, 38.

Leggett, S. K., Harris, H. C. & Dahn, C. C. (1994), 'Low mass stars in the central region of the Hyades cluster', *AJ* **108**, 944.

Leggett, S. K. & Hawkins (1988), 'The infrared luminosity function for low-mass stars', *MNRAS* **234**, 1065.

Leggett, S. K. & Hawkins (1989), 'Low mass stars in the region of the Hyades cluster', *MNRAS* **238**, 145.

López Martí, B., Eislöffel, J., Scholz, A. & Mundt, R. (2004), 'The brown dwarf population in the Chamaeleon I cloud', *A&A* **416**, 555.

Low, C. & Lynden-Bell, D. (1976), 'The minimum Jeans mass or when fragmentation must stop', *MNRAS* **176**, 367.

Lucas, P. W. & Roach, P. F. (2000), 'A population of very young brown dwarfs and free-floating planets in Orion', *MNRAS* **314**, 858.

Lucas, P. W., Roach, P. F., Allard, F. & Hauschildt, P. H. (2001), 'Infrared spectroscopy of substellar objects in Orion', *MNRAS* **326**, 695.

Luhman, K. L. (2000), 'The intial mass function of low-mass stars and brown dwarfs in Taurus', *ApJ* **544**, 1044.

Luhman, K. L. (2004), 'The first discovery of a wide binary brown dwarf', *ApJ* **614**, 398.

Luhman, K. L., Briceño, C., Stauffer, J. R., Hartmann, L., Barrado y Navascués, D. & Caldwell, N. (2003), 'New low-mass members of the Taurus star-forming region', *ApJ* **590**, 348.

Luhman, K. L. & Rieke, G. H. (1998), 'The low-mass intitial mass function in young clusters: L1495E', *ApJ* **497**, 354.

Luhman, K. L., Rieke, G. H., Young, T., Cotera, A. S., Chen, H., Rieke, M. J., Schneider, G. & Thompson, R. I. (2000), 'The initial mass function of low mass stars and brown dwarfs in young clusters', *ApJ* **540**, 1016.

Lui, M. C., Fischer, D., Graham, J. R., Lloyd, J. P., Marcy, G. W. & Butler, R. P. (2002), 'Crossing the brown dwarf desert using adaptive optics: A very close L-dwarf companion to the nearby solar analog HR7672', *ApJ* **571**, 519.

Macintosh, B., Zuckerman, B., Becklin, E. E. & McLean, I. S. (1992), 'Searches for brown dwarfs in the Hyades', *AAS* **24**, 773.

Magazzù, A., Rebolo, R., Zapatero-Osorio, M. R., Martín, E. L. & Hodgkin, S. T. (1998), 'A brown dwarf candidate in the Praesepe open cluster', *ApJ* **497**, L47.

Marcy, G. W., Butler, R. P., Vogt, S. S., Liu, M. C., Laughlin, G., Apps, K., Graham, J. R., Lloyd, J. P., Luhman, K. L. & Jayawardhana, R. (2001), 'Two substellar companions orbiting HD168443', *AJ* **555**, 418.

Martín, E. L., Basri, G. & Zapatero-Osorio, M. R. (1999), 'The lithium test in young brown dwarf candidates', *AJ* **118**, 1005.

Martín, E. L., Basri, G., Zapatero-Osorio, M. R., Rebolo, R., López, R. & García, R. J. (1998), 'The first L-type brown dwarf in the Pleiades', *ApJ* **507**, L41.

Martín, E. L., Brandner, W., Bouvier, J., Luhman, K. L., Stauffer, J., Basri, G., Zapatero-Osorio, M. R. & Barrados y Navascués, D. (2000), 'Membership and multiplicity among very low mass stars and brown dwarfs in the Pleiades cluster', *ApJ* **543**, 299.

Martín, E. L., Delfosse, X., Basri, G., Goldman, B., Forveille, T. & Zapatero-Osorio, M. R. (1999*a*), 'Spectroscopic classification of late-M and L field dwarfs', *AJ* **118**, 2466.

Martín, E. L., Delfosse, X., Basri, G., Goldman, B., Forveille, T. & Zapatero-Osorio, M. R. (1999*b*), 'Spectroscopic classification of late-M and L field dwarfs', *AJ* **118**, 2466.

Martín, E. L., Dougados, C., Magnier, E., Ménard, F., Magazzù, A., Cuillandre, J. C. & Delfosse, X. (2001*a*), 'Four brown dwarfs in the Taurus star forming region', *ApJ* **561**, L195.

Martín, E. L., Dougados, C., Magnier, E., Ménard, F., Magazzù, A., Cuilllandre, J.-C. & Delfosse, X. (2001*b*), 'Four brown dwarfs in the Taurus star forming region', *ApJ* **561**, L195.

Martín, E. L., Rebolo, R. & Zapatero-Osorio, M. R. (1996), 'Spectroscopy of new substellar candidates in the Pleiades:Toward a spectral sequence for young brown dwarfs', *ApJ* **469**, 706.

McCarthy, C., Zuckerman, B. & Becklin, E. E. (2003), 'There is a brown dwarf desert of companions orbiting stars between 75 and 1000 AU', *IAU Symposium, Brown Dwarfs* **211**, 279.

McCaughrean, M. J., Close, L. M., Scholz, R. D., Lenzen, R., Biller, B., Brandner, W., Hartung, M. & Lodieu, N. (2004), 'εIndi Ba/b: The nearest binary brown dwarf', *A&A* **413**, 1029.

McCaughrean, M. J. & Stauffer, J. R. (1994), 'High resolution near-infrared imaging of the Trapezium: A stellar census', *AJ* **108**, 1382.

Mennickent, R. E., Diaz, M. P. & Tappert, C. (2004), 'Search for brown dwarf like secondaries in cataclysmic variables II', *MNRAS* **347**, 1180.

Mermilliod, J. C. (1981), 'Comparative studies of young open clusters. III - Empirical isochronous curves and the zero age main sequence', *A&A* **97**, 235.

Minkowski, R. L. & Abell, G. O. (1963), The National Geographic Society - Palomar Observatory Sky Survey, *in* K. A. Strand, ed., 'Stars and Stellar Systems', Vol. 3, Chicago University Press, Chicago, p. 481.

Mokler, F. & Stelzer, B. (2002), 'X-ray emission near the substellar limit: The σ Orionis and Taurus star forming regions', *A&A* **391**, 1025.

Moraux, E., Bouvier, J., Stauffer, J. & Cuillandre, J.-C. (2003*a*), 'IZ photometry of Pleiades brown dwarfs', *A&A* **400**, 891.

Moraux, E., Bouvier, J. & Stauffer, J. R. (2001), 'Proper motion of very low mass stars and brown dwarfs in the Pleiades cluster', *A&A* **367**, 211.

Moraux, E., Bouvier, J., Stauffer, J. R. & Cuillandre, J.-C. (2003*b*), 'Brown dwarfs in the Pleiades cluster: Clues to the substellar mass function', *A&A* **400**, 891.

Muench, A. A., Lada, E. A., Lada, C. J. & Alves, J. (2002), 'The luminosity and mass function of the Trapezium cluster: From B stars to the deuterium burning limit', *ApJ* **573**, 366.

Naef, D., Mayor, M., Beuzit, J. L., Perrier, C., Queloz, D., Sivan, J. P. & Udry, S. (2004), 'The ELODIE survey for northern extra-solar planets. III. Three planetary candidates detected with ELODIE', *A&A* **414**, 351.

Nakajima, T., Oppenheimer, B. R., Kulkarni, S. R., Golimowski, D. A., Matthews, K. & Durrance, S. T. (1995), 'Discovery of a cool brown dwarf', *Nature* **378**, 463.

Napier, W. M. & Guthrie, B. N. G. (1975), 'Black dwarf stars as missing mass in clusters of galaxies', *MNRAS* **170**, 7.

Nelson, L. A., Rappaport, S. A. & Joss, P. C. (1986), 'The evolution of very low mass stars', *ApJ* **311**, 226.

Neugebauer, G. & Leighton, R. B. (1969), 'Two-micron sky survey; A preliminary catalogue', *NASA SP* **3047**.

Neuhäuser, R. & Comerón, F. (1998), 'Rosat x-ray detection of a young brown dwarf in the Chamaeleon I dark cloud', *Science* **282**, 83.

Neuhäuser, R. & Guenther, E. W. (2004), 'Infrared spectroscopy of a brown dwarf companion candidate near the young star GSC 08047-00232 in Horologium', *A&A* **420**, 647.

Oliveira, J. M., Jeffries, R. D., Kenyon, M. J., Thompson, S. A. & Naylor, T. (2001), 'No disks around low mass stars and brown dwarfs in the young σ Orionis cluster', *A&A* **382**, L220.

Oliveira, J. M., Jeffries, R. D. & van Loon, J. T. (2003), 'An L-band survey for circumstellar disks around low mass stars in the young σ Orionis cluster', *MNRAS* **347**, 1327.

Oppenheimer, B. R., Basri, G., Nakajima, T. & Kulkarni, S. R. (1997), 'Lithium in very low mass stars in the Pleiades', *AJ* **113**, 296.

Osborne, S. L., Casewell, S. L. & Jameson, R. F. (2005), 'A survey of the entire Hyades for low mass members', *in preparation* .

Palla, F. & Stahler, S. W. (2000), 'Accelerating star formation in clusters and associations', *ApJ* **540**, 255.

Pepe, F., Mayor, M., Galland, F., Naef, D., Queloz, D., Santos, N. C., Udry, S. & Burnet, M. (2002), 'The CORALIE survey for southern extra-solar planets VII', *A&A* **388**, 632.

Perryman, M. A. C., Brown, A. G. A., Lebreton, Y., Gomez, A., Turon, C., de Strobel, G. C., Mermilliod, J. C., Robichon, N., Kovalensky, J. & Crifo, F. (1998), 'The Hyades: Distance, structure, dynamics and age', *A&A* **331**, 81.

Phan-Boa, N., Crifo, F., Delfosse, X., Forveille, T., Guibert, J., Borsenberger, J., Epchtein, N., Fouqué, P., Simon, G. & Vetois, J. (2003), 'New neighbours: V. 35 DENIS late m dwarfs between 10 and 30 parsecs', *A&A* **401**, 959.

Phan-Boa, N., Guibert, J., Crifo, F., Delfosse, X., Forveille, T., Borsenberger, J., Epchtein, N., Fouqu, P. & Simon, G. (2001), 'New neighbours: IV. 30 DENIS late-M dwarfs between 15 and 30 parsecs', *A&A* **380**, 590.

Pinfield, D. J., Dobbie, P. D., Jameson, R. F., Steele, I. A., Jones, H. R. A. & Katsiyannis, A. C. (2003), 'Brown dwarfs and low mass stars in the Pleiades and Praesepe: Membership and binarity', *MNRAS* **342**, 1241.

Pinfield, D. J., Hodgkin, S. T., Jameson, R. F., Cossburn, M. R., Hambly, N. C. & Devereux, N. (2000), 'A six-square-degree survey for Pleiades low-mass stars and brown dwarfs', *MNRAS* **313**, 347.

Pinfield, D. J., Hodgkin, S. T., Jameson, R. F., Cossburn, M. R. & von Hippel, T. (1997), 'Brown dwarf candidates in Praesepe', *MNRAS* **287**, 180.

Pinfield, D. J., Jameson, R. F. & Hodgkin, S. T. (1998), 'The mass of the Pleiades', *MNRAS* **299**, 955.

Pinsonneault, M. H., Stauffer, J., Soderblom, D. R., King, J. R. & Hanson, R. B. (1998), 'The problem of HIPPARCOS distances to open clusters. I. Constraints from multicolor main-sequence fitting', *ApJ* **504**, 170.

Potter, D., Martín, E. L., Cushing, M. C., Baudoz, P., Brandner, W., Guyon, O. & Neuhäuser, R. (2002), 'Hokupa'a/Gemini discovery of two ultracool companions to the young star HD130948', *ApJ* **567**, L133.

Pozio, F. (1991), 'Lithium in brown dwarfs and very low mass pre-main sequence stars', *MmSAI* **62**, 171.

Rana, N. C. (1987), 'Mass function of stars in the solar neighbourhood', *A&A* **184**, 104.

Rebolo, R., Martín, E. L., Basri, G., Marcy, G. W. & Zapatero-Osorio, M. R. (1996), 'Brown dwarfs in the Pleiades cluster confirmed by the lithium test', *ApJ* **469**, L53.

Rebolo, R., Martín, E. L. & Magazzù, A. (1992), 'Spectroscopy of a brown dwarf candidate in the Alpha Persei open cluster', *ApJ* **289**, L83.

Rebolo, R., Zapatero-Osorio, M. R. & Martín, E. L. (1995), 'Discovery of a brown dwarf in the Pleiades star cluster', *Nature* **377**, 129.

Rees, M. (1976), 'Opacity-limited hierarchical fragmentation and the masses of protostars', *MNRAS* **176**, 483.

Reid, I. N. (1992), 'Proper motions from Schmidt plates. II - The Hyades', *MNRAS* **257**, 257.

Reid, I. N. (1993), 'Low mass stars in the Hyades', *MNRAS* **265**, 785.

Reid, I. N. (1999*a*), *ApJ* **521**, 613.

Reid, I. N., Brewer, C., Brucato, R. J., McKinley, W. R., Maury, A., Mendenhall, D., Mould, J. R., Mueller, J., Neugebauer, G., Phinney, J., Sargent, W. L. W., Schombert, J. & Thicksten, R. (1991), 'The second Palomar Sky Survey', *PASP* **103**, 661.

Reid, N. I. (1999*b*), Low mass stars and brown dwarfs, *in* 'Proceedings of Star Formation 1999', p. 327.

Reipurth, B. & Clarke, C. (2001), 'The formation of brown dwarfs as ejected stellar embryos', *AJ* **122**, 432.

Robichon, N., Arenou, F., Mermilliod, J. C. & Turon, C. (1999), 'Open clusters with Hipparcos. I. Mean astrometric parameters', *A&A* **345**, 471.

Ruiz, T. M., Leggett, S. K. & Allard, F. (1997), 'Kelu-1: A free-floating brown dwarf in the solar neighborhood', *ApJ* **491**, 107.

Salpeter, E. E. (1955), 'The luminosity function and stellar evolution', *ApJ* **121**, 161.

Schneider, D. P., Knapp, G. R., Hawley, S. L., Covey, K. R., Fan, X., Ramsey, L. W., Richards, G. T., Strauss, M. A., Gunn, J. E., Hill, G. J., MacQueen, P. J., Adams, M. T., Hill, G. M., Ivezic, Z., Lupton, R. H., Pier, J. R., Saxe, D. H., Shetrone, M., Tufts, J. R., Wolf, M. J., Brinkmann, J., Csabai, I., Hennessy, G. S. & York, D. G. (2002), 'L dwarfs found in Sloan Digital Sky Survey commissioning data. II. Hobby-Eberly telescope observations', *AJ* **123**, 458.

Scholz, R. D., McCaughrean, M. J., Lodieu, N. & Kuhlbrodt, B. (2003), 'εIndiB: A new benchmark T dwarf', *A&A* **398**, L29.

Siegler, N., Close, L. M., Mamajek, E. E. & Freed, M. (2003), 'An adaptive optics survey of M6.0-M7.5 stars: Discovery of three very low mass binary systems including two probable Hyades members', *ApJ* **598**, 1265.

Simons, D. A. & Becklin, E. E. (1992), 'A near-infrared search for brown dwarfs in the Pleiades', *ApJ* **390**, 431.

Skrutskie, M. F., Schneider, S. E., Stiening, R., Strom, S. E., Weinberg, M. D., Beichman, C., Chester, T., Cutri, R., Lonsdale, C., Elias, J., Elston, R., Capps, R., Carpenter, J., Huchra, J., Liebert, J., Monet, D., Price, S. & Seitzer, P. (1997), 'The Two Micron All Sky Survey (2MASS): Overview and status', *2nd DENIS Euroconference; In the impact of large scale near-ir sky surveys* **ed. F. Garzon et al**, 25.

Slesnick, C. L., Hillenbrand, L. A. & Carpenter, J. M. (2004), 'The spectroscopically determined substellar mass function of the Orion nebula cluster', *ApJ* **610**, 1045.

Smith, M. C., Mao, S. & Woźniak, P. (2003), 'A brown dwarf microlens candidate from the second phase of the optical gravitational lensing experiment', *ApJ* **585**, L65.

Stauffer, J., Schultz, G. & Kirkpatrick, J. D. (1998), 'Keck spectra of Pleiades brown dwarf candidates and a precise determination of the lithium depletion edge in the Pleiades', *ApJ Letters* **499**, L199.

Steele, I. A., Jameson, R. F., Hodgkin, S. T. & Hambly, N. C. (1995), 'Infrared spectroscopy of low-mass stars and brown dwarfs in the Pleiades', *MNRAS* **275**, 841.

Stothers, R. B. & Chin, W. C. (1992), 'Stellar evolution in blue populous clusters of the Small Magellanic Cloud and the problems of envelope semiconvection and convective core overshooting', *ApJ* **390**, 136.

Strauss, M. A., Fan, X., Gunn, J. E., Leggett, S. K., Geballe, T. R., Pier, J. R., Lupton, R. H., Knapp, G. R., Annis, J., Brinkmann, J., Crocker, J. H., Csabai, I., Fukugita, M., Golimowski, D. A., Harris, F. H., Hennessy, G. S., Hindsley, R. B., Ivezic, Z., Kent, S., Lamb, D. Q., Munn, J. A., Newberg, H. J., Rechenmacher, R., Schneider, D. P., Smith, J. A., Stoughton, C., Tucker, D. L., Waddell, P. & York, D. G. (1999), 'The discovery of a field methane dwarf from Sloan Digital Sky Survey commissioning data', *ApJ* **522**, L61.

Strom, K. M. & Strom, S. E. (1994), 'A multiwavelength study of star formation in the L1495E cloud in Taurus', *ApJ* **424**, 237.

Tarter, J. C. (1975), The interaction of gas and galaxies within galaxy clusters, PhD thesis, University of California, Berkley.

Tinney, C. G. (1998), 'The intermediate-age brown dwarf lp944-20', *MNRAS* **296**, L42.

Tsuji, T. (1969), Model atmospheres of M dwarf stars, *in* S. S. Kumar, ed., 'Low Luminosity Stars', Gordon & Breach Science Pulications, New York, p. 457.

Tsuji, T. (2002), 'Dust in the photospheric environment: Unified cloudy models of M, L, and T dwarfs', *ApJ* **575**, 264.

Tsuji, T. & Nakajima, T. (2003), 'Transition from L to T dwarfs on the colour-magnitude diagram', *ApJ* **585**, L151.

Tsuji, T. & Ohnaka, K. (1995), Opacities of very cool and dense gaseous mixtures - an extension of stellar opacities to the substellar regime, *in* 'Astrophysical Applications of Powerful Databases', Vol. 78 of *ASP Conference Series*, p. 69.

Tsuji, T., Ohnaka, K. & Aoki, W. (1996), 'Dust formation in stellar photospheres: A case of very low mass stars and a possible resolution on the effective temperature scale of M dwarfs', *A&A* **305**, L1.

Tsvetanov, Z. I., Golimowski, D. A., Zheng, W., Geballe, T. R., Leggett, S. K., Ford, H. C., Davidsen, A. F., Uomoto, A., Fan, X., Knapp, G. R., Strauss, M. A., Brinkmann, J., Lamb, D. Q., Newberg, H. J., Rechenmacher, R., Schneider, D. P., York, D. G., Lupton, R. H., Pier, J. R., Annis, J., Csabai, I., Hindsley, R. B., Ivesic, Z., Munn, J. A. & Waddell, A. R. T. P. (2000), 'The discovery of a second field methane brown dwarf from Sloan Digital Sky Survey commissioning data', *ApJ* **531**, L61.

van Leeuwen, F. (1980), Mass and luminosity function of the Pleiades, *in* 'Star Clusters', IAU Symposium 85, p. 157.

Walter, F. M., Vrba, F. J., Matieu, R. D., Brown, A. & Myers, P. C. (1994), 'X-ray sources in regions of star formation. 5: The low mass stars of the upper scorpius association', *AJ* **107**, 692.

White, R. J. & Basri, G. (2003), 'Very low mass stars and brown dwarfs in Taurus-Auriga', *ApJ* **582**, 1109.

Wichmann, R., Bastian, U., Krautter, J., Jankovics, I. & Rucinsky, S. M. (1998), 'Hipparcos observations of pre-main-sequence stars', *MNRAS* **301**, L39.

Wolk, S. J. (1996), 'Watching the stars go 'round and 'round', *PhD Thesis, Univ. New York at Stony Brook* .

York, D. G. (2000), 'The Sloan Digital Sky Survey: Technical summary', *AJ* **120**, 1579.

Zapatero-Osorio, M. R., Bejar, J. J. S., Martín, E. L., Barrados y Navascués, D. & Rebolo, R. (2002*a*), 'Activity at the deuterium burning mass limit in Orion', *ApJ* **569**, L99.

Zapatero-Osorio, M. R., Bejar, V. J. S., Martín, E. L., Rebolo, R., Barrados y Navascués, D., Bailer-Jones, C. A. L. & Mundt, R. (2000), 'Discovery of young, isolated planetary mass objects in the σ Orionis star cluster', *Science* **290**, 103.

Zapatero-Osorio, M. R., Bejar, V. J. S., Pavlenko, Y., Rebolo, R., Prieto, C. A., Martín, E. L. & López, R. J. G. (2002*b*), 'Lithium and Hα in stars and brown dwarfs of σ Orionis', *A&A* **384**, 937.

Zapatero-Osorio, M. R., Bejar, V. J. S., Rebolo, R., Martín, E. L. & Basri, G. (1999*a*), 'An L-type substellar object in Orion: Reaching the mass boundary between brown dwarfs and giant planets', *ApJ* **524**, L115.

Zapatero-Osorio, M. R., Caballero, J. A., Bejar, V. J. S. & Rebolo, R. (2003), 'Photometric variability of a young, low mass brown dwarf', *A&A* **408**, 663.

Zapatero-Osorio, M. R., Lane, B. L., Pavlenko, Y., Martín, E. L., Britton, M. & Kulkarni, S. R. (2004), 'Dynamical masses of the binary brown dwarf GJ 569Bab', *ApJ* **615**, 958.

Zapatero-Osorio, M. R., Rebolo, R., Martín, E. L., Basri, G., Magazzù, A., Hodgkin, S. T., Jameson, R. F. & Cossburn, M. R. (1997), 'New brown dwarfs in the Pleiades cluster', *ApJ* **491**, L81.

Zapatero-Osorio, M. R., Rebolo, R., Martín, E. L., Hodgkin, S. T., Cossburn, M. R., Magazzù, A., Steele, I. A. & Jameson, R. F. (1999*b*), 'Brown dwarfs in the Pleiades cluster', *A&AS* **134**, 537.

The information used to write the basic introductory background material contained in this thesis was gathered from a number of different sources. However, the main books that were used are listed below.

An Introduction to Modern Astrophysics
B. W. Carroll & D. A. Ostlie
Addison Wesley Publishing, 1996, USA

Introductory Astronomy and Astrophysics
M. Zeilik, S. A. Gregory & E. P. Smith
Harcourt Brace Jovanovich College Publishing &
Saunders College Publishing, 1992, USA

An Introduction to the Theory of Stellar Structure and Evolution
D. Prialnik
Cambridge University Press, 2000, USA

Low Light Level Detectors in Astronomy
M. J. Eccles
Cambridge University Press, 1983, UK

Stars and Planets
P. Moore
Chancellor Press, 1992, UK